

University of St Andrews



Full metadata for this thesis is available in
St Andrews Research Repository
at:

<http://research-repository.st-andrews.ac.uk/>

This thesis is protected by original copyright

Photocapacitance Studies
of
Transition Metal Related
Deep Levels in
III-V and II-VI
Semiconductors

A thesis presented by
Ralph Stephen Hall, B.Sc.,
to the University of St. Andrews
in application for the
Degree of Doctor of Philosophy



Th A922

Career

I first matriculated in the University of Edinburgh in October 1981 to study physics. In June 1984 I obtained the Degree of Bachelor of Science with First Class Honours in physics.

In October 1984, being in receipt of a Quota award from the Science and Engineering Research Council, I was enrolled as a Research Student in the University of St. Andrews under the then current resolution of the University Court, as a Higher degree candidate and subsequently enrolled for the degree of Doctor of Philosophy.

Declaration

I, Ralph Stephen Hall, hereby certify that this thesis has been composed by myself, that it is a record of my own work, and has not been accepted previously in partial or complete fulfillment of any other degree or professional qualification.

Ralph S. Hall

Dated *2nd August 1988*

The research was carried out in the Wolfson Institute of Luminescence, within the Department of Physics and Astronomy in the University of St Andrews under the supervision of Professor J W Allen.

Certificate

I hereby certify that the candidate, Ralph Stephen Hall, BSc., has fulfilled the conditions of the Resolution and regulations appropriate to the Degree of Doctor of Philosophy.

Research Supervisor

Date 2nd August 1958

Copyright

In submitting this thesis to the University of St. Andrews I understand that I am giving permission for it to be made available for use in accordance with the regulations of the University Library for the time being in force, subject to any copyright vested in the work not being affected thereby. I also understand that the title and abstract will be published, and that a copy of the work may be made and supplied to any bona fide library or research worker.

Acknowledgements

I thank the Science and Engineering Research Council for the award that made this project possible.

I am deeply grateful to my parents for all the support they have given me through many years. Their financial support released me from potential anxieties, but most of all their love helped to sustain me.

The staff and Research Students of the Physics department help provide an excellent, but relaxed working atmosphere, I thank them. In particular I thank the members of J W Allen's research group who were able to give me many interesting conversations (including physics!).

Life in St. Andrews has changed me greatly, I hope for the better, this would not have been possible without the love of so many of the friends I have made in St. Andrews.

Finally, I thank John Allen who, whilst not perfect as a research supervisor, came as close as I can practically imagine to that ideal. I thank him for his availability, affability, patience and interest.

ABSTRACT

The properties of transition metal impurities in semiconductors are interesting for theoretical and practical reasons. In this thesis the results of photocapacitance experiments on three semiconductor-impurity systems, nickel in gallium phosphide (GaP:Ni), chromium in zinc selenide (ZnSe:Cr) and vanadium in zinc selenide (ZnSe:V) are given and discussed. Two types of photocapacitance experiments were used, namely double light source steady state (DLSS) photocapacitance and single beam photocapacitance transient experiments ('transient experiments').

Two DLSS photocapacitance experiments were performed on a GaP:Ni diode. The first experiment, with a red (2.00eV) pump source, largely confirmed earlier photothermal ionisation experiments on Ni d^9 ; whereas the second, with an infrared (1.00eV) pump beam, revealed new photothermal d^8 to valence band transitions.

Photocapacitance transient measurements on ZnSe:Cr indicated two levels in the samples. One level, only seen below 140K, was 0.45 ± 0.05 eV from the conduction band edge and was probably due to a chromium complex. The second level had a threshold of about 1.1eV and is most probably the substitutional chromium $d^5 \rightarrow d^4 + e_{cb}$ transition, not previously reported in photocapacitance.

Very large capacitance changes were found in transient measurements on a ZnSe:V diode resulting from electrons from a well occupied level going to the conduction band. The transition threshold energy was in agreement with recent theoretical predictions of the d^2/d^3 level position, which had not been seen previously.

Finally, tables of known absolute photoionisation cross sections were compiled. The data was analysed for trends and compared to several simple transition rules. Both host-dependent variations and trends across the series are discussed. Anomalies of the cross section magnitudes in InP:Co and ZnTe:Co with respect to the most successful selection rule might be explained by low-spin d^6 ground states.

Contents

Chapter One : Introduction

1.0 Preamble	1
1.1 Deep Levels and their description	2
1.1.1 What is a Deep Level?	2
1.1.2 Level Diagrams	3
1.1.3 Configuration Coordinate Diagrams	4
1.1.4 Why study deep levels in Binary Semiconductors?	5
1.2 Review of Experimental Techniques	8
1.2.1 An Overview	8
1.2.2 Optical Spectroscopies	8
1.2.3 Electrical Techniques	10
1.2.4 Capacitance-based Techniques	10
1.2.5 Spin Resonance Techniques	13
1.3 Deep Level Kinetics	16
1.4 Role of the present work	19

Chapter Two Experimental Apparatus and Methods

2.0 Introduction	21
2.1 Description of Apparatus	21
2.1.1 Cryostats	22
2.1.2 Sample Contacts and Mounting	22
2.1.3 Light Sources	23
2.1.4 The Bridge	27
2.1.5 Measurement System	28
2.1.6 Automation	30

Contents

2.2	Procedures	32
2.2.1	DLSS Spectra	32
2.2.2	Wavelength Scanned DLSS	34
2.2.3	Transient Experiments	36
2.2.4	Temperature Control	36
2.2.5	Electrical Experiments	38
2.3	Techniques for Analysing Results	39
2.3.1	DLSS Capacitance Changes	39
2.3.2	Analysis of Capacitance Transients	40
	Appendix 2.I Measuring the Photon Flux	42
	Appendix 2.II Measuring the Bridge Response Time	43

Chapter Three : Nickel in Gallium Phosphide

3.1	Introduction	44
3.2	Sample and Experiments Performed	47
3.3	Results	50
3.4	Discussion and Interpretation of Results	54
3.4.1	2.00eV Pump Source Experiments	54
3.4.2	1.00eV Pump Source Experiments	58
3.5	Conclusions	63

Chapter Four : Chromium in Zinc Selenide

4.1	Introduction	64
4.2	Experiment	67
4.3	Results	71
4.4	Discussion	74
4.5	Conclusions	78

Contents

Chapter Five : Vanadium in Zinc Selenide

5.1 Introduction	79
5.2 Samples and Experiments	82
5.3 Results	87
5.4 Discussion	93
5.5 Conclusions	99
Appendix 5.1 Sudden Changes in the High Photon Energy Capacitance Spectrum of ZnSe:Cr and ZnSe:V	100

Chapter Six : Absolute Photoionisation Cross Sections:
A Review

6.1 Introduction	104
6.2 Basic Theory: Symmetries, Crystal Fields and e & t ₂ orbitals	108
6.3 Methods used to Measure the Cross Section	113
6.3.1 Optical Absorption	113
6.3.2 Optical Capacitance based Techniques	115
6.3.3 Photo-EPR	116
6.4 Possible Selection Rules and Expected Trends in Cross Section Values	118
6.5 Discussion	124
6.5.1 Are Low-Spin Ground States Possible? The Cases of InP:CO and ZnTe:Co.	130
6.6 Conclusions	136
Appendix 6.1 Deriving the Photoionisation Selection Rule	137
Appendix 6.2 Further Comments on Low-spin Systems	139

Chapter Seven: Conclusions 141

<u>References</u>	i-x
-------------------	-----

Chapter One: Introduction

Deep Levels, Experimental Techniques and Deep Level Kinetics.

1.0 Preamble

The title of this thesis is "Photocapacitance Studies of Transition-Metal Related Deep Levels in III-V and II-VI Semiconductors". In the introduction the terms "deep level", "transition-metal related deep level", "photocapacitance", III-V and II-VI will be examined and explained. I shall take the liberty of assuming the reader has some familiarity with the term semiconductor. I shall try to prepare the ground for the presentation of my experimental results and the interpretations of my results, in the light of results in the literature, which are to be presented in Chapters Three through Six.

Firstly, in Section 1.1 we shall examine briefly what deep levels are and why they are produced by 3d transition metal impurities. We shall also look at the reasons why deep levels are studied, including how deep levels are or could be utilised. Then we shall look at how deep levels can be characterised through the use of simple visually-based aids including level diagrams (Section 1.1.2) and configuration coordinate diagrams (Section 1.1.3). Next in Section 1.2 we will examine the various techniques used to study deep levels. Special reference will be given to techniques by which level depths can be calculated. Questions which have to be considered include the following. How must a sample be prepared to use a particular technique? Must it be conducting or semi-insulating? Has it to be prepared as a diode? What information can be obtained from the experiment? How easy is it to obtain important centre characteristics from

the results? What are the drawbacks to the technique? This work is not definitive but a reasonable attempt is made to answer these questions in a restricted space. In Section 1.3 we examine the kinetics of the occupation of deep levels with particular regard to the situations encountered later in the thesis. Lastly, a short summary of the rest of the thesis is given in Section 1.4.

1.1 Deep Levels and their Description

1.1.1 What is a Deep Level?

When a defect has more than one stable charge state (say x) it must produce a related number of levels in the energy gap ($x-1$). In the case of impurities which lie close in the periodic table to the host element(s) the impurity levels are found to have large effective electron orbitals, electrons from which can be easily completely delocalised because of the small binding energies (up to perhaps 20meV) involved. They are therefore said to be *donors* in the case of the lattice bonded impurity with an extra electron(s), or *acceptors* if the impurity has an excess of holes with respect to the atom it replaces. Shallow donor levels are thus close to the conduction band within the gap and shallow acceptors close to the valence band (see figure 1.1). Shallow impurity wavefunctions can be adequately expressed as a linear combination of a tractably small number of lattice wavefunctions from one band.

On the other hand, deep impurities are well localised and would require a linear combination of an impossibly large number of Bloch states to represent their wavefunctions accurately. Transition metal impurities, normally at a (cationic) substitutional site, have incomplete 3d shells after accounting for electrons participating in bonding orbitals. This leads to

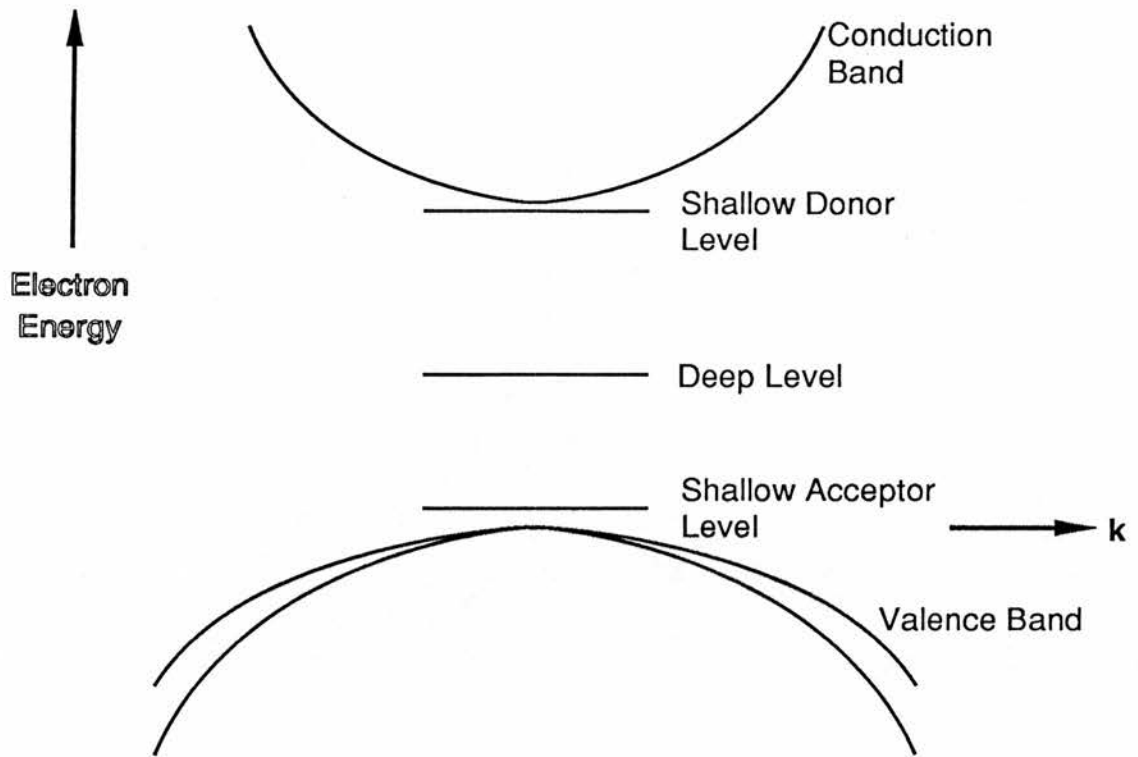


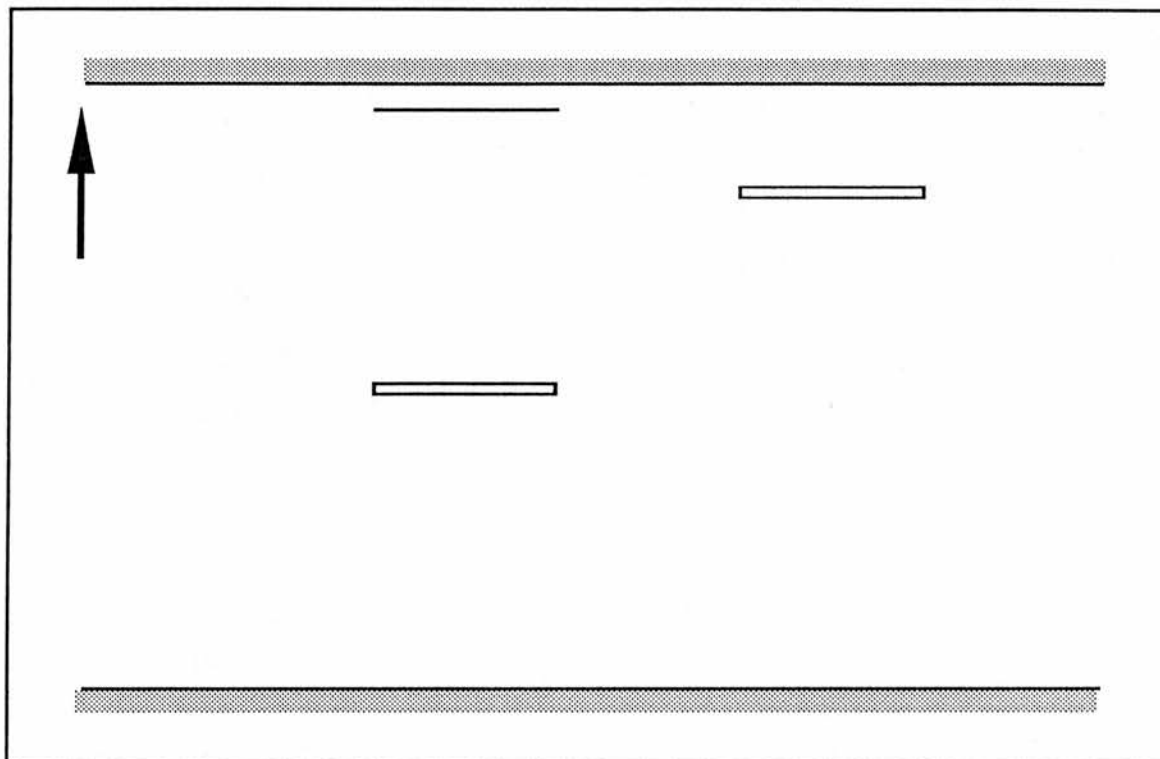
Figure 1.1 Illustration of the labels 'deep' and 'shallow' on an energy-momentum diagram. Deep levels might lie as illustrated in the mid-gap region but could also lie close to a band edge.

totally different behaviours from shallow impurities. The energy required to remove an electron or hole from the impurity to the nearest carrier band is not necessarily confined to be small (see figure 1.1). It could be any value up to half of the bandgap energy. Even when a transition metal produces a level close to a carrier band extremum, it does not behave at all like a typical shallow impurity (such as P in Si or Al in ZnSe). As an example of the differences we notice that the excited state structure is quite different – not at all like the "modified hydrogen atom" states seen for many shallow impurities. "Deep", therefore, refers more to the localisation of the impurity wavefunction than energy gap position.

1.1.2 Level Diagrams

A level diagram is a useful, simple tool to indicate the ground and excited states of an impurity with respect to the conduction and valence bands in a certain manner. Such a diagram is shown in figure 1.2. However simple these diagrams appear some thought is necessary to avoid possible later confusion. The level position only makes sense when comparing systems before and after a charge transfer transition. Thus in figure 1.2 we have a transition indicated between a configuration of d^n electrons and the energy of the d^{n-1} electron system + the electron in the conduction band. The level diagrams can be constructed in terms of electron energies (which increase going upwards) or in terms of hole energies (which increase downwards towards the valence band). This difference is trivial until one considers transitions involving excited states. There are two possible energy scales to use: hole energies which increase towards the valence band and electron energies which increase towards the conduction band. The usefulness of the two representations will become apparent in the discussion contained in Chapter Three.

a



b

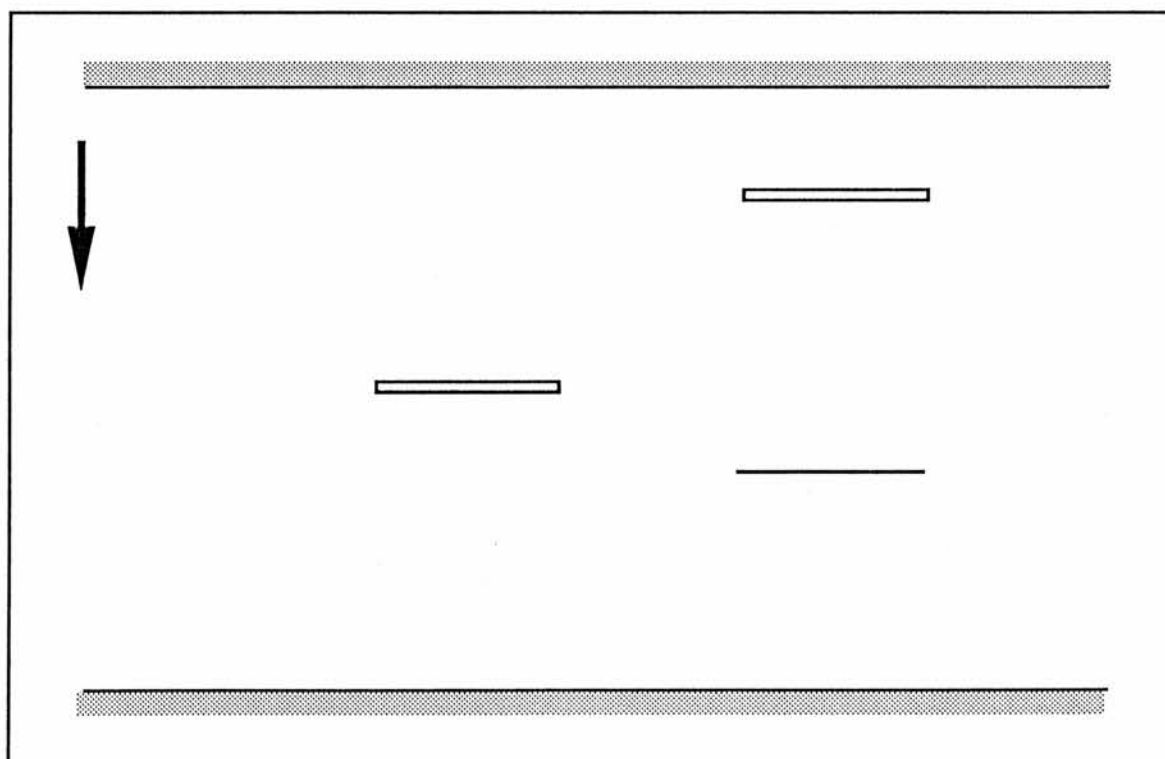

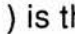


Figure 1.2 One level diagram drawn for electron and for hole energy representations. The blocked lines () are ground states and the thin line () is the same excited state as it must be shown in the two representations. The 'd' values show the ground state when the Fermi level is in a particular energy region. The system shown has three stable charge states, therefore two levels in the gap. The middle charge state is taken to have n d-orbital electrons. Hole occupations are given in **b**.

1.1.3 Configuration Coordinate Diagrams

A configuration coordinate diagram (CCD) helps to take account of the coupling of lattice vibrations to the electronic energy levels of a defect. Vibrational interactions can be thought of as being mediated through particles known as phonons. The interaction between electronic levels and phonons produces a set of so-called vibronic levels. The linear vibrations of the system can be described, in the harmonic approximation, by a parabola (or a set of parabolae when involving band states) in a one-dimensional configuration space^[1]. This is illustrated in figure 1.3. The configuration coordinate is related to (is a linear combination of) real displacements from equilibrium lattice positions. If the quantum nature of the system is taken into account the energy levels must be discrete. In fact, to a first approximation in configuration coordinate space, the system is a quantum harmonic oscillator with equally spaced energy levels ($E_n = h\omega_0(n + \frac{1}{2})$). However, if the system is at a temperature such that the thermal energy kT is large compared to the energetic spacing of the vibronic levels (given by the effective phonon energy $h\omega_0$) it is often a reasonable approximation to regard the vibronic levels as forming a continuum. If the lowest energy state parabola minima for two different charge states of the same centre occur at different configuration coordinate values then there exists a Franck-Condon shift or *relaxation energy* between the configurations. This can be seen in figure 1.3.

Different levels belonging to the same centre can be represented on the same CCD, as is the case with level diagrams. Such a system is illustrated in figure 1.3. Optical transitions are assumed to take place in a time which is short compared to the relaxation time between different

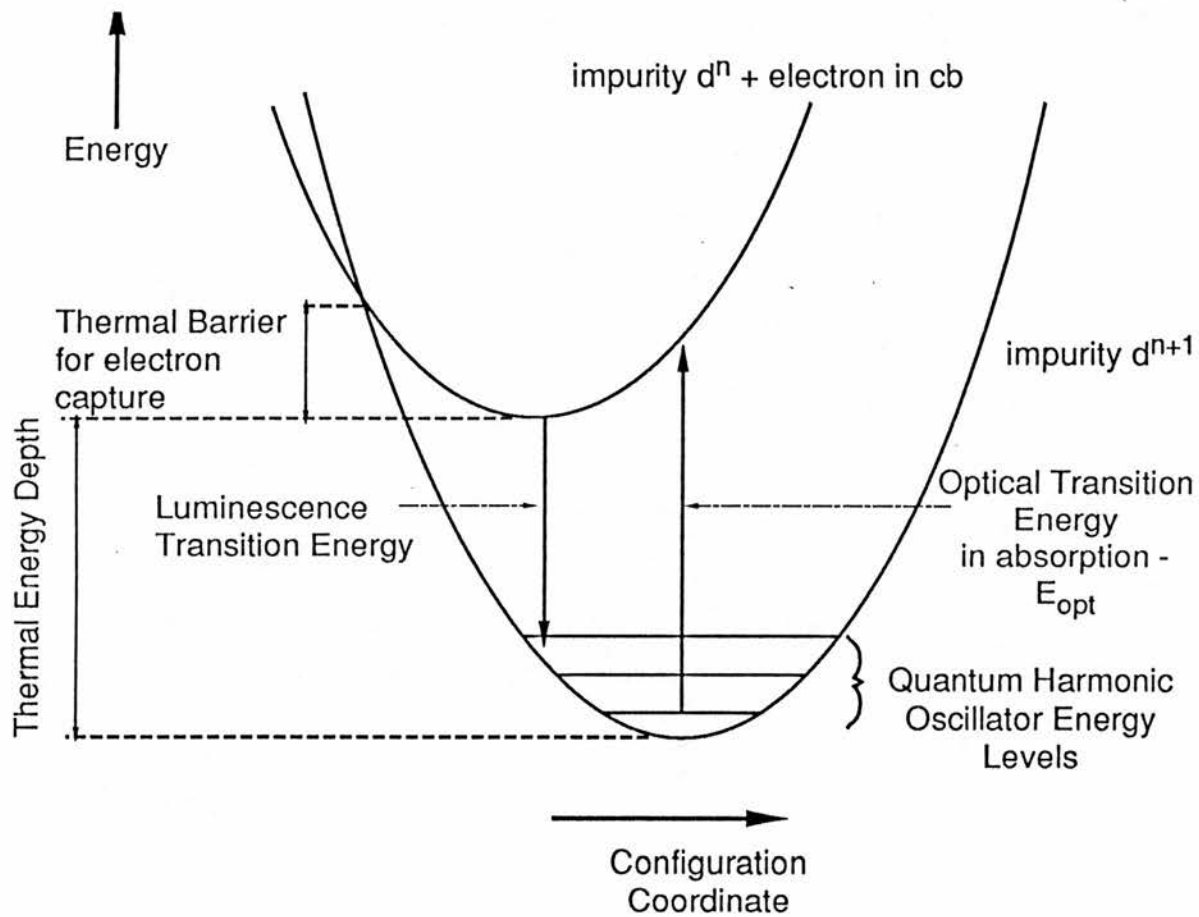


Figure 1.3 A hypothetical one-dimensional configuration coordinate diagram.

vibronic levels. Therefore optical transitions are represented by vertical transitions on the CCD. Thermal relaxation processes can take place from a higher to a lower vibronic level on the same diagram. The difference between the energies of the minima of two parabolae gives the thermal energy separation between the levels, this is not the same as the optical transition energy unless the minima of both parabolae occur at the same configuration coordinate value. More information on this subject can be found in the literature.

Figure 1.4 is an attempt to represent the relationship between experimental data, in this case idealised cross sections, and the two pictorial models we have discussed above. It should be noted that to construct either a level diagram using thermal energy depths or a CCD one cross section provides insufficient information without either the other cross section or shape fitting the cross section to a particular photoionisation model.

1.1.4 Why study deep levels in Binary Semiconductors?

Deep levels have a number of properties of interest. Some materials are of use in the optoelectronic and electronic industries. Deep levels exhibit properties which are of fundamental interest to solid-state physicists.

III-V and II-VI semiconductors are binary semiconductors. They consist of two chemical elements which can grow as a regular crystal. III-V semiconductors contain an equal number of group IIIB atoms (Al or Ga or In) and group VB atoms (N or P or As or Sb). The different elements lie on distinct sub-lattices so that the nearest-neighbouring

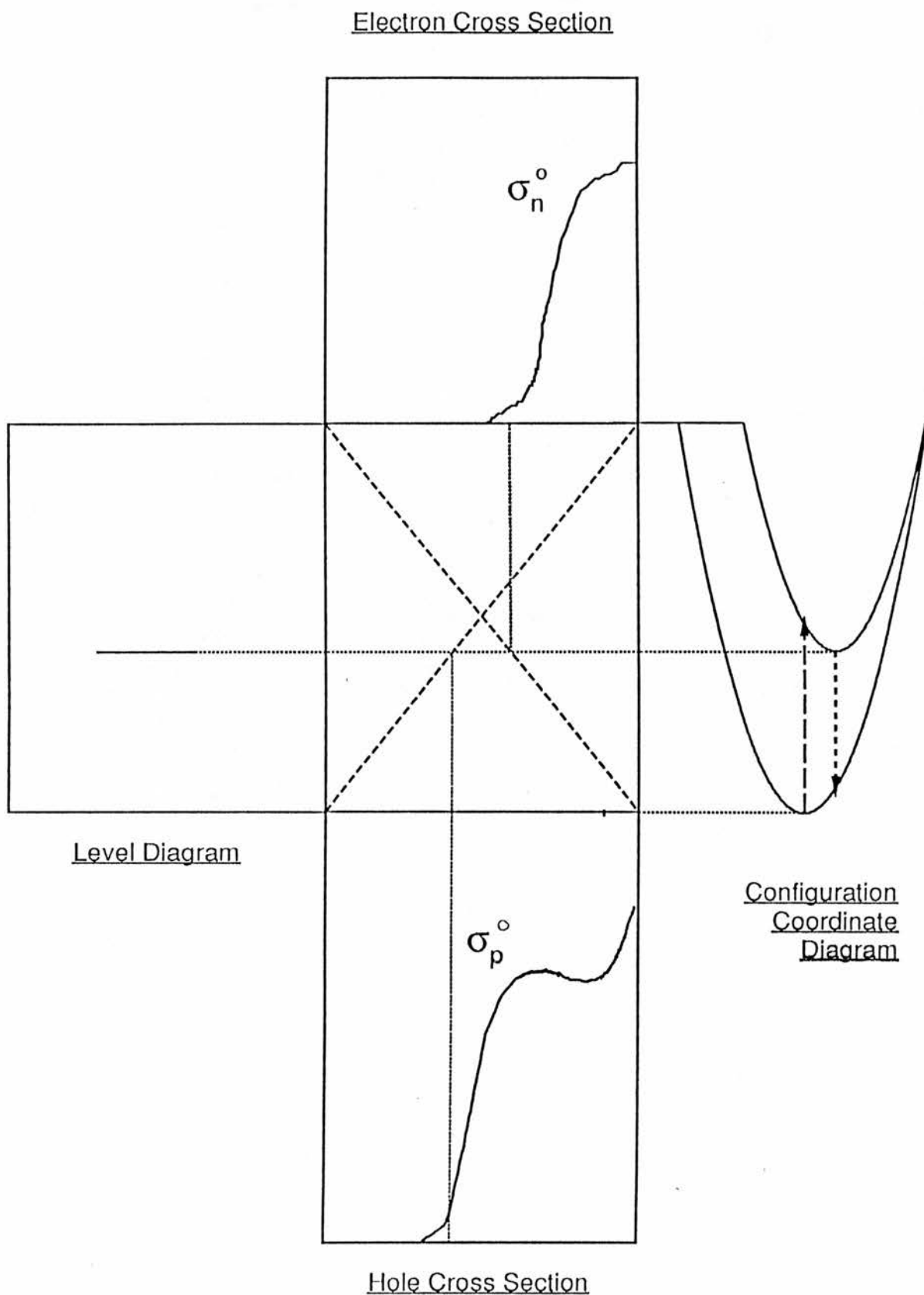


Figure 1.4 Diagram giving a crude relationship between modelling aids (level diagrams and configuration coordinate diagrams) and cross section spectra for charge transfer transitions.

atoms are of the opposite type. This is also the case for II–VI semiconductors with groups IIB (Zn or Cd or Hg) and VIB (S or Se or Te).

Substrate materials of high resistivity, either in the conductivity ranges corresponding to the terms insulating or semi-insulating (SI), are required to ensure that devices grown upon them are stable in their performance and that closely spaced devices do not interfere with each other. To ensure that a material is of at least SI resistivity at room temperature the Fermi level must be approximately in the middle of the energy gap. Deep levels in suitably high concentrations which are approximately mid-gap can often act as carrier traps "forcing" the Fermi level down/up into the mid-gap region. Here we look briefly at the most common electronic and optoelectronic substrate materials – GaAs and InP.

To produce SI GaAs three techniques have so-far been used commercially. (1) Very pure GaAs (nearly intrinsic) has been used as an SI substrate. Excluding all undesirable impurities is expensive. (2) Chromium has been used most often as a deep level electron trap to reduce conductivity. (3) Vanadium has been used most recently to produce a mid-gap Fermi level. The mechanism for the production of SI material is still not fully understood, although a number of papers have been published since 1984^[2–6].

Similarly iron in indium phosphide has been used to pin the Fermi level to a near mid-gap position, but this material is 'dirty', containing other defects making it far from ideal. Recently titanium-doped indium phosphide has been suggested as an alternative because of the mid-gap position of the d^0-d^1 level^[7–9] at about 0.63eV below the conduction band.

Manganese has been used to dope zinc sulphide to produce electroluminescent phosphors which emit a characteristic yellow–orange light. Other impurities, apart from transition metals have been used in zinc sulphide to produce different phosphors emitting different colours. Light emitting diodes (LEDs) have been produced which use transitions via deep levels. Solid state lasers are a possible future application but there are many problems associated with maintaining a population inversion. Laser action has only been observed in iron–doped indium phosphide^[10].

There are many points of fundamental interest in the study of transition metals in semiconductors. One of the major points of discussion is how far can the impurity be treated as a free ion perturbed by the effect of a crystalline environment? When can it not be so treated? The 3d transition–metal series impurities produce highly localised centres in semiconductors as stated before, however, the precise degree to which centres are localised varies from system to system. Much of the spin density is often found to be outside the impurity cell (ENDOR experiments—(See Section 1.2.5)). Chapter Six contains some discussion of this question.

Impurities in semiconductors typically have ionisation energies, and differences between successive ionisation energies, more than an order of magnitude lower than the free ion values. This implies a very substantial degree of effective screening of the nuclear charge by the crystal field. The precise screening mechanism is not fully understood. Excited states are also typically one electron–Volt in magnitude – again reduced from free ion values.

1.2 Review of Experimental Techniques

1.2.1 An Overview

Here a review of some of the most important techniques which have been used for the characterisation of transition metal impurities in semiconductors is given. The techniques are broken up into categories: optical techniques, electrical techniques, junction capacitance techniques and magnetic resonance techniques. This categorisation is loose, the list is far from exhaustive and some techniques could be included in more than one category.

1.2.2 Optical Spectroscopies

Optical Absorption

Absorption experiments can be useful in finding the energy difference between a ground and an excited state, or the energy necessary to remove a carrier on an impurity to the conduction or valence band edge. Unfortunately absorption measurements have the drawback of requiring fairly thick samples of good optical quality, thus it is extremely difficult to work on some epitaxial materials, which could be only a few hundred Angstroms thick (on top of a much thicker substrate material).

Photoluminescence

Photoluminescence (PL) is another well known, routinely used technique. The basic principle behind the technique is very simple. A monochromatic light source of high intensity (often a powerful laser) is shone onto the sample and the intensity of the light emitted from the sample is measured over a range of photon energies less energetic than

the excitation beam. A schematic diagram of apparatus to perform a photoluminescence experiment is shown as figure 1.5. A general review of photoluminescence of impurities in semiconductors can be found in an article by Dean^[11].

Luminescence techniques are quite sensitive and can give very good energy resolution. If a magnetic field is present the levels will be split into Zeeman sub-levels. Resolving the split lines gives information on the symmetry of a level, perhaps even the position of the centre in the lattice. Luminescence competes, however, with non-radiative channels for decay and this can make luminescence data misleading at times. Whilst luminescence can produce accurate values for the energy differences between states, it provides no quantitative concentration measurement. One example of a non-radiative channel is the energy transfer mechanism by which one centre can de-excite through energy being transferred to excite another centre, which in turn decays producing a detectable luminescence. Other non-radiative processes include Auger processes. Free carrier Auger processes are important in II-VI:Mn materials^[12] and Auger effects involving three centres have been seen in a few materials – ZnS:Fe^[13] to give an example.

Induced absorption can give additional information on excited states and might help to locate the ground state of an impurity relative to a band edge^[14].

Photoluminescence Excitation

Photoluminescent excitation (PLE) is a related technique where the excitation light source photon energy is varied and a broad-band detector and monochromator (or narrow pass-band filter) is used to select a particular energy which should usually correspond to a single transition.

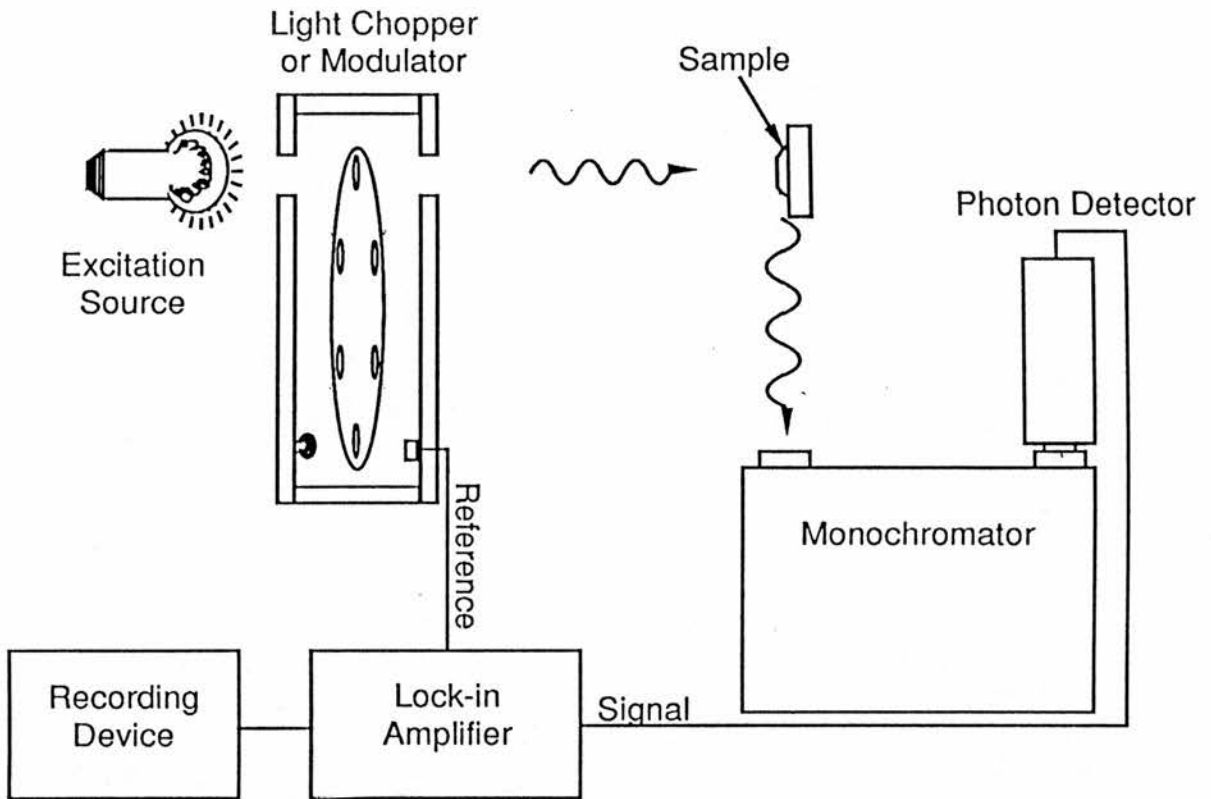


Figure 1.5 A schematic diagram of apparatus to perform a room temperature photoluminescence experiment.

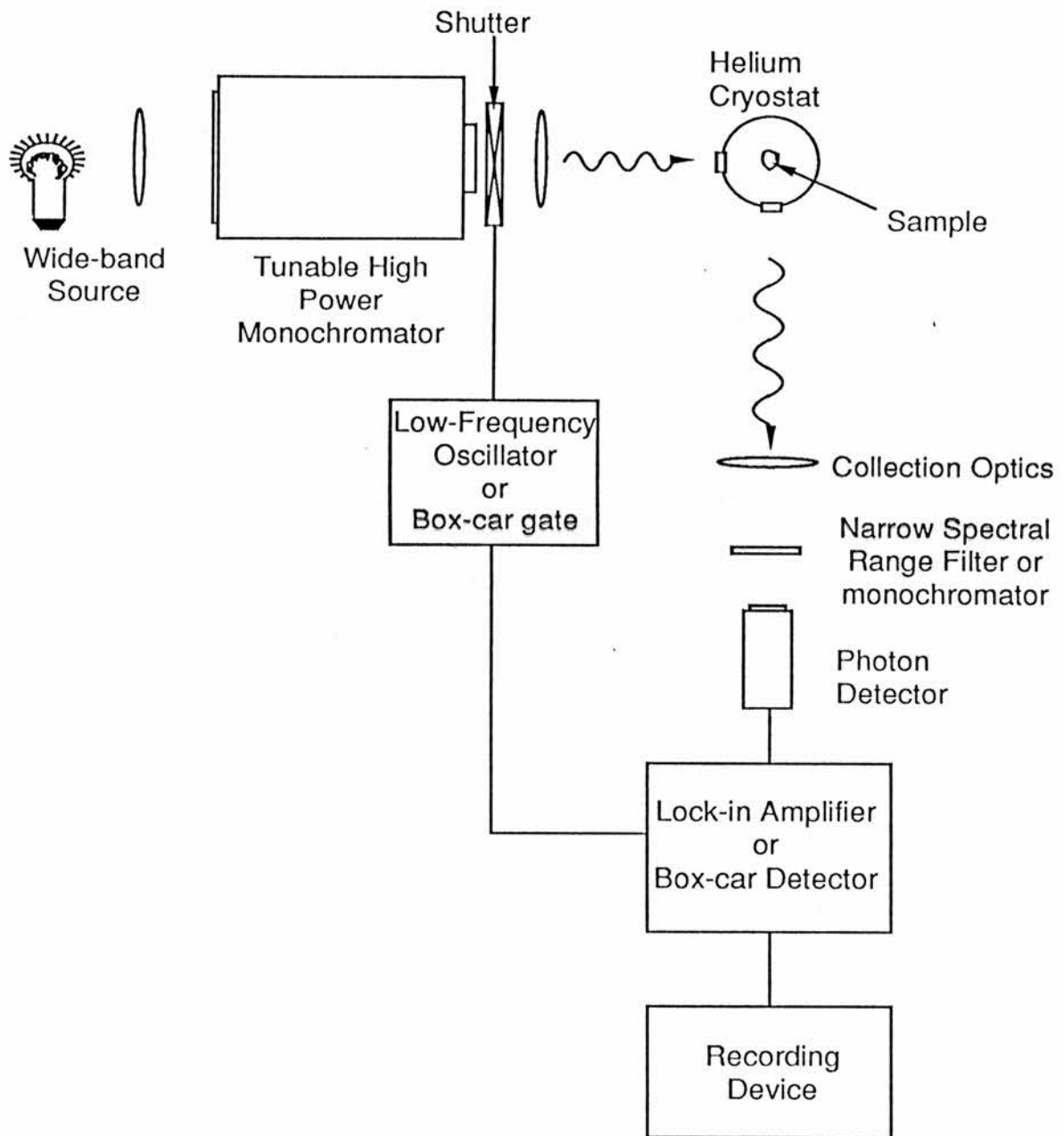


Figure 1.6 Schematic diagram of apparatus that could be used to perform photoluminescence excitation (PLE) experiments at low temperatures.

PLE can be viewed as a method of detecting absorption transitions by luminescence. An outline of the apparatus needed is given in figure 1.6.

1.2.3 Electrical Techniques

Hall Effect

The Hall effect is the production of an electric field (hence voltage) orthogonal to an electric current flowing through a conductor in the presence of a transverse magnetic field. The Hall effect can give the sign of the majority carrier (electrons or holes) and carrier concentration over a wide range of temperatures. The temperature dependence of the Hall coefficient can give an estimate of the energy depth of a level from a carrier band. The Hall effect can be performed under illumination (photo-Hall experiment). A suitable sample geometry for Hall measurements is shown in figure 1.7.

1.2.4 Capacitance-based Techniques

In this section we will look at techniques based on measuring capacitance changes, both time dependent and total capacitance changes, in the depletion region near a junction in the sample. In these techniques the sample must be conducting. It is prepared either as a p-n junction or, more usefully for material characterisation, as a Schottky diode. The techniques are photocapacitance, deep level transient spectroscopy and deep level optical spectroscopy. There are many more different techniques and variants on the basic ones described above which we will not have space to discuss. Capacitance based techniques have an advantage over the optical techniques outlined in Section 1.2.3 in that they can differentiate between transitions to the conduction band and transitions to

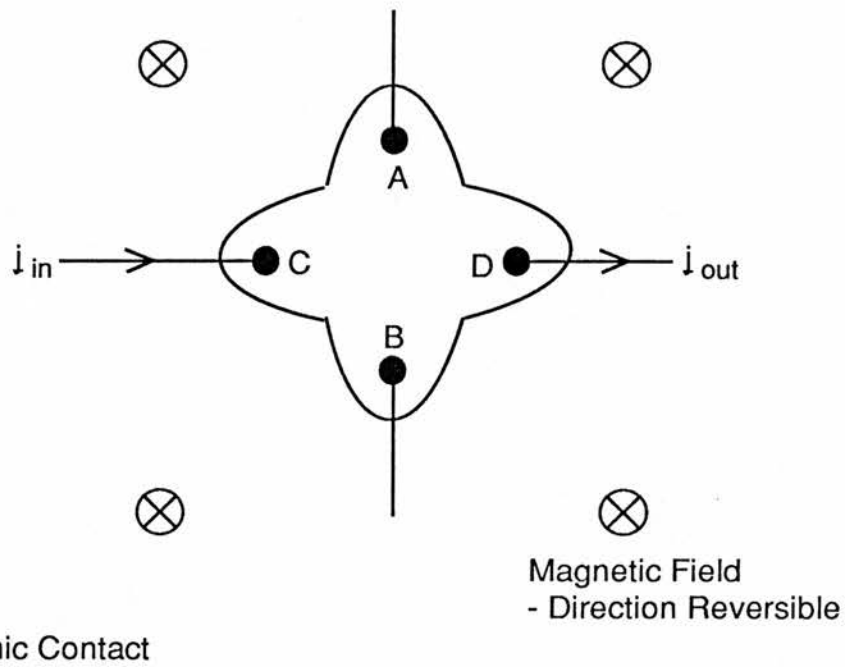


Figure 1.7 A typical sample geometry and contact arrangement for a Hall effect experiment. In the arrangement shown the Hall voltage will develop across the contacts labelled A and B. In order to obtain good carrier concentration measurements the functions of the two pairs of contacts must be varied, as must the direction of the magnetic field.

the valence band because of their sensitivity to charge change in the depletion region.

Deep Level Transient Spectroscopy (DLTS)

In this technique the junction is biased with electrical pulses and the capacitance transient sampled after each pulse^[15]. The sample temperature is slowly increased, from typically 77K. In the most usual version of this technique the capacitance transient is sampled at two fixed times (in the order of milliseconds) after the excitation pulse. If the decay time is very short or very long compared to the interval between the sample times then this difference will be very small (figure 1.8). A peak is seen in the signal at the temperature at which the decay time is equal to the sampling interval ("rate window" – see figure 1.8). The height of the peak is an indication of the concentration of the level and its characteristic temperature is an indication of where the level lies within the gap. Plotting the DLTS data in a suitable manner can give the thermal activation energy of the level. If the decay is not exponential then the technique requires much more careful interpretation of the data, a fact not realised in some early papers. The analysis of DLTS spectra is a subject which has itself spawned many applied research papers, for example Morimoto *et al.*^[16]. The method is most useful for the easy concentration measurement of levels with known DLTS signatures. Suitable apparatus is shown in figure 1.9.

Similar experiments can be performed detecting the current produced by the voltage excitation pulses^[17]. This is useful in high resistivity materials. DLTS and this current transient spectroscopy have become standard industrial quality control techniques.

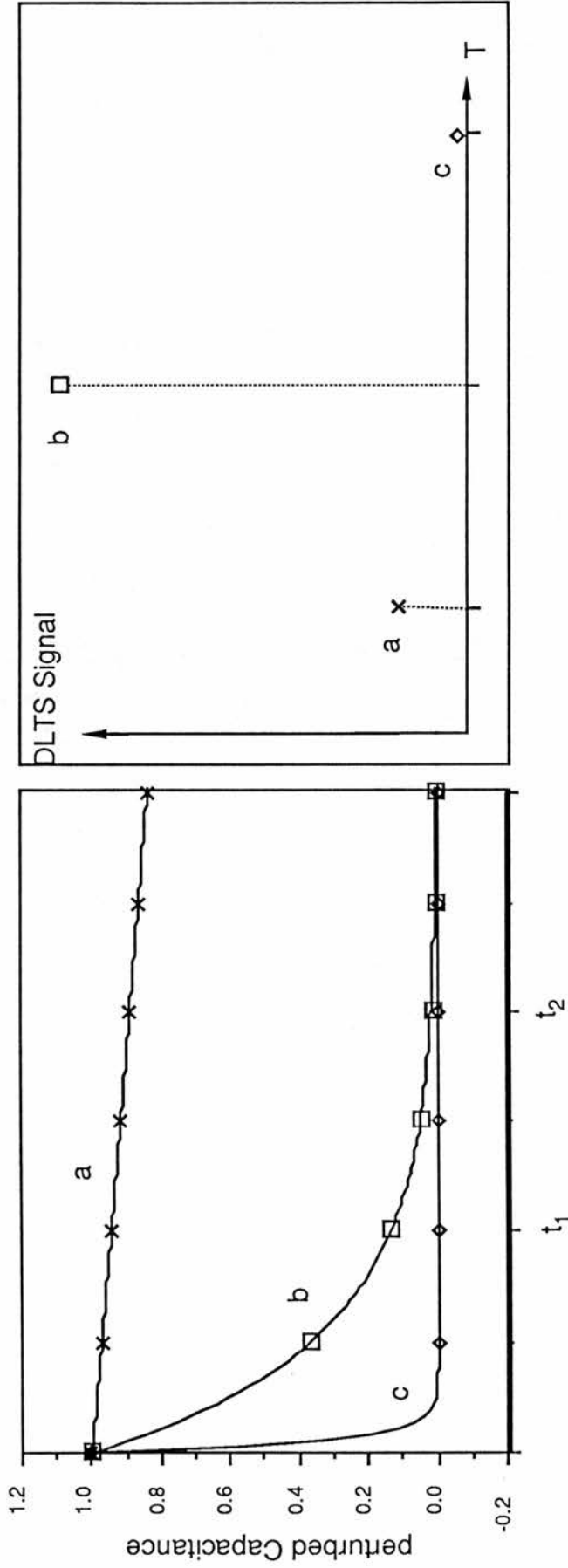


Figure 1.8 Illustration of the principle of DLTS and related transient sampling techniques. For a particular level the DLTS signal will be a maximum when the transient decay time is equal to the transient sampling window time.

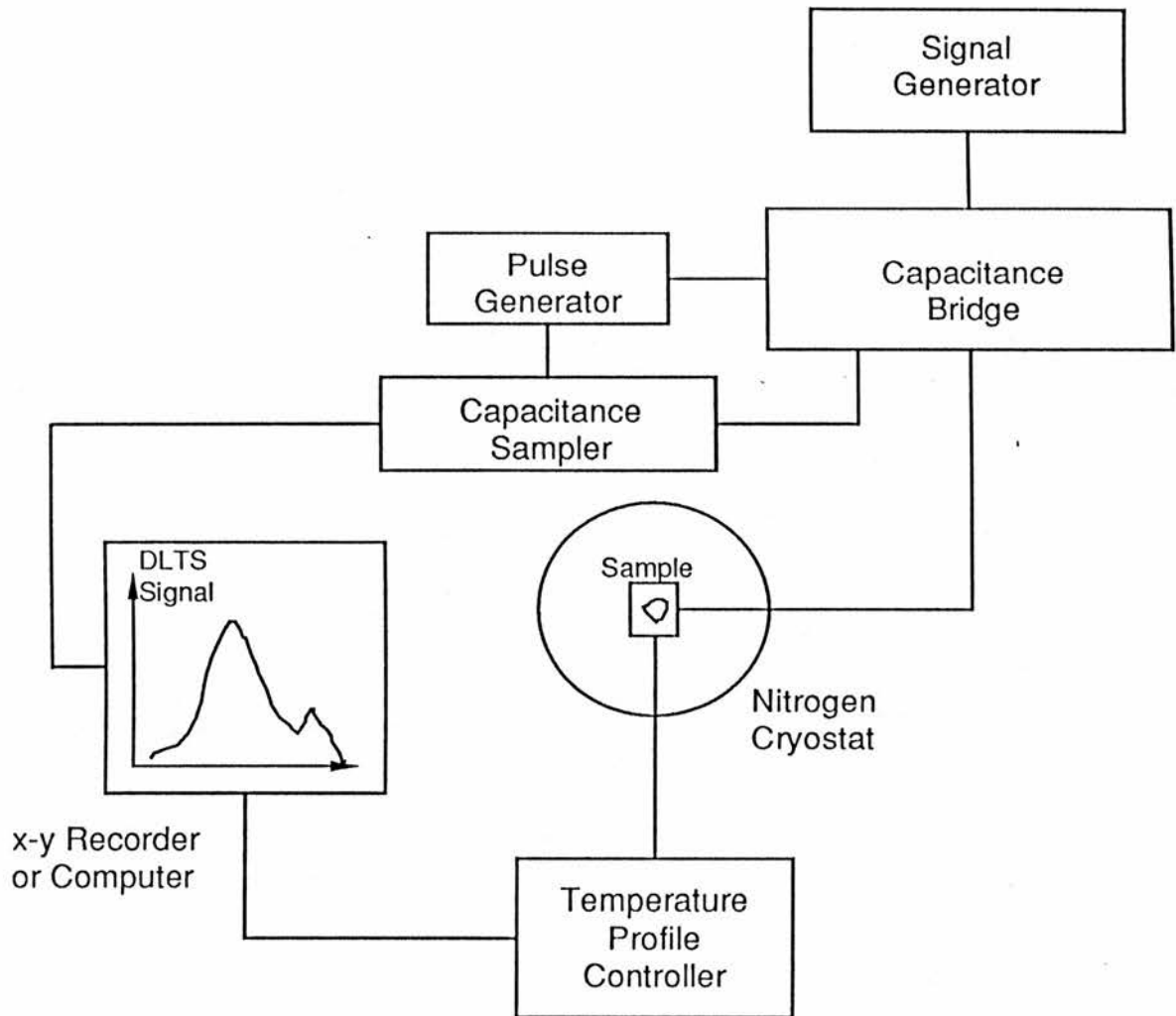


Figure 1.9 Schematic diagram of apparatus to perform simple electrical DLTS measurements.

Photocapacitance

The capacitance of the depletion region depends on the Schottky barrier height (which in turn depends on the nature of the Schottky contact, the bias applied to the sample, and on the fixed charge within the depletion region. The charge in the depletion region of course depends on the concentration of all levels within the energy gap, deep levels and net shallow donor or acceptor concentrations as well as the depletion region width. If light of the appropriate energy is shone on the depletion region then transitions to or from the level to a carrier band can take place. One such process is shown in figure 1.2a. The change in the charge state in the depletion region leads to a change in the capacitance of the sample. Changes in the capacitance of less than 10^{-14} F can be resolved with suitable equipment, enabling levels to be studied at trace concentrations of about 10^{13} cm⁻³ in a sample with a capacitance of 100pF and a shallow donor concentration of about 10^{17} cm⁻³.

One major advantage of this technique is that the cross section for an optical transition can be obtained directly giving good information on how the centre interacts with its environment. The sign of the capacitance change indicates whether a hole or an electron is involved, which is a point often in doubt with many other techniques.

This method has practical disadvantages, a major one being the length of time necessary to take a spectrum as the value for each photon energy might take any time from a few minutes to several hours to obtain. Photocapacitance was the technique used for all the impurity systems investigated in this thesis. More information on photocapacitance can be found in the article by Grimmeiss and Ovrén^[19].

Deep Level Optical Spectroscopy

Another capacitance-based technique is deep level optical spectroscopy (DLOS)^[20]. In this technique the sample is excited by optical pulses and the capacitance changes examined in a similar manner to DLTS (DLOS apparatus – figure 1.10). The measured signal is the time derivative of the capacitance transient calculated from two or more samples of the capacitance transient. The signal divided by the incident flux is plotted against the energy of the excitation light. Simple modifications of the basic DLOS method are to electrically excite the level by pulsing the bias voltage at low temperature or to thermally excite the levels by pulsing the light source at high temperature.

The technique being based on changes in capacitance it is possible to find out whether a hole or an electron is involved in the transition like in photocapacitance.

1.2.5 Spin Resonance Techniques

EPR and Photo-EPR

Electron paramagnetic resonance (EPR), also known as electron spin resonance (ESR), is a technique which uses the microwave transitions between magnetically-split levels to determine the characteristics of a centre. Usually a fixed frequency microwave generator (GHz frequencies) is used and the magnetic field splitting varied with the magnetic field. The absorption of microwave power in the sample cavity is measured as a function of magnetic field. The magnetic field values at which these resonances occur gives the g value for the lines; together with hyperfine splittings it can identify – at best – the spin, the nucleus involved and the

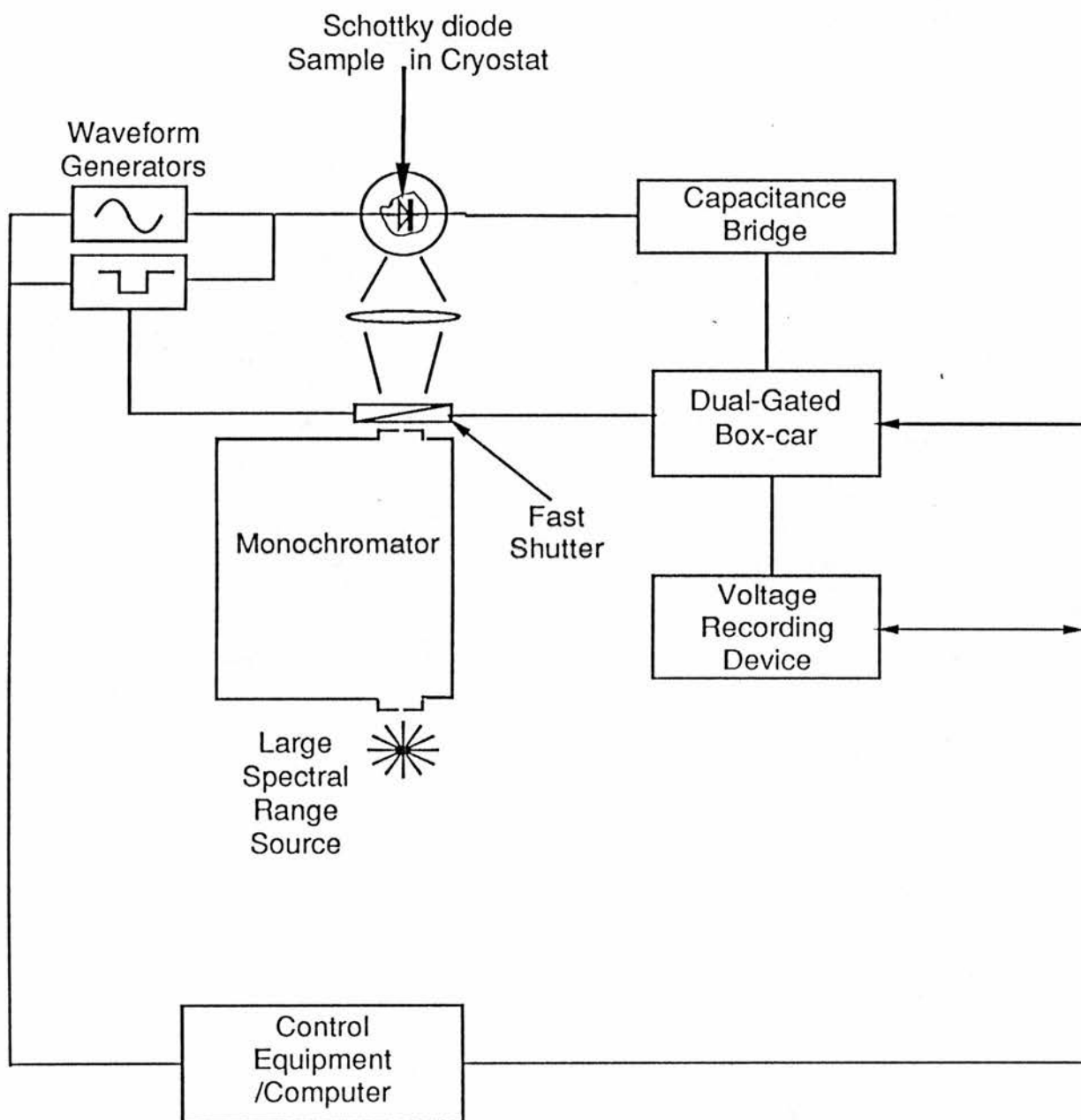


Figure 1.10 A schematic diagram of a set of apparatus for performing a deep level optical spectroscopy (DLOS) experiment.

symmetry of a centre. A variant photo-EPR looks at the changes in the EPR signals induced by illumination. Both the steady state and system dynamics can be studied. An extensive review of the uses of the photo-EPR technique for deep level characterisation and identification has been given by Godlewski^[21].

Optically Detected Magnetic Resonance

The optically detected magnetic resonance (ODMR) technique looks at microwave transitions through detecting optical radiation. The basic principles of this technique have been around for some time – first having been used to study atomic systems^[22]. It thus combines the sensitivity of optical detection with the advantages of magnetic resonance in probing level spins and symmetries. It is usually more sensitive than straightforward photoluminescence. A schematic diagram of an ODMR apparatus is given in figure 1.11. It enables the magnetic resonance properties of the excited states of impurities to be studied as well as their ground states (figure 1.12). The recombination radiation can be examined for its polarisation properties as well as the overall intensity. (There are selection rules for the polarised optical transitions between Zeeman split levels belonging to different base levels.) This technique is especially useful for studying transitions which produce only broad, unstructured bands in photoluminescence spectra. A general review of the technique can be found in the article by Cavenett^[23] and a specific review of ODMR in II-VI materials has been recently published by Davies^[24].

ENDOR (Electron-Nuclear Double Resonance)

ENDOR^[25] is a technique which involves the double resonance of magnetically split levels ($\propto \underline{B} \cdot \underline{J}$) with the hyperfine splitting ($\propto \underline{I} \cdot \underline{S}$) produced by the interaction between the nuclear and electron spins.

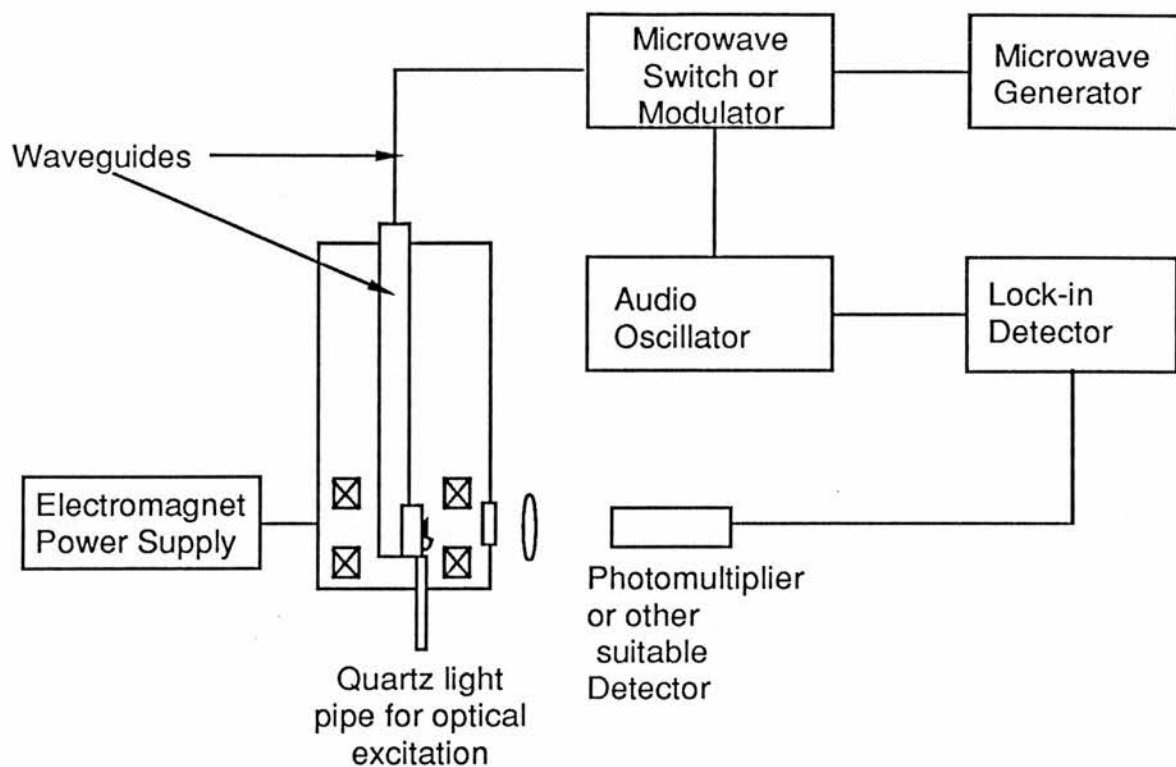


Figure 1.11 A schematic diagram of apparatus to perform a simple optically detected magnetic resonance (ODMR) experiment.

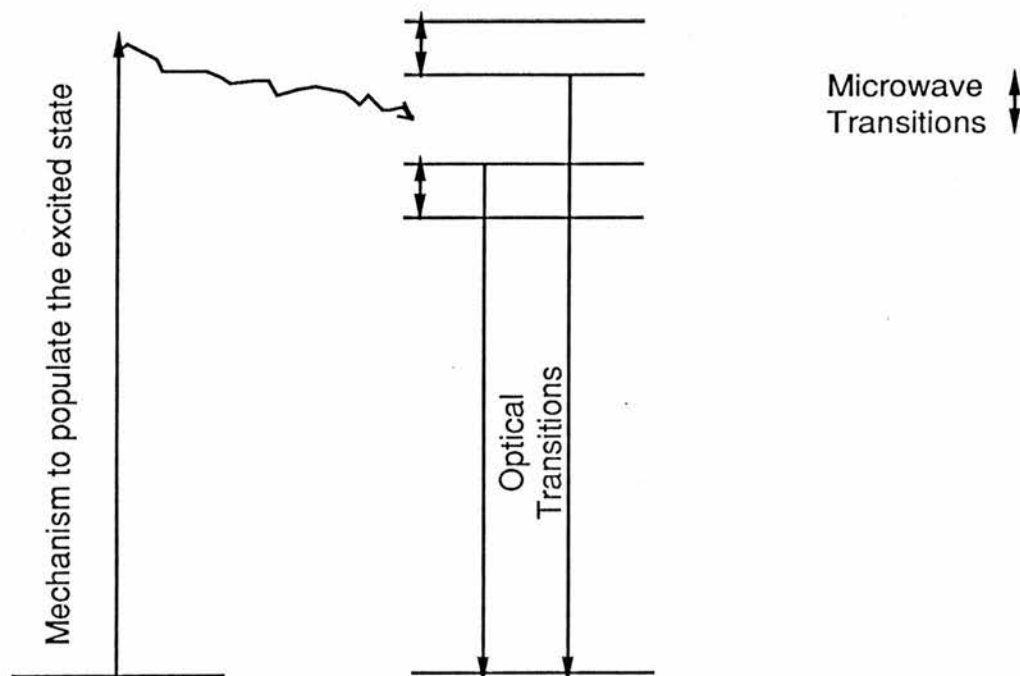


Figure 1.12 A rough diagram illustrating how ODMR can in principle give detectable changes in luminescence transitions, leading to information on the splitting of an excited state in a magnetic field.

Transitions between the hyperfine levels are produced by a radio-frequency coil, the effect being monitored by the microwave absorption between the electronic lines (figure 1.13). ENDOR can give information on the number and atomic type of some of the shells of atoms surrounding the impurity. It can also determine the impurity spin and the spin density around the impurity^[26,27]. Often the chemical identity of the centre can be determined. ENDOR is the only technique we have looked at so far which can 'get a handle on' the impurity wavefunction. If ENDOR experiments still leave ambiguities it is possible to perform triple resonance experiments to clarify the situation^[28].

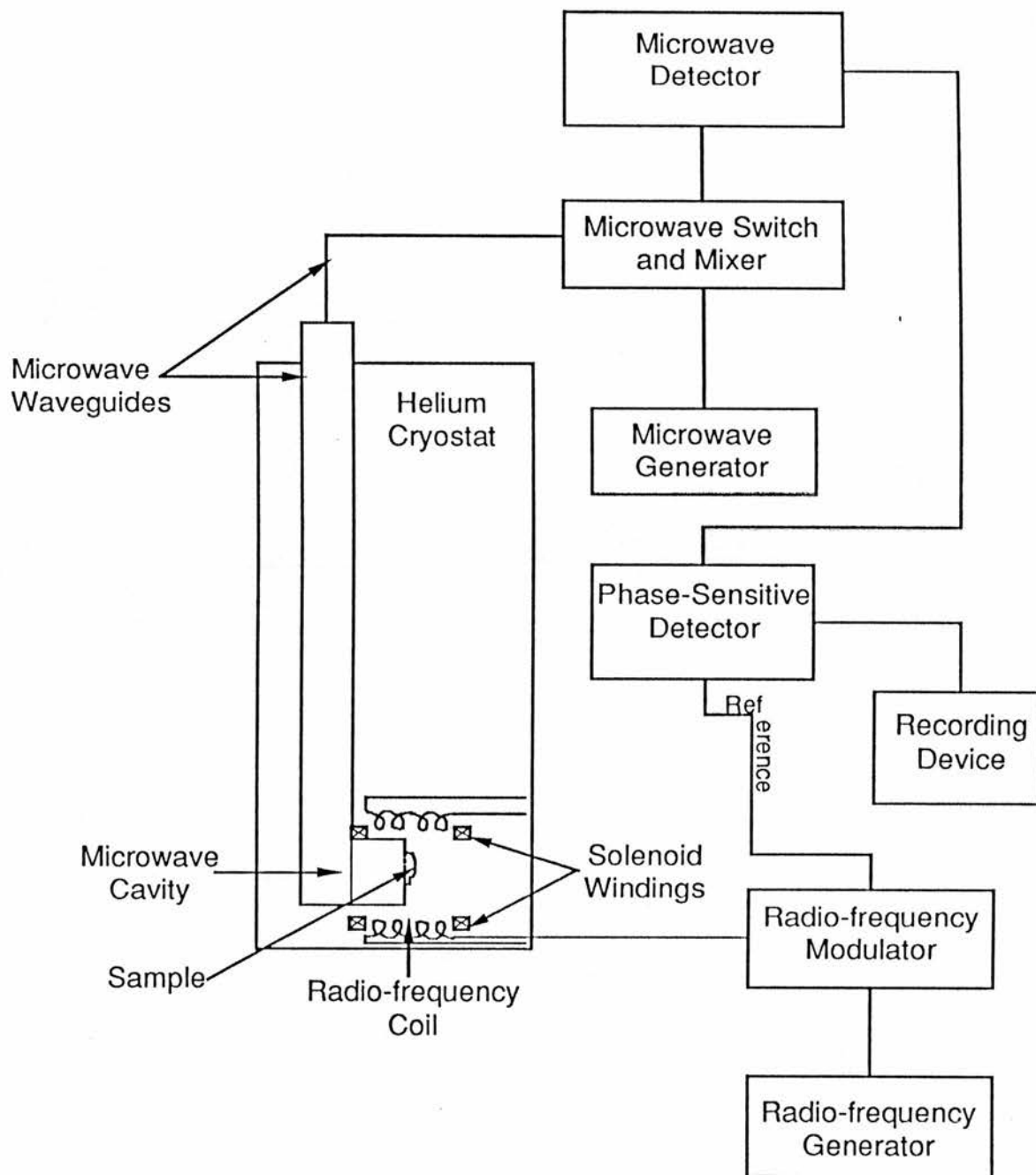


Figure 1.13 A schematic diagram of apparatus required for Electron- Nuclear Double Resonance (ENDOR) experiments.

1.3 Deep Level Kinetics

A study of the processes which can empty or fill a level is useful. We take a single level in the gap which has a total number of N centres. Each individual trap can be 'empty', with concentration n_e , or 'occupied' (n_g), such that $N = n_g + n_e$. The processes are illustrated in figure 1.14. The processes are divided here into six categories, characterised by emission (e) rates and carrier capture rates (c). The superscripts 'o' and 't' refer to optical and thermal processes respectively. The subscripts 'n' and 'p' denote that the carrier involved is an electron or a hole respectively. The full expression for the rate of change of the level occupation is then

$$\boxed{\frac{dn_g}{dt} = n_e \{-c_p p + e_p^o + e_p^t\} - n_g \{-c_n n + e_n^o + e_n^t\}} \quad 1.1$$

If there is insignificant carrier capture (in a depleted region) and we are at low temperatures where thermal rates are also negligible then (1.1) reduces to

$$\boxed{\frac{dn_g}{dt} = n_e e_p^o - n_g e_n^o} \quad 1.2$$

If we have a level which does not lie in the region close to the middle of the forbidden gap and if illumination is restricted to a photon energy region less than half of equivalent bandgap energy we have

$$\boxed{\frac{dn_g}{dt} = n_e e_p^o = (N - n_g) e_p^o} \quad 1.3$$

for levels in the lower half of the energy gap and

$$\boxed{\frac{dn_g}{dt} = -n_g e_n^o} \quad 1.4$$

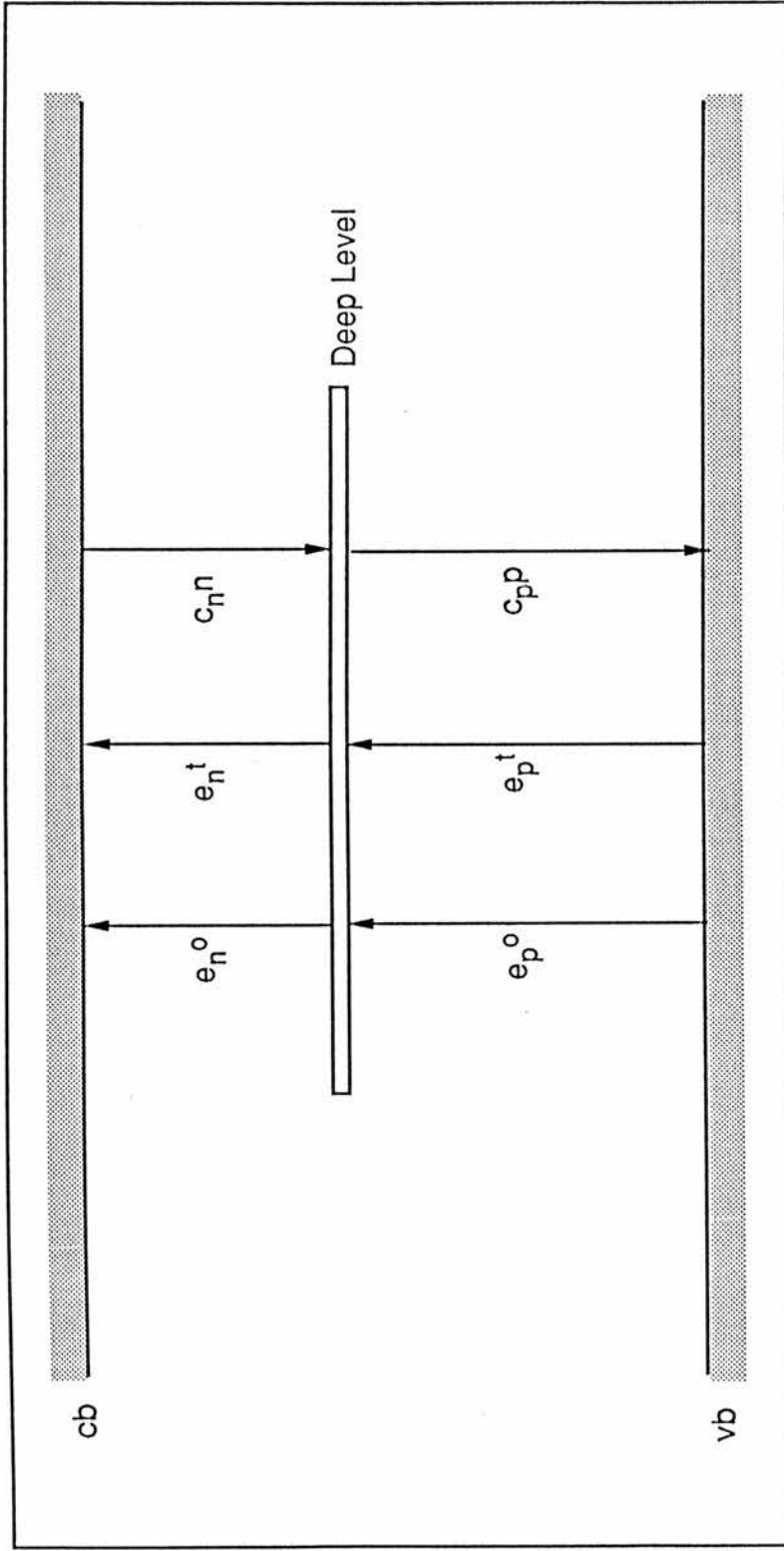


Figure 1.14 The simplified charge transfer processes possible at a deep level are indicated in the figure. The subscript _n refer to transitions involving the conduction band and likewise _p involves the valence band. The superscript ^o refers to an optical process and ^t to a thermal process. The concentrations of the carriers in the cb and vb are respectively denoted by 'n' and 'p'. The carrier capture processes 'c' depend on the carrier concentrations. The arrows represent the directions of *electron* movement.

for levels in the upper half of the gap. In the second case we have a simple exponential time dependence of the level occupation

$$\boxed{n_g(t) = n_g(t=0) \exp(-e_n^o t)} \quad 1.5$$

The optical emission rates are related to the optical cross sections by

$$\boxed{e^o = \sigma^o \phi} \quad 1.6$$

where ϕ is the photon flux.

In the case of a "mid-gap" level with an excited state close to the conduction band (refer to figure 1.15) we have the set of coupled equations

$$\boxed{\frac{dn_g}{dt} = n_e e_p^o - n_g \{e_n^o + e_i^o\} + n_x c_i} \quad 1.7a$$

$$\boxed{\frac{dn_x}{dt} = n_e c_{x,n} n + n_g e_i^o - n_x \{e_{x,n}^t + c_i\}} \quad 1.7b$$

neglecting thermal emission and capture processes directly involving the ground state and direct photoionisation of the excited state. The extra term not previously defined is c_i the internal decay rate. The subscript x is used to denote the excited state. Equations (1.7a,b) can be re-written as

$$\boxed{\frac{dn_g}{dt} = e_p^o N - \{e_n^o + e_i^o + e_p^o\} n_g + \{c_i - e_p^o\} n_x} \quad 1.8a$$

$$\boxed{\frac{dn_x}{dt} = c_{x,n} n N + \{e_i^o - c_{x,n} n\} n_g - \{e_{x,n}^t + e_{x,n}^o + c_i + c_{x,n} n\} n_x} \quad 1.8b$$

These coupled equations can in general be solved by using the properties of Laplace transforms. The general solution is a sum of exponential terms. The time constant is thus much more complex than in the case of the single level without an excited state^[29,30]. It is still possible to obtain information on the relative optical cross sections by the use of two

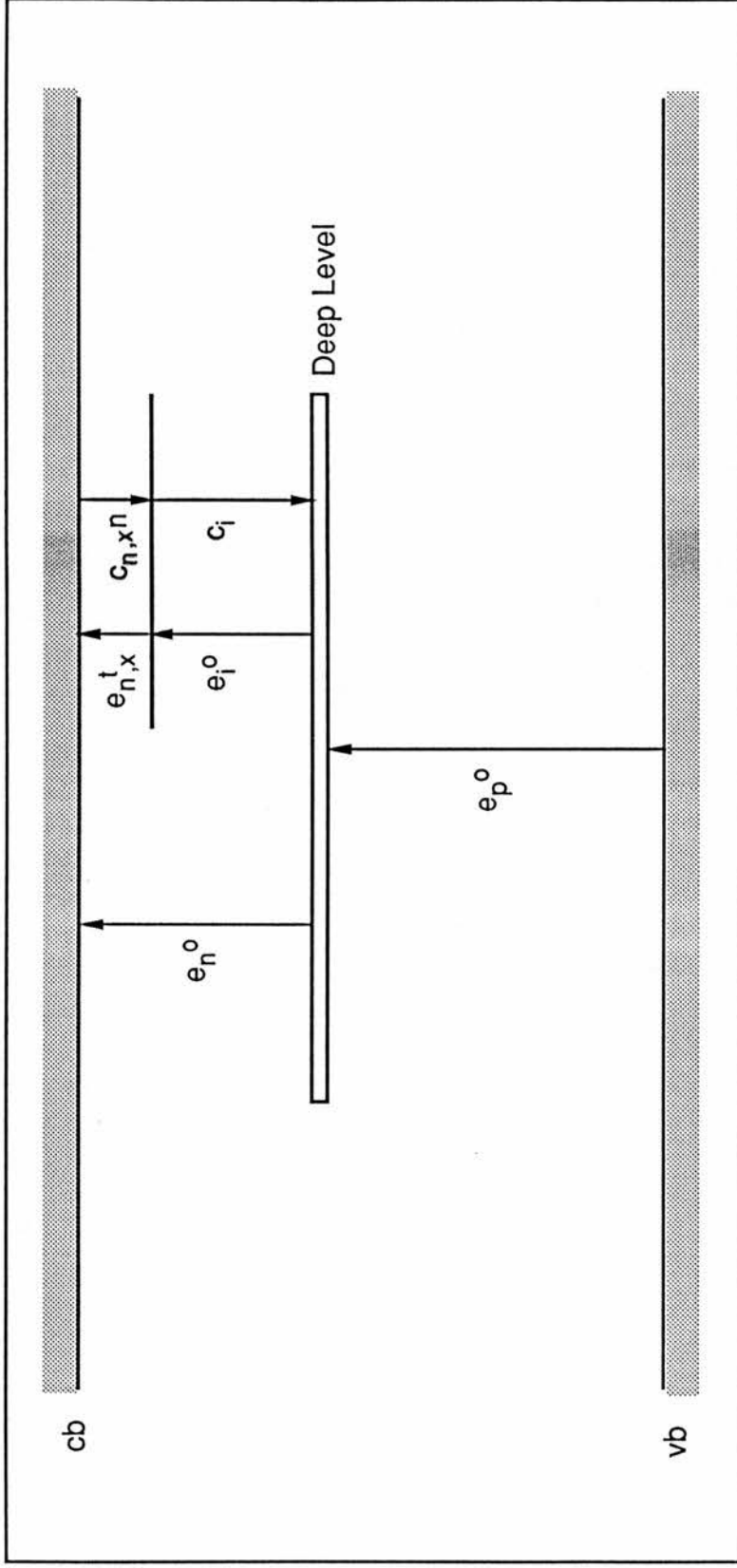


Figure 1.15 The simplified kinetic processes possible at a deep level with an excited state close to the conduction band, are indicated in the figure. The subscript n refer to transitions involving the conduction band and likewise p involves the valence band. The superscript o refers to an optical process and t a thermal process. The concentrations of the carriers in the cb and vb are respectively denoted by 'n' and 'p'. The carrier capture processes 'c' depend on the carrier concentrations. Comparing this diagram to figure 1.14 it can be seen that the thermal emission from and carrier capture processes directly to the deep level ground state have been assumed to be negligible.

beam steady state capacitance techniques. A certain distribution of levels is established with a high intensity beam and a second, lower intensity beam is used to perturb the distribution^[31,32].

If one works through the algebra, as has Mudhar^[31], one can establish that if the thermal emission is strong enough compared to the capture process into the excited state and the internal relaxation then the empty level occupation is perturbed by an amount Δn_e

$$\Delta n_e = \frac{e_p^o}{(e_p^o + e_n^o)^2} e_i^o N \quad . \quad 1.9$$

(Capacitance techniques can only differentiate between different charge states and so the difference in either n_e the empty level concentration or $n_g + n_x$ is the quantity being measured.)

1.4 Role of the present Work

How does this introductory chapter relate to the work presented in this thesis? This is a question which can only be satisfactorily answered after the chapters concerned have been examined in detail. However, as an interim measure, a short summary of the main points in each chapter is presented here.

In the next chapter, Chapter Two, there is a look at the experimental apparatus, experimental procedures and data analysis techniques necessary to extract deep level parameters from the samples studied.

Chapter Three looks at the transitions of nickel in n-type gallium phosphide (GaP:Ni) which can be observed with the dual beam steady state *photocapacitance* experiments. Two different experiments show that, depending on the experimental conditions, it is possible to see *photothermal transitions* originating from two different charge states of an impurity in one sample.

Chapter Four is concerned with the chromium transitions in zinc selenide (ZnSe:Cr). The chromium $d^5 \rightarrow d^4 + e_{cb}$ transition was studied by single beam *photocapacitance*. The *optical depth* of the impurity level from the conduction band was determined. The absolute cross section for the transition was measured and was shown to be of similar magnitude to that previously determined for the complementary transition ($d^4 \rightarrow d^5 + h_{vb}$).

The work in Chapter Five is on vanadium-doped zinc selenide (ZnSe:V), a material about which few papers have been published. The *optical depth* of the $d^3 - d^2$ level has been established from the determined *photocapacitance* cross section spectrum to the conduction band. Absolute

cross section measurements were taken. Charge transfer transitions for this level had not been studied before, although the excited state spectra for the two charge states had been investigated (d^3 and d^2).

Finally, in Chapter Six an effort is made to unify the results from the isolated materials studied in Chapters Three, Four and Five and also to tie the absolute cross section measurements in with those available in, or calculable from, the literature. Simple theories of the comparative magnitudes of optical cross sections for photoionisation transitions will be examined and compared to the data available, including the values obtained in Chapters Four and Five. Comments also will be made on the variation of cross section magnitude with host crystal. Discrepancies do exist between predicted and experimental cross section magnitudes for two examples of the cobalt $d^7 \rightarrow d^6 + e_{cb}$ transitions (in InP and ZnTe). The plausibility of a possible reason for this discrepancy is discussed.

Chapter Two:

Experimental Apparatus and Methods

2.0 Introduction

In this chapter the experimental techniques and procedures adopted are described. Firstly the experimental apparatus is described in Section 2.1, with some brief notes on the automation of the experiment. In Section 2.2 procedures are described. Finally in Section 2.3 the techniques used to examine the results are themselves analysed.

2.1 Description of Apparatus

The experiments were carried out using components already used in a proven photocapacitance system (used for example by Szawelska *et al.*^[32] and Mudhar^[31]). The basic system was as illustrated in figure 2.1. The diode in the cryostat can be illuminated with light from one or two monochromators or from filtered lamps. The capacitance and series resistance of the diode is measured on a capacitance bridge against a series combination of capacitance and resistance. The off-balance voltage (OBV) is amplified and detected on a CRO and an a.c. voltmeter. In the rest of Section 2.1 we examine cryostats, sample contacts and mounting, light sources, bridge and measurement systems in turn, finishing with a brief examination of how the system was automated with the use of a simple microcomputer and the advantages gained thereby.

2.1.1 Cryostats

Two different cryostats were used. For the GaP:Ni experiments low temperatures were not required, so the most important requirement became temperature stability. To this end a nitrogen bath cryostat was used. This had a single optical window made of spectrosil B (pass band 0.3–3.0 μm). The sample was mounted directly onto a copper cold-finger. The cryostat used for the other experiments was an Oxford Instruments continuous flow helium cryostat model CF1204, with a temperature range of 4–500K. This was configured with two sets of sapphire optical windows (pass band 0.25 to 5.0 μm) which were mounted at right angles to each other. The sample rod was fitted with ten electrical connections into the sample space of which three were used (high, low and ground).

2.1.2 Sample Contacts and Mounting

Two different types of contacts have to be made to the sample. Ohmic contacts were made by alloying a dot of clean indium metal onto a clean semiconductor surface at about 400 $^{\circ}\text{C}$. Schottky contacts were made by evaporating thin layers of gold or aluminium onto a clean semiconductor surface. Depending on the semiconductor and on the Schottky contact material the height of the barrier thus formed varies. Gold has a 1.30V^[33] (at 300K) barrier on n-type gallium phosphide and 1.36V^[34] (at 300K) on zinc selenide. Aluminium has a 0.76 V^[34] (at 300K) barrier on zinc selenide.

For the GaP:Ni experiments, when the nitrogen-bath cryostat was used, the sample was mounted directly onto an earthed copper cold finger.

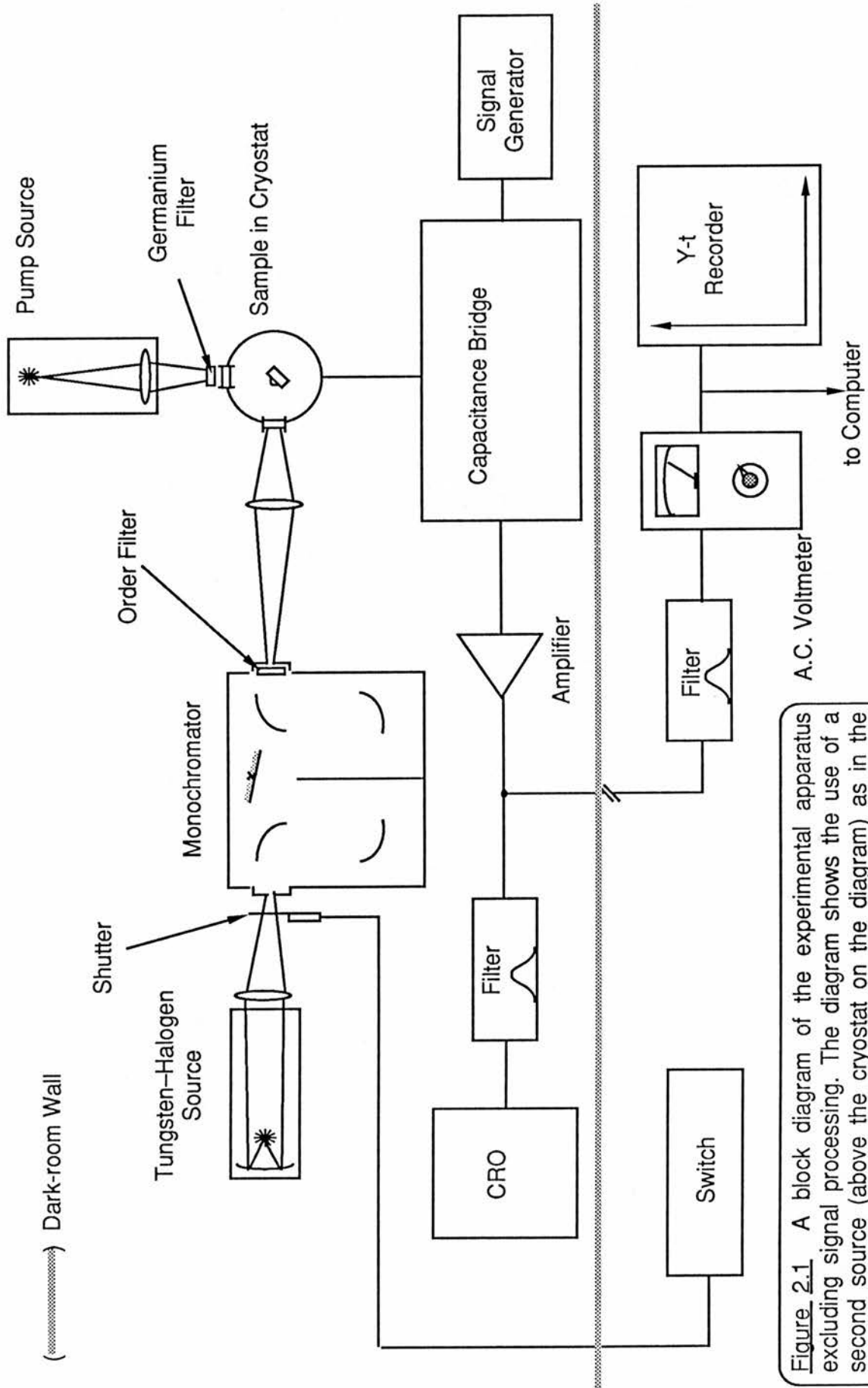


Figure 2.1 A block diagram of the experimental apparatus excluding signal processing. The diagram shows the use of a second source (above the cryostat on the diagram) as in the 'bleaching' experiments described in Chapters Four and Five.

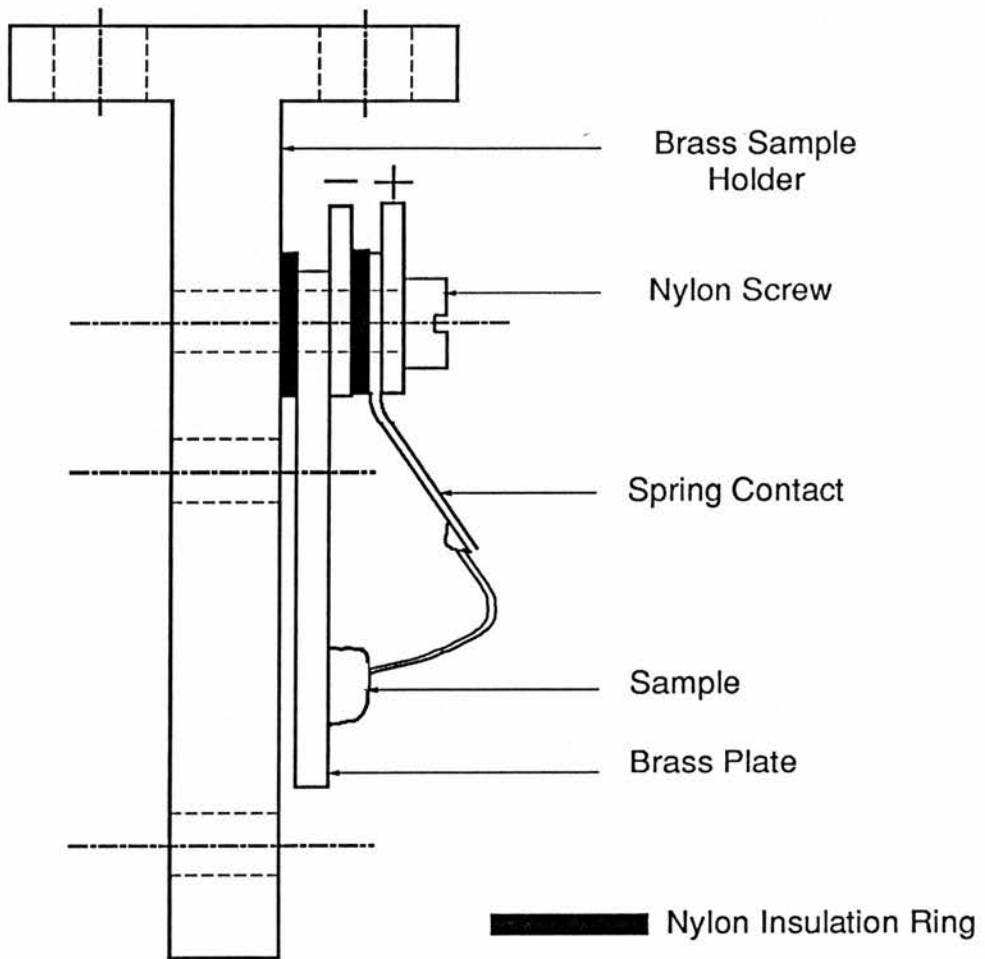


Figure 2.2 A diagram of the sample holder for the Oxford Instruments CF1204 cryostat. The scale, whilst not exact, is approximately four times the real size of the insert. The sample holder was earthed, the terminal marked - was connected to the series resistor (used to help balance the resistance in the bridge). The terminal marked + was connected directly to the bridge input.

A thin spring clip made contact with the gold Schottky contact. A 50Ω resistor was connected between the Ohmic contact on the sample and the screen of the coaxial cable to the bridge.

In all the zinc selenide experiments the CF1204 helium cryostat was used. The samples were mounted on a small brass plate attached to, but electrically insulated from both the sample holder and the spring contact (figure 2.2). The plate is necessary to avoid earthing the Ohmic contact. An earth wire was connected to the sample holder. A 50Ω resistor was mounted in series with the sample for ease of balancing the bridge. Originally, the resistor had been mounted in a box with a screened two core cable leading from the box to the top connector of the sample rod. There were problems of unstable capacitances associated with the contacts within the box. Placing the 50Ω resistor at the top of the sample holder eliminated the instability and also greatly reduced the stray capacitance in parallel with the sample.

2.1.3 Light Sources

The light source used to induce the measured capacitance changes, the primary or "excitation" light source, was a tungsten-halogen projection lamp coupled into a Spex Minimate 1670 grating monochromator. The lamps were run from a Coutant ASC 1000 24V, 10A stabilised d.c. power supply.

Initially it was found that the highest power lamp that could be utilised in the first, fully enclosed, uncooled lamp housing was one of 150W. Higher power bulbs were tried, to attempt to improve the resolution of the experiments by decreasing the excitation bandwidth (using

narrower monochromator slits) without decreasing sensitivity, but overheating in the lamp housing led to greatly reduced bulb lifetimes. Later a fan-cooled housing was constructed which allowed lamps up to 250W, the limit of the Coutant supply, to be used. The latter housing was, necessarily, less light-proof than the uncooled, fully enclosed housing.

This led to occasional misinterpretation of some spectra due to light screening around the cryostat being sometimes inadequate.

A Spex 600 lines/mm grating was used throughout the GaP:Ni experiments as it was blazed at 1000nm. For the spectral range 1000–350nm a 1200 lines/mm (500nm blazing) and for 3.2–2.0 μ m a 300 lines/mm (2 μ m blazing) were employed.

It should be noted that the output intensity of the tungsten lamps peaks at about 1160–1180nm making these lamps very inefficient above 4eV (310nm) or below 0.4eV (3 μ m).

Upon installation of a fresh bulb it was found that very unstable signals occurred for a period of a few hours. Thus it became standard procedure to leave a new bulb, or a freshly switched on bulb, for at least eight hours before any serious measurements were taken. The instability is attributed to the bulb slowly reaching an equilibrium temperature. The lifetime of a 150W bulb in the excitation source was approximately six to eight days.

For one bulb two calibration spectra were taken, the first about half an hour after the installation of a new bulb, and the second after about six hours of continuous use in the uncooled housing. The shapes of the two

spectra were not significantly different but the later spectrum showed more than double the total light output of the one recorded earlier.

A Bausch and Lomb high intensity grating monochromator fitted with a 45W tungsten-halogen lamp was used to provide the intense light source which was intended to fill or empty a particular centre in the GaP:Ni experiments. This I will usually refer to as the "pump" or second light source. For the experiment on the GaP:Ni diode with the 2.00eV pump source a grating covering the range 350–800nm was used, and for the 1.00eV pump light GaP:Ni experiment one which covered the range 800–1600nm.

This second source needed to be of much greater intensity than the excitation source, this was ensured by measuring the photocurrent produced by each source at 620 nm. The photocurrent was measured with a Keithley 602 electrometer.

In some of the experiments performed in Chapter Four (ZnSe:Cr) and Chapter Five (ZnSe:V) a long wavelength pass germanium filter was used in front of a powerful (45–150W) tungsten lamp to 'bleach out' the more shallow levels.

The excitation source could be blocked off from the sample with a mechanical shutter. The power supply to the shutter could be switched off remotely using a TTL compatible input^[31].

With grating monochromators there are nearly always problems with higher orders of diffraction. In order to reduce spurious effects due to these second and higher orders certain optical filters were used in front of the exit slit of the monochromators. The filter chosen depended on the

spectral range of light which was to be used in a particular experiment. Details are listed in table 2.1.

TABLE 2.1: Filters used in Photocapacitance Experiments

<u>GaP:Ni</u>		
<u>SPEX</u> <u>WAVELENGTH</u>	<u>SPEX</u> <u>FILTER</u>	<u>BAUSCH AND LOMB</u> <u>FILTER</u>
2000–1550 nm	Ealing 26–3046	Ealing 26–3038 (620 nm)
1540–1300 nm	Grubb–Parsons Silicon	Ealing 26–3038 (620 nm)
1240–680 nm	Ealing 26–3319	Grubb–Parsons Silicon (1240nm)

ZnSe:Cr and ZnSe:V

3.2–1.7 μ m	Grubb–Parsons Germanium
2.00–1.05 μ m	Grubb–Parsons Silicon
1.24–0.70 μ m	Ealing 26–3319
700–350 nm	Ealing 26–3038

2.1.4 The Bridge

The radio-frequency bridge is a unity-ratio transformer arm bridge which was designed and built specially in this laboratory (see figure 2.3). The sample capacitance and the sample resistance plus added series resistance is balanced against a series combination of capacitance and resistance within the bridge. The bridge has been used previously for phot capacitance work within the same laboratory^[31,32]. Szawelska^[35] showed that the off-balance voltage (OBV) signal is directly proportional to the capacitance change and calibrated the capacitance scale.

An electrical bias could be applied to the diode through the bridge. Biases of up to 3V were applied, the voltage being provided by two 1.5V dry cells in series, tapping the precise required voltage with a potentiometer.

The input voltage to the bridge was derived from a Farnell LFM1 signal generator. This was set to give a frequency of 400 kHz, sufficiently high enough to avoid capacitance effects due to surface levels, and an amplitude such that the peak-to-peak voltage across the diode was kept always less than 20mV. (The voltage was changed from sample to sample to give a suitable output signal strength.) When a bias was applied to the diode through the bridge circuitry, it was found that the transformer within the bridge caused a power surge within the signal generator, which eventually led to damage. The problem was eliminated by placing two silicon diodes in anti-parallel across the output terminals of the signal generator. There was no effect on the waveform of the signal going into the bridge at the r.m.s. voltages used.

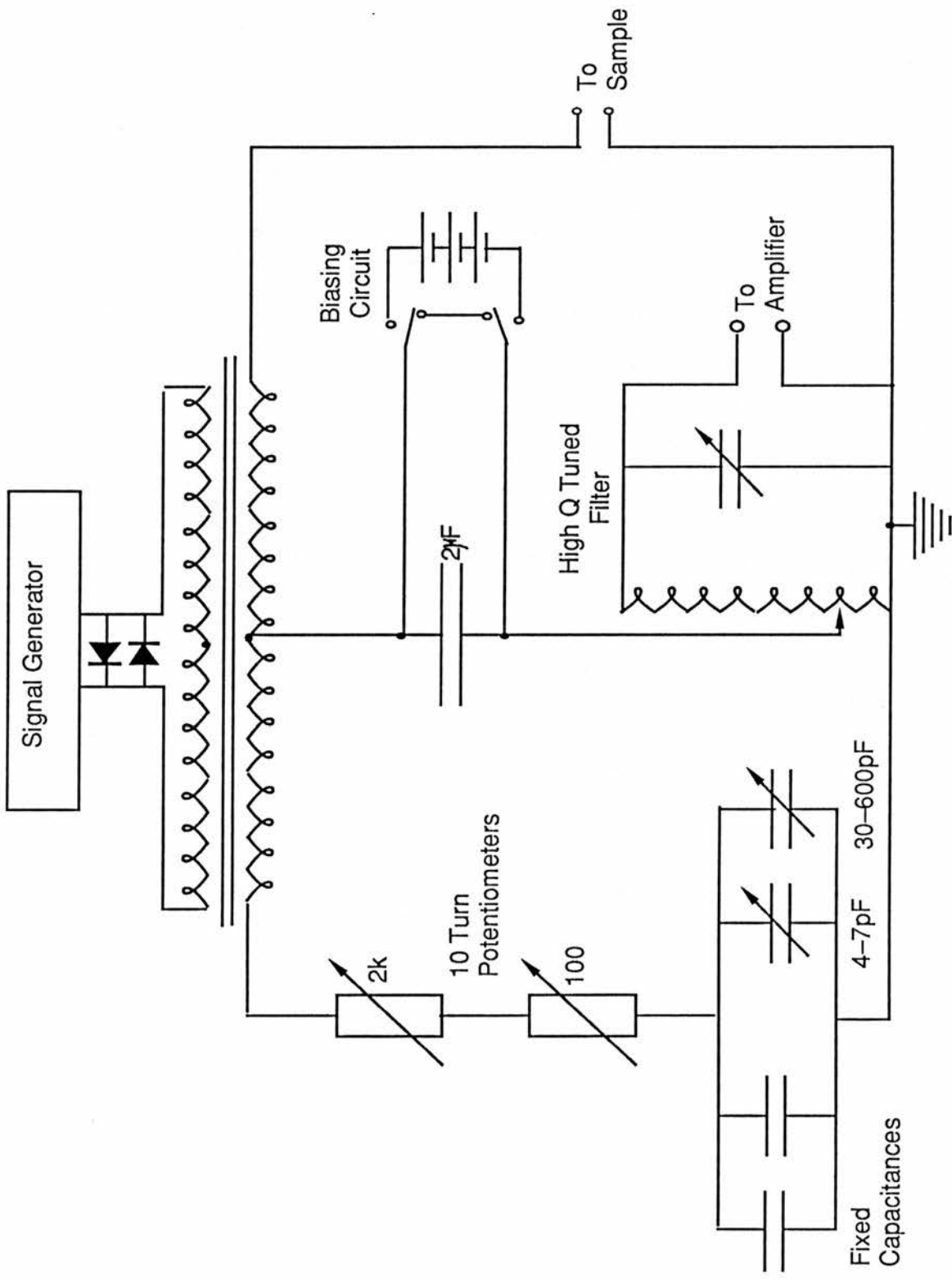


Figure 2.3 A diagram of the unity-ratio transformer arm bridge used in the photocapacitance experiments.

2.1.5 Measurement System

The OBV was amplified by a Brookdeal model 451 systems amplifier, which has gain continuously variable between 28 and 80 dB and operates at frequencies up to 1 MHz. Usually the gain was fixed at approximately 60 dB which provided a reasonable trade-off between signal and increased noise.

The mains power supply was found to be very 'dirty' containing both repetitive and irregular noise over many frequency-decades which adversely affected the signal quality. In order to eliminate as much of this noise as possible the following steps were taken. The mains power to the signal generator and bridge amplifier was passed through a mains voltage line conditioner. Additionally, mains filters were placed as close as possible to the signal generator and amplifier, minimising the length of cable between the filters and the devices; hopefully reducing the radio frequency pick-up by aerial effects. A second line conditioner was used outside the darkroom to provide the power for the signal detection equipment (voltmeters and chart recorder). Finally, a separate earth, well grounded in damp soil, was connected to all sensitive equipment.

The signal was taken from the output of the amplifier, via a tunable filter to a CRO within the darkroom. This oscilloscope was not for measurement but to enable the bridge to be easily balanced. Also, the signal was taken through the wall of the darkroom to a 400 kHz LCR filter and then into an average responding a.c. voltmeter, the Hewlett-Packard 400E. The HP-400E has full scale sensitivities down to 1 mV r.m.s.. It was found that the most convenient scale in the GaP:Ni experiments was 3 mV fsd, in some of the other experiments less sensitive scales were used.

There is a 1V full scale d.c. output, of 1000Ω output impedance, on the back of the instrument.

The d.c. signal is taken to a Farnell PR1 chart recorder ($10^6 \Omega$ input impedance) and also, via a 5:1 voltage divider ($10 \text{ k}\Omega$ resistance), into a 200 mV full scale 4.5 digit Analogic model AN2574 digital voltmeter ($10^{12} \Omega$ input impedance).

The bridge and measurement system's overall stability was tested by replacing the diode with a high quality capacitor and a resistor in series, of similar values to those of the diode, in a shielded box. The system was balanced and the OBV monitored. When the bridge was in good repair, that is all its parts were mechanically stable and electrically isolated from each other, then a good balance with only a very small drift from the residual noise OBV could be achieved for several hours. If the system was found to be stable with the boxed capacitor-resistor combination simulating the sample, but unstable with the sample itself, then the problem most often originated with poor contacts to the sample and could often be corrected by mechanical manipulation of the spring contact.

At one time it was attempted to move the HP-400E into the darkroom to minimise the length of coaxial cable needed to connect the voltmeter with the amplifier, but when this was done the sensitivity of the system was found to decrease appreciably. It is thought that this is due to better impedance matching between the devices when the 2-3m of coaxial cable is providing extra capacitive coupling between instruments.

2.1.6 Automation

The most essential component of an automated system is the system controller. A Commodore PET model 4016 computer, up-graded to 32KB and fitted with a Supersoft HR-40 high-resolution graphics board, was obtained for this purpose. Although already an old design of microcomputer at the start of the automation project (1983), the PET still possessed some redeeming features: two were an IEEE-488 standard interface and a 6522 versatile interface adaptor (VIA). A double floppy disk drive and a dot-matrix printer were connected to the IEEE-488 bus.

Interfaces for reading the Analogic AN2574 digital voltmeter or a Control Readout model 207 temperature reader have already been described in detail elsewhere^[31].

It will suffice here to state that there were four VIA lines remaining free after connecting these interfaces. One line was taken for switching the excitation light shutter. Another was used to switch a fixed bias voltage on or off (or could switch between two fixed non-zero biases) by means of a relay. Finally one line was used to cut the mains power to the wavelength drive stepper motor controller (the reason for which will be shown below).

A stepper motor was attached to the wavelength drive of the Minimate, the stepper motor drive unit was a Spex model GS/4. This unit had an IEEE-488 bus and could be driven under software control from the PET computer, as well as at rates preset by front panel control. A problem arose: when the GS/4 unit had been addressed once it continued to remain addressed when the computer was communicating with the disk drive

(data dumping), resulting in the motor often being accidentally switched on. A crude solution was found by using a spare VIA line to switch off the power to the GS/4 unit, via a solid-state relay, before the computer addressed the disk drive.

Software for the control of individual interfaces had been written previously^[31], but no overall program to control an experiment had been written. The author of the present work wrote programs to control the three different types of experiment (DLSS, wavelength scanned DLSS and transient photocapacitance) described below in Section 2.2.

To summarise, automation of the experiment produced many benefits; some of these are now described. Re-writing the data capture software, including using some machine code subroutines (the PET uses a 6502 microprocessor), resulted in an order of magnitude improvement in the voltage sampling time from 15s down to 1.2s, (approximately the same as the bridge-HP400E system's response time (see Appendix 2.II)). As well as sampling being quicker, the resolution of the AN 2574 (one part in 20000 of fsd) is much improved over that which can be achieved from a chart recording (perhaps 0.5 mm in 250 mm, or one part in 500 of fsd). Automation, also in removing the experimenter from the immediate environment of the diode and capacitance bridge, greatly reduces the influence of the observer on the results (stray capacitances remain more constant; darkroom can be more dark). Subsequent processing of the data was, obviously, much easier.

2.2 Procedures

This section describes the methods for obtaining single points on DLSS spectra, joining the points to form the spectra and wavelength scanned spectra. Finally there is information on the control of sample temperature.

2.2.1 DLSS Spectra

The standard method for taking DLSS spectra consists of taking one or more transients at each of many different photon energies in the range of interest, a process which can be very time consuming. However the method remains more reliable, yields more information and is less prone to misinterpretation than the wavelength scanned method described in Section 2.2.2.

The steps of the procedure for taking a single point on a DLSS spectrum were as follows.

- i) The bridge was balanced in the dark.
- ii) The diode was illuminated with the intense pump light source.
- iii) When the OBV remained within a small range of a constant value for a reasonable period of time, say one hour, then the diode was in thermal equilibrium with its environment, level occupancies were constant and the measurement system was stable. The bridge was then re-balanced to offset the large capacitance change due to the pump source. Re-balancing enabled greater resolution of the small capacitance

changes resulting from the less intense monochromatic source (typically changes as small as 0.01 pF can be detected).

iv) The shutter was opened allowing light from the excitation source to reach the sample.

v) The OBV was monitored for either a preset time based on previous runs, or until the signal reached a determined 'degree of flatness'. This measure of 'flatness' was usually just the difference between successive values of the OBV being less than a set figure (certainly much smaller than the typical noise voltage on the signal). When the system was automated a combination of these two methods was used. When the difference between successive voltmeter readings became less than about 20% of the noise on the signal only then did the computer check whether the set time had passed.

vi) The shutter was then closed and the decay of the OBV monitored. If the decay 'bottomed out' at a value close to that which pertained prior to opening the shutter then the system could be inferred to be stable. (With the proviso that the OBV during the run followed smooth curves.)

vii) The wavelength of the excitation source was changed for the next point on the spectrum.

viii) Steps iii) to vii) were repeated for different photon energies of the light from the excitation source.

These steps are illustrated on a flow diagram in figure 2.4. There is a difference between the procedure sketched here and that used by Mudhar^[31] in previous experiments on the GaP:Ni material. The bridge was not re-balanced in the dark for every point, but only once at the start

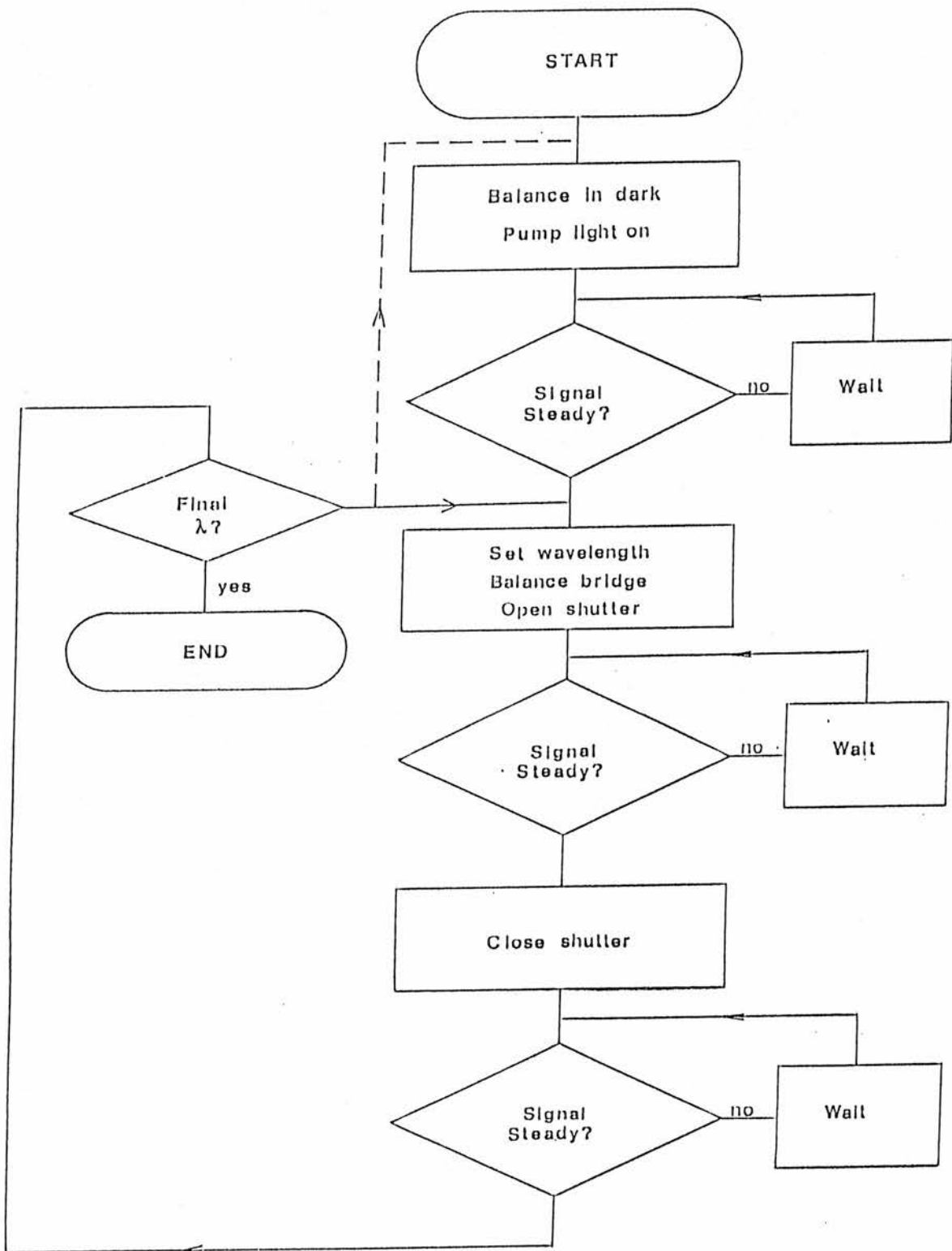


Figure 2.4 A flow chart illustrating the steps which were used to take a series of DLSS photocapacitance measurements at different wavelengths to form a part of a DLSS spectrum. The differences between the procedure used in the present work and that used by Mudhar [31] are noted. (---)

of a period of measurement. The new procedure is quicker than the previous one and is justified, for this case, by the fact that the system relaxes by thermal and optical transitions induced by the pump source to a state indistinguishable from that existing before the excitation source was shone on the diode.

Observing these steps lessens, or at least draws the experimenter's attention to, potential errors such as: variations with time in the intensity of the light from the monochromators; knocking the beam focus out of alignment whilst filling the cryostat with ice; changes in the temperature of the sample (Section 2.2.4); or instability in the measurement system (most commonly in the bridge during the GaP:Ni experiments).

2.2.2 Wavelength Scanned DLSS

This technique involves the scanning of the excitation source wavelength through a range without re-balancing the bridge or re-biasing the sample. Using this technique a DLSS spectrum can be taken in a matter of hours rather than the weeks that the 'standard' procedure of Section 2.2.1 might take. Two of the many disadvantages are that all time resolved data contained in the transients is lost, and that if the scan is not slow enough, compared with the longest rise or decay time that could be resolved in the 'standard' method, then what is measured is a complex convolution in time of many factors.

The following steps were taken to do a wavelength scanned spectrum.

- i) The bridge was re-balanced and system left for at least 30 minutes to check for stability.

ii) The total time for the run, the wavelength sweeping rate and the OBV sampling rates were calculated and the appropriate parameters input into the program controlling the run.

iii) The shutter was opened at the initial wavelength for the run, then it was necessary to wait until a reasonably steady signal was achieved.

iv) Control of the experiment was passed to a program which slowly changed the excitation source wavelength in very small steps at a rate determined in ii) and regularly sampled the OBV until a preset time expired (preset wavelength reached).

v) The program then closed the shutter and stored the data on a floppy disk.

Wavelength scanned photocapacitance experiments using a single source could also be performed. This technique can sometimes provide a quick method of discovering the rough energy positions of occupied levels within the energy gap. A slow sweep can be taken in a matter of a few hours, compared to days to weeks for a complete single source photocapacitance or DLSS cross-section measurement.

The disadvantages are the lack of information. In the DLSS case when one is not usually utilising rates of change or time constants the swept results are very close to those taken from in single shot-mode.

This technique was used to quickly characterise samples of ZnSe:Cr and ZnSe:V in the photon energy range 0.4 to 0.6eV (refer to Chapters Four and Five). If a sharp threshold to a transition exists (and the fastest time constant associated with the transitions is small compared to the total wavelength scanning time) the method will detect it. Sensitivity can be

increased by connecting the output of the a.c. voltmeter to a double differentiator circuit.

2.2.3 Transient Experiments

The procedures adopted for use in single transient experiments are briefly outlined here. First it is necessary to wait until a stable temperature was achieved (Section 2.2.4). The sample could then be forward biased to fill the centre under study with carriers (electrons). Again, after the cessation of biasing we waited until the OBV was steady. The bridge was re-balanced. The shutter over the excitation source was opened. It was to remain open until the OBV was again steady, or until the change was clearly into a non-exponential 'tail' region. After shutter closure and a few minutes observation of the start of the decay, the wavelength was changed and the above procedure repeated from the point of forward biasing.

2.2.4 Temperature Control

Comments on the control of sample temperature are presented for the various experimental situations encountered.

At ice temperature the background signal, with only the pump source incident on the sample, would only remain in a useful range, after an ice refill, for a maximum period of about 7–8 hours. Within this time period the background was not constant but fluctuated in a manner which can be typified by figure 2.5. The main features to be noted are as follows.

i) Initial rapid fall in signal in the first 15–20 minutes.

ii) 'Overshoot'. A slower rise, then a fall, in the next 30–60 minutes.

iii) A period of 4–8 hours when the signal oscillates gently up and down by an amount which corresponds typically to 10% of the residual noise signal at balance. This is the useful period for carrying out the experiment with reasonable accuracy.

iv) A period of increased instability lasting up to an hour.

v) A quite sharp and steady increase in background signal due to a steady rise in temperature after all the ice in the cryostat has melted.

The behaviour of the background signal at room temperature must be contrasted with that mentioned above. With the cryostat empty the signal showed a large amount of instability with a diurnal cycle. The temperature was checked at regular intervals for 3 days and a daily variation of 2°C was found in the sample temperature. This problem was eliminated by filling the cryostat with water which had been allowed to stand at room temperature for several hours. The temperature then remained stable to within 10% of residual noise signal for up to 48 hours, after which the bridge needed to be re-balanced due to a combination of bridge and amplifier drift.

The helium flow rate, when using the CF1204 cryostat (ZnSe host experiments), was set to the minimum value necessary to achieve the required temperature. Temperature control was provided by a Thor 3010II temperature controller. Using proportional control temperature fluctuations could be kept to less than 0.1K within two to three hours after first reaching the set-point temperature. The fluctuating heater voltage is

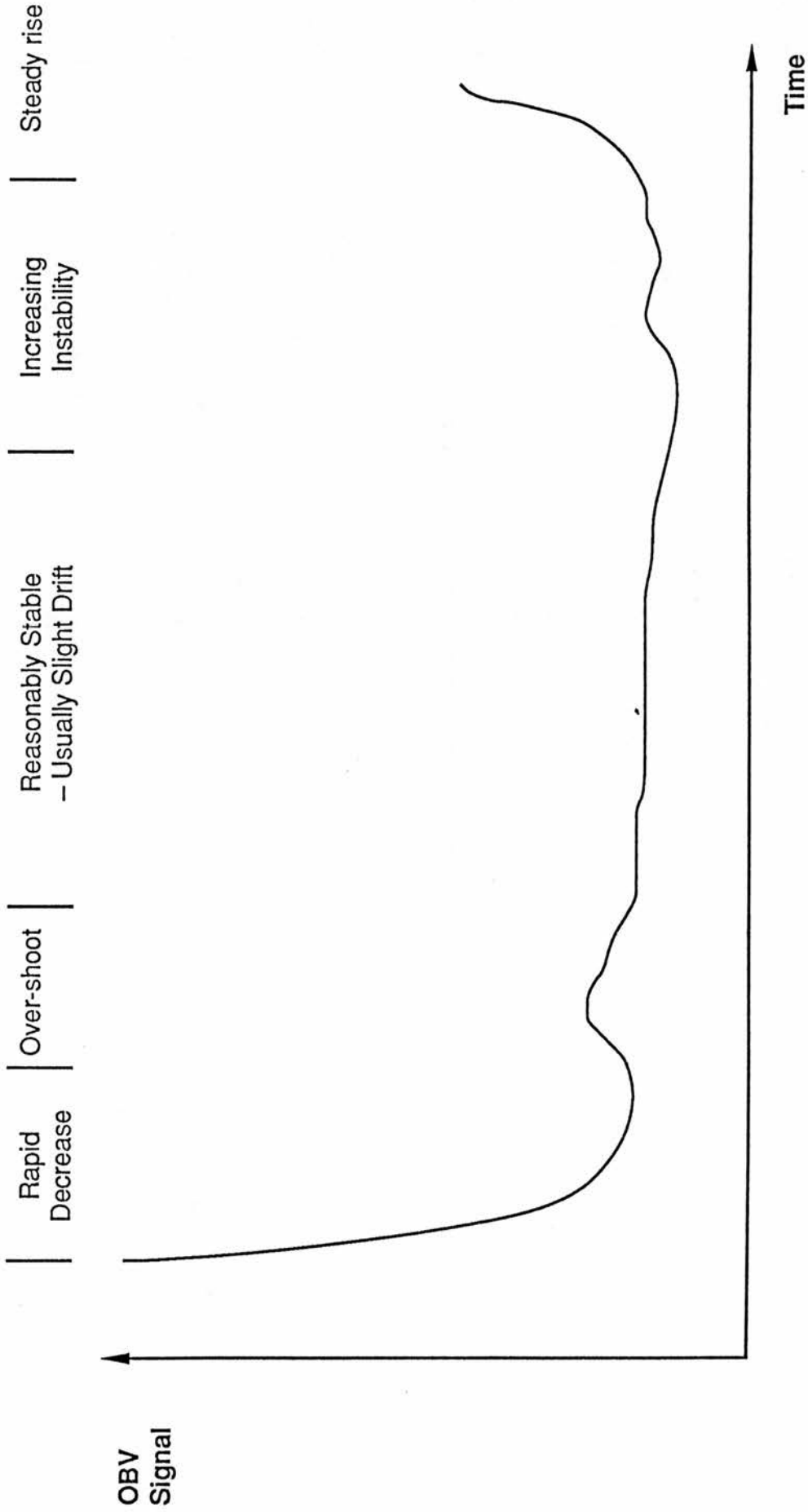


Figure 2.5 A figure illustrating the typical time variation of the temperature adjacent to the GaP:Ni diode after refilling the cryostat with ice. The time scale is approximately five to nine hours. Several distinct regions could be consistently identified.

one of the sources of noise in the signal. If the voltage applied to the heater is kept as constant and as small as possible, the electrical interference is minimised.

2.2.5 Electrical Experiments

The sample was in the same bath-type nitrogen cryostat which was used for the phot capacitance experiments. The optical window was covered so that photogenerated currents would not affect the results. The current through the diode and the voltage across the diode were measured with very high impedance ($100T\Omega$) Keithley 602 electrometers. The outputs of the electrometers were connected to digital multi-meters to take readings easily and with greater accuracy. The voltage source was a Farnell L30A stabilised d. c. supply. Fine control of the applied voltage was provided by a 10-turn potentiometer. The sample temperature was measured with a copper-constantan thermocouple connected to a Control and Readout Ltd. model 207 digital thermometer. With this arrangement it was found that currents of about 1nA could be measured to 10% accuracy.

2.3 Techniques for Analysing Results

Once results, a collection of numbers representing voltages at particular times, have been collected they must be processed in order to extract useful information. In the case of a DLSS experiment we require to know the OBV change which is proportional to a capacitance change. For the transient experiments we require to know, in addition to the OBV change, the time constant of the transient modelled to an exponential. How these quantities were calculated is outlined in the sub-sections below.

2.3.1 DLSS Capacitance Changes

The initial background (R_1) was read within a minute before the opening of the shutter. When the 'signal flat' condition had been reached, at a time interval t_1 after reading R_1 , the second reading was taken (R_2). After the shutter was closed the signal settled to a final value, read as R_3 , at a time t_2 . The drift rate in the system was estimated from R_1 and R_3 as $(R_3 - R_1)/t_2$. So the drift corrected DLSS signal value, S_{DLSS} , was calculated as:

$$S_{DLSS} = R_2 - \left[R_1 + (R_3 - R_1) \frac{t_1}{t_2} \right] \quad 2.1.$$

In fully automated experiments, once the drift rate had been worked out the 'excitation light on' final OBV was calculated by looking for a stable value relative to a drift-corrected base-line.

2.3.2 Analysis Of Capacitance Transients

The principal quantity of interest in a photacapacitance transient experiment is the rise-time of the transient. The calculational method is that due to Mangelsdorf^[36], which does not require knowledge of the final value of the transient. The manual procedure is to draw lines on the chart recording, spaced at distances equivalent to, or smaller than, an estimation of the rise-time. The values are read and plotted in the form $C(t+T)$ vs. $C(t)$. Here: T is the estimated rise-time. The gradient of a perfect exponential would be given by $\exp(-T/\tau)$, where τ is the actual rise-time or time constant.

The transients were usually not exponential and often points at the start and the end of a run had to be discounted. There are several reasons for removing the first part of the trace. One is that the measuring system has a not insignificant response time. A second is thermal refilling of states within a characteristic length of the depletion layer boundary^[37]. Thermal refilling is at a maximum in the zero-bias case. Finally, there can be some small amplitude, but very fast capacitance changes if there is not a simple single level in the gap. One example of this could be the bi-exponential behaviour predicted in photoionisation transitions proceeding via an excited state close to the conduction band^[29,38,39].

Many transients also possessed 'tails' with very long time constants, which often were not reproducible. These could be due to other levels with much smaller cross sections or could be simply due to some form of drift in the sample or apparatus, for example drift in temperature. The remaining points gave the time constant(s) calculated by the Mangelsdorf method (above). A program called 'ANARISE' was written to remove

points from the beginning and the end of the transient as requested, to draw the Mangelsdorf plots with any given time constant estimate (T) and to calculate the resultant time constant. The program also possessed the capability of displaying both the calculated theoretical transient and the raw data for comparative purposes.

The time constant is multiplied by the photon flux at a particular wavelength and the reciprocal taken to find the cross section. The photon flux is calculated as the product of the light intensity (Appendix 2.I) at a particular wavelength and the wavelength itself. A spectrum should be taken 'all at once' in order that the photon intensity does not change. For similar reasons great care was taken when changing filters in the middle of a spectrum. If the photon flux at one wavelength does change for any reason then we must make sure that the measurements are normalised in an appropriate manner by repeating the last photon energy measurement and normalising all subsequent calculated cross sections by the ratio of the two results taken at the single wavelength. The normalisation can be effected by the procedure of multiplying the first set of results, for example, by the ratio $\tau(h\nu)_a/\tau(h\nu)_b$, where the subscript refers to the set of results. This process is illustrated in figure 2.6.

This normalisation process breaks down if the results for a particular wavelength have a large error associated with them.

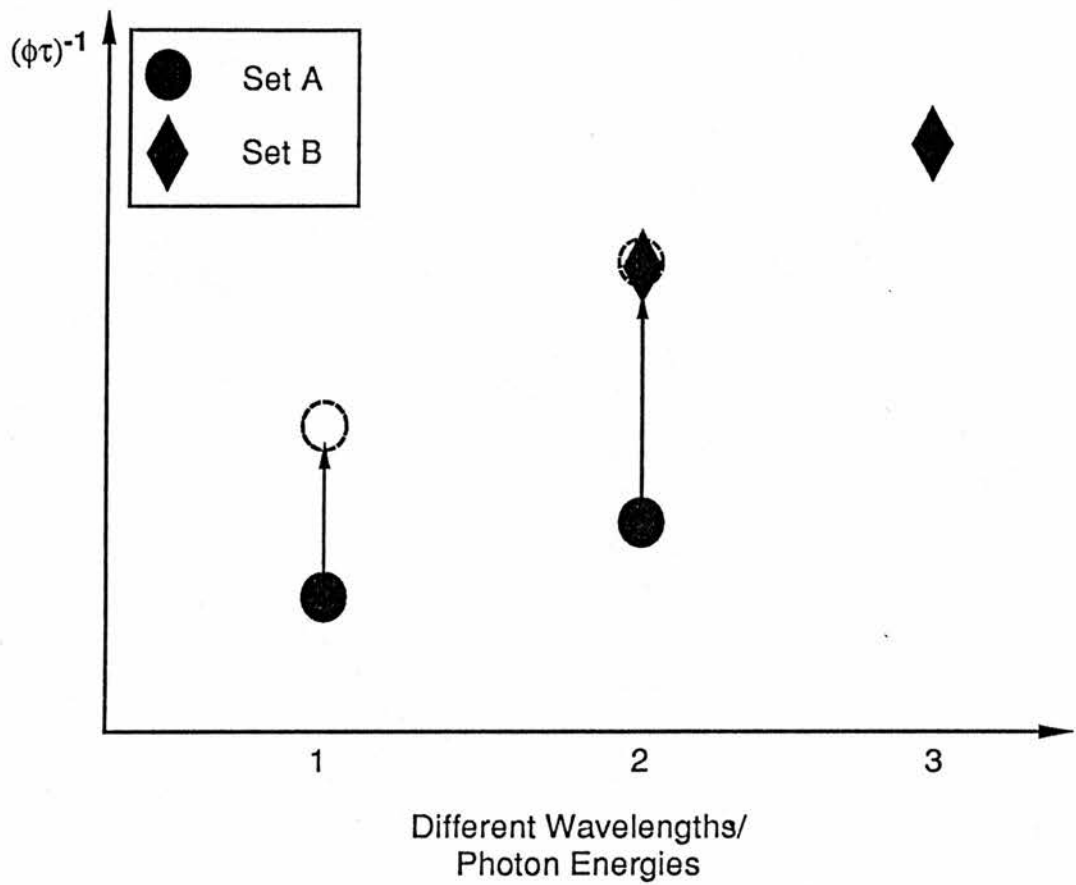


Figure 2.6 An illustration of the 'linking-up' procedure for sets of DLSS measurements taken over a longer period than the OBV signal would remain steady without adjusting the bridge.

Appendix-2.I: Measuring The Photon Flux

The data obtained from measuring the time constants, or sometimes the OBV changes, has to be normalised for different photon fluxes incident on the sample when different photon energies are used. A calibration curve of the output intensity of the light from the monochromator was taken for each of the optical order filters used with the excitation source.

The light from the monochromator exit slit was focused by a lens onto the aperture of a Hilger-Schwartz FT 17-A thermopile, which has a linear voltage output response from 110nm to 10 μ m. The voltage from the thermopile was measured on a Keithley 155 micro-voltmeter. No focussing optics were used with the germanium filter when operating in the 2.0–3.2 μ m wavelength range because of high absorption losses in the glass lenses.

The information was read into the computer and stored on disk. Once the information was stored on the disk it was easy to normalise spectra with respect to photon flux.

Appendix 2.II:

Measurement of The Bridge Response Time

The apparatus used to measure the system response time is illustrated in figure 2.II.1. Basically it consisted of the bridge, amplifier, filter, HP-400E with the output connected to a Nicolet Explorer II digital storage oscilloscope. The diode was replaced by a series capacitor (2200pF) and resistor (50 Ω) with a second capacitor (220pF) in parallel with the first that could be switched in and out of the circuit. (CR time constant $O(10^{-7}$ s))

The measured change in OBV on switching the capacitor in and out was exponential, with a measured response time of ≈ 1.2 seconds. It is thought that most of this is due to the 'averaging' of the HP-400E voltmeter.

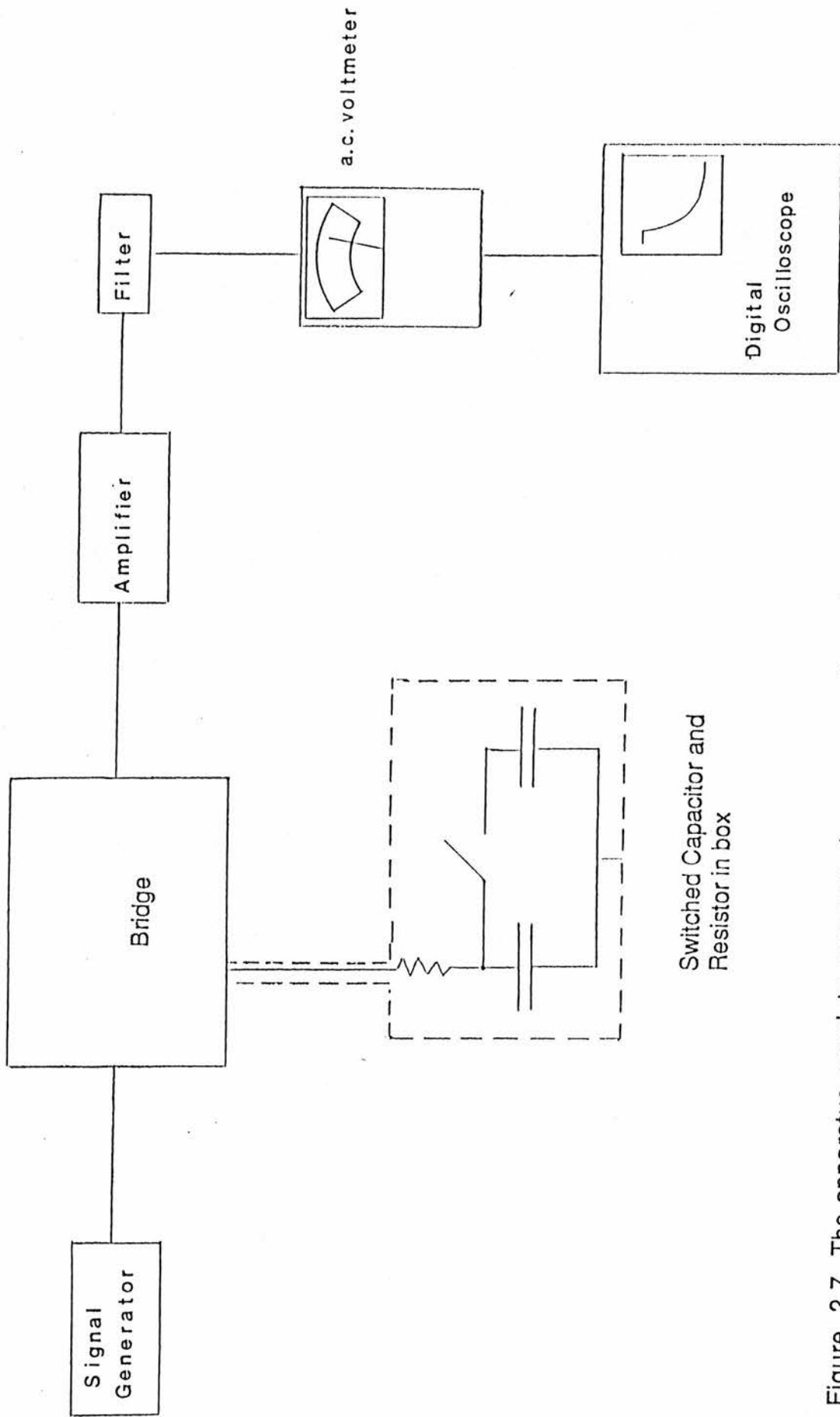


Figure 2.7 The apparatus used to measure the response time of the capacitance bridge. A bounce-free switch was used to switch the smaller 220pF capacitor in and out of the circuit.

Chapter Three:

Nickel in Gallium Phosphide

3.1 Introduction

Nickel in gallium phosphide is a transition metal impurity system in which three stable charge states with 3d electron configurations d^7 , d^8 , d^9 have been found. The GaP:Ni system is now quite well studied, but there remain some details of the system to be resolved.

It is desirable to understand how the presence of nickel can affect the operation of devices. An early part of this process is to gain knowledge about the energy levels nickel introduces into the gap and the kinetics of the level populations. Nickel is found to be present in all material grown using stainless steel apparatus^[40]. Gallium phosphide is a possible material for making optoelectronic devices operating at visible wavelengths (the bandgap is approximately 2.25eV at 300K which is equivalent to a wavelength of 550nm).

It has been shown that one of the nickel charge states exhibits *photothermal* behaviour in photocapacitance^[30–32] and photoconductivity^[41]. The GaP:Ni system is useful to test theories of the kinetics of such processes.

In n-type material the d^8 and d^9 configurations are in the highest concentrations, whereas in p-type material d^7 predominates.

The observed charge state can be changed by illumination^[42]. This fact is exploited in the experiments described in this chapter. The positions of the levels in the gap are known to within a tenth of an electron-Volt. An intense beam in the red end of the visible spectrum will fill the d^8 - d^9 level

with electrons creating a d^9 majority population. A beam of lower energy radiation, below the $d^8 \rightarrow d^9$ photoionisation threshold, but still above the threshold of the complementary transition will produce a d^8 majority. The experiments described below attempted to produce these population changes.

The paramagnetic (odd-spin) states have been studied using the EPR (d^7 [43] and d^9 [44]) technique. ENDOR experiments[27] have shown nickel atoms in the d^7 configuration to be on substitutional sites in the gallium sub-lattice, from analysis of the quadrupole interaction with the nearest-neighbour shell of gallium atoms.

Several bands have been seen in absorption spectra. One of the bands lies at an energy of about 0.67eV, originally it had been attributed to the ${}^3T_1(F) - {}^3T_2(F)$ transition of the d^8 [45] configuration, but Zeeman experiments by Kaufmann *et al*[44] unambiguously demonstrated that this band was due to the internal transition of the crystal field split nickel d^9 configuration.

The bands which occur at roughly 1.23eV and 1.41eV are well known, first being seen by Baranowski *et al*[45]. The 1.23eV transition is agreed, by most workers, to be the ${}^3T_1(F) - {}^3T_1(P)$ internal d^8 transition. The 1.41eV band is the subject of more controversy. It was assigned by Baranowski *et al* to be the d^8 internal transition from the ground state to the ${}^3A_2(F)$ level and recently by Jeźnewski *et al*[46] to be that which terminated on the 1T_2 level.

Jeźnewski *et al*[46] have seen an absorption band near 0.8eV at a very low temperature (9K) which they interpret as the sought after, but previously unreported, ${}^3T_1(F) - {}^3T_2(F)$ internal d^8 transition in a compensated GaP:Ni:S sample.

The $d^7 \rightarrow d^8 + h_{\nu b}$ transition has been seen by Abagyan *et al*^[45] in Hall effect experiments which show a level lying at an energy of $0.50 \pm 0.03 \text{ eV}$ above the top of the valence band. There are reports that the optical and thermal energies for this transition are very similar^[48]. Szawelska^[35] has reported the complementary photoionisation transition $d^8 \rightarrow d^7 + e_{cb}$ in photocapacitance with a threshold energy in the range $1.6\text{--}1.7 \text{ eV}$. Saidov *et al*^[49] have seen a band at 1.3 eV which they claim to be the $d^8 \rightarrow d^9 + h_{\nu b}$ transition. This is the complementary transition to that seen by Yang *et al*^[30] at low temperatures (where there are no complications because of photothermal peaks) and also seen in the 2.00 eV pump light DLSS experiments to be discussed in this chapter.

Nickel can form associates with nearest neighbour shallow donors such as sulphur and germanium^[50], which can complicate the structural details of absorption and photoluminescence experiments.

Clerjaud^[51] has given a review of recent work on 3d series transition metals in III–V semiconductors (GaP, GaAs and InP) including an analysis of GaP:Ni.

3.2 Sample and Experiments Performed

The sample used in these experiments was n-type (identity of the donor is not known), commercially grown gallium phosphide with nickel impurities introduced by high temperature diffusion (The process has been described by Szawelska^[35]). The complete history of this sample is not recorded which leaves this description more vague than it should be. The sample was polished, etched, an alloyed indium-tin Ohmic contact was made on one side of the diode and a 1mm diameter, semi-transparent gold Schottky contact was evaporated onto the opposite face.

The experimental apparatus, the phot capacitance methods used and the techniques for the analysis of the results obtained are described in detail in Chapter Two. The electrical measurements are described first, then the constant 2.00eV photon energy beam phot capacitance experiments and finally those performed with a constant 1.00eV source. The last mentioned set of experiments have not, to our knowledge, been performed before.

Current-voltage (I-V) characteristics were measured to verify that we had, in fact, a diode and to check the statement in Szawelska *et al*^[32] (this paper will be referred to as SMA for the rest of this chapter) that the shallow donors froze out below 140K, making low temperature phot capacitance measurements impossible. I-V characteristics were taken at room temperature and at liquid nitrogen temperature. The temperature variation of the series capacitance at zero bias was investigated.

At room temperature (296K) readings were taken at reasonably small (0.05-0.10V) voltage intervals. The maximum current allowed to pass

through the sample was 10mA in order to avoid possible damage due to self-heating.

The I-V characteristic at liquid nitrogen temperature (-190°C [83K] – according to the CRL model 207) was recorded half an hour after liquid nitrogen had been poured into the cryostat, so that the system had had time to reach thermal equilibrium.

For the experiments carried out using a constant 2.00eV photon energy pump light a spectrum using the 'standard' DLSS method of Chapter Two was carried out at a temperature of 0°C only. The 'wavelength swept' double light source method, again described in Chapter Two, was used to obtain spectra at 0°C and at 30°C .

A series of DLSS capacitance transients were taken at 0°C under illumination with a constant pump beam of photon energy 2.00eV (bandwidth 12.5nm equivalent to 0.04eV). The excitation source used had a bandwidth of 20nm (0.01eV at a photon energy of 0.75eV). Transients were recorded at 10nm intervals over most of the wavelength range 1900 to 1350nm.

Wavelength swept spectra were taken at 0°C and at 30°C . The scan speed was kept as low as possible, considering the time over which the background OBV signal could be kept steady. Later, it was thought prudent to check that the shape of the spectrum was independent of scan speed. Therefore the scan speed was increased and a new spectrum recorded.

Now to discuss the experiments performed with a 1.00eV (bandwidth 0.02eV) photon energy pump light source. Both transient and wavelength scanned spectra were recorded at 0°C and at 30°C .

Two sets of transient measurements were taken at both 0°C and 30°C. The wavelength separation between individual transients was 40nm. This was so that the experiments could be completed in a shorter time than the 2.00eV pump source experiment. Ideally the spacing should be closer: as the bandwidth of the excitation light used in this experiment was 10nm more detail might have become apparent.

The resulting files were processed by the program 'ANALYSE' to determine the total change in OBV and when necessary, scaled relative to each other by the 'link-up' procedure described in section 2.2.6.

Swept wavelength results were taken starting at the pump light wavelength of 1240nm (1.0eV) and usually continuing until the end of the filter pass band (760nm or 1.63eV). Spectra were taken sweeping the wavelength in the opposite direction to check differences between the spectra.

3.3 Results

Firstly we will look briefly at the electrical measurements, followed by the results from the 2.00eV photon energy pump beam experiments before looking at those undertaken with a constant 1.00eV source.

The room temperature current–voltage characteristic is plotted on a linear scale in figure 3.1a and on a log–linear scale in figure 3.1b. The forward currents are obviously much larger than those in the reverse direction at the same voltage. Thus the sample is acting as a diode. There appears to be a threshold at $0.65\pm 0.03\text{V}$ forward bias, after which the current passed increases much more rapidly than below this value. The characteristic at 83K is shown similarly in figure 3.2, where the much higher resistance can be noted. As can be seen in figure 3.3 the dark capacitance decreased rapidly with temperature below 140K. The reason why measurements could not be performed below about 140K is that the sample resistance became too large to be balanced by the bridge resistors. Decreased capacitance also makes photocapacitance measurements increasingly difficult as the capacitance change observed in photocapacitance techniques is proportional to the total junction capacitance.

The results taken with the standard method under the constant 2.0eV light are shown in figure 3.4, whilst examples of wavelength swept spectra can be seen in figure 3.5. Some of the features observed in these two forms of the spectra will now be described.

i) The general shape of the band around 0.7–0.8eV is a skewed Gaussian in wavelength swept spectra, but appears less regular, less easily classified, in transient spectra. In both measurements there was a

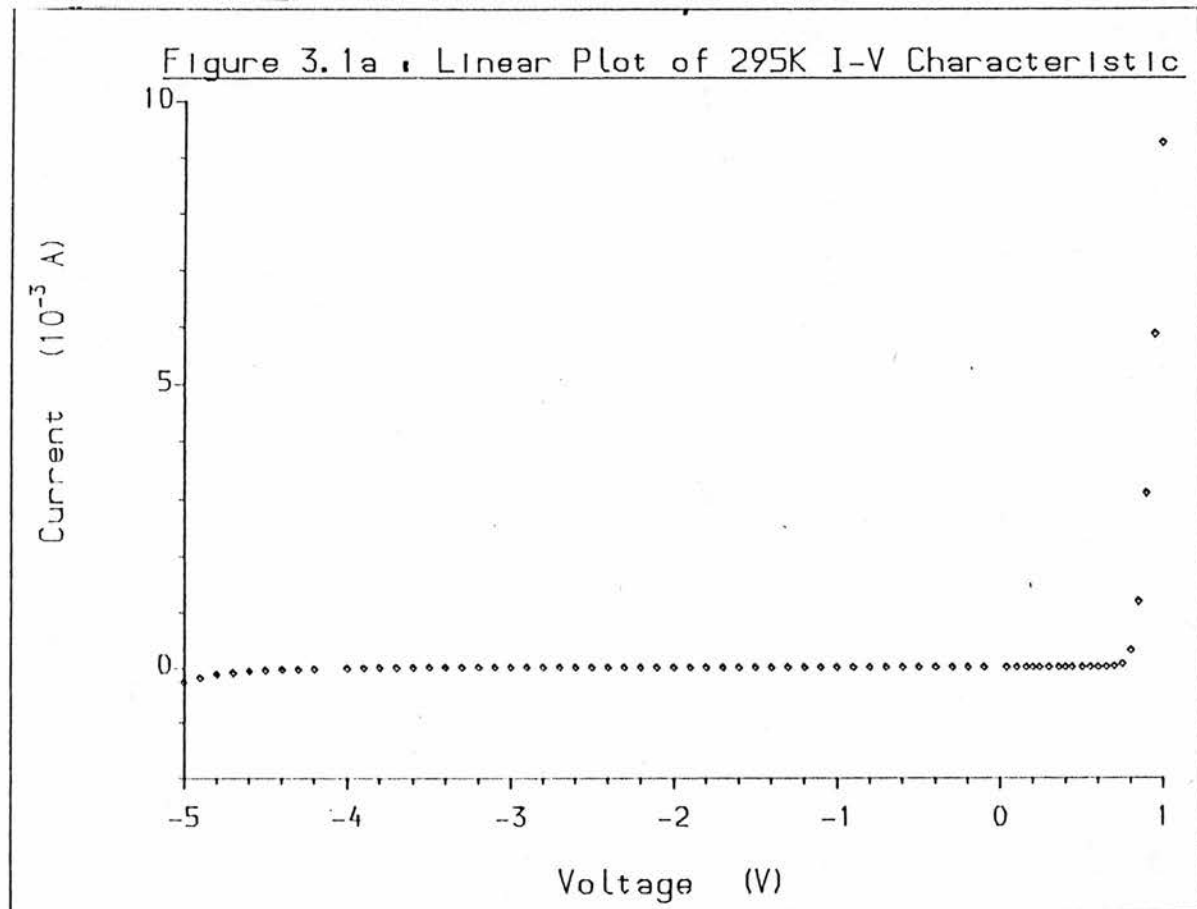


Figure 3.1a The room temperature current–voltage characteristic of the GaP:Ni diode. The rectifying behaviour is clearly apparent.

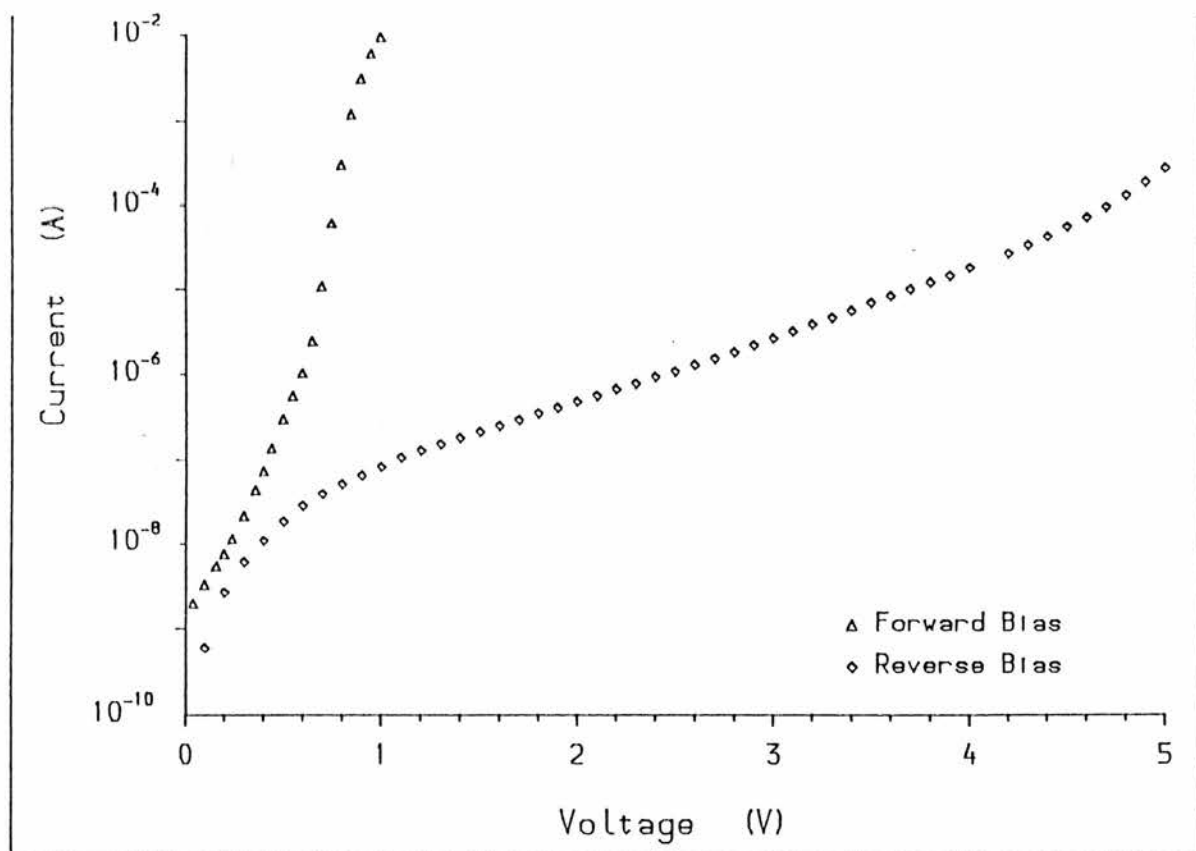


Figure 3.1b A log–linear plot of the room temperature current–voltage characteristic shown in figure 3.1a.

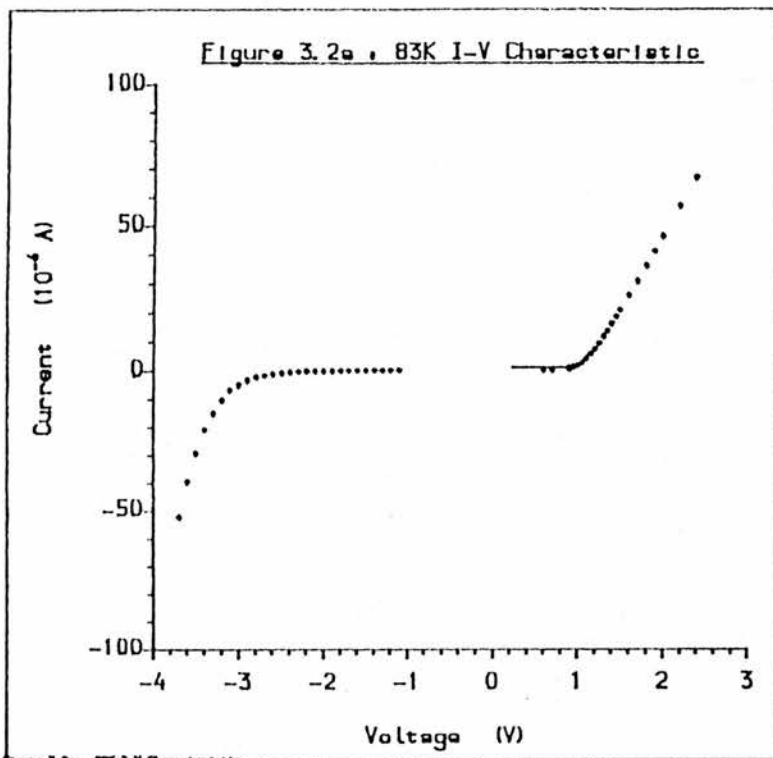


Figure 3.2a - 83K I-V Characteristic

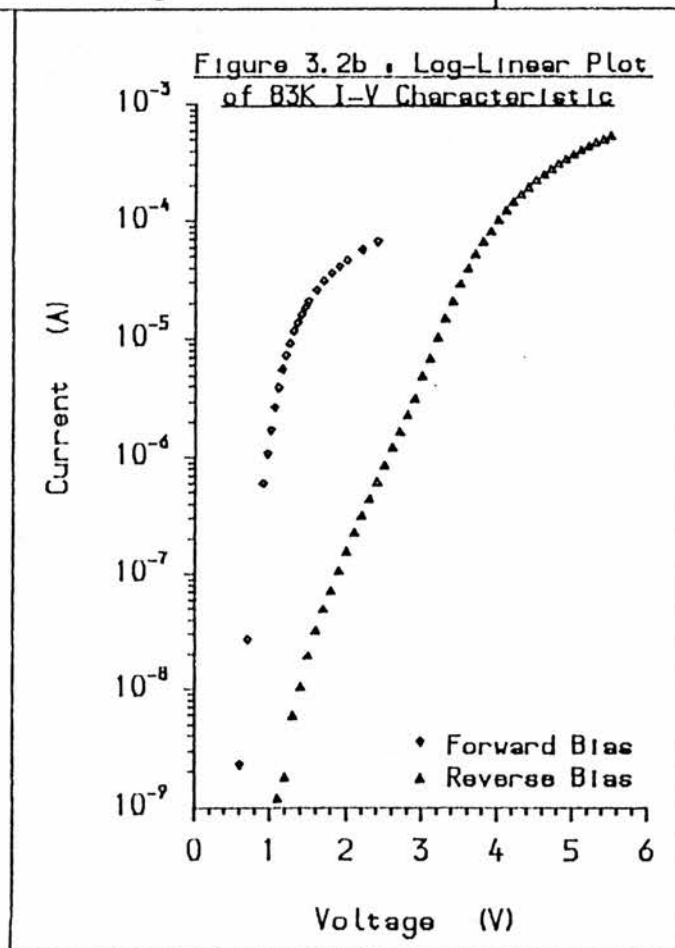


Figure 3.2 Linear (3.2a) and log-linear (3.2b) plots of the current-voltage characteristic of the GaP:Ni Schottky diode at a temperature of 83K.

Figure 3.3 : Dark Capacitance
against Temperature

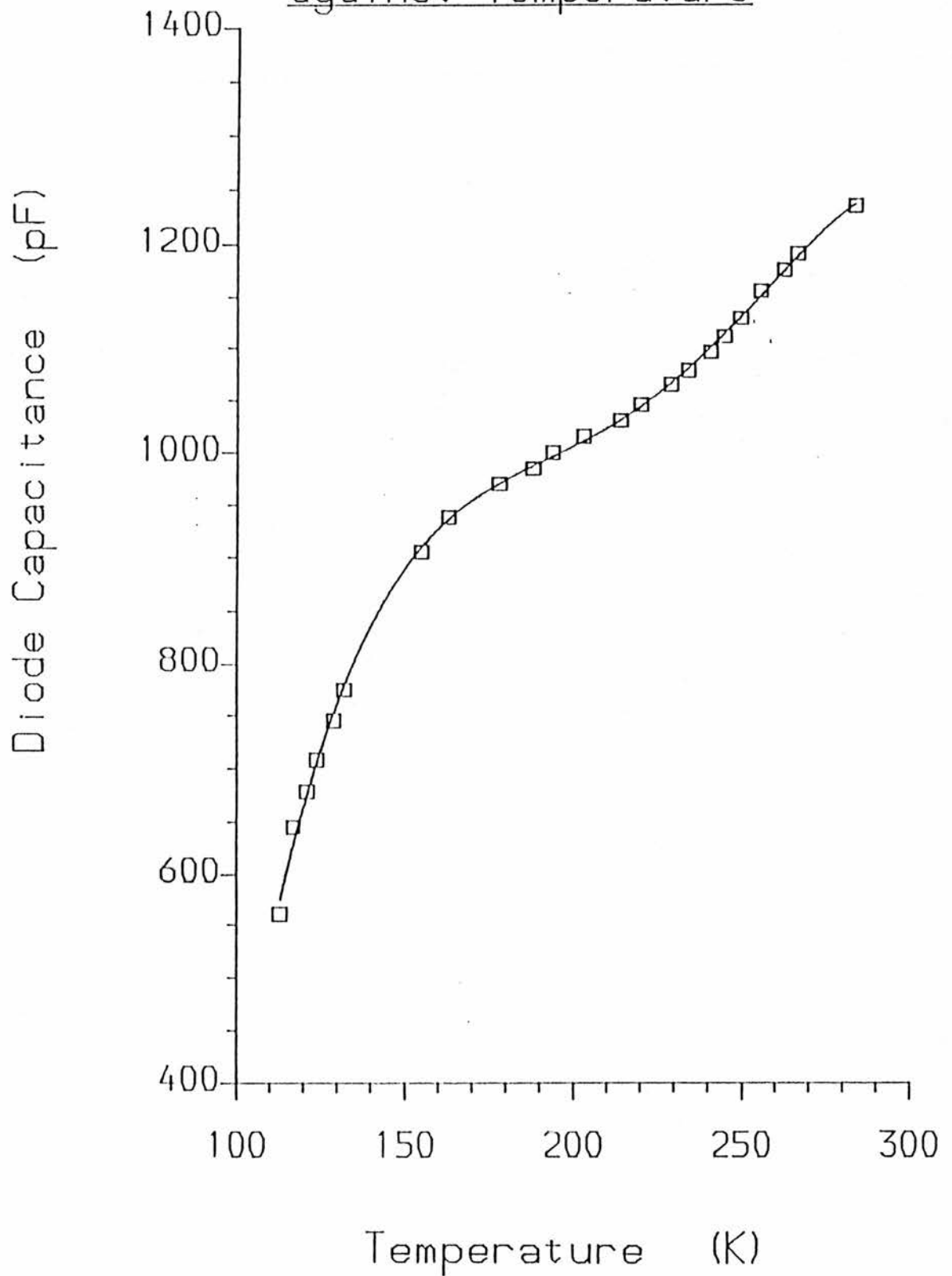


Figure 3.3 A graph of the dark capacitance of the GaP:Ni Schottky diode against temperature. The line is an empirically-fitted polynomial.

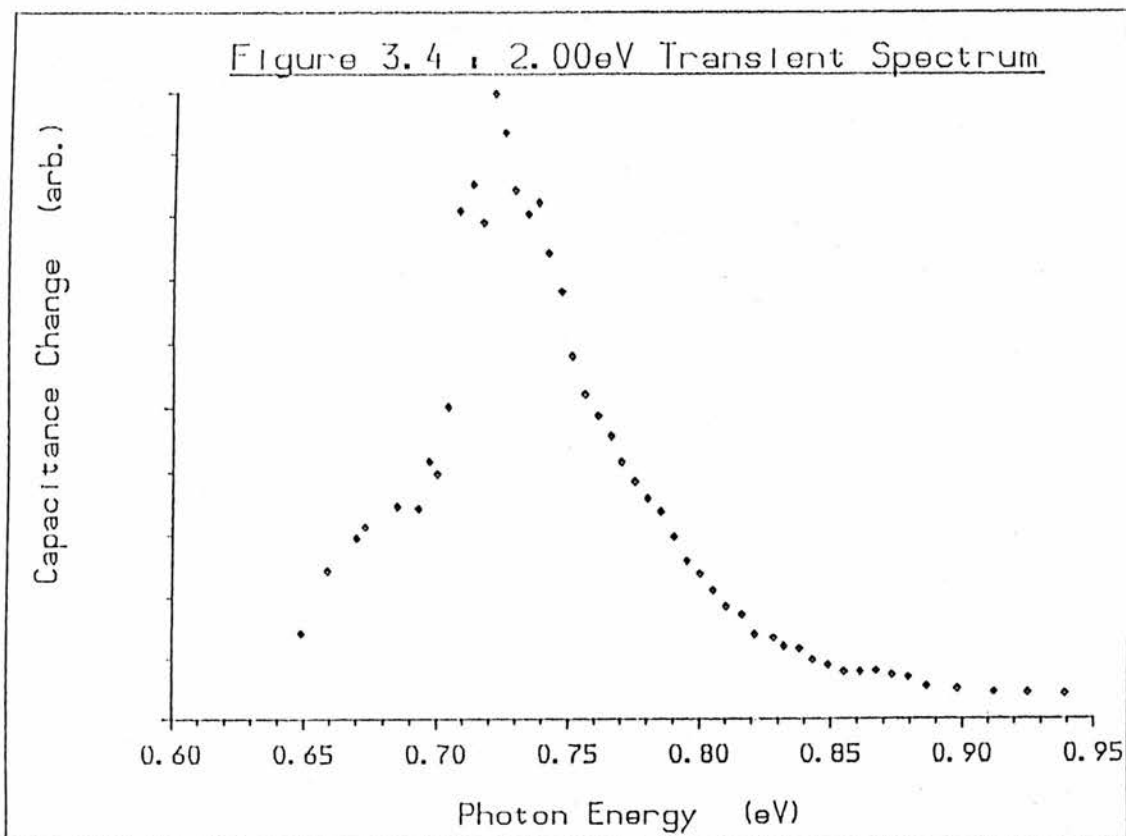


Figure 3.4 A plot of the spectral dependence of the capacitance change due to a perturbation of a steady state condition established by an intense red (2.00eV) light source. Each point is calculated from (usually) more than one, transient. The spectrum represents the photothermal detection of the nickel d^9 ${}^2T_2 \rightarrow {}^2E$ transition.

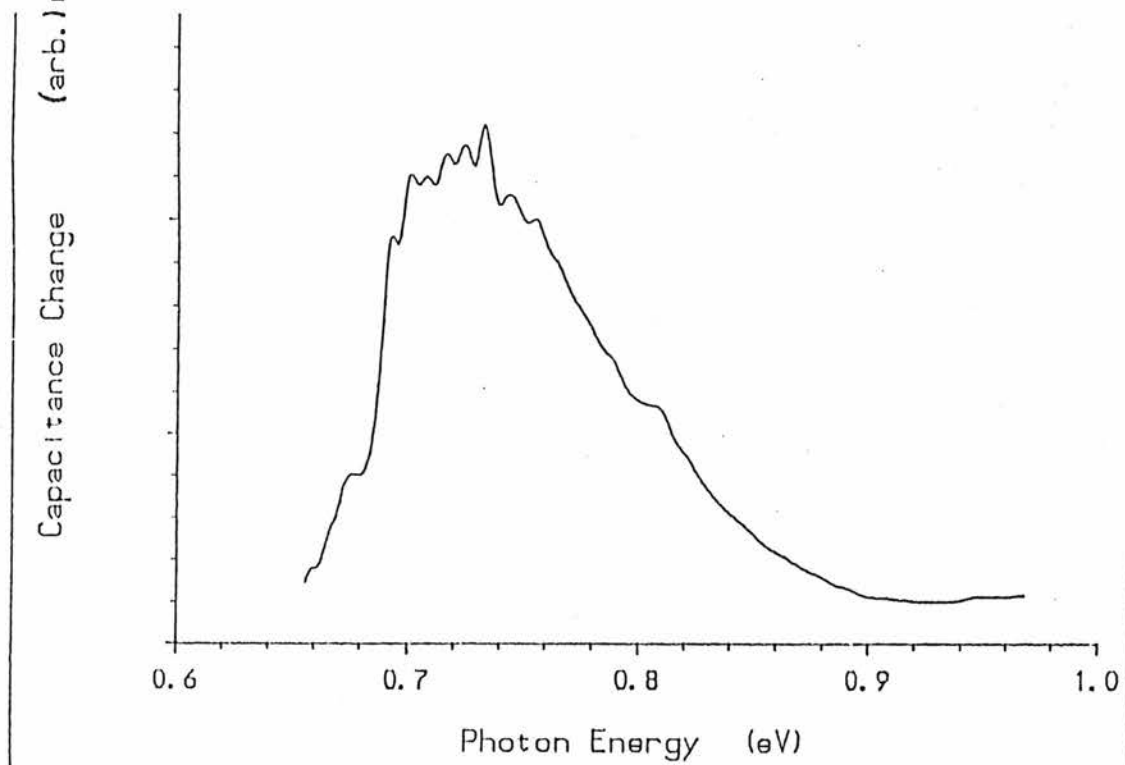


Figure 3.5 A plot of the spectral dependence of the capacitance change due to the perturbation of a steady state condition established by an intense red (2.00eV) light source. In this case the wavelength of the perturbing source was slowly swept from longer to shorter wavelengths. This spectrum should also represent the photothermal detection of the nickel d^9 ${}^2T_2 \rightarrow {}^2E$ transition.

steep rise in the cross-section at a photon energy of $0.69\pm 0.01\text{eV}$, as had been noted by previous workers^[32].

The width of the peak was $0.09\pm 0.01\text{eV}$ in transient measurements and $0.12\pm 0.02\text{eV}$ in wavelength swept experiments.

ii) The band maximum occurred at an energy of 0.725eV in transient spectra and at about $0.745\pm 0.010\text{eV}$ in wavelength swept results.

iii) Structure was observed close to the maximum of the peak but was not well resolved at these relatively high temperatures. In particular a 'bump' (or small peak) in the wavelength swept spectra was found to occur in wavelength swept data at a photon energy of 0.82eV . It is not certain whether this feature is a property of the diode or of the measurement system (bulb output). The uncertainty arises from the fact that there is a similar bump in the intensity spectrum of the tungsten-halogen lamps. A normalisation for photon flux, carried out as a standard procedure for obtaining single source transient photocapacitance spectra, should have removed any such bump due to the lamp output in the transient spectra. No such improvement was observed.

iv) There is a rising edge to the spectrum beginning at about 0.9eV .

v) A dip in the spectrum first observed by Mudhar^[31] with a minimum at an energy of 1.24eV was found in wavelength swept spectra which were taken with the intention of seeking this feature (figure 3.6). There is a local maximum in the spectrum at about $1.15\pm 0.01\text{eV}$ and the bottom of the dip was found to be at $1.24\pm 0.01\text{eV}$. The size of this dip, relative to the peak maximum at 0.75eV , was larger than had been observed by SMA.

Figure 3.6a : Dip In 2.00eV Swept Spectrum

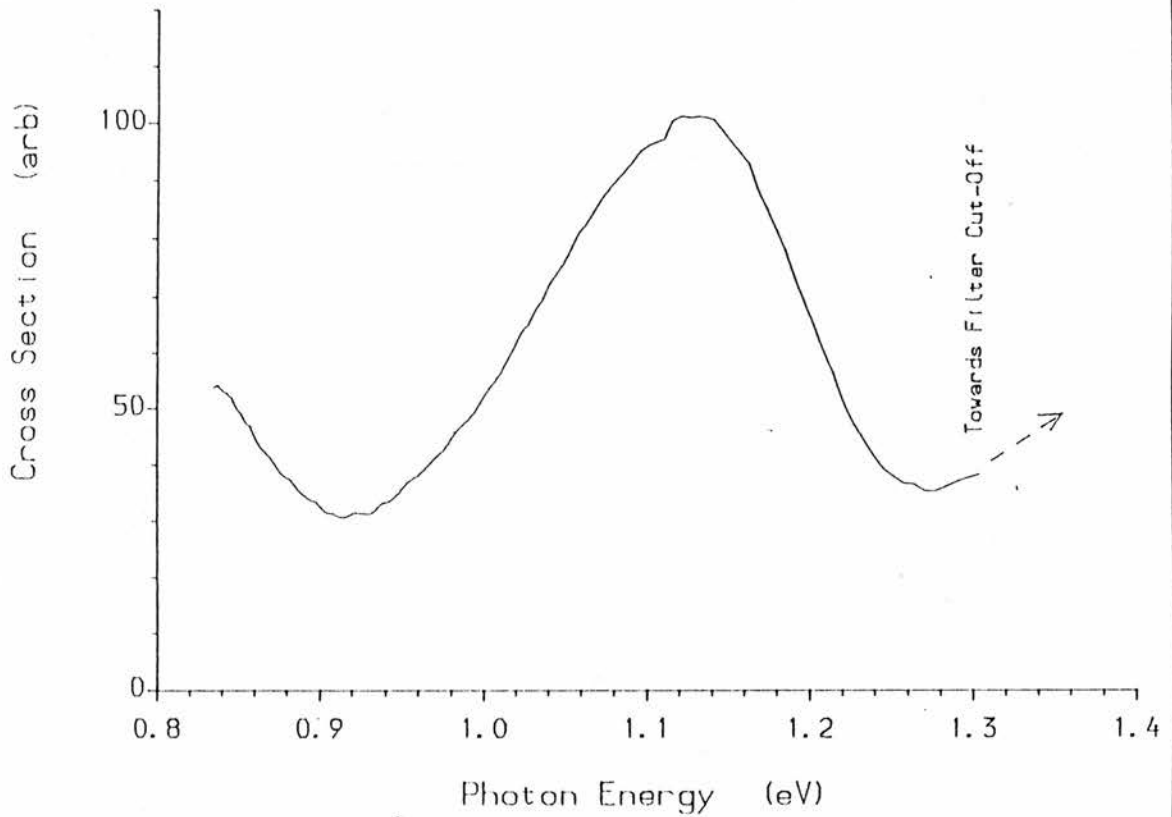


Figure 3.6a This graph shows the capacitance perturbation spectrum for the GaP:Ni diode illuminated by a constant intense red (2.00eV) light source in the perturbing photon energy region 0.8–1.3eV. The features to note are the rise in ΔC between approximately 0.9eV and 1.1eV, and the marked dip at higher energies.

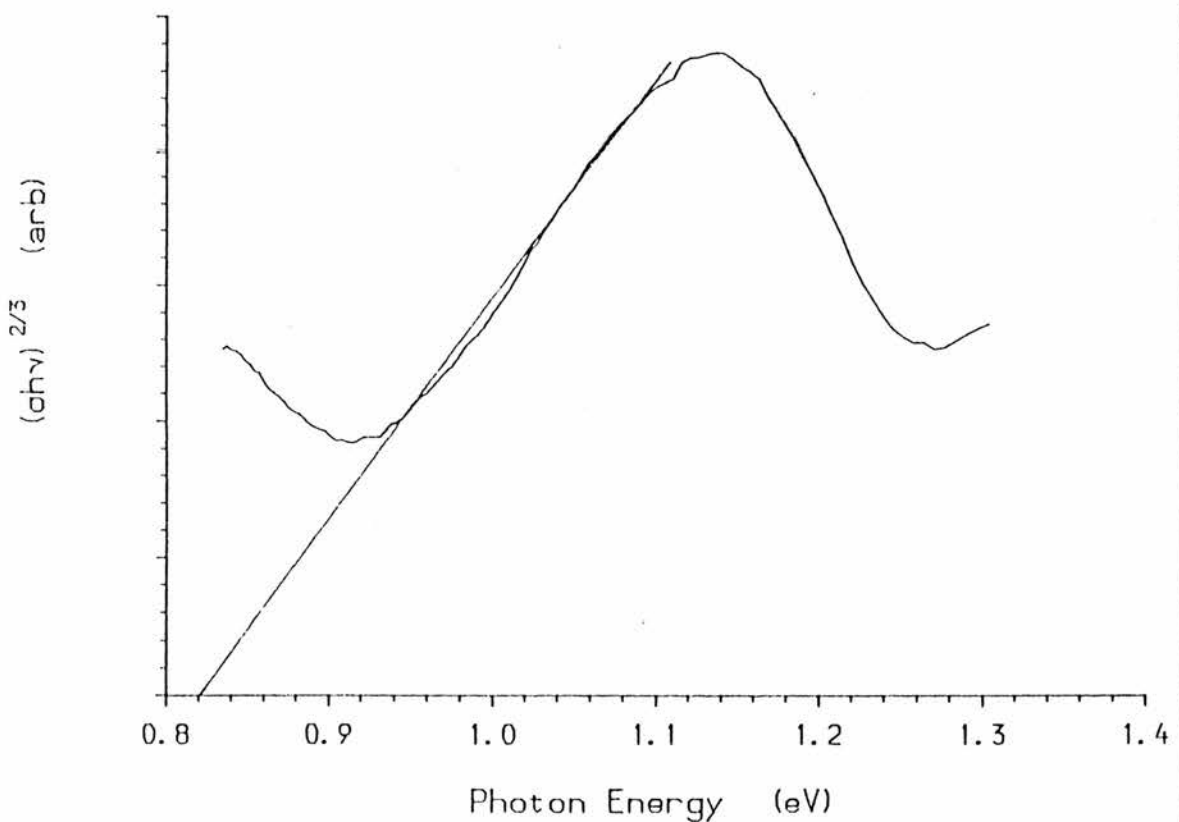


Figure 3.6b This graph is an Allen-2/3 plot of the cross section (capacitance change) plotted in figure 3.6a. The line is a best fit to the rising edge, which is probably a photoionisation transition, extended to intercept the x-axis in an attempt to give the optical threshold energy for the transition.

About eighty of the transients taken at 0°C were examined using a transient analysis program, called 'PMANGEL6' based on the Mangelsdorf^[36] method. In general the transients were found to be non-exponential. The initial part (5 to 10 points) of the transient was discarded and the Mangelsdorf method applied to the final part of the transient.

The spread of time constant values obtained was large. Little meaningful information could be obtained from the analysis. A possible reason for this was that many of the transients had bumps or other irregularities. The irregularities were not sufficient to disrupt calculation of a final OBV but ruin a Mangelsdorf analysis which requires accurate data from the final part of the transient recorded. Secondly, the wavelength difference between successive transients was very small, so a >10% error in each calculated time constant would completely obscure the small intrinsic differences between neighbouring transients, particularly with the effect of the extra multiplications introduced by the 'link-up' procedure of Section 2.3.2.

Now, we switch attention to the results from the experiments carried out under a constant 1.00eV photon energy pump light. Transient (figure 3.7) and swept wavelength spectra (figure 3.8) show the same general features up to about 1.45eV. The main features of these spectra are listed below.

- i) There is a maximum in the spectrum at $1.15 \pm 0.02\text{eV}$.
- ii) A minimum occurs at an energy of about $1.21 \pm 0.02\text{eV}$.
- iii) The spectrum rises monotonically between 1.2 and 1.3eV.
- iv) There is a second maximum at an energy of $1.35 \pm 0.02\text{eV}$.

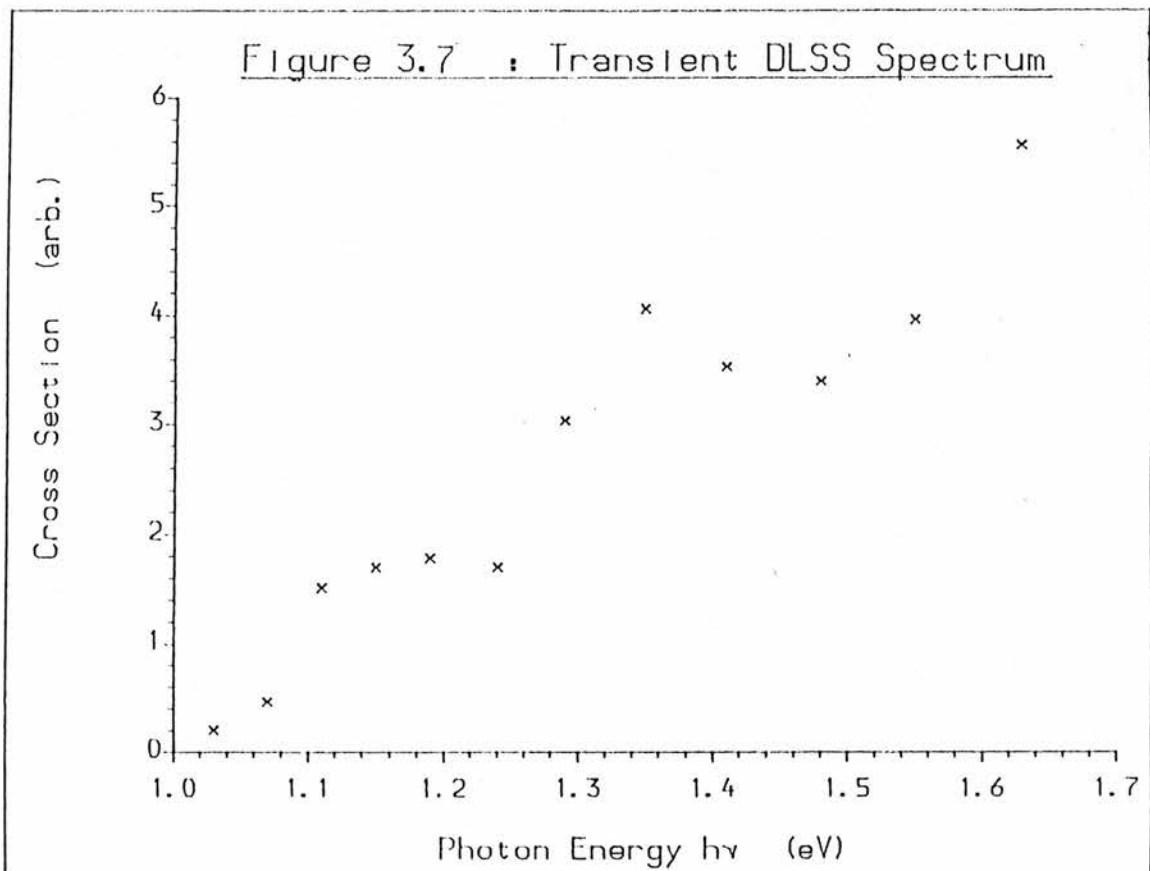


Figure 3.7 A plot of the spectral dependence of the capacitance change due to a the perturbation of a steady-state condition established by an intense infrared (1.00eV) light source. Each point is calculated from individual transients starting from equilibrium.

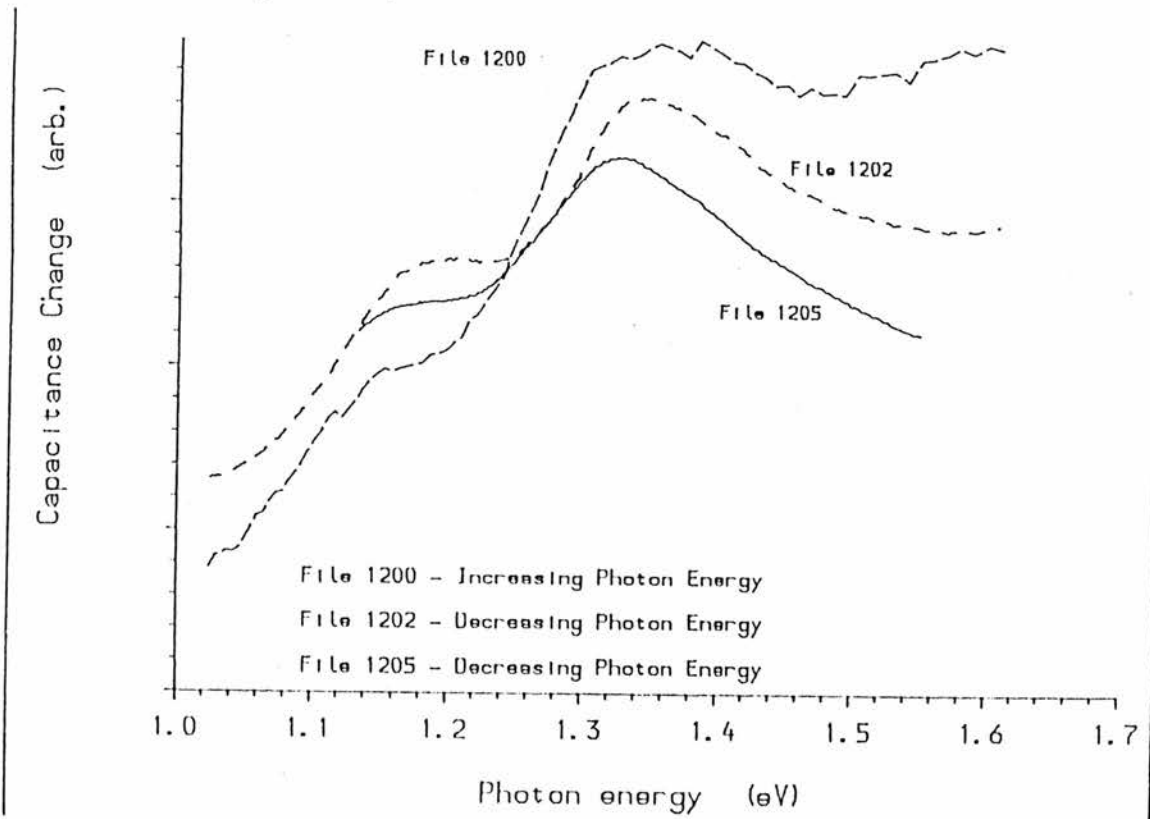


Figure 3.8 Three plots of the spectral dependence of the capacitance change due to a the perturbation of an equilibrium established by an intense infrared (1.00eV) light source. The perturbing beam wavelength was slowly swept. It is seen that the general shape of the spectra is independent of the direction of the wavelength sweep.

v) There is a second minimum at an energy of $1.42 \pm 0.02 \text{eV}$.

vi) The transient spectrum rises quite sharply for all energies above the second dip. (Up to at least 1.85eV , but no good quantitative results were obtained in this high energy region.) Wavelength swept spectra were taken up to 1.6eV and hardly rose at all.

A scanned wavelength spectrum was taken in the photon energy range 0.66 to 1.00eV . No signal significantly larger than the background drift could be seen.

3.4 Discussion And Interpretation Of Results

This section is split into two parts dealing with the two pump source photon energies used. The first part discusses the photothermal peak, the 0.9eV edge and the dip in the spectrum found above 1.2eV – all seen in the 2.00eV photon energy pump source experiments. The second part chiefly discusses the two broad peaks seen in the lower pump source energy (1.00eV) experiments.

3.4.1 2.00eV Pump Source Experiments

The results are consistent with the assumption that the 2.00eV pump source creates a large population of d^9 in the depletion region. In retrospect it can be seen that the choice of 2.00eV as a pump source photon energy is ideal as this is approximately where the maximum in the electron ($d^9 \rightarrow d^8$) photoionisation cross section occurs^[30]. The interpretation of the results is in general agreement with the level schemes used by SMA amongst others. The level scheme, described in terms of both electron energies and hole energies, is shown in figure 3.9. A peak was found in the 2.00eV pump beam DLSS spectrum below the rising $d^9 \rightarrow d^8 + e_{cb}$ photoionisation threshold in both the photocapacitance transient and swept wavelength results. This peak is due to the photothermal ionisation of d^9 to the conduction band via the T_2 excited state. At both temperatures (30^oC and 0^oC) for which measurements were carried out, the maximum of the peak was found to occur at a photon energy of 0.725 ± 0.005 eV, inconsistent with the value obtained by SMA (0.752 ± 0.002 eV at 47^oC). Yang *et al*^[30] have found a maximum in their data at "about 0.73eV" with little variation from this value above 200K. It is not clear why there is this variation: possible reasons include differences

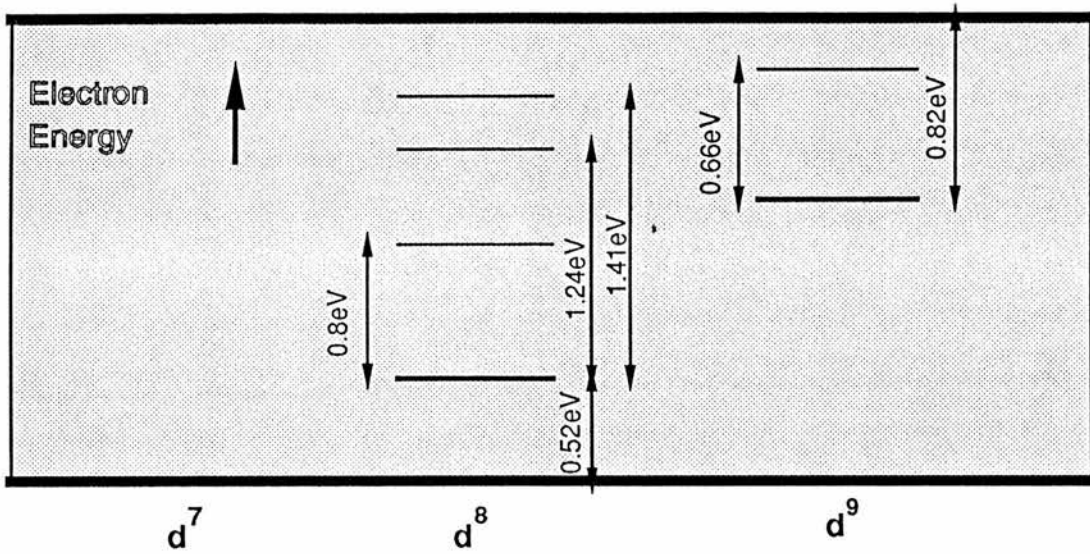


Figure 3.9a : Energy level diagram for nickel in GaP in terms of electron energies. Thicker lines are the d^7 - d^8 and d^8 - d^9 levels and the thinner lines are excited states.

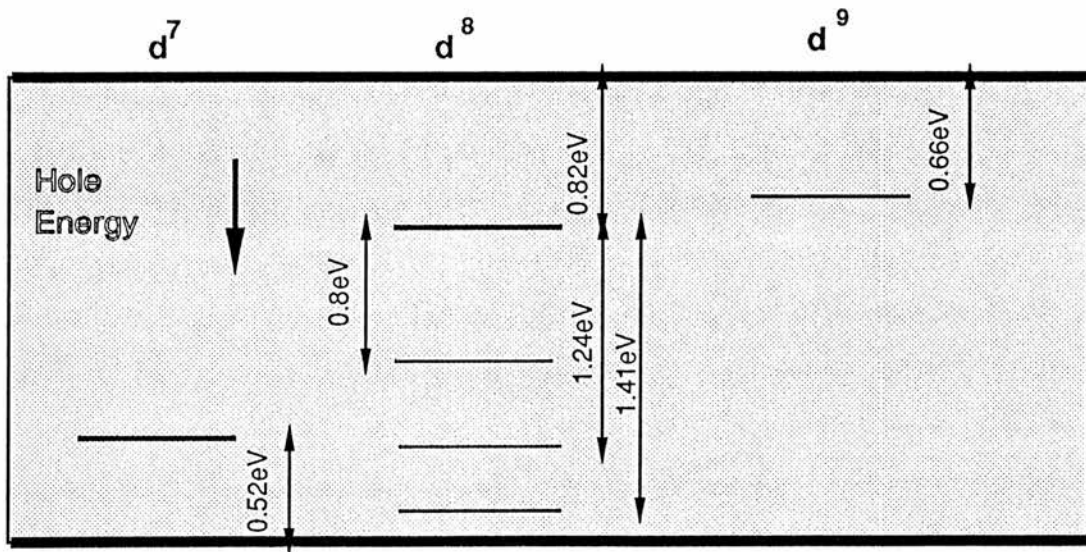


Figure 3.9b : Energy level diagram for nickel in GaP in terms of hole energies. Thicker lines are the d^7 - d^8 and d^8 - d^9 levels and the thinner lines are excited states.

between samples and differences in what precisely is measured when using a particular technique.

There are some problems concerning the width of the photothermal peak. The measured width in the transient experiments was 0.09 ± 0.01 eV. This differs significantly from the measurements of SMA, who obtained values of 0.15 eV from single source transient spectra and 0.17 eV from DLSS spectra. Wavelength swept spectra show an increased width of 0.13 ± 0.01 eV, not inconsistent with that measured by SMA, and by Yang *et al.*^[30] The nature of the wavelength swept spectra is likely to distort the shape of the peak if the scan speed is too fast, generally broadening it. Spectra taken with scan rates differing by a factor of two from the spectrum given in figure 3.5 did not, however, show significant differences in overall shape, or in the width of the peak.

The edge arising from energies of 0.9 eV was taken to be a photoionisation edge. The threshold energy of the transition from the best set of data in this energy region, a wavelength swept spectrum, was found according to the following formula,

$$\sigma = \frac{(h\nu - E_i)^{3/2}}{h\nu} \quad 3.1$$

Thus a plot of $(\Delta C(\infty).h\nu)^{2/3}$ against $h\nu$, a so-called Allen two-thirds plot, should produce an x-intercept equal to the photoionisation threshold E_i (using eqn 1.9 and $\Delta n/N = 2\Delta C/C$). The set of data so processed produced a threshold of 0.82 eV. It is necessary to consider the possible effect of even a slow (several hours) sweep through the wavelengths. Because of the extremely slow transients in the photoionisation energy region the slope of the photoionisation edge will be reduced, this is seen as a reduction of the measured threshold energy. The threshold is calculated assuming no drift

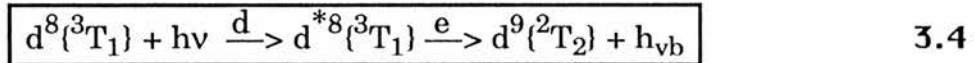
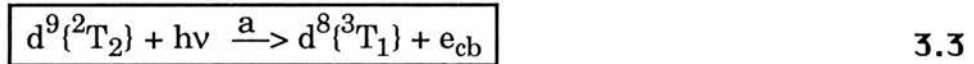
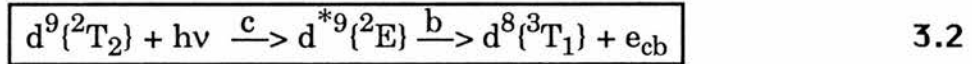
from the background OBV present at the start of the sweep and no contribution from other levels. An under-estimated true background again would lead to a lowering of the threshold. For these two reasons the figure of 0.82eV must be taken as a minimum bound on the estimate of the threshold energy. Therefore this figure is not necessarily inconsistent with the 0.82eV obtained by Yang *et al*, by the summation of the luminescence zero phonon line energy 0.66eV, for the internal d^9 transition, and the 0.16 eV thermal activation energy of the excited state. Neither can the 0.88eV determined by SMA be discounted. For the level scheme of figure 3.9 I have adopted the 0.82eV result.

The dip at 1.23eV is almost certainly due to a transition to the valence band. Reasons for this are outlined in SMA. Additionally, we will show below that we have transients in the 1.00eV pump light source experiments which display bi-exponential behaviour in the region of 1.19–1.23eV photon energy and in which one of the pre-exponential factors is negative. The relatively large size of the 1.23eV dip compared to that found by SMA is possibly a consequence of the different methods used to provide the pump light source. In SMA a lamp with two glass filters was used to obtain a very intense source. The experiment discussed here used a high intensity monochromator only which is a source less intense, but more monochromatic, relative to the excitation source than that which was used by SMA. Accordingly the proportion of nickel impurities in the d^8 state should be appreciably larger. Thus the dip is almost certainly due to a photothermal excitation to the valence band, via an excitation within the d^8 configuration. This process is illustrated in the lower part of figure 3.10.

Yang and Allen^[38,39] have attempted to bring together apparently inconsistent results in DLTS and photocapacitance measurements on n-type GaP:Ni, by constructing a more complete one-dimensional single-

mode configuration coordinate diagram than has been proposed before. DLTS measurements of activation energy and photocapacitance photoionisation thresholds are made to fit on one diagram, all the results being corrected to a temperature of 200K. This diagram is sketched in figure 3.14. Seven relevant energies can be seen. Two energies are vertical transition energies to the excited state (labelled as 6 in figure 3.14) and directly to the conduction band (5). Two more are thermal threshold energies (1 and 2) and there are also three activation energy barriers where the curves (parabolaes in the harmonic approximation) cross (3, 4 and 7).

To summarise this section, we have seen in this experiment with a constant 2.00eV energy pump light the following transitions (illustrated in figure 3.10 – transitions labelled a–e),



3.4.2 1.00eV Pump Source Experiments

The interpretation of the data from these 1.00eV pump source experiments, intended to study excitations originating from a d^8 population (1.00eV light should efficiently photoionise d^9 to d^8), presents more problems than the 2.00eV experiments.

The principal problems are:

- i) Are the principal features in the DLSS spectra the peaks or the dips and what causes them?
- ii) What produces the rising positive capacitance change background?

The majority of the features found in the spectra can, however, be explained using the same level scheme which was presented to explain features occurring in the 2.00eV pump source experiments.

One of the models presented for discussion in the arguments below requires, as well as the presence of the simple substitutional nickel in the three possible charge states, additionally, requires the presence of a nickel-related hole trap with a level about 0.95eV above the valence band. This level has been seen, or is claimed to have been seen, by many workers including a detailed study by Hamilton and Peaker^[52] using thermal capacitance measurements. The position of this level in the bandgap is illustrated in figure 3.11.

Firstly, it must be noted that the capacitance change is always positive indicating that the depletion region is becoming more positively charged. Either electrons are promoted to the conduction band or holes captured from the valence band. Since the sample is n-type and the active region is largely depleted of carriers the former of these possibilities is the most likely.

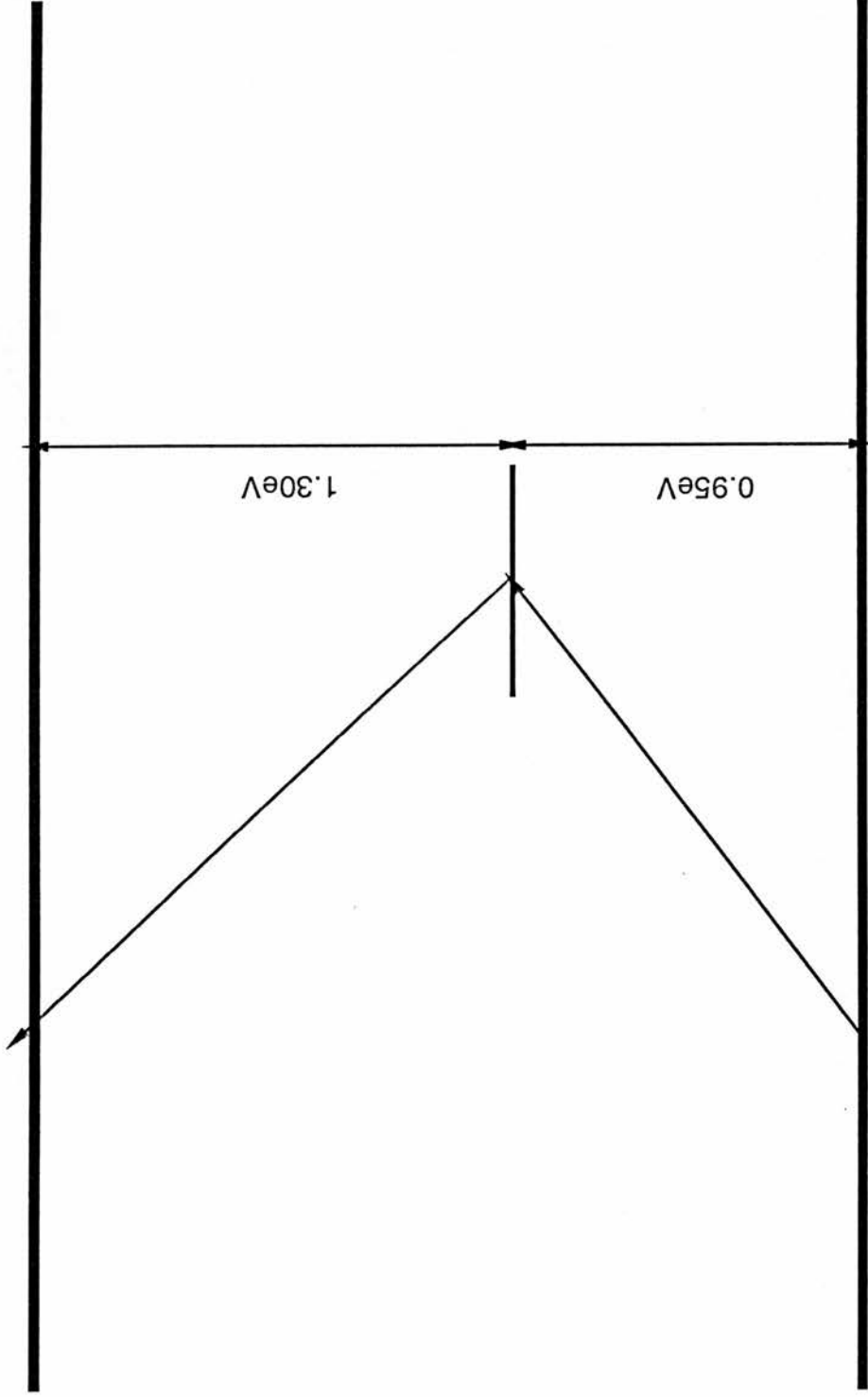


Figure 3.11 : Diagram showing the position of the "0.95eV nickel-related hole trap" in gallium phosphide

The fact that no signal is observed at an excitation source energy of 0.75eV is interpreted to mean that the d^9 level is being emptied quite efficiently by the pump source, leaving a large d^8 concentration.

We now proceed to a discussion specifically on the origin of the features in the spectrum occurring between photon energies of 1.15eV and 1.25eV. At first, it was thought that the peaks in the DLSS spectra were due to photo-thermal or optical transitions from the d^8 ground state to the conduction band, via the excited states of the d^8 configuration seen in absorption measurement, leaving the nickel in a d^7 configuration. This would have meant that the experiment was a close analogue of that using the 2.00eV pump light, except that $d^8 \rightarrow d^{8*} \rightarrow d^7 + e_{cb}$ transitions were involved instead of $d^9 \rightarrow d^{9*} \rightarrow d^8 + e_{cb}$ transitions. However this interpretation did not stand up to detailed examination of the results.

If it were the case that the 0.95eV hole trap was involved, then the peaks would be the significant features. However, the peak positions are at too low energies to agree with the positions of the d^8 excited states found in absorption experiments. Secondly, at 1.24eV (1000nm) and at 1.19eV (1040nm) we have transients which show a bi-exponential behaviour with one negative pre-exponential coefficient (figure 3.12) contradictory to the positive coefficient expected for this model with electrons ending in the conduction band.

Transients for these two photon energies showed a large initial quite fast rise (time constant approximately 30s), followed by a slower (time constant approximately 150s), much smaller magnitude, decrease in OBV. It was found empirically that these transients could be fitted quite well with a bi-exponential, as can be seen in figure 3.12. The bi-exponential behaviour with one negative pre-exponential factor results in the OBV

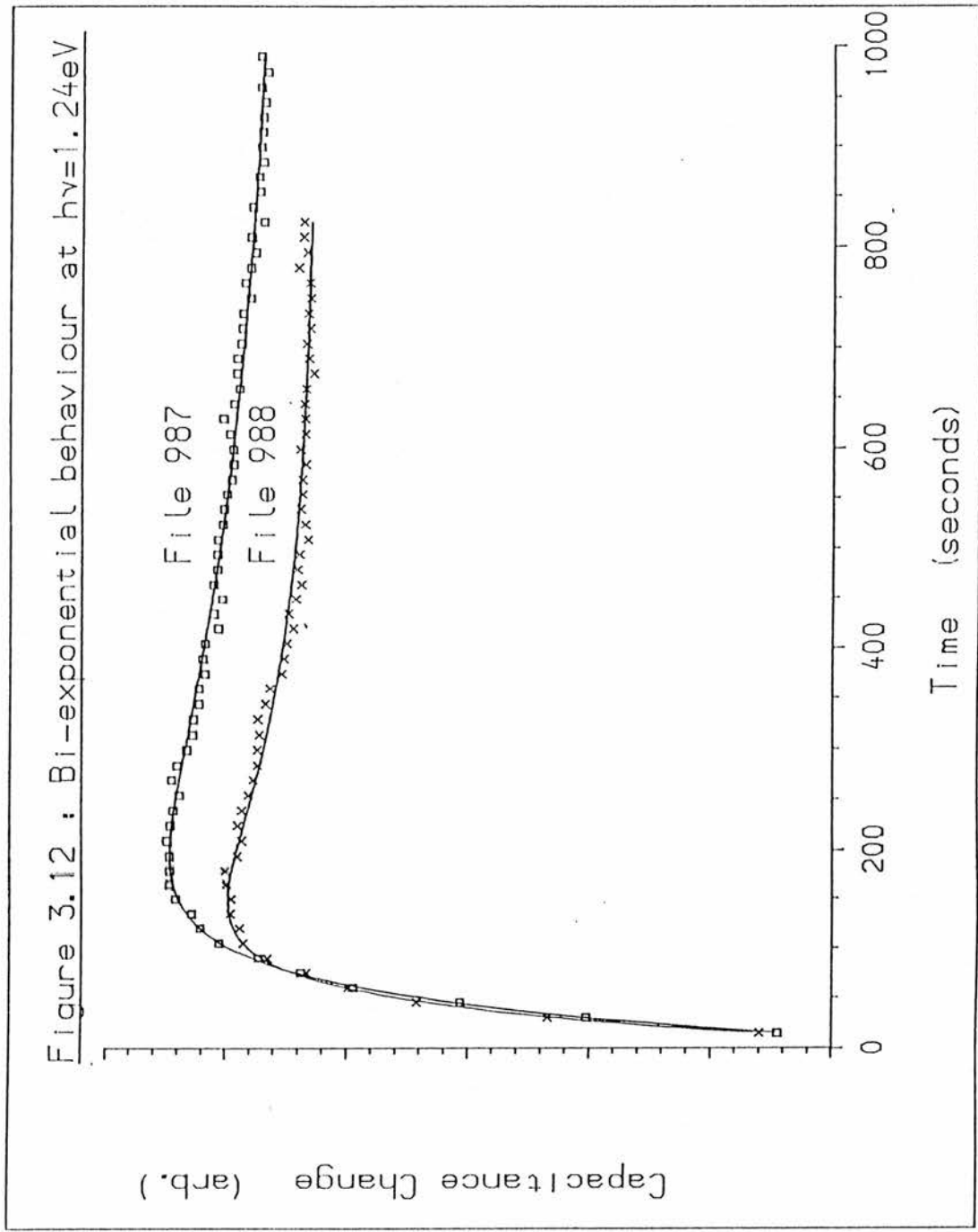
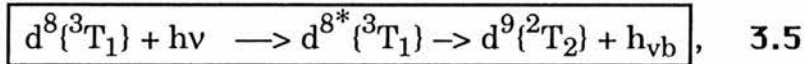


Figure 3.12 Two examples of DLSS transients recorded with a 2.00eV pump beam at a perturbing photon energy of 1.24eV. The lines are bi-exponentials with one short time constant of about 50s and a second, longer time constant in the range 250-300s.

transient reaching a maximum and then decreasing appreciably (and reproducibly).

This can also help to explain the peak in the graph calculated from the time variation of the last part of the OBV transients, as the Mangelsdorf exponential fitting program had interpreted the flat top of the curve as a very fast time constant.

The most compelling assignment for the dip in the spectrum at around 1.21eV is that it is due to the transition,

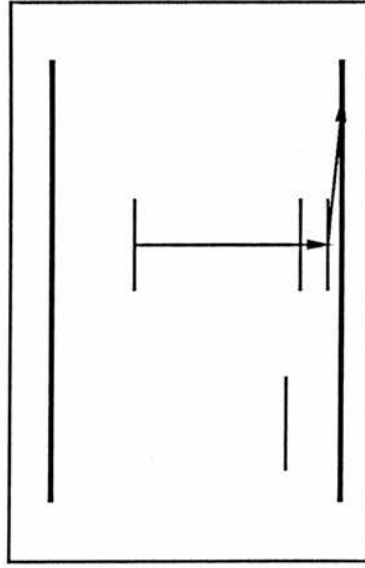


which had already been observed in the 2.00eV pump light experiment (Equation 3.4) and in absorption at 1.23eV.

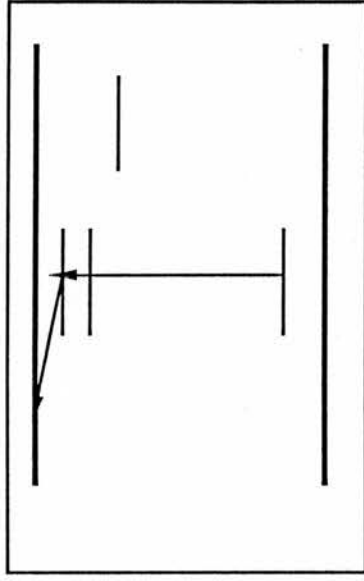
In the light of the above assignment of the dip at around 1.21eV it is not certain whether the peak at around 1.15eV has some significance itself, or is just a consequence of the dip at 1.21eV. It should be noted that Fung and Nicholas^[53] also see a maximum in their photoconductivity spectra at 1.16eV. We believe that the maximum does not have independent significance.

The dip around 1.24eV having been assigned to a likely transition, we now attempt to do the same for the other peak/dip at 1.35/1.41eV. Several possibilities are discussed. The processes are all illustrated in figure 3.13. It might be thought that the 1.35eV peak could be caused by the photoionisation of the 0.95eV nickel-related hole trap (seen by many workers). Fung and Nicholas^[53] attribute a point of inflection in their spectra at approximately 1.30eV to the photoionisation of the nickel-related hole trap to the conduction band. The transition is included as part of figure 3.13. This centre is likely to have a low concentration compared to

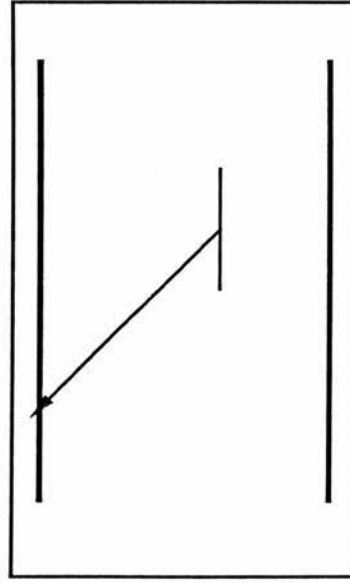
d^8 Photothermal Ionisation to the Valence Band



d^8 Photothermal Ionisation to Conduction Band



Hole Capture by 0.95eV hole Trap



d^8 to d^9 Photoionisation Transition

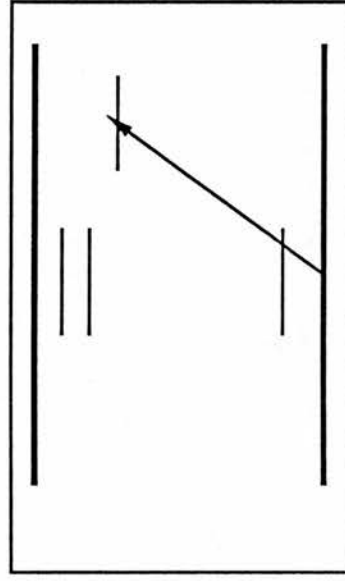


Figure 3.13 : The four candidate models for the 1.35eV peak/1.41eV dip in the 1.00eV pumped Spectra

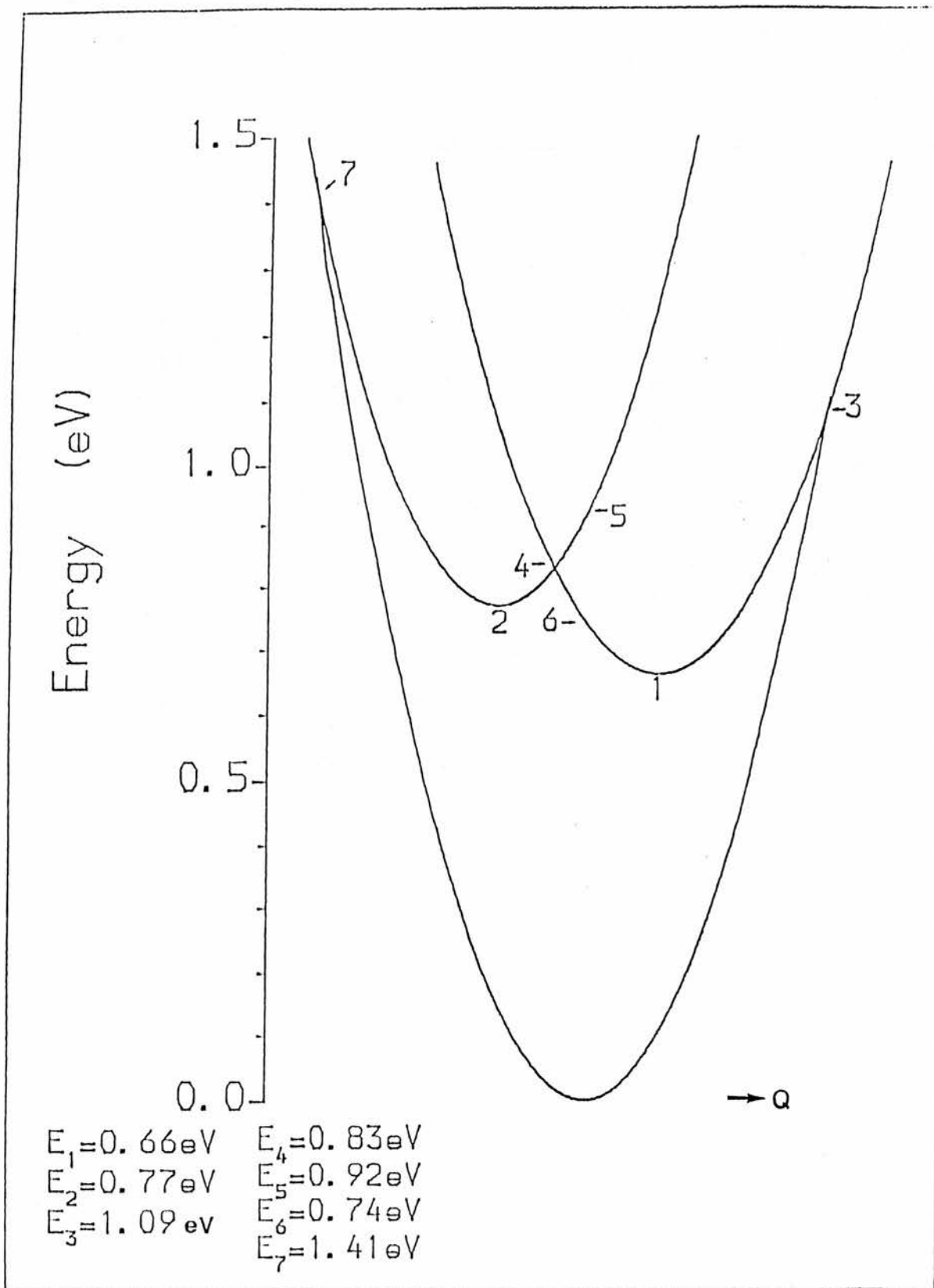


Figure 3.14 : An illustration showing the one-dimensional configuration coordinate diagram proposed by Yang and Allen[38,39] to explain the absorption, luminescence and junction capacitance effects arising from transitions involving the nickel d^9 state in GaP.

the simple substitutional impurity in samples intentionally doped with nickel. It could have a much higher optical cross section, due to its reduced symmetry, resulting in a noticeable peak in the absorption spectrum, but is not likely to be seen in a photocapacitance spectrum unless in high concentration^[32].

No indication of negative coefficient bi-exponential behaviour was found in the transients taken in the 1.4 eV photon energy region, which would have been directly analogous to those taken into 1.19–1.24eV energy region.

Another possibility for the interpretation of the 1.35eV peak, considered at first to be a stronger candidate model, is the photothermal promotion to the conduction band of an electron via an excited state of the d^8 configuration (a two stage optical process would be of second order and therefore improbable). It is now considered that this excited state will be much more likely to result in a hole in the valence band. In a hole excitation energy scheme the 1.43eV d^8 excited state is close to, if not degenerate with, the valence band. Once the hole is in this excited state thermal excitation, if still in the energy gap, or autoionisation, if not, will quickly follow.

A final candidate transition, included here because its onset should be at about 1.3eV, is the direct photoionisation transition $d^8 \rightarrow d^9 + h_{vb}$. This hypothesis can be rejected because being a photoionisation transition the cross section should increase, that is the OBV decrease on a positive capacitance change background, for photon energies up to at least several tenths of an electron-Volt above the onset of the transition. If this transition is taking place then it is well masked by other transitions which result in transfer of electrons to the conduction band.

A peak had been observed by Szawelska^[35] at approximately 1.37eV in single source steady state photocapacitance measurements, but this feature was not discussed in her text. The sign of the capacitance change of the peak was again positive.

3.5 Conclusion

A photothermal peak in the GaP:Ni d^9 photocapacitance experiment was seen and studied using a 2.00eV photon energy pump source to ensure a large d^9 population. Some unresolved discrepancies in peak position and peak width have become apparent. New experiments were performed with a 1.00eV photon energy pump light initially depleting most of the d^9 population. A photothermal ionisation transition from the d^8 configuration to the valence band at 1.21eV was confirmed by the analysis of bi-exponential transients. A similar photothermal transition, also to the valence band, might have been seen for the first time at a photon energy of about 1.41eV.

Chapter Four:

Chromium in Zinc Selenide

4.1 Introduction

The study of chromium in II-VI semiconductors is of interest for several reasons. Zinc selenide, is an increasingly important material in the optoelectronic industry. It is used to make visible pass, ultra-violet absorbing filters and Fabry-Perot optical transistor elements for example. It is necessary to know how the presence of impurities, both deliberate and unintentional, can affect the properties of the materials and hence the performance of devices constructed from those materials. There is also the theoretical interest in determining how the many experimental parameters vary as one either changes the 3d impurity in the same host, or looking at the same elemental impurity in different host crystals.

Chromium in zinc selenide is thought to be present mostly as a simple substitutional impurity on zinc sub-lattice sites. The electronic configuration of the free chromium atom in its lowest energy state is [Ar] $3d^5 4s^1$. Two of the outermost electrons are involved in bonds with the neighbouring selenium atoms (the term ion can not be used without qualification in a material which does not have a completely ionic character), leaving a $3d^4$ configuration, also labeled as Cr^{2+} . Chromium can accept an electron to give a d^5 (Cr^+) configuration. Chromium might also be capable of losing an electron, giving d^3 ^[54] (Cr^{3+}). The d^5 state has been observed in EPR measurements by Title^[55] at 77K. It has been suggested from EPR and absorption data that most of the zinc substitutional chromium is present in the d^4 configuration^[56].

A thermally broadened band has been seen in absorption and was assigned to the transition $d^4 \rightarrow d^5 + h\nu_b$. Photo-EPR measurements by

Kamińska *et al.*^[57] suggest the d^4-d^5 level can be described by a one-dimensional configurational coordinate diagram (figure 4.1). The temperature dependence of the broadening was accounted for by suggesting that chromium induces a large lattice relaxation^[57] (for a 3d impurity in a II-VI compound). It was an aim of the present study to look for and study the complementary transition ($d^5 \rightarrow d^4 + h_{\nu b}$) using the photocapacitance technique.

The measurements of Kamińska *et al.*^[57] on the $d^4 \rightarrow d^5 + h_{\nu b}$ transition lead to values of the optical ionisation parameter, E_{opt} , of 2.26eV and a thermal activation energy of 1.93eV to the valence band (refer to figure 4.1). The relaxation energy, E_{rel} , being the difference between E_{opt} and E_{th} , is thus equal to 0.33eV. This value is quite large indicating a strong coupling between the impurity and the lattice. Kamińska *et al.* calculate a large lattice distortion from their thermally broadened EPR data of about 4.5% in the impurity to nearest-neighbour bond-length.

Infrared absorption measurements on cubic ZnSe by Vallin *et al.*^[58] show a broad absorption band at 0.68eV (5500 cm^{-1}) at room temperature probably arising from the ${}^6T_2-{}^5E$ transition of the d^4 configuration. At helium temperatures a zero-phonon line was identified at 0.616eV and assigned to this transition. Grebe *et al.*^[59,60] have seen in luminescence experiments what they believe to be a series of d^4 excited states which fit quite well to a Tanabe–Sugano diagram calculated under tetrahedral (T_d) symmetry with parameter $Dq/B=0.94$.

The photocapacitance measurements presented in this chapter show that there are two levels contributing to the low temperature photocapacitance spectra. One is largely thermally quenched at temperatures significantly above 100K. At low temperatures the dominant

contributor to the phot capacitance signal in the photon energy range 0.5 to 1.1 eV has a thermal activation energy of 0.21 ± 0.02 eV.

The sample history and details of the experimental methods used are given in Section 4.2. Section 4.3 states the results obtained from capacitance-voltage, phot capacitance and thermal level emptying experiments. The results obtained are discussed with reference to other information known about the impurity system in Section 4.4, with the summarised conclusions in Section 4.5.

4.2 Experiment

The sample used in these experiments was n-type zinc selenide with chromium impurities introduced by diffusion. The material was obtained from R.A. Stradling by H.R. Szawelska. It was labelled ZnSe P193 and had a date (6/29/71) associated with it (taken to be the growth date). The material underwent a zinc-aluminium conductivity enhancement process in June 1980 (6g of Zn to 0.5g of Al), being heated for 66 hours in a furnace at 960°C. It was then relabelled 'P193 Z.T.'.

One piece of the P193 Z.T. material was chromium doped in July 1980. It was heated to 750°C (this was the set temperature, the temperature of the sample could have been significantly lower) with 1g of chromium and 7.1g of zinc for 25 hours. The material was then labelled 'P-193 CR1'. This material was treated a second time for 25 hours with zinc and chromium at 850-900°C. The P-193 CR1 material was a dull red-orange colour. After grinding to half thickness the material looked more yellow. The material was from then called 'P-193 CR2'. Indium contacts alloyed to it gave a sample resistance of approximately 5Ω. Later a 1mm diameter, semi-transparent gold dot was evaporated onto the opposite surface to the indium contacts. The final sample designation as a diode was 'P193-CR2*1'. The sample was stored under propanol between 1982 and 1986.

The sample was mounted in the Oxford Instruments CF1204 cryostat as described in Chapter Two. The peak-to-peak signal voltage across the diode was 3 mV throughout this work. The rest of the measurement system has already been described in Chapter Two. The order filters used in conjunction with the Spex Minimate monochromator are given in table 2.1.

A capacitance against voltage measurement was taken at room temperature as follows. The diode was balanced on the bridge at room temperature with the three smallest variable capacitors in their minimum (non-zero) capacitance positions. The 'switched in' or fixed capacitor labelled No.1 (10pF) was used, the smallest of the fixed capacitors that it is possible to use on the bridge. The position of the largest variable capacitor, C_1 , was noted. The bridge was rebalanced using C_1 and the variable resistors at each new bias voltage. When as good balances as possible were achieved the position of C_1 was noted along with the exact bias voltage applied across the sample and 50Ω resistor. A check was made that virtually all the voltage drop was across the sample, and less than 1% was dropped across the resistance. The readings on the bridge dials were converted into capacitance values by comparing them with a table compiled by earlier workers. The zero-bias capacitance of the sample itself was later measured on a Wayne-Kerr 601 radio-frequency bridge. The latter bridge allows nulling of the cable capacitances.

No photocapacitance change was found at room temperature for photon energies below about 1.7eV. For a photon energy of 1.24eV a capacitance change was found upon illumination when a temperature of 60K was used. Single wavelength photocapacitance transients were taken at temperature of 60K in order to take a photocapacitance cross section spectrum. The spectrum was initially taken only for photon energies up to 1.181eV. Later, with a different order filter the range was extended up to 1.46eV. A second spectrum was taken at the higher temperature of 150K, a convenient temperature at which sufficiently large photocapacitance changes were observed. That is, large enough that the transients could still be analysed by the Mangelsdorf^[36] method.

It was thought that since both the total capacitance change and the cross section exhibited thresholds and also because the total capacitance

change decreased markedly with increasing temperature, at low photon energies, that the levels under discussion were being thermally emptied. Measurements of the thermal emptying rates could therefore give information on the thermal activation energies of the levels. This can be achieved by filling the level by an application of forward bias which decreases the contact barrier potential. The system relaxes back to a steady-state condition mostly through thermal emission processes. A preliminary thermal emptying experiment was carried out by the application of a 1.5V forward bias pulse for times varying between 1 and 600 seconds. It was found that pulse widths greater than about a second had only an insignificant effect on the thermal relaxation time of the capacitance signal; the bias pulse-width was then kept constant at 10s. The pulse height used was 0.6V. Initially a bias of 1.5V was used but this was later decreased to 1.0V and finally to 0.6V. This parameter affects which depth range of levels are filled by the forward bias. The final pulse voltage used must be sufficient to bring all traps deeper than 0.8eV (from the conduction band minimum) below the Fermi level. The decay in the capacitance with time was recorded for five temperatures between 100 and 150K. This temperature range produces results between the extremal decay-times measurable with our system.

A photoionisation spectrum was taken under steady illumination by a second light source at 60K. The second source was a 50W tungsten bulb, placed close to the cryostat, illuminating the sample through the second optical window, which had a germanium filter placed in front of it. This was an attempt to ionise all centres with gap levels within an energy of 0.75eV of the conduction band minimum, particularly the 0.5–0.6eV level, in order to study any levels present at low temperatures, but which were not easily discernible in the masking presence of energy levels closer to the conduction band.

Finally, a set of swept wavelength photocapacitance measurements was taken at 60K for the photon energy range between 1.77eV and 3.1eV. A double differentiator circuit was used to help to identify the exact position of the weaker capacitance thresholds observed. The differentiator circuit had a time constant of about 2s, corresponding to a wavelength interval of 0.4nm at the fastest scan rate used.

4.3 Results

The donor concentration in the depletion region was determined by taking a plot of capacitance against reverse bias, as described in the preceding section. A graph of inverse square capacitance against reverse bias was plotted (figure 4.2). The resultant curve had a very poor fit to a straight line as stray capacitance had not been taken into account. A fit was made by subtracting capacitance until the calculated value of the Schottky barrier height agreed with the literature value of $1.36\text{V}^{[61]}$. From this 'corrected' C-V plot the donor concentration was calculated to be $8.0 \pm 1.5 \times 10^{15} \text{cm}^{-3}$. The corrected capacitance figure at zero-bias of 146pF is in good agreement with the result obtained from the Wayne-Kerr bridge capacitance result of $144 \pm 4\text{pF}$.

Photoionisation cross-section spectra were calculated from the rise-times (τ) of capacitance transients taken at different photon energies (see Chapter Two). A graph showing the experimentally determined cross-section ($(\phi\tau)^{-1}$) at 60K against photon energy is given as figure 4.3 for photon energies up to 1.1eV . Below 0.6eV the spectrum drops quite sharply, to less than 15% of its 0.7eV value by 0.5eV . It was not possible to go to lower energies due to the instability of the background capacitance level over long (tens of minutes) times imposing a limit on the measurable range of transient rise-times. The practical range of rise-times that can be measured with the equipment at this time was about 3 to 10^3 seconds. The tungsten-halogen lamps used as light sources have a decreasing output at lower energies, this also contributes to increasing the time constant.

The low temperature photoionisation spectrum was, later, extended to higher photon energies, up to 1.46eV , using the appropriate order filters. The results are shown in figure 4.5.

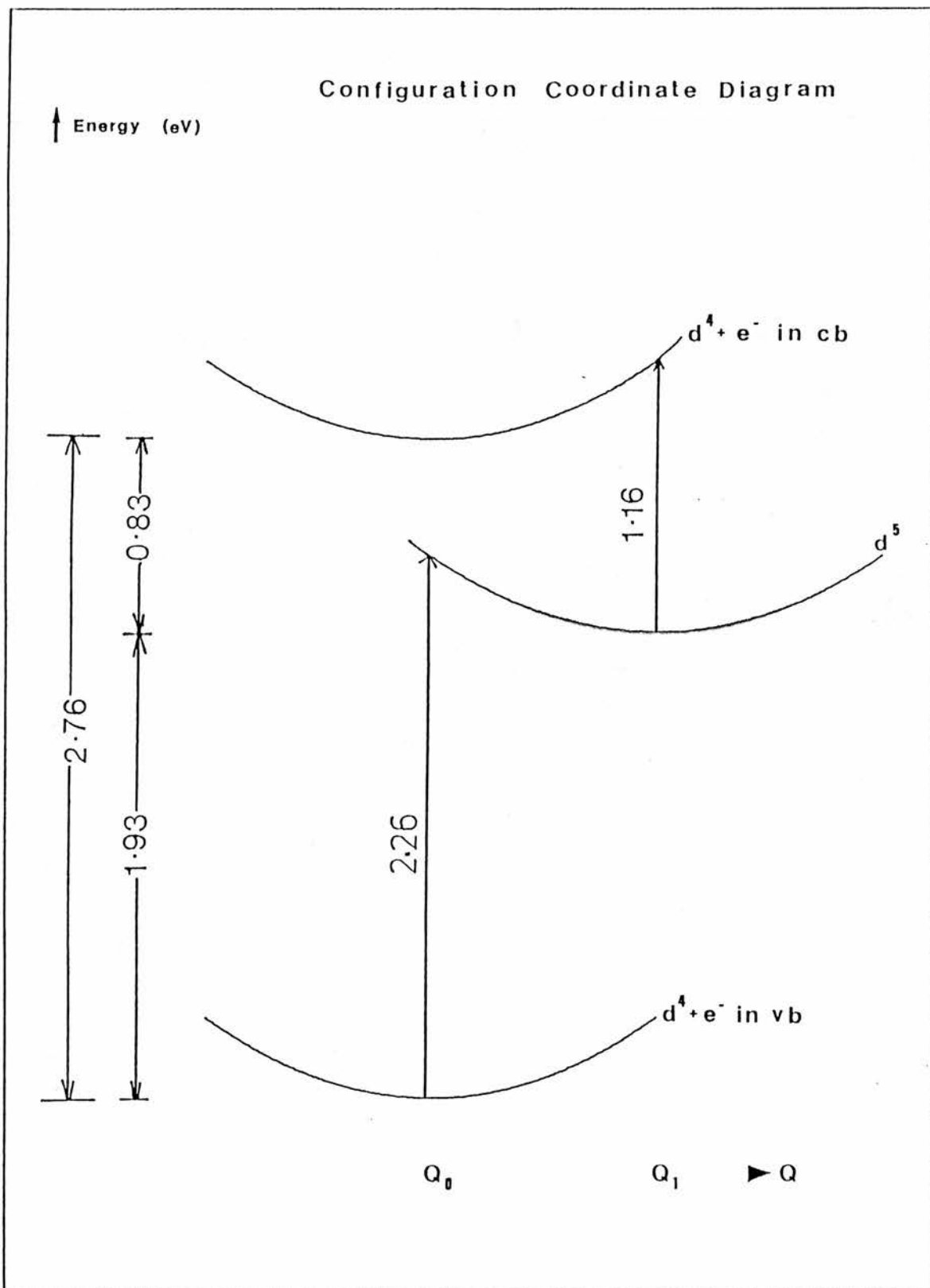


Figure 4.1 A one-dimensional configuration coordinate diagram for the substitutional chromium d^4-d^5 level in zinc selenide based on the data obtained in this chapter and that of Kamińska *et al.*^[57].

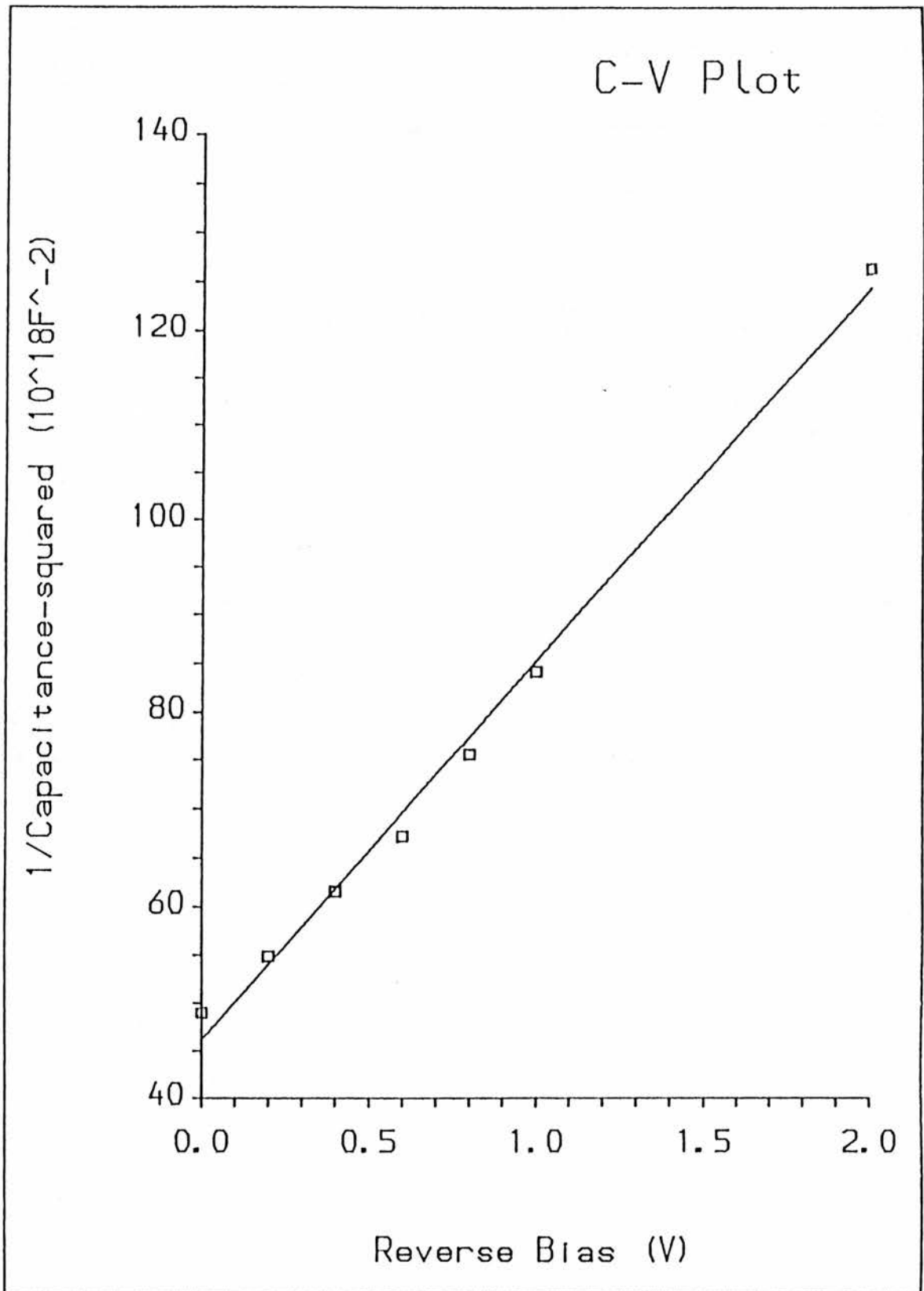


Figure 4.2 A graph showing the inverse squared sample capacitance of sample P193-CR2*1 against reverse bias. The measurements were performed in the dark at room temperature. The gradient of the best-fit line corresponds to a donor concentration of $8.0 \pm 1.5 \times 10^{15} \text{cm}^{-3}$.

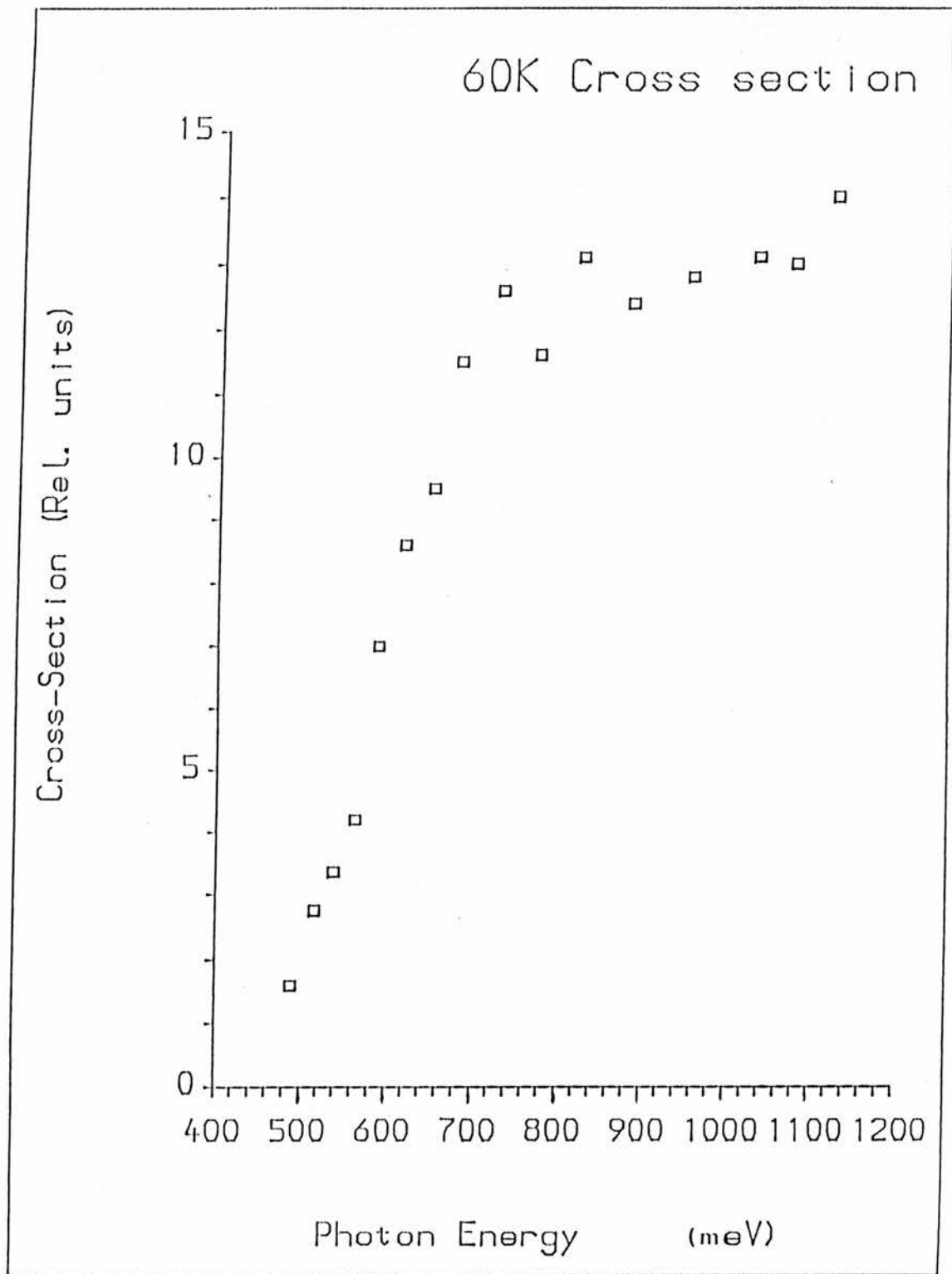


Figure 4.3 The low temperature (60K) photoionisation cross section spectrum of diode P193-CR2*1 calculated from $(\text{Photon-Flux} \cdot \text{rise-time})^{-1}$ plotted against photon energy.

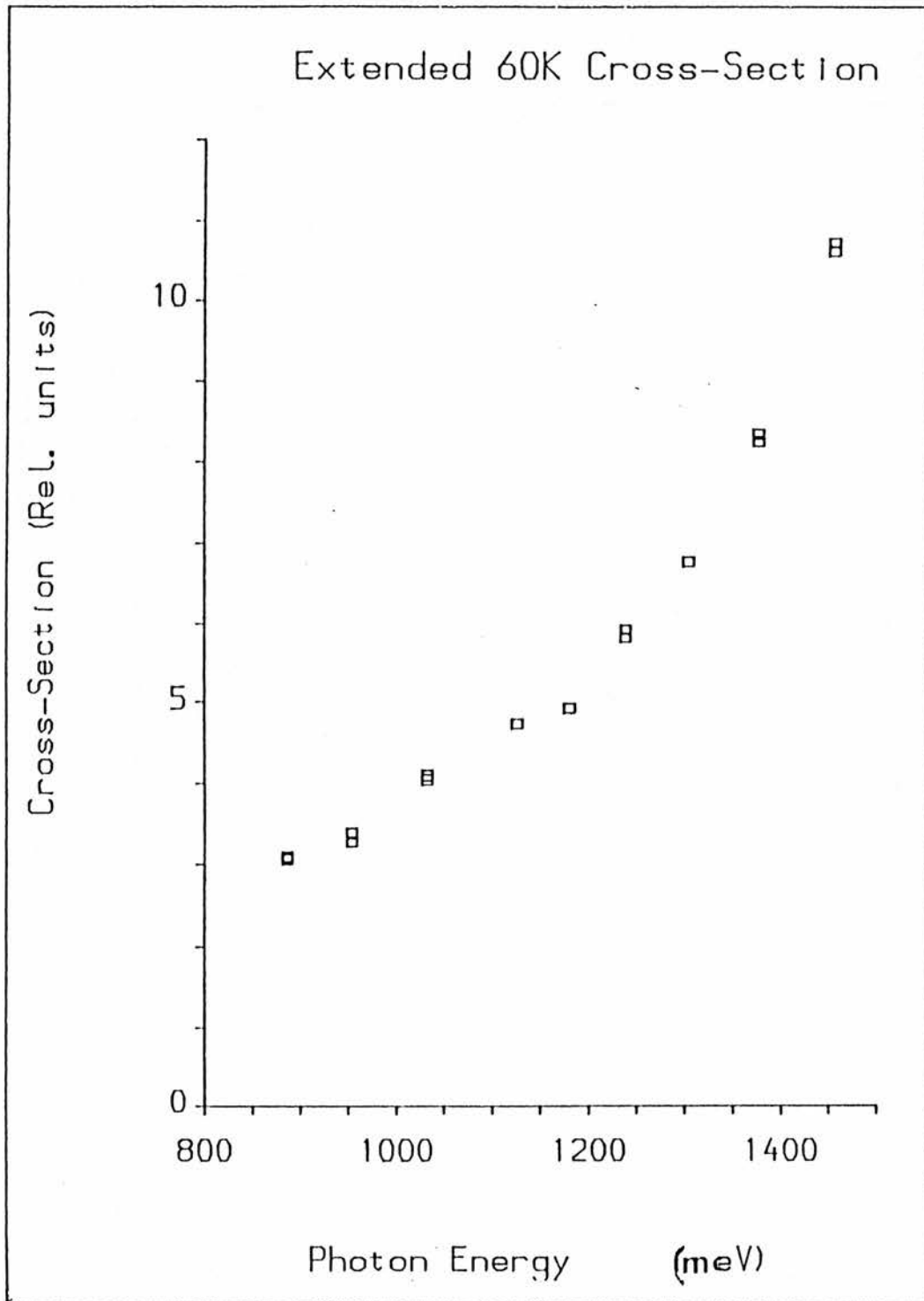


Figure 4.4 The low temperature (60K) photoionisation cross section spectrum of diode P193-CR2*1 extended to higher photon energy values. A different order filter was used to obtain this spectrum to that used to obtain the spectrum of figure 4.3.

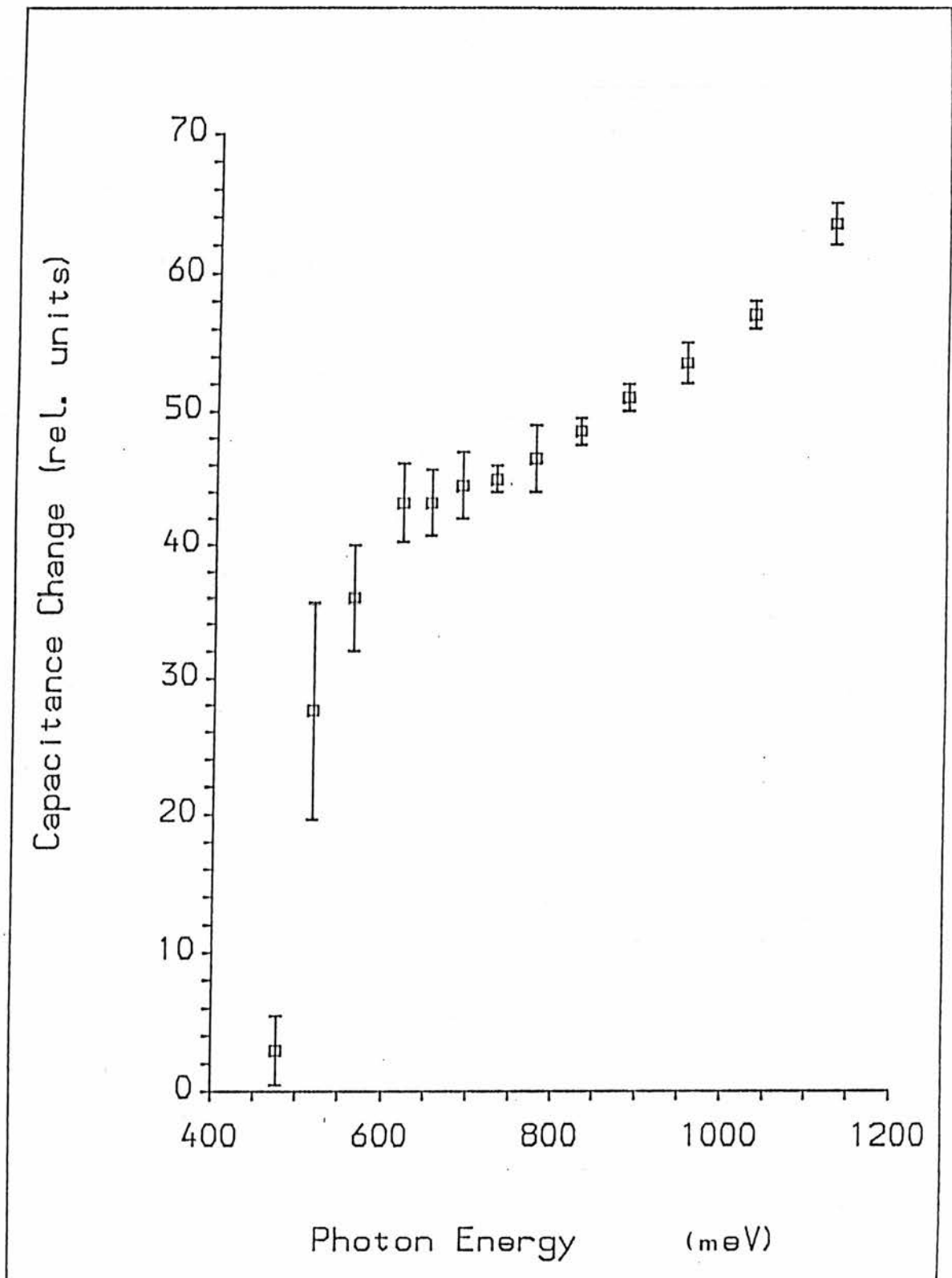


Figure 4.5 A graph showing the low temperature (60K) spectral dependence of the total capacitance change after illumination, $\Delta C(\infty)$, for the chromium doped zinc selenide diode P193-CR2*1.

Figure 4.5 shows the measured total capacitance change against photon energy at 60K. This quantity is difficult to measure accurately at low photon energies because of the aforementioned long term drift. It is, however, noticeable that the capacitance change does not vary much over the range 0.65 to 1.0eV. This capacitance change corresponds, using equation ($\Delta n = 2 \times N_t \times \Delta C / C$), to a change in level occupancy of $3 \times 10^{14} \text{ cm}^{-3}$. Above about 1.0eV there is a rapidly growing capacitance change, which continues up to the highest photon energies that were used.

The experimentally determined photoionisation cross-section at 150K is shown in figure 4.6. Photon energies from 0.70 to 1.46eV were used. The spectrum was not extended to higher photon energies because of the need to change order filters again. This introduces additional errors which it would not be easy to distinguish whether other states had been excited (a likely possibility considering the scanned wavelength results above 1.77eV). It can be seen that the spectrum is completely different in shape to that at 60K. There is no measurable capacitance change at energies below 0.75eV. The cross section rises rapidly above energies of 0.9eV and continues to rise up to the highest photon energy used, 1.46eV.

The capacitance change at 150K against photon energy is shown in figure 4.7. The total capacitance change is very small ($< 0.05 \text{ pF}$) up to an energy of between 0.8 and 0.9eV, after which it grows increasing rapidly up to the highest photon energies used. The measured capacitance change at a photon energy of 1.181eV corresponds to a level occupancy change of approximately $1.5 \times 10^{14} \text{ cm}^{-3}$

We now look at the thermal emptying experiment. A plot of the logarithm of the time constant of the capacitance decay, after removing the forward bias, against inverse temperature is shown in figure 4.8. The

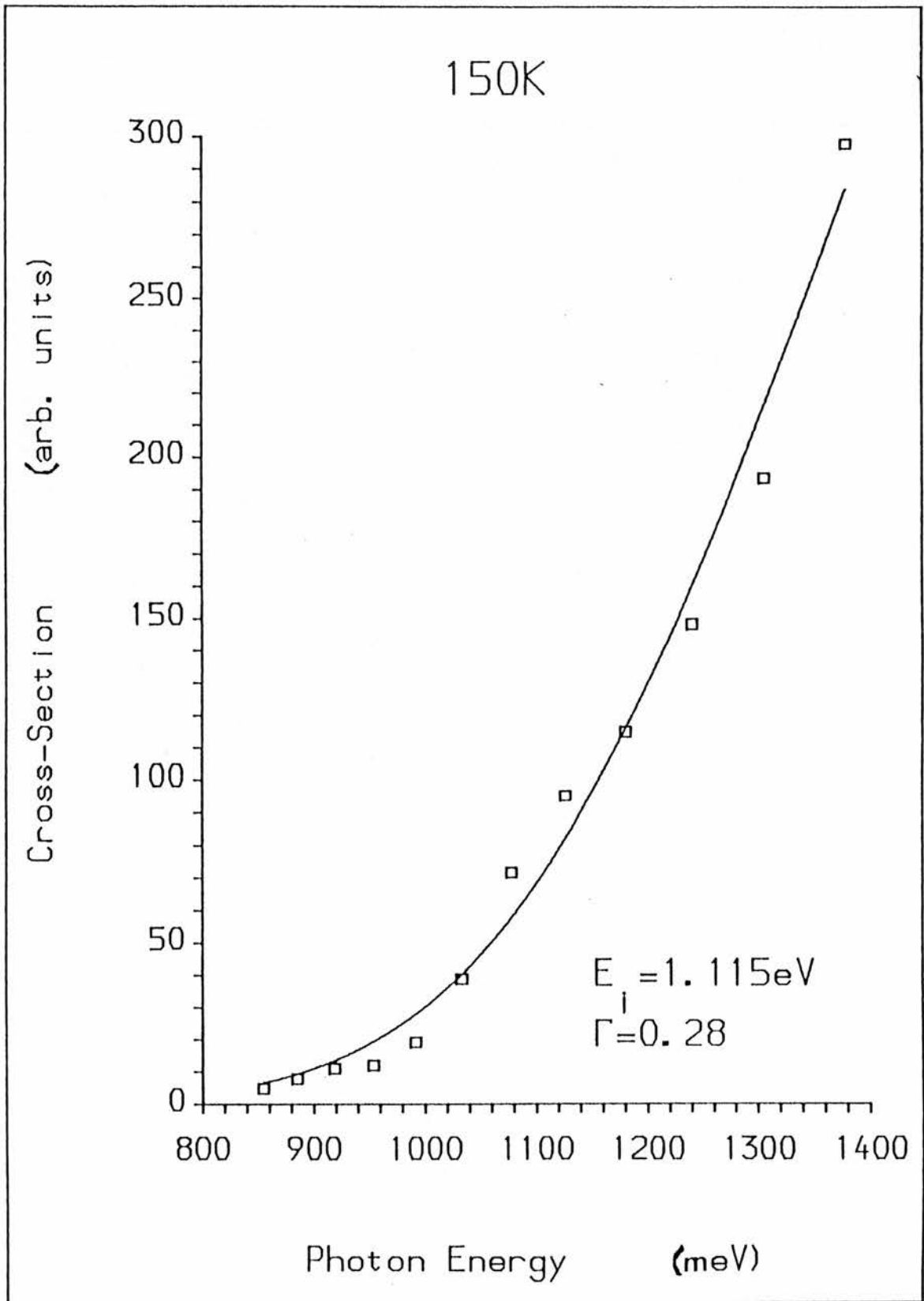


Figure 4.6 The transient photoionisation cross section spectrum at 150K for diode P193-CR2*1. The line is a least squares fit with $E_{opt}=1.115\text{eV}$ and a thermal broadening parameter, Γ , of 0.28.

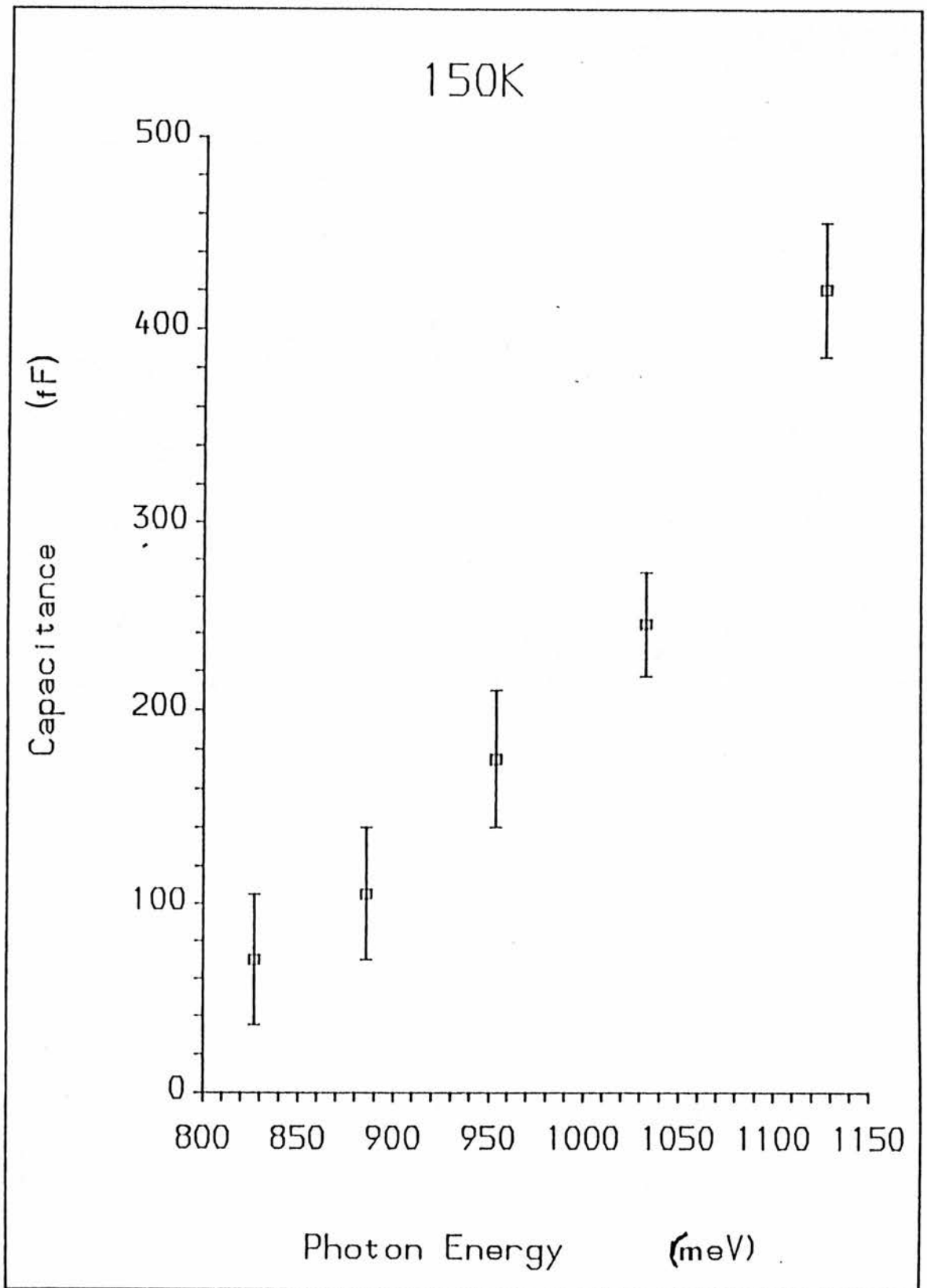


Figure 4.7 The total capacitance change $\Delta C(\infty)$ against photon energy at 150K for diode P193-CR2*1.

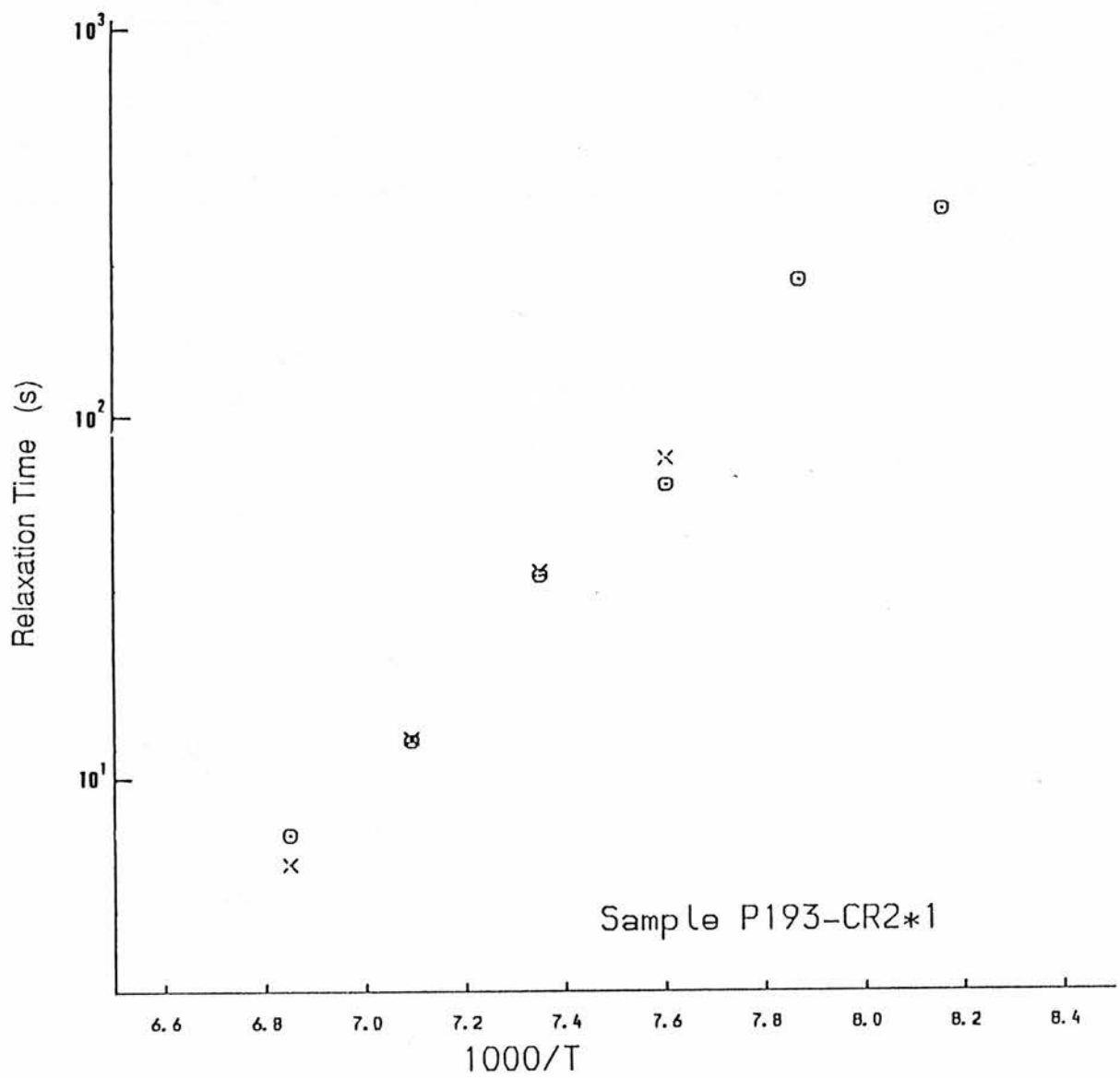


Figure 4.8 A graph plotting the logarithm of the time constant for the thermal emptying of deep levels in diode P193-CR2*1 against reciprocal temperature. Thermal relaxation occurs after ceasing to apply a forward-bias pulse intended to fill levels in the energy gap. A least-squares fit to these points gave an energy of $0.21 \pm 0.02 \text{ eV}$

activation energy calculated from the gradient of the graph was $0.21 \pm 0.02 \text{ eV}$.

The resulting spectrum and total capacitance change resulting from the photocapacitance transient experiments under secondary illumination, with the un-photoquenched results for comparison, are shown in figure 4.9 and figure 4.10. It can be clearly seen that the spectrum and the associated capacitance change are much closer in form to the 150K spectrum with the bias light applied.

Swept wavelength photocapacitance measurements produced a series of sharp, but sometimes very small ($O(10^{-2} \text{ pF})$) capacitance changes when photon energies greater than about 1.8eV were used (described as "thresholds"). Most of the onsets were visible over a large temperature range from below 50K to above 300K. A chart recording of a capacitance spectrum taken at 150K is shown in figure 4.11. A table of the "thresholds" can be found in Appendix 5.1, where they are to be more fully discussed in relation to a similar set of thresholds found in vanadium doped ZnSe. In order to make the very small capacitance changes visible, the output from the a.c. voltmeter was taken through a double differentiator circuit. The total capacitance change was about 24pF for photon energies from 1.8 to 2.1eV at 60K, incrementally changing by less than 1pF over this range.

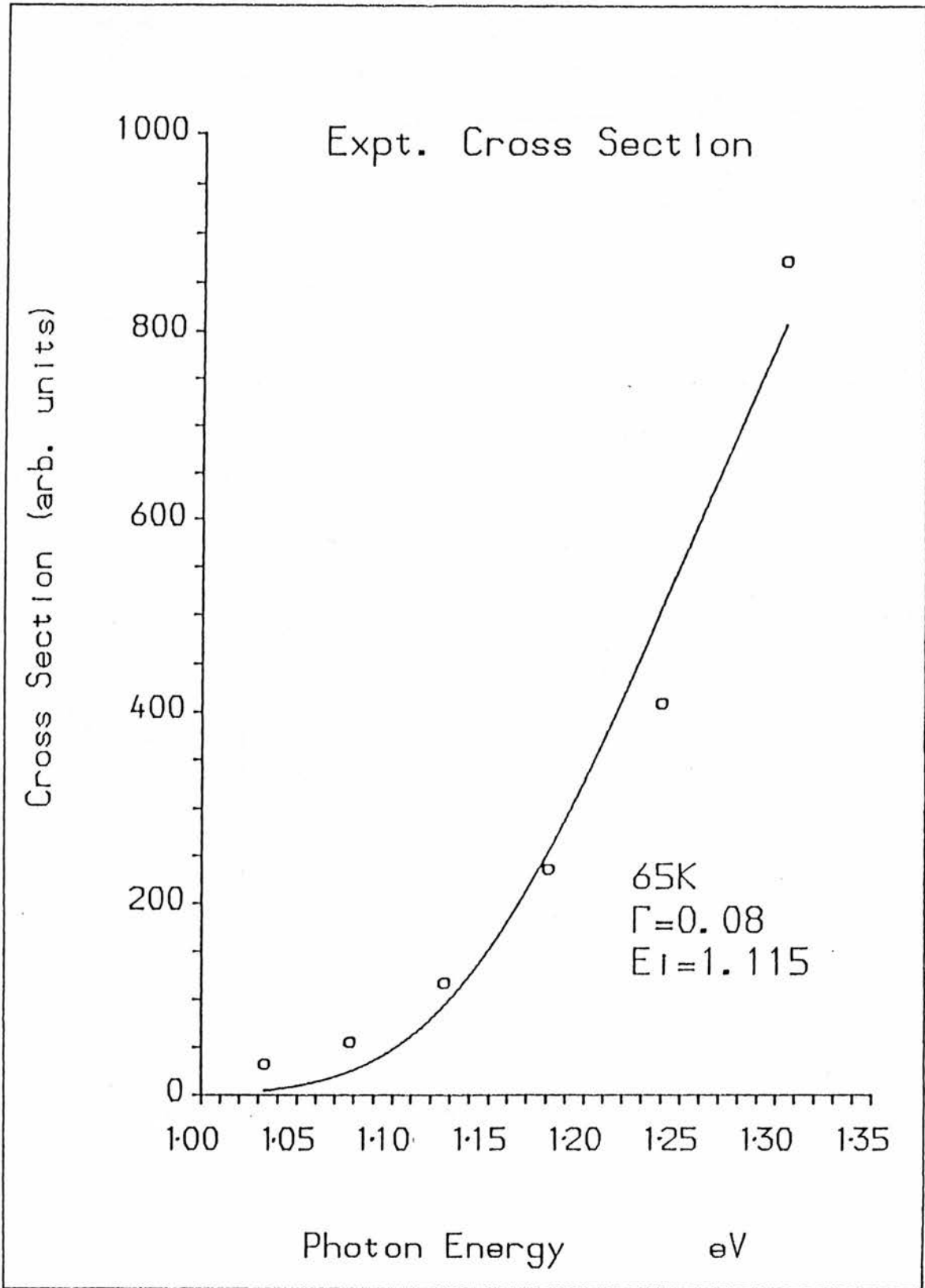


Figure 4.9 The $(\text{photon-flux} \cdot \text{rise-time})^{-1}$ plotted against photon energy at 65K when diode P193-CR2*1 is under secondary illumination with germanium filtered tungsten light ($h\nu < 0.7\text{eV}$). The line is a least squares fit to the thermal broadening formula of Piekara *et al.*^[63] with an optical ionisation parameter (E_i) of 1.115eV and a thermal broadening parameter, Γ , of 0.08.

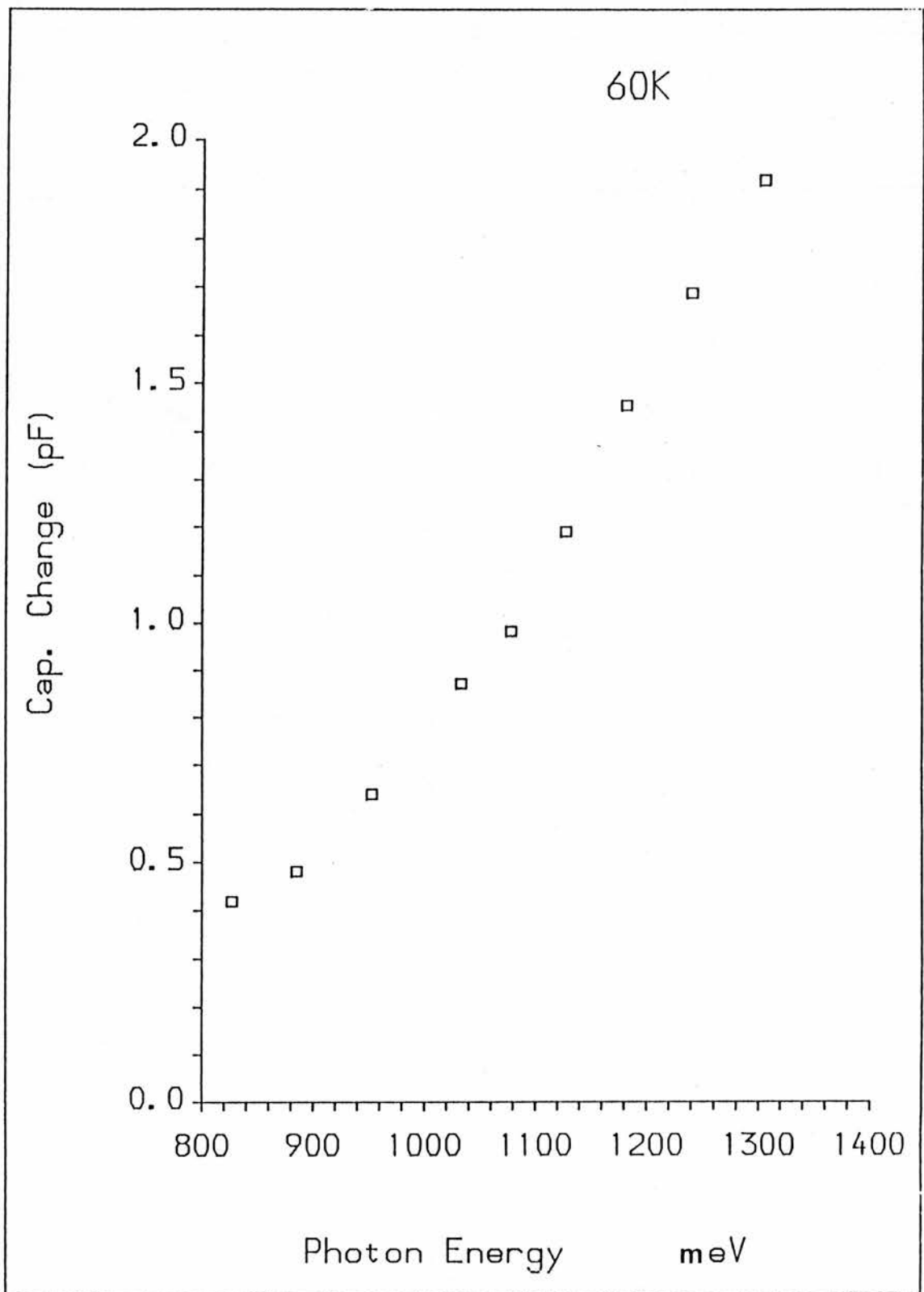


Figure 4.10 The total capacitance change against photon energy at 60K when diode P193-CR2*1 was under secondary illumination with germanium filtered tungsten light.

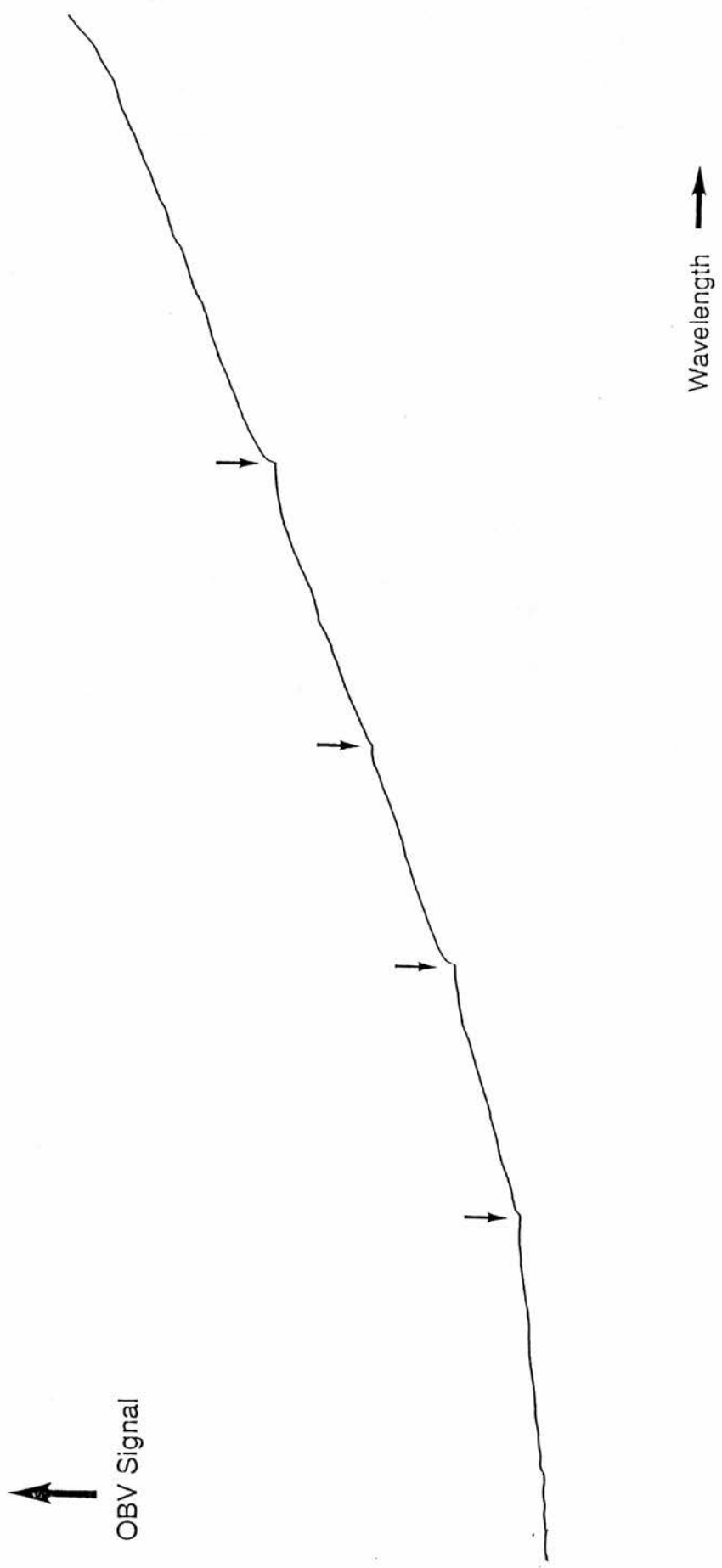


Figure 4.11 A trace showing the cumulative capacitance change against photon energy at 150K showing sharp changes in capacitance ("thresholds") at certain well-defined energies (diode P193-CR2*1).

4.4 Discussion

The capacitance changes upon illumination in this present work are positive, from 0.4eV up to above 2eV photon energies, indicating more positive charge in the depletion region thus showing that the transitions result in electrons in the conduction band.

There appear to be two centres detected in these present photocapacitance experiments. One has a concentration (or more correctly, a maximum occupancy change) of $3 \times 10^{14} \text{ cm}^{-3}$ at 60K, an optical ionisation energy of less than 0.6eV, and is only seen at temperatures below about 130–140K. The other centre shows an occupancy change of $1.5 \times 10^{14} \text{ cm}^{-3}$, an optical ionisation energy of 1.1eV and is present from the lowest temperatures used (40K) up to above 200K.

It seems reasonable to associate the first level referred to in the last paragraph (the shallower level) with the level which gives a thermal activation energy of 0.21eV through thermal emptying measurements in the same (100–150K) temperature range as the capacitance change due to the lower level decreases to near zero values. It was not possible to fit one of the photoionisation cross-section models to the data, as the errors associated with the points are too large for the information obtained to be meaningful. However, the cross-section rises to very close to its maximum value by 0.7eV (neglecting the onset of the higher photon energy level). Since the simple Lucovsky^[62] model predicts a maximum in the cross-section at twice the optical threshold energy, E_i , as does the Lucovsky derived thermally broadened model of Piekara *et al.*^[63], then we can suggest that the optical ionisation energy parameter for this transition is between 0.35 and 0.5eV. This is a large energy uncertainty.

At first, it was thought that this transition, with the lower energy threshold, was due to photoionisation of the isolated substitutional Cr d^5 configuration to the conduction band (as was reported by Szawelska^[35]), but this hypothesis was rejected for a two-fold reason: the energy depth is inconsistent with energy parameters found for the complementary transition^[57]; the transition with the higher threshold is a much improved candidate for the $d^5 \rightarrow d^4 + e_{cb}$ transition.

One possible candidate centre, responsible for the 0.35–0.5eV optical threshold level, could be a complex consisting of a chromium on a zinc site associated with another defect also present in quite high concentrations. A possible associate is a selenium vacancy, since it is thought that selenium vacancies exist in high concentrations and are quite stable. Attempts to test this idea by annealing out the vacancies would probably be very difficult, as the zinc ions are much more mobile, and even if successful the vacancy is one source of donors for electrons, so the conductivity would be decreased making the experiment more difficult. Suto *et al.*^[64] found a maximum in the EPR photoexcitation spectrum of the d^5 level at 2.55eV, which they believed due to the $d^5 - d^4$ level of the isolated substitutional chromium being at an energy of about 0.3eV below the conduction band minimum. This energy is similar to that expected for the hole transition to the valence band from the unidentified 0.35–0.5eV (relative to the conduction band) deep level, as 2.55eV plus (0.35 to 0.50)eV equals E_g plus (0.15 to 0.30)eV, could give a relaxation energy in the range 0.08–0.15eV. Röppischer *et al.*^[56] have EPR photo-quenching spectra which show a threshold at 0.4eV which is more pronounced in their more heavily chromium doped sample (samples doped using Cr_2Se_3 during growth), whereas chromium–vacancy complexes are more likely to be found at low chromium concentrations (as in our sample).

Similar complexes between transition metal ions and native defects, as is suggested above, are thought to exist in GaAs:Cr and in GaP:Ni. The evidence in GaAs is particularly strong for the 0.839eV intracentre photoluminescence line seen by Fujiwara *et al.*^[65], among others, to be due to a complex between chromium and an arsenic site vacancy, after a suggestion by Skolnick *et al.*^[66]. Baranowski *et al.*^[67] have suggested a similar nickel-related centre in gallium phosphide. It is well to remember that the identification of these centres is often a long process with several quite convincing 'red herrings'.

The size of the capacitance change in the photon energy regime up to 1.1eV decreases with increasing temperature until there is no change at all discernible at 150K when a photon energy of 0.70eV was used. The fact that there is a threshold in the photocapacitance spectrum at 150K, even if it is not very clearly defined, suggested that it could be possible to fit this spectrum to the thermal photoionisation broadening model of Piekara *et al.*^[63] ('the Piekara model') as Kamińska *et al.* had done for the complementary transition^[57]. The spectrum has a good fit to the Piekara model using an optical energy parameter of 1.12 ± 0.01 eV. This is not inconsistent with the expected energy, of 1.15eV, using the Kamińska *et al.* configurational coordinate diagram, and an energy gap of 2.75eV at 150K. The fitting of the 150K spectrum using the Piekara model generates a thermal broadening parameter, Γ , equal to 0.28 which seems unreasonably large when compared with the 60K photoquenched spectrum (with low photon energy background cross-section subtracted) which yielded $\Gamma = 0.10 \pm 0.03$. These compare with the values taken from the Kamińska^[57] *et al.* paper of 0.14 ± 0.01 at 150K and 0.10 ± 0.01 at 60K. It should be noted that the ground state of the d^4 configuration is Jahn-Teller split^[68] making a single coordinate description of the state a fairly crude approximation.

The Kamińska *et al.* values for E_{opt} and Γ were calculated with the assumption that the level is pinned to the valence band as the energy gap decreases with increasing temperature. Fits were made to the data of Kamińska *et al.*^[57] using assumptions of the energy level being pinned: 1) to the conduction band minimum and 2) to the valence band maximum. Equally good fits to their data can be obtained by either of the pinning assumptions, as can be seen in figures 4.12 and 4.13. The values for Γ calculated are then increased (to $\Gamma = 0.16 \pm 0.01$ at 150K). In reality the level will almost certainly not be pinned to either the conduction band minimum or valence band maximum, but will move in some manner between these two extremes. It might be that the position of the deep level, with respect to the vacuum energy level, varies less than the position of either of the band extrema.^[69] Values for the energy gap of ZnSe at different temperatures used in the fittings were taken from the temperature dependency of the bandgap excitons as measured by Hite *et al.*^[70].

The positive capacitance change seen in the high photon energy regime up to band gap energies means that the capacitance change is not due to the $d^4 \rightarrow d^5 + h_{\text{vb}}$ transition. I cannot see any reason to exclude the possibility of the creation of the d^3 configuration. This could be true only if the $d^4 - d^3$ level lies well within the bottom half of the energy gap, as is thought to be the case. Grebe *et al.*^[60] have an absorption band which they suggest to be the photoionisation of the d^4 state at a photon energy of 2.36eV. Above bandgap photon energies the capacitance decreases at each threshold indicating decreases in the positive charge in the depletion region.

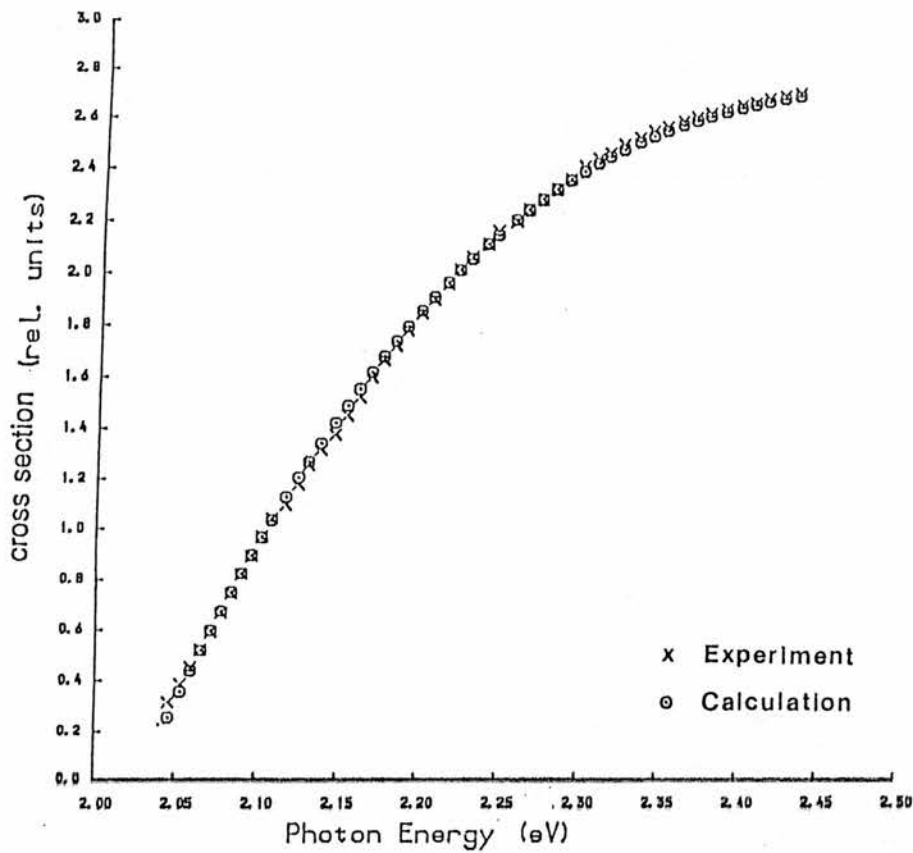


Figure 4.12 The EPR-derived photolionisation cross section data of Kamińska *et al.*^[57] (at 150K) is fitted by a line calculated from the photolionisation broadening theory of Plekara *et al.*^[63] with an optical ionisation parameter of 1.15eV (level pinned to valence band maximum).

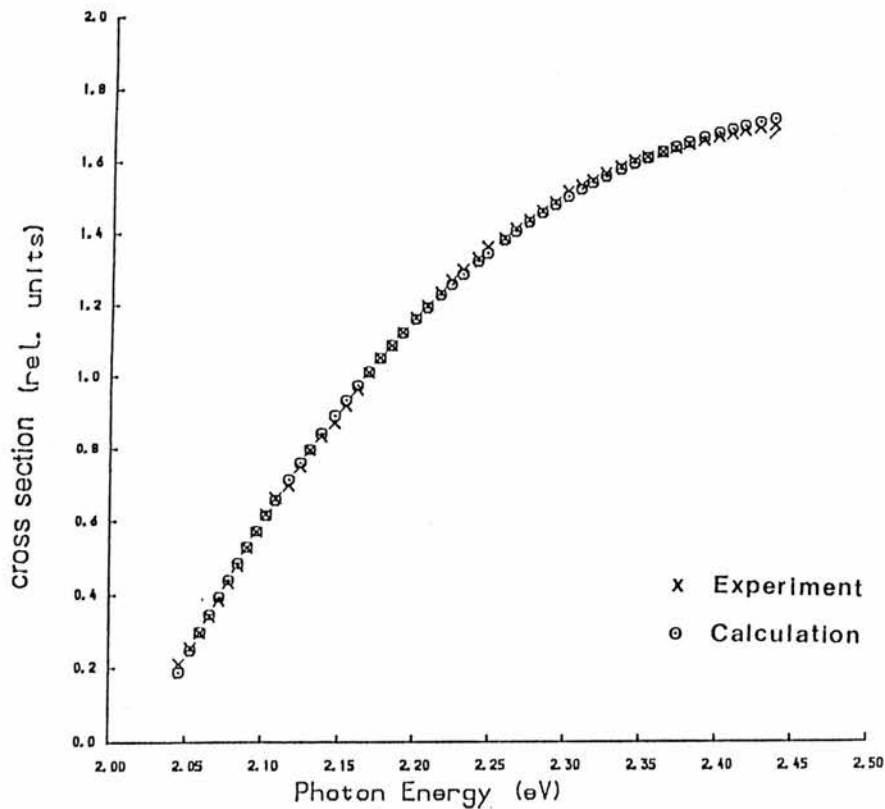


Figure 4.13 The EPR-derived photoionisation cross section data of Kamińska *et al.*^[57] (at 150K) is fitted by a line calculated from the photoionisation broadening theory of Plekara *et al.*^[63] with an optical ionisation parameter of 1.115eV (level pinned to conduction band minimum).

4.5 Conclusions

In this work we believe that we have seen charge transfer transitions involving two centres. One involves the isolated zinc substitutional chromium d^4-d^5 level, lying 1.1eV below the conduction band and having a minimum d^5 concentration of $1.5 \times 10^{14} \text{ cm}^{-3}$ when in thermal equilibrium at 150K. The energy position of the level is consistent with previous reports. The other level, optically 0.35–0.5eV below the conduction band (for a vertical transition on a configuration coordinate diagram), could be the product of a zinc substitutional chromium atom complexing with another defect, possibly a selenium vacancy. This level showed occupancy changes of up to $3 \times 10^{14} \text{ cm}^{-3}$ at 60K. The level is thermally quenched above 150K.

Chapter Five:

Vanadium in Zinc Selenide

5.1 Introduction

Vanadium is becoming a much studied impurity in III-V materials, particularly since it had been shown that vanadium doping of GaAs could produce material which is semi-insulating^[71]. Vanadium in II-VI materials has been, in comparison, not much studied and its behaviour is not well understood. Experimental investigations of ZnSe:V have been very scarce in recent years; however some theoretical predictions of level positions and excited state structure have been made.^[72,73] The work presented in this chapter probably represents the first study of the ZnSe:V system with the photocapacitance technique. Before we look at the present experiments, a short review of many of the experimental studies which have been performed on the system will be given. The known applied techniques include optical absorption, luminescence and EPR measurements. The structure of the rest of the chapter is as follows: in Section 5.2 the history and preparation of the samples, together with the experiments performed upon the samples, are described. The results are presented in Section 5.3 and are discussed in Section 5.4. The chapter ends with a short summary of the main conclusions (Section 5.5).

Meijer and Avinor^[74,75] in the early 1960s measured the luminescence emission from vanadium doped ZnSe, ZnS, CdS and CdSe powder phosphors at room temperature and liquid nitrogen temperature. The excitation light used was wide-band with a lower cut-off at an energy at about 0.9eV. They found the luminescence emission from ZnSe:V in three bands at about 0.56eV. The emission was very weak compared to similar emissions from the other vanadium doped materials. In contrast to the enhancement of luminescence seen in other II-VI materials, co-

doping ZnSe:V with either copper or silver severely attenuated the luminescence. The results were later interpreted by Allen^[76] to be consistent with an energy level distribution arising from a d^2 configuration in a tetrahedral crystal field with $|\Delta| = 0.653\text{eV}$ (5150 cm^{-1}).

Holton *et al.*^[77] performed EPR experiments on zinc sulphide doped with vanadium, concluding that they had observed the d^2 configuration with a g value of 1.9433 ± 0.0005 .

Allen and Wray^[78] in the late 1960s performed a series of absorption measurements at liquid helium temperature on several different 3d impurities in ZnSe (V, Cr, Fe, Ni, Co and Cu) in an attempt to show the variation of the crystal field parameter (Δ) across the 3d transition series. In the case of ZnSe:V they found a set of very strong absorption lines with a dominant group of lines near 1.18eV (9500cm^{-1}) (the width of the group of lines/band was approximately 0.25eV), as well as groups of lines at both lower (around 0.75eV) and at higher energies.

Hoang and Baranowski^[79] conducted a series of absorption experiments on vanadium in several different II-VI semiconductors (ZnS, ZnSe, CdSe and CdTe). They obtained the same strong ($> 50\text{cm}^{-1}$) absorption in ZnSe:V, at slightly different photon energies, as was obtained by Allen and Wray. Hoang and Baranowski suggest that the differences in energy positions of the lines were due to spectrometer calibration. The 50cm^{-1} maximum value for the ZnSe:V absorption compares with 15cm^{-1} in ZnS:V and 18cm^{-1} in CdSe:V. (Of course, the absorption coefficient depends on the concentration of the impurity centre and the degree to which the level is filled as well as the oscillator strength of the transition. So, although large in ZnSe:V this figure might be a

concentration effect.) They found many other lines in the range 0.5eV to 2.0eV. Many of these lines are given in the first column of Table 5.2.

In photoluminescence experiments^[79], excitation at 1.18eV (9500cm^{-1}) was found to give the maximum luminescent intensity. The emission maxima occurred at 0.558eV, 0.577eV and 0.639eV (4500 , 4650 and 5150cm^{-1}). The difference in energy between the excitation light and the emission is too large to be accounted for by a Franck–Condon shift in the excited states of the vanadium ion. The relaxation processes must include thermal as well as radiative effects. The authors believed that the absence of a structure in the absorption spectrum mirroring that in luminescence suggested that the d^3 ground state was not the state at which the radiative transition terminated. There is a rising edge, possibly a photoionisation edge, in their spectrum with a threshold at around 1.9eV.

There has been some discussion as to whether the lines seen in absorption spectra arise from the d^2 or d^3 configurations. Allen & Wray^[78] and Hoang & Baranowski^[79] have suggested a d^3 configuration is responsible for the absorption lines seen, but assign different values to the crystal field splitting parameter. In fact whether the d^2 or d^3 or a distribution of both states is seen depends on the position of the d^2 – d^3 level and the Fermi level position in the energy gap. Another question arises if the d^2 – d^1 level lies within the gap then it might be possible to see effects due to the d^1 configuration in some circumstances (such as a p-type crystal or two-stage photoionisation (refer to Section 6.4 [eqn 6.6]).

5.2 Samples and Experiments

This section describes the preparation of the samples used and the experiments performed upon them. Two samples, obtained from different sources, were utilised. The first sample, upon which the majority of the experiments were conducted, was grown from its elemental constituents at St Andrews in January 1971. The material, known as E11, was doped with aluminium during the growth. In July 1977 the material was made conducting by means of a zinc/aluminium treatment^[35,80]. In February 1978 the material was diffusion doped with 3.5g vanadium and 4g zinc in an ampoule at a temperature of 900°C. The material was removed after 170 hours. The material was then labelled as 'E-11 Vanadium'. The material was found to have remained conducting and its colour was a fairly uniform yellow. H. R. Szawelska performed some preliminary photocapacitance experiments on a diode made from this material in March 1978^[80]. The contacts were removed immediately after this experiment. In November 1981 one piece of the material was remade into a diode by forming Ohmic indium/tin contacts on one side of the sample and evaporating a 1mm diameter semi-transparent gold dot onto the opposite side. The sample was stored under propanol until I started work with it in March 1987. The five year old contacts appeared still to have good rectifying properties. The diode was labelled as and will be referred to as 'E11-V-1'.

The second sample was obtained from a piece of ZnSe grown in June 1971, obtained from R. A. Stradling (P193). A piece of the material underwent a zinc-aluminium conductivity process in July 1981, after which it was found to be conducting. In November 1981 one piece from the 'P-193 Z.T. (18/7/81)' material was diffusion doped with vanadium by heating the sample, vanadium and zinc together in a silica tube to 900°C.

for 140 hours. Although the material had a dark appearance it remained conducting. Similar gold Schottky and In/Sn contacts to those put on the E11-V-1 diode were made. The sample was not stored under propanol between the fabrication of these contacts and March 1987. When I tried to use the existing diode contacts a capacitance balance could not be achieved. The diode was remade. Two Ohmic indium contacts were contacted onto on one side and an aluminium Schottky contact was evaporated onto the opposite side. During the process the sample split into two unequal parts. The larger fragment was used for the experiments.

The first sample to be studied was the first described above, that is E11-V-1. Capacitance–voltage plots were taken, in the dark and whilst under constant illumination with a source of photon energy 1.378eV (900nm), at a temperature of 37K, in order to find the concentration of donors in the sample. The capacitance was measured on the photocapacitance bridge described in Chapter Two. Initial photocapacitance measurements produced a very large positive capacitance change (off scale – subsequently found to be overloading the amplifier) at photon energies greater than about 1.1eV. The pleasant 'problem' of amplifier overload was resolved by reducing the signal generator voltage by a factor of four from its last value of 6mV to 1.5mV peak–to–peak.

Photocapacitance transient experiments were performed over a wide range of photon energies from 0.39eV (3.2 μ m) to 1.91eV (650nm). A Spex 1670 monochromator with appropriate diffraction gratings and order filters for different spectral ranges was used as a monochromatic light source. In the photon energy range 0.39eV (3.2 μ m) to 0.62eV (2.0 μ m) no glass focussing lenses were used because ordinary glasses absorb strongly in this region. Scanned wavelength photocapacitance spectra were taken

at room temperature in several ranges covering the interval 0.39eV to 3.1eV. The lowest scan rates possible with the stepper motor driver were used.

Extraordinary phot capacitance transients were taken to measure the absolute value of the photoionisation cross section at room temperature. A Bausch and Lomb high intensity monochromator was used together with interference filters of pass-band centres 950nm (1.305eV) and 850nm (1.459eV) to provide the necessary monochromatic light. The bandwidth of both the interference filters was 10nm (0.013eV at 950nm). The light was shone directly onto the diode with no focussing optics. The absolute intensity of the light incident on the depletion region was estimated by placing a thermopile in an exactly (as far as possible) equivalent position. The reason why no focussing optics were used was to ensure that the re-positioning of the thermopile at the exact position occupied by the sample is not crucial. A small discrepancy will only produce a small error between the flux on the sample and that on the thermopile.

Whilst the diode was illuminated it was found that to balance the bridge the series equivalent resistance in the bridge had sometimes to be changed somewhat more than in other materials studied in this thesis. This fact suggested that the photoconductive behaviour of the sample should be investigated. To this end, photoconductivity transients were taken using the same Schottky contact and Ohmic contact as in the phot capacitance work. The method of illumination was also unchanged. The photocurrent was measured with a Keithley 602 electrometer with the 1V output connected to a chart recorder. The measurements were carried out at room temperature in the photon energy range 1.033eV (1200nm) to 1.908eV (650nm), since lower energies had not shown any detectable

photocurrent (less than 10^{-13} A). Swept wavelength photoconductivity measurements were taken over the range 1.033 to 1.771eV (1200–700nm).

Thermal emptying measurements were performed to attempt to find the thermal depth of levels below the conduction band. A positive bias was applied for ten seconds to fill the level to be emptied. Traces were set running ready for when the bias was relaxed. The time of the applied positive bias was varied but no change in the form of the thermal relaxation was detected. In the temperature range 60K to 120K initially a voltage of +1.2V was used. It was found that this value could be decreased to +0.6V without affecting capacitance relaxation times. In the case of the higher temperature emptying experiment the initial bias used was +1.9V which was later reduced to +1.3V.

Experiments were performed with two light sources. A tungsten lamp with a germanium filter was used to attempt to bleach out centres closer to the conduction band than the filter cut-off energy (0.75eV). Measurements were taken in the range 0.85eV to 1.15eV (1500–1100nm).

A smaller number of experiments were carried out on the diode labelled as P193-V-1. A low temperature photocapacitance sweep showed no measurable capacitance change between 0.39eV and 0.80eV ($3.1\mu\text{m}$ to $1.55\mu\text{m}$). Preliminary photocapacitance investigations, carried out at room temperature, revealed a small peak below a rising edge. The maximum of the peak was at a photon energy of just under 1.0eV. A maximum at about the same photon energy was found in the magnitude of the capacitance change after illumination for many minutes, the maximum remained even after correcting for incident photon flux. This feature subsequently proved to be an experimental artifact arising from reflections from the monochromator entering the unused second optical

window of the cryostat which had been left unscreened since the second sample was first introduced into the cryostat. Once this problem had been recognised and corrected photocapacitance measurements were repeated at room temperature (300K), 78K and 150K. Measurable photocapacitance changes were recorded at photon energies well below 1.0eV. This was in marked contrast to the room temperature case. Photocapacitance spectra were taken at room temperature and at 78K. Double light source 'bleaching' experiments were performed as for the first diode E11-V-1.

5.3 Results

First we will look at the results of the experiments performed on the diode labelled E11-V-1 and then the smaller number of experiments carried out on diode P193-V-1 will be presented for comparison.

The capacitance–voltage measurements at 37K yielded donor concentrations of the reasonable order of 10^{16} – 10^{17} cm^{-3} with significant increases after illumination, increases which were significant enough to be measured easily using C–V measurements. The increase in capacitance during illumination shows that the positive charge concentration in the depletion region increases during 1.378eV illumination. The precise values for the donor concentrations and measured barrier heights are given in table 5.1. Szawelska performed a C–V measurement on an earlier diode made from this sample obtaining a donor concentration of 3.1×10^{17} cm^{-3} [80] at room temperature, very similar to the result obtained here at 37K, if the cable capacitance is not subtracted before calculating the donor density. Szawelska, however used a Wayne–Kerr 601 bridge for this measurement. The nulling procedure for this bridge takes most of the cable capacitance into account in the measurement. Therefore the donor density decreases from 3.1×10^{17} at 300K to 4.4×10^{16} cm^{-3} at 37K, probably due to the freezing-out of the deeper lying donors.

The room temperature transient photocapacitance spectrum is given as figure 5.1. The capacitance changes associated with these transients are shown in figure 5.2. The corresponding results at 37K are given as figures 5.3 and 5.4. It can be seen from the first four figures, that at all temperatures in the range 35–300K the dominant transition in the transient photocapacitance spectrum has a threshold of a little over 1 eV.

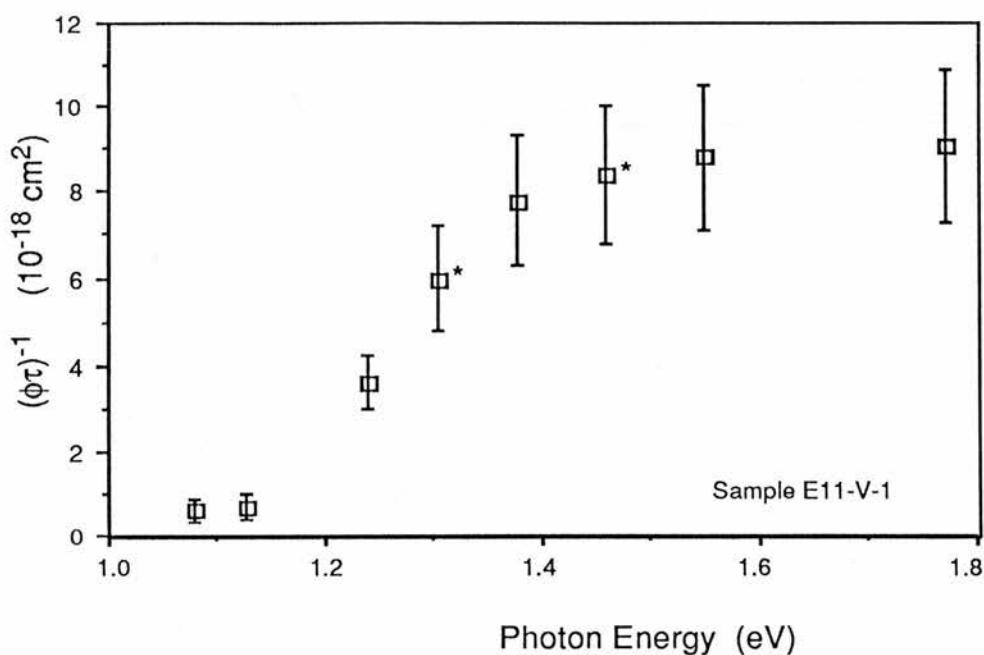


Figure 5.1 The absolute photoionisation cross section spectrum of the ZnSe:V d^2-d^3 level in diode E11-V-1 at room temperature. The symbol * marks the two points for which the absolute value of the cross section was determined experimentally. The other points have been normalised relative to the starred points.

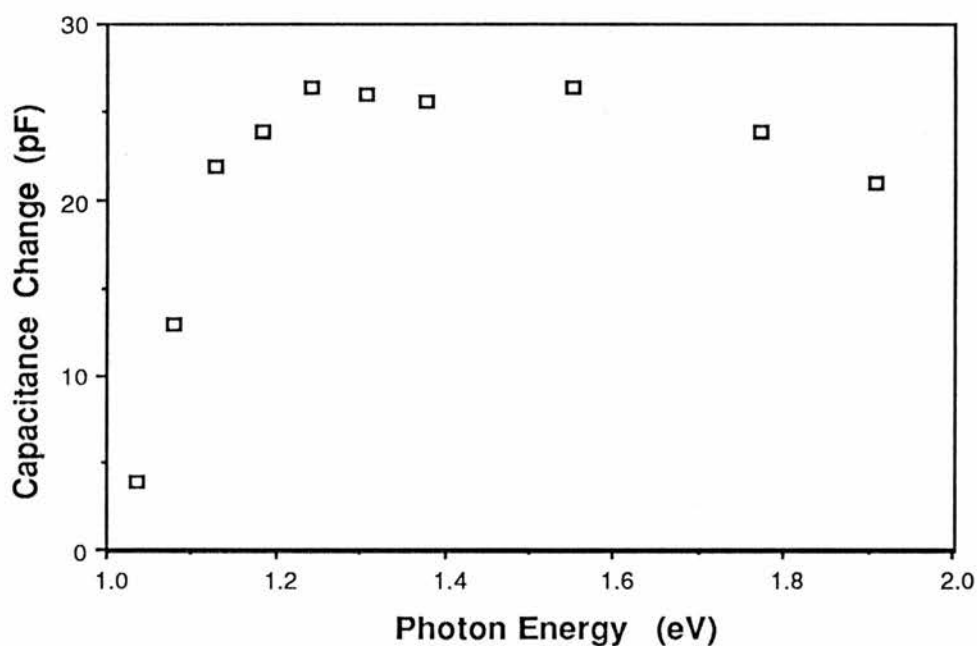


Figure 5.2 The total change in capacitance seen in transient photocapacitance experiments on the vanadium doped zinc selenide diode E11-V-1 at room temperature (300K).

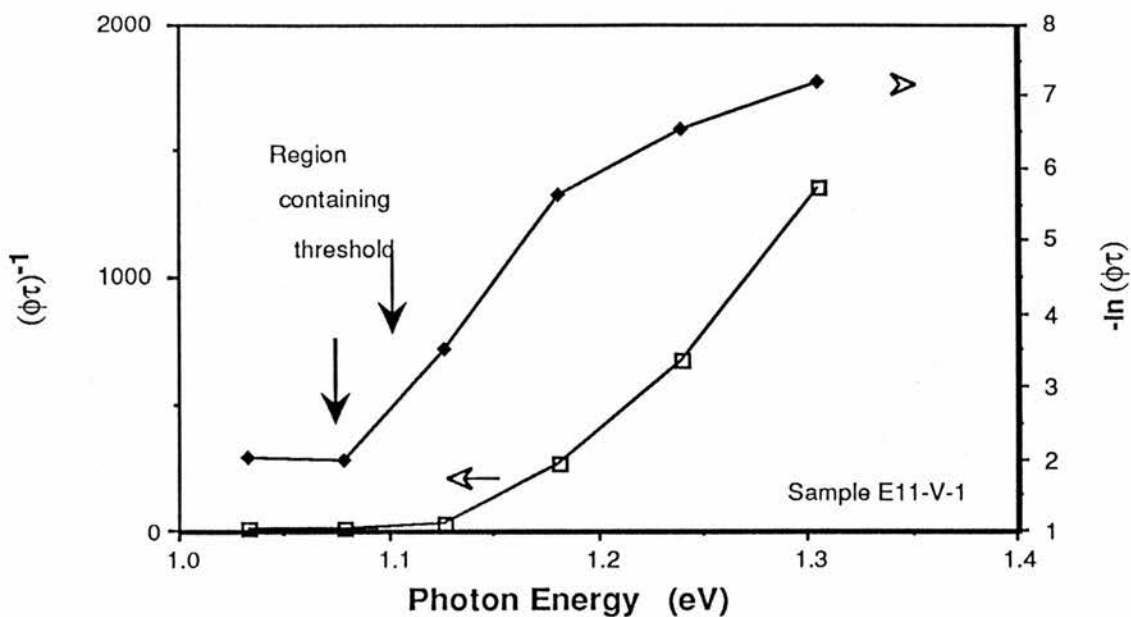


Figure 5.3 The photoionisation cross section spectrum of vanadium in zinc selenide diode E11-V-1 at 37K. The data is plotted both linearly (axis to left) and logarithmically to base e (axis to right). The vertical scale is in relative units.

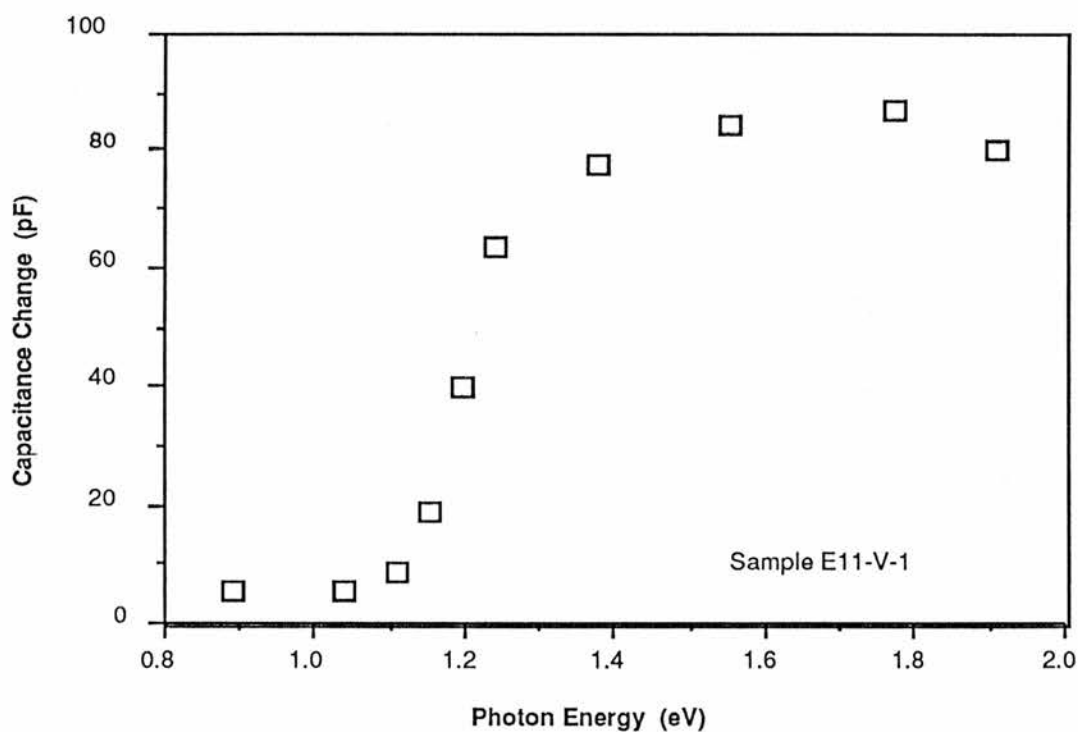


Figure 5.4 A graph of the total capacitance change against photon energy for ZnSe:V diode E11-V-1 due to monochromatic light. The sample temperature was 37K.

At the lowest temperatures light in the photon energy range 1.3–1.6 eV promotes a maximum capacitance change of about 85pF on a total device capacitance of approximately 350pF. At higher temperatures the capacitance change decreased, until at room temperature the same photon energy range as quoted above gave a change of approximately 30pF. The transition appears to be thermally quenched at temperatures around 500K as can be seen from looking at the capacitance change at 1.127eV (1100nm) against temperature which is illustrated in figure 5.5.

The absolute value of the optical cross section for the photoionisation transition at room temperature was calculated from the measured transient time constant and photon flux to be $6.0 \pm 1.0 \times 10^{-18} \text{ cm}^2$ at a photon energy of 1.305eV. A second result was obtained for 1.459eV photon energy, the value of which was found to be $8.3 \pm 1.6 \times 10^{-18} \text{ cm}^2$. No allowance has been made in the calculation for losses in photon flux at the cryogen–gold and gold–semiconductor interfaces. Thus these figures represent minimum values of the absolute photoionisation cross section.

At lower temperatures, a lower photon energy threshold occurred at around an energy of 0.47eV. The associated total level occupancy change was $1.4 \pm 0.1 \text{ pF}$ at 37K when a photon energy of 0.517eV ($2.4 \mu\text{m}$) was used. This capacitance change equates to a level occupancy change of about $4 \times 10^{14} \text{ cm}^{-3}$. A graph of the capacitance change against photon energy at 37K for this spectral region is shown in figure 5.6. The only significant threshold found in low temperature swept photocapacitance measurements in the 0.39eV to 1.0eV photon energy range occurred at an energy of $0.47 \pm 0.01 \text{ eV}$ ($2.635 \mu\text{m}$).

Swept wavelength photocapacitance spectra at room temperature showed two "thresholds" (the distinction between a threshold and a

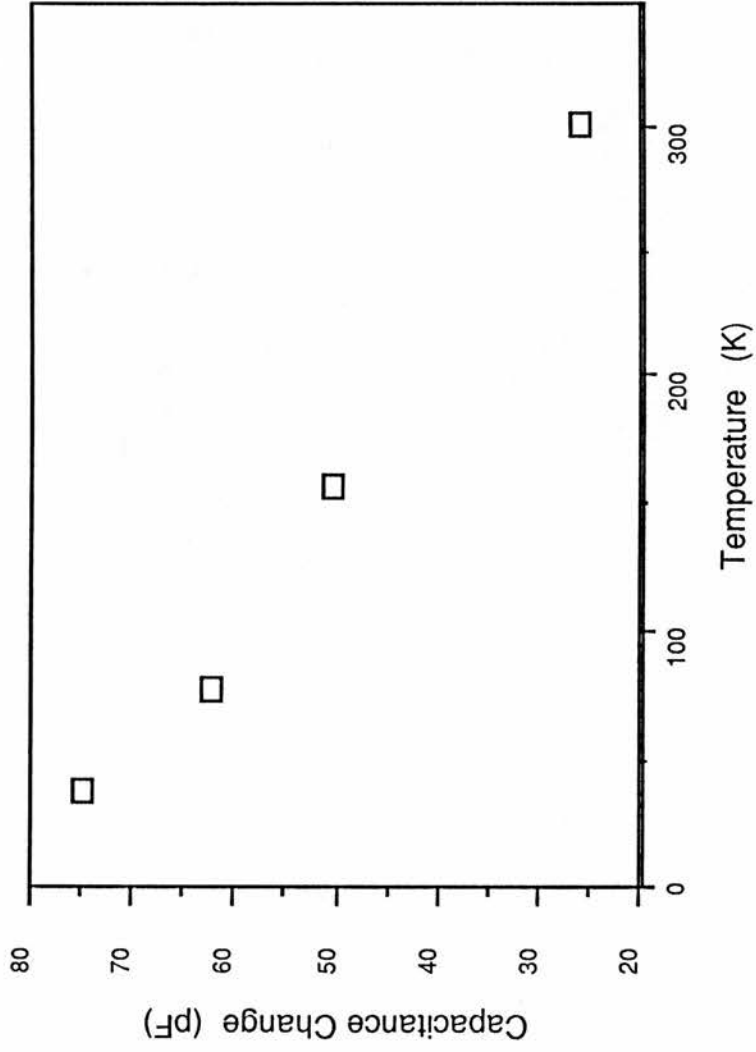


Figure 5.5 A graph of the total capacitance change of diode E11-V-1 against temperature after illumination with light of photon energy 1.378eV (900nm).

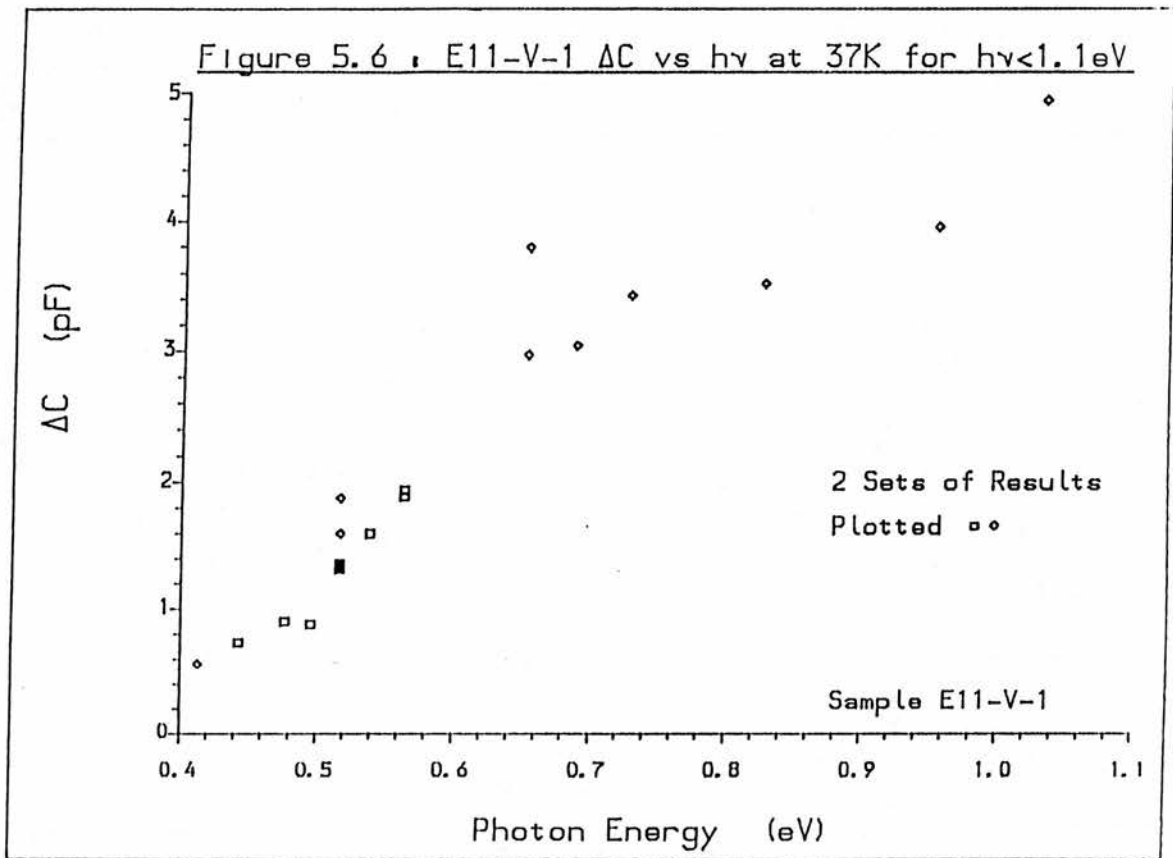


Figure 5.6 The total capacitance change for low photon energies (0.4–1.0eV) in ZnSe:V diode E11-V-1 at 37K.

"threshold" is discussed in the following section), at 1.075eV (1.155 μ m) and at 1.150eV (1.080 μ m) in the region of the $d^3 \rightarrow d^2$ photoionisation edge. A portion of the OBV from a typical swept spectrum recording is shown in figure 5.7. At higher photon energies more positive capacitance "thresholds" were found. All the "thresholds" found at photon energies up to 1.9eV are tabulated in Table 5.2. Swept wavelength results in the higher photon energy range 1.9 to 3.6eV showed a large number of capacitance "thresholds". Upon comparison with similar measurements on the ZnSe:Cr diode many of these "thresholds" could be attributed to the host crystal or common impurities present at lower concentrations than the intentional dopants. A longer discussion of these so-called "thresholds" can be found in Appendix 5.1.

The two sets of thermal emptying experiments gave two very different activation energies. The one which was performed over the temperature range 80–120K, with a 0.6V forward bias, gave an activation energy of 0.08 ± 0.04 eV (figure 5.8). In the range 290–450K with a 1.3V forward bias, an activation energy of 0.41 ± 0.03 eV was obtained (figure 5.9).

Photoconductivity transients in the photon energy region 1.03–1.55eV showed both transient and steady-state components, as can be seen in the example transient shown in figure 5.10. The variation of the maximum value of the transient component with photon energy (figure 5.11) showed a similar general behaviour to the capacitance change spectrum. In particular there is a threshold in the region 1.0–1.1eV, rising until 1.38eV after which the maximum transient photocurrent decreased again to less than half of the peak value. The maximum value of any transient current after subtracting the (assumed constant) steady state photocurrent was 2.2pA. A study of the photocurrent integrated with respect to time was undertaken for the transient element of the current. This should be

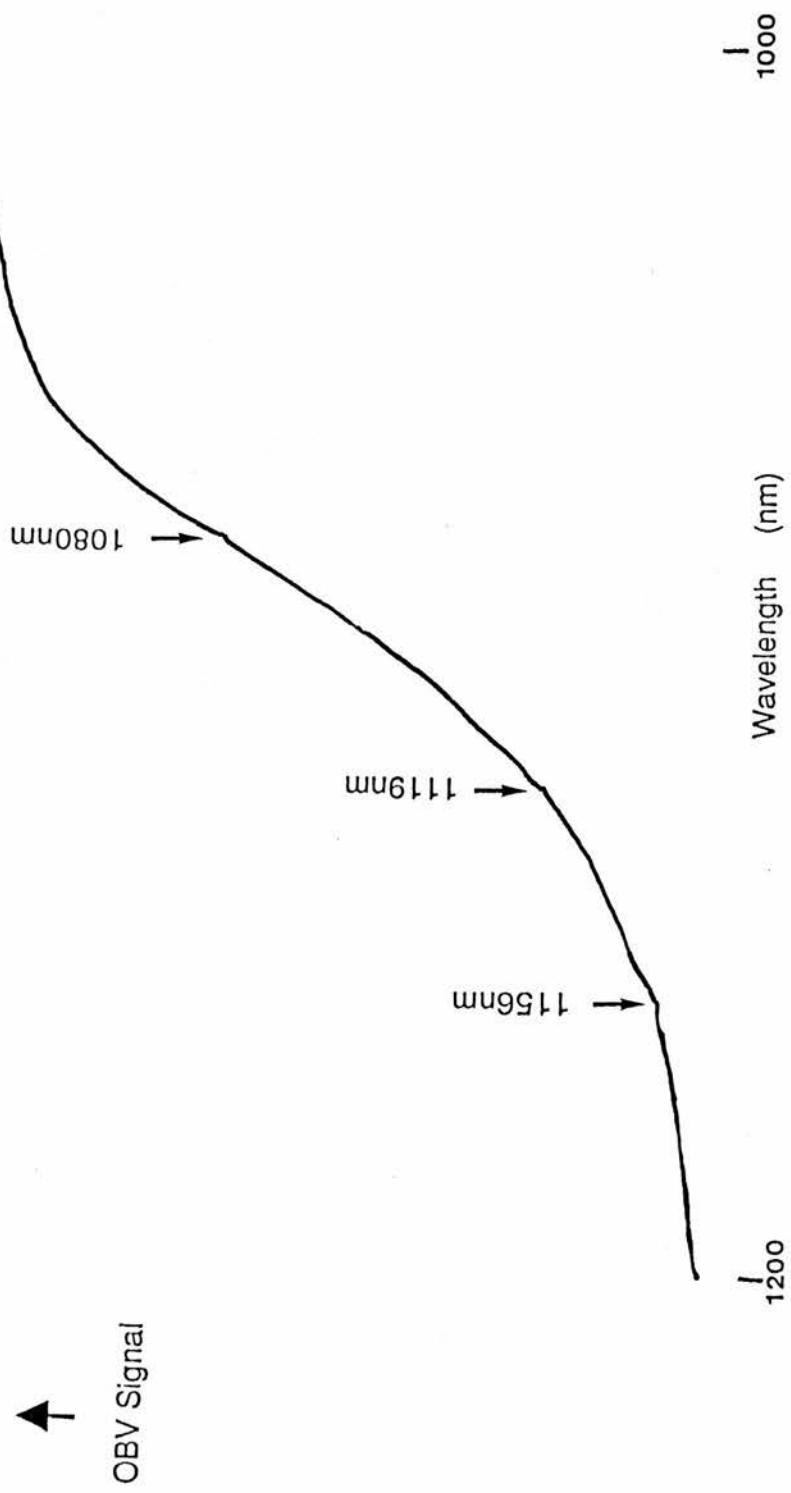


Figure 5.Z An example of a swept capacitance spectrum for sample E11-V-1

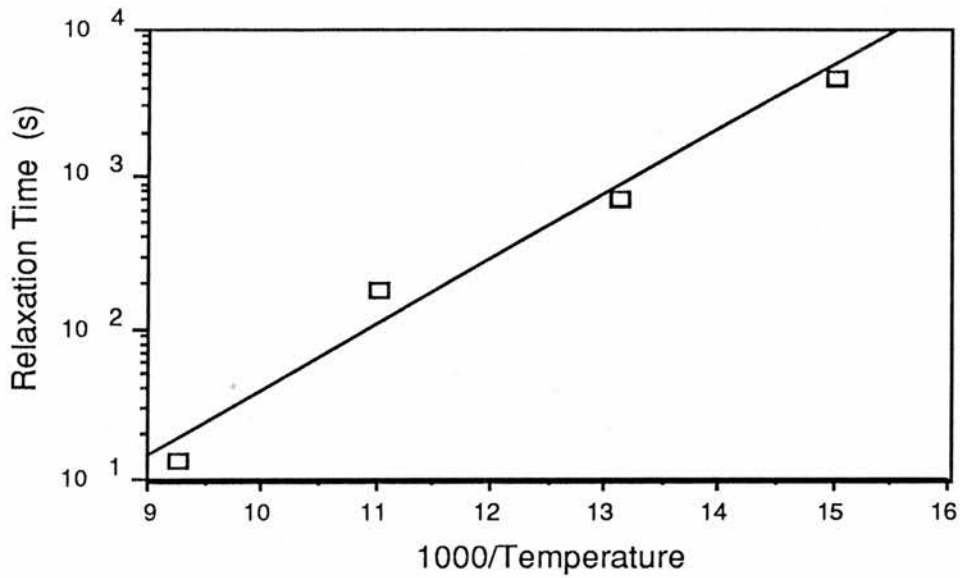


Figure 5.8 A plot of the low temperature (67K–108K) thermal relaxation time of the capacitance of diode E11-V-1 after the cessation of an applied forward-bias. The best fit line corresponds to an activation energy of $0.08 \pm 0.04 \text{ eV}$.

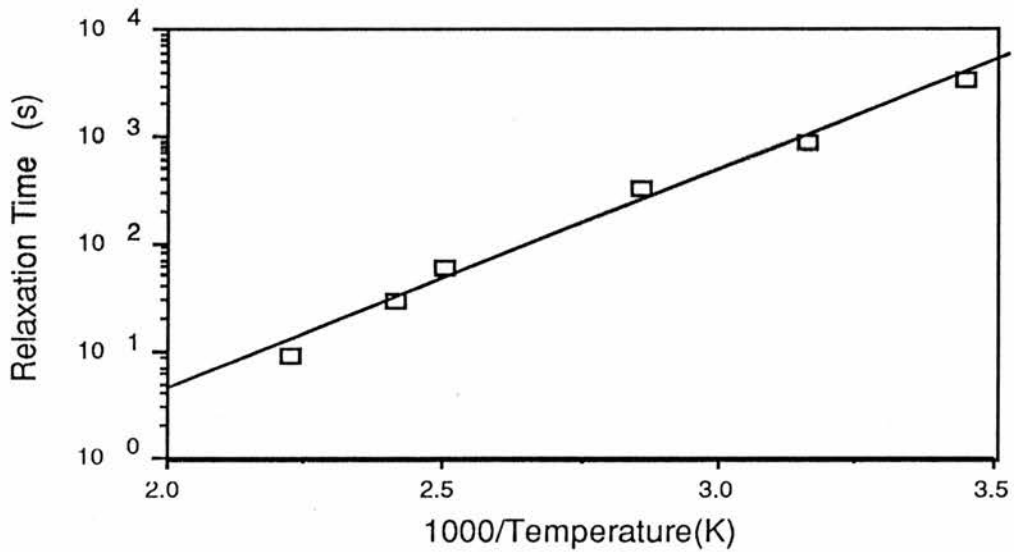


Figure 5.9 A plot of the high temperature (290K–450K) thermal relaxation time of the capacitance of diode E11-V-1 after the cessation of an applied forward-bias. The best fit line has a slope (error) corresponding to an activation energy of $0.41 \pm 0.03 \text{ eV}$.

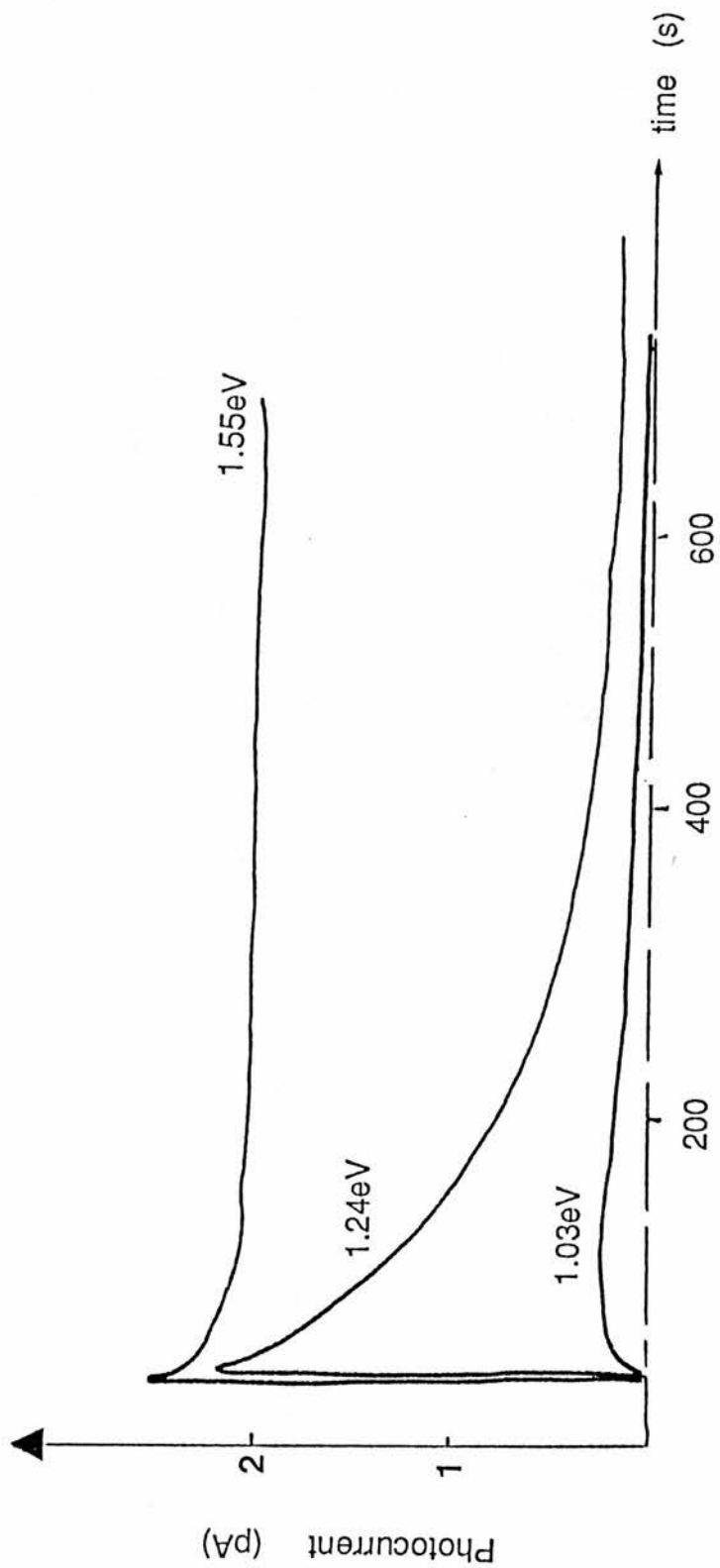


Figure 5.10 Three examples of photocurrent transients for sample E11-V-1 at different photon energies ($h\nu = 1.03, 1.24$ and 1.55eV). It can be seen how the transient photocurrent increases at lower energies than the steady state photocurrent.

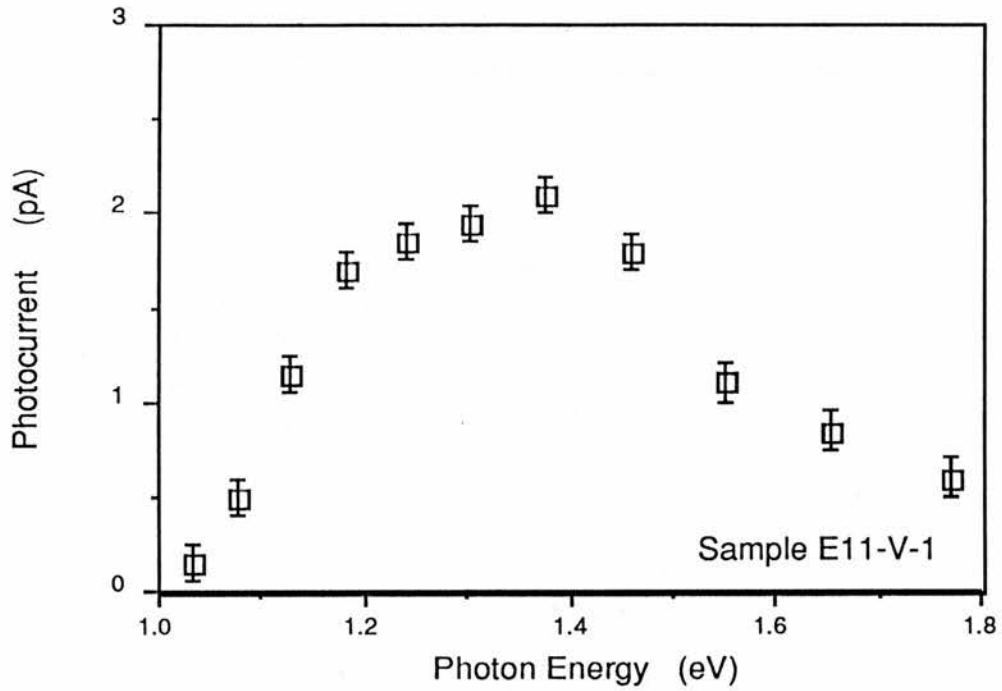


Figure 5.11 A graph of the maximum transient photocurrent (steady-state photocurrent subtracted) for sample E11-V-1 at room temperature.

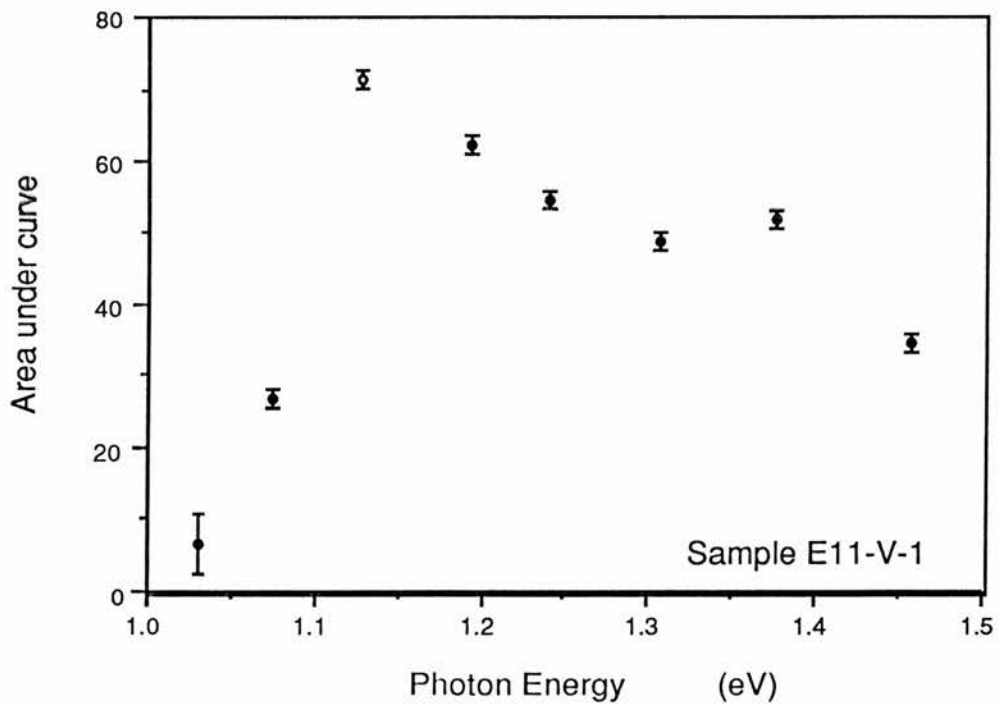


Figure 5.12 A graph of the spectral dependence of the area under the transient part of the photoconductivity trace produced by monochromatic light, on sample E11-V-1. The area of the trace is a measure of total transient charge flowing through the sample.

related to the total charge released from the depletion region. The results are given as figure 5.12. The steady state element of the photocurrent traces had a higher threshold (about 1.30–1.35eV) than the transient part. The value is similar to the theoretical Schottky barrier height. The maximum steady state photocurrent measured was 2.6pA. Swept wavelength photoconductivity measurements gave threshold behaviours (slow scan – quasi-steady state) at 1.075eV (1155nm), 1.102eV (1125nm), 1.108eV (1119nm) and 1.148eV (1080nm). These thresholds can be seen alongside the swept photocapacitance thresholds in column four of Table 5.2. A tracing from a chart recording containing photoconductivity thresholds is shown in figure 5.13.

The second sample, diode P193-V-1, had a capacitance of the order of one hundred picofarads at room temperature. A lower value was expected because of the aluminium Schottky contact which has a lower barrier height than that for a gold contact. Upon illumination with light of near infra-red photon energies (0.8–1.2eV) capacitance changes of the order of one pF were observed, certainly a small change in overall capacitance, when compared to the first sample. The capacitance change against photon energy is shown in figure 5.14. The cross section spectrum is shown in figure 5.15. The double light source photocapacitance changes at 78K are also shown in figure 5.14, alongside the capacitance changes with no secondary illumination.

A room temperature swept wavelength spectrum showed no detectable changes in capacitance over the range 0.39–0.62eV (3.2–2.0 μ m) as has been stated previously.

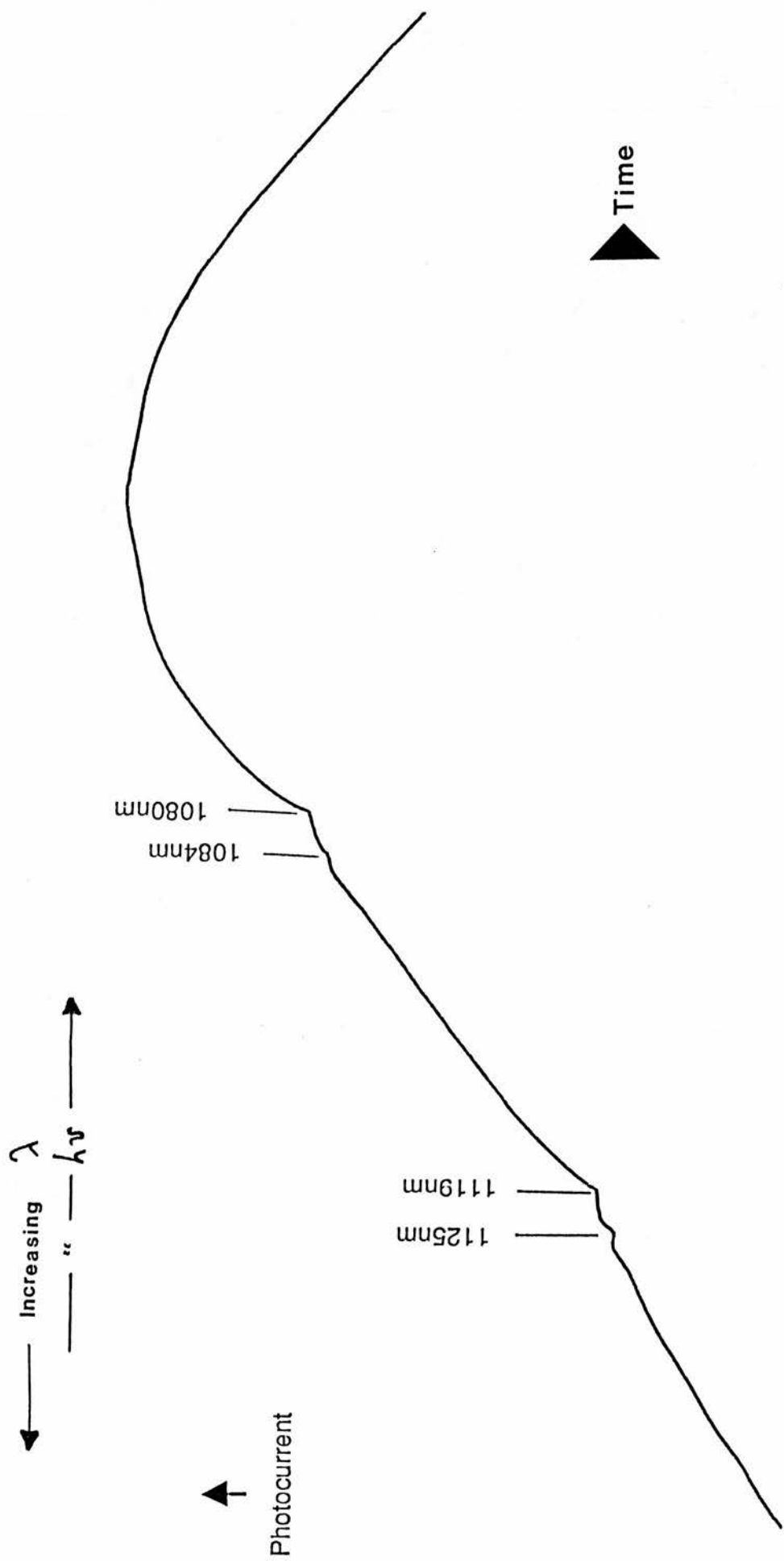


Figure 5.13 Wavelength swept steady state photoconductivity for ZnSe:V diode E11-V-1 at 300K. This spectrum shows features associated with transitions proceeding through excited states.

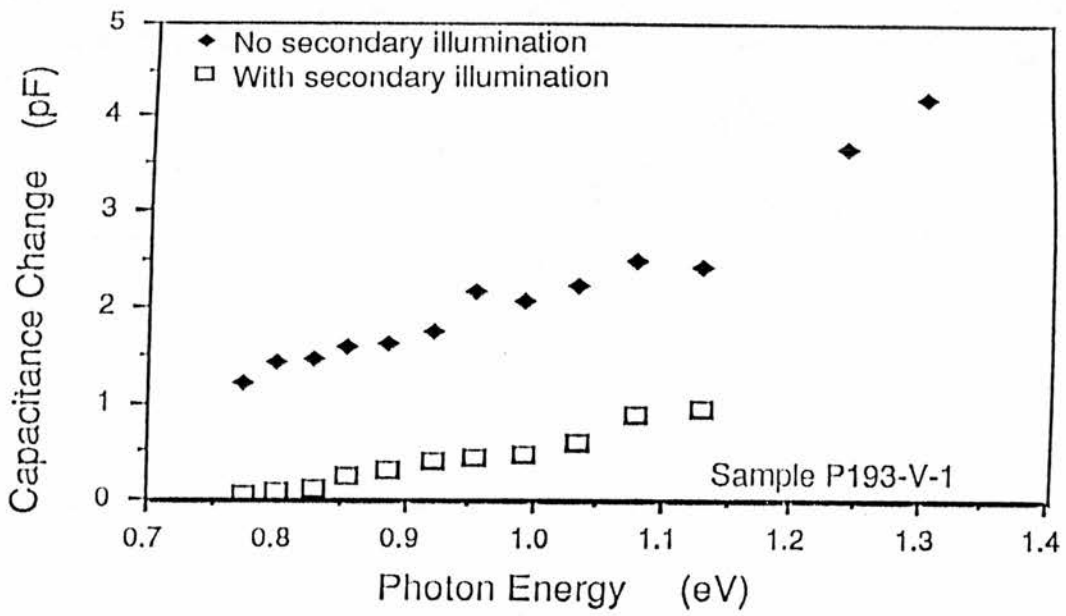


Figure 5.14 Photocapacitance changes for sample P193-V-1 at 78K with and without additional illumination with a constant ($h\nu < 0.75\text{eV}$) second source.

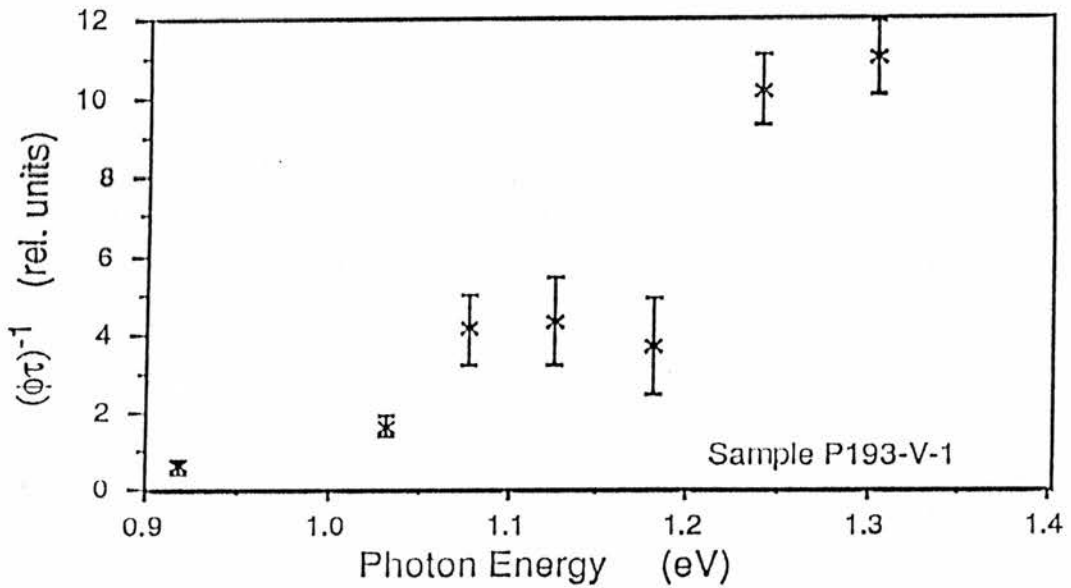


Figure 5.15 The room temperature (300K) relative photoionisation cross section for sample P193-V-1. The cross section is calculated from $(\phi\tau)^{-1}$ for single transients

Table 5.1Results of C-V Measurements on Sample E11-V-1 at 36K

<u>No Illumination</u>		<u>1.378eV Illumination</u>	
<i>Donor Density</i>	<i>Barrier Height</i>	<i>Donor Density</i>	<i>Barrier Height</i>
	<i>V</i>		<i>V</i>
	10^{17} cm^{-3}		10^{17} cm^{-3}
Uncorrected	3.5	4.9	3.3
Corrected	0.44	0.70	1.4

Table 5.2Literature Absorption Lines/Bands and Experimental Thresholds(All Energies in eV– MyPCON and MyPCAP repeatability $\approx 0.002\text{eV}$)

<u>A&W</u>	<u>H&B</u>	<u>Assign</u>	<u>MyPCON</u>	<u>MyPCAP</u>
1.027	1.020			
1.051	1.042			
1.064		4A_2	1.075	1.075
	1.087	2T_1	1.102	
	1.104	2T_2	1.108	
1.178	1.178	4T_1	1.148	1.150
	1.364			1.390
1.798	1.634		1.640	
	1.767			1.779
	1.777			
	1.794	2T_1		
				1.826
				1.834
				1.879

'A&W' is Allen and Wray reference [78].

'H&B' is Hoang and Baranowski reference [79].

'Assign' is the symmetry of the excited state assigned to a line or band by Hoang and Baranowski.

'MyPCON' is a list of the photon energies at which "thresholds" (bumps) were found in the photocurrent in swept wavelength photoconductivity experiments.

'MyPCAP' is a list of the photon energies at which "thresholds" were found in the OBV in swept photocapacitance experiments.

5.4 Discussion

In this section an attempt is made to draw conclusions from the data shown in the previous section taking account of the reports of earlier workers. The d^3 configuration is neutral with respect to the host crystal. The expected distribution of orbitals is $e^2t_2^1$ in d^3 and $e^2t_2^2$ in d^2 (see Chapter Six).

There is reasonable evidence from these results to suggest that the ground state of the d^2-d^3 energy level in ZnSe:V has been observed to lie at an energy of 1.05–1.10eV below the conduction band minimum. This result agrees with the recent prediction that this level lies at a depth of approximately 1.1eV below the conduction band minimum.^[72] The prediction is consistent with the observation that the binding energies of many transition metal impurities in different semiconductors are almost constant with respect to the vacuum energy level (only weakly dependent on the host crystal). In the paragraph below we examine the reasons for concluding that this is the d^2-d^3 level and the transition is to the conduction band.

The sign of the photoionisation change was positive, up to bandgap photon energies, which indicated that there was an increase of the positive charge in the depletion region. Thus, a transition which resulted in an electron in the conduction band had taken place. The d^3-d^4 level of vanadium in zinc selenide is believed to lie above the conduction band minimum. If we accept that prediction then we are left with only one possibility – the transition must be the vanadium $d^3 \rightarrow d^2 + e_{cb}$ transition.

The shape of the photoionisation spectrum is quite sharp at low temperatures and the threshold energy does not decrease greatly with increasing temperature, suggesting that the thermal broadening effects

are small in this system (compare with the ZnSe:Cr results of Chapter Four). The thermal emptying experiments did not provide any results which could possibly be interpreted as a manifestation of the thermal depth of this level. The values of 0.08eV and 0.41eV obtained are impossibly low for the thermal depths of a transition metal induced level over 1eV from the conduction band by an optical process. Even if a large relaxation, as in ZnS:Cr (0.40eV)^[57], existed we should expect a thermal energy of about 0.65eV as a minimum). We are lacking sufficient information to construct a good working configuration coordinate diagram, as in the case of ZnSe:Cr (Chapter Four).

At room temperature it can be seen that there is one clear photoionisation threshold. At a photon energy of 0.95eV the capacitance change is less than 1pF, at 1.078eV it is about 13pF and by 1.24eV has risen to 26pF. Above this photon energy the capacitance change did not vary much until close to 2.0eV. Similarly at low temperature we start from a low capacitance change – quite constant in the range 0.6–0.9eV – rising to over 85pF at 1.55eV. The 85pF capacitance change under 1.55eV illumination at low temperatures corresponded to a level occupancy change of about $2.5 \times 10^{16} \text{ cm}^{-3}$ using the formula $\Delta n = 2 \times N \times \Delta C / C$. In fact this formula is inappropriate because the capacitance change is not small compared with the total capacitance. Using the exact formula^[81] the occupancy change is found to be $3.1 \times 10^{16} \text{ cm}^{-3}$. The result is roughly in agreement with the change in donor charge concentration under illumination calculated from the capacitance–voltage measurements at 37K given in Table 5.1 (7.0×10^{16} subtract 4.4×10^{16} equals $2.6 \times 10^{16} \text{ cm}^{-3}$). The capacitance change does not contain any noticeable broad 'bumps' at higher photon energy. This indicates there are no levels up to 1.9eV from

the conduction band, detectable by this technique, of a size comparable to the transition taken to be the $d^3 \rightarrow d^2$ photoionisation transition.

We refer to as "thresholds", always using double quote marks to distinguish the energetic positions of these sudden rises/falls in recorded OBV (experimental features) from the threshold for a photoionisation transition which is a more precisely defined quantity. The similarity of the "thresholds" discovered in both swept photocapacitance and swept photoconductivity results should be compared to the positions of absorption and luminescence bands previously reported^[78,79]. The general agreement is good as we shall see in detail below. We observe many of the absorption lines and can attribute the "thresholds" to photoionisation transitions which are photothermal in character. This is supported by the fact that only those absorption lines which lie close to or above the conduction band minimum are seen. The capacitance "threshold" at 1.075eV (1154nm) and the photoconductivity "threshold" at 1.075eV probably arise from the same transition as that seen in absorption measurements at 1.085eV (from FCZ who quote Hoang & Baranowski – reckoned here to be 1.087eV). The photoconductivity "thresholds" at 1.102eV (1125nm) and 1.108eV (1119nm) are close to the value of 1.104eV found by Hoang and Baranowski. In the table the break lines mean that there are some absorption lines in the literature which are not listed here because no "thresholds" were seen in the present work close to the unlisted lines. The comparison in the table between the local minimum in the capacitance, not a "threshold", at 1.390eV (892nm) with the 1.364eV absorption line/band is probably not significant. The highest photoconductivity "threshold" found was at 1.640eV (750nm) which would correspond to an absorption line at 1.634eV. The situation is represented pictorially in figure 5.16 which shows the ground state and excited states

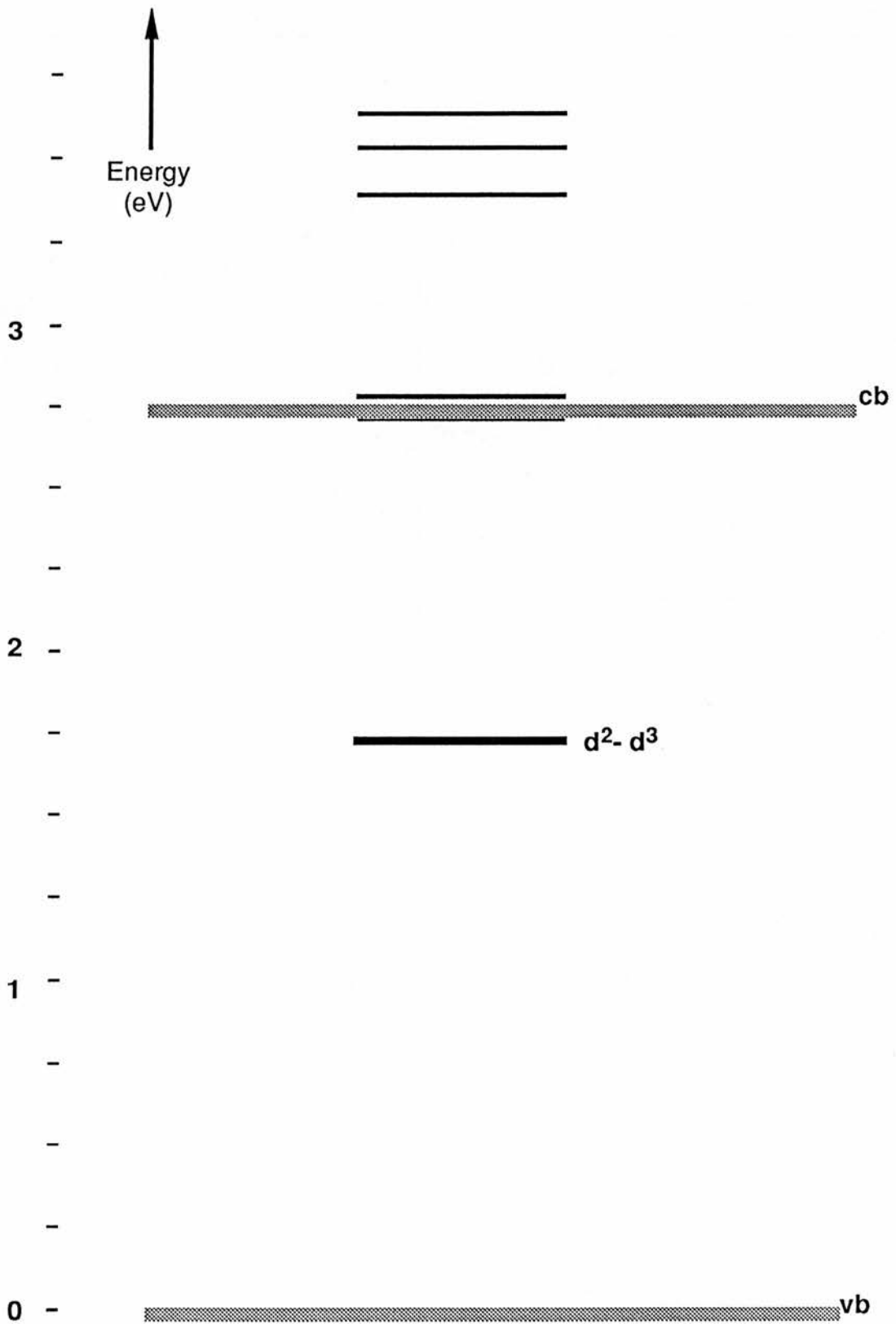


Figure 5.16 This diagram illustrates the position of the vanadium d^2-d^3 level in the energy gap of zinc selenide according to the photocapacitance data presented in this chapter. The relative energy positions of excited states seen in photocapacitance and photoconductivity are also shown.

at the observed "threshold" energies relative to the conduction and valence band extrema.

At higher energies, above 1.9eV, many more "thresholds" were found in the swept phot capacitance spectra. It is necessary to compare the values found at these higher photon energies with the series of values found in the spectra of ZnSe:Cr samples because of the coincidence of many of the "threshold" energies. This discussion has been postponed to Appendix 5.1 when a comparison with similar effects seen in chromium doped zinc selenide is undertaken.

Data obtained from photoconductivity measurements must be interpreted very carefully. A few of the complicating factors will now be discussed. Photoconductivity measurements at photon energies above the Schottky barrier height must take account of the steady state photoconductivity which can be due to effects at the gold-semiconductor interface or (less likely) to a deep level being filled by a mechanism from one carrier band and emptying a carrier to the opposite band. Two possible mechanisms are suggested in figure 5.17. 1) Electrons at the Fermi level in the region of the gold-semiconductor boundary could gain sufficient energy to surmount the Schottky barrier and then would be accelerated out of the depletion region. 2) At photon energies greater than the bandgap energy there exists the possibility of photocurrents generated by two complementary photoionisation processes ($x^{n-1} \rightarrow x^n \rightarrow x^{n-1}$). Band structure is another factor that should be taken into account when analysing photoconductivity results. Having pointed out the problems, we note that the threshold energy for the photoconductivity is very similar to the phot capacitance threshold energy. It is not thought that this fact is coincidental, but that there is a transient current associated with the photoionisation of the d^3 state.

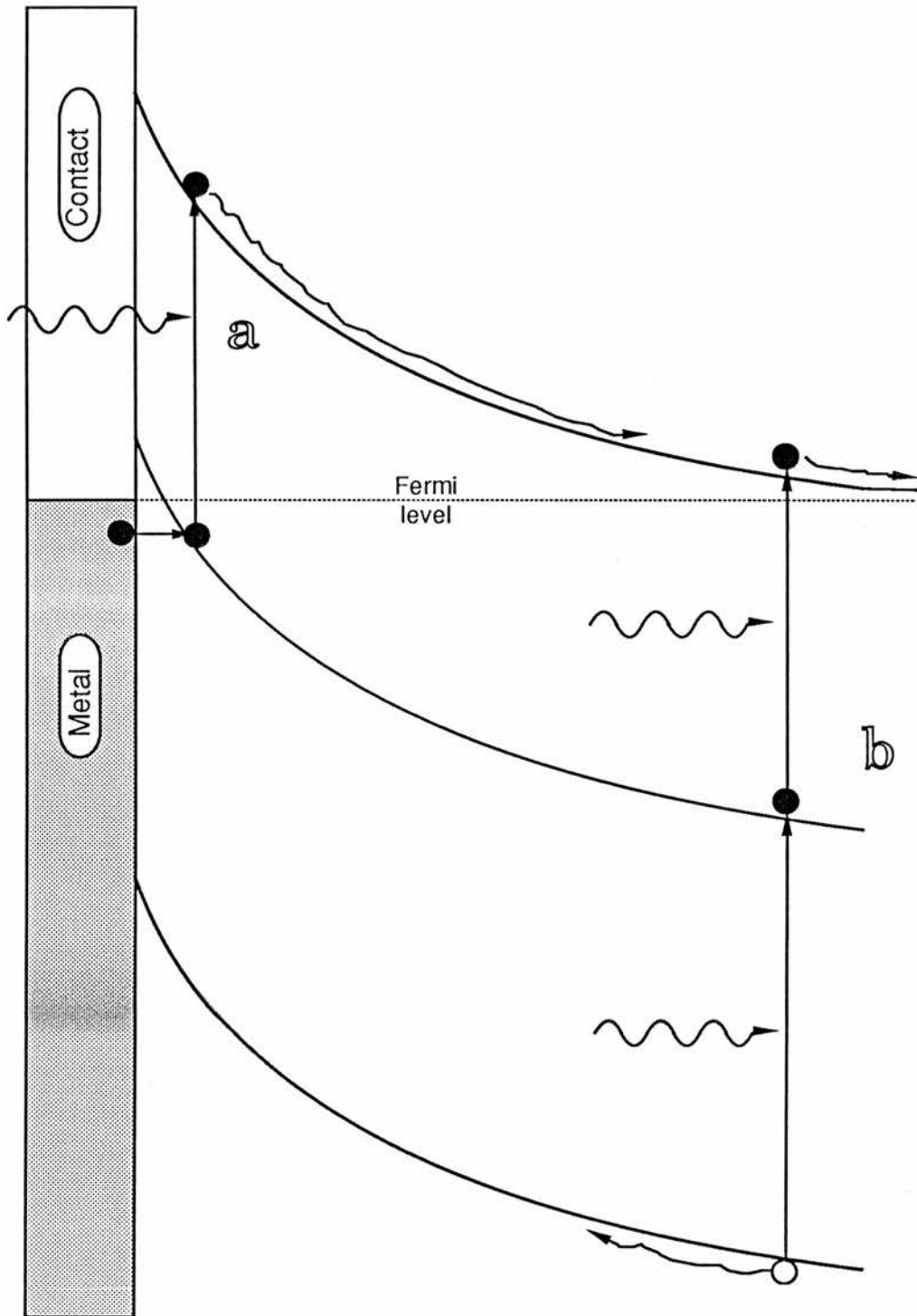


Figure 5.17 A diagram illustrating two possible photoconductivity mechanisms involving a deep level. **a** An electron tunnels from a surface state to a centre responsible for a deep level close to the interface. Photoionisation follows to one of the carrier bands. **b** Two-stage photoionisation takes place. Here is shown a centre undergoing photoionisation to produce a hole in the valence band. Secondly, the centre is converted back to its original state by photoionisation to the conduction band. The arrows show the direction of electron transport. Filled circles indicate electrons; unfilled circles holes. There are several other possible mechanisms.

It has already been noted that the high temperature (300–450k) thermal emptying experiment resulted in an activation energy determination of $0.41 \pm 0.03 \text{eV}$. Below it will be argued that this activation energy is to be associated with the impurity level producing a photocapacitance threshold at $0.47 \pm 0.01 \text{eV}$.

If we are correct in surmising a common origin for these two results then taking the difference between the results gives a relaxation energy of $0.06 \pm 0.03 \text{eV}$. The level is closer to the conduction band than the dominant level at $E_c - 1.1 \text{eV}$ and so is likely to have a much higher electron capture cross section. If the defect is a complex this would produce a lower symmetry and again the electron capture rate would be increased. The concentration of this defect is low since no occupancy changes greater than $4 \times 10^{14} \text{cm}^{-3}$ were found. This level has a threshold at similar energies to the level found in the chromium doped zinc selenide sample of Chapter Four. The change in level occupancy calculated for each level is very similar $\{(4 \pm 1) \times 10^{15} \text{cm}^{-3}\}$. No thermal activation energies in the same area were found in the chromium doped samples. In both ZnSe:V and ZnSe:Cr we have diodes which were made from material grown in the same batch (P193) of zinc selenide. Any contaminants introduced at the growth stage would be common to both ZnSe:Cr and ZnSe:V samples. In Chapter Four it was suggested that the unknown level with the 0.35–0.50eV photocapacitance threshold might be the result of a complex between a selenium vacancy and a chromium on a zinc sub-lattice site. A similar complex is possible in ZnSe:V as the d^2/d^3 level is at a similar position within the energy gap to the d^4/d^5 level in ZnSe:Cr. It is emphasised that these speculations require more sensitive identification techniques to be applied in order to test their veracity.

It is necessary to offer some possible reasons as to why the behaviour of diode P193-V-1 differed from that of E11-V-1 so markedly in the size of the capacitance change above 1.0eV. Three reasons have been considered.

- 1) The sample was of intrinsically poorer quality. We have no details of the growth conditions of the P193 material and thus no indication of possible co-dopant materials or contaminants. The dirty brown colour suggests a poorer sample quality than the uniform yellow E11-V-1.
- 2) The surface was damaged or contaminated. The sample had been exposed to air for more than five years. Although the surface was cleaned with a hot alkali bath prior to forming the contacts, perhaps this did not remove a sufficiently thick layer of material.
- 3) The aluminium Schottky contact was probably several times thicker than the evaporated gold contact and so not as transparent. This was due to lack of control in evaporation time, itself partly due to the equipment used and partly to operator inexperience.

Having found possible reasons for poor sample quality, the fact that the 78K double light source results (figure 5.14) show, to a large degree, the expected quenching below 1.0eV, it must be remarked that the sample could still yield similar results to E11-V-1, with suitable device preparation, if either of reasons 2) or 3) were true.

5.5 Conclusion

A level was found in V doped ZnSe (ZnSe:V), 1.1eV below the conduction band minimum as measured optically. The level appeared to have only a small associated lattice relaxation because of the absence of appreciable thermal broadening. The most likely identification of this level is that it is due to the $d^3 \rightarrow d^2 + e_{cb}$ photoionisation transition of vanadium – almost certainly incorporated into the host lattice on a zinc substitutional site. This is to our knowledge the first confirmation of the position of the energy level induced in zinc selenide by vanadium doping. The level position agrees with recent theoretical predictions. The absolute value of the cross section for a transition from the level (d^3-d^2), involving the promotion of electrons to the conduction band, was measured and found to be of the same order of magnitude as other determined 3d transition metal level photoionisation cross sections in II-VI materials. Several excited states of the d^3 configuration, which lie close below, or above the conduction band minimum, are believed to have been observed.

Appendix 5.1High Photon Energy Capacitance
Changes in ZnSe:Cr and ZnSe:V

In this appendix we examine some phenomena mentioned in both Chapters Four and Five but not described there in great detail. We look at the similarities and differences between the high photon energy (above 1.8eV) sudden changes in capacitance ("thresholds") seen in swept wavelength experiments. (Rebalancing the bridge showed the OBV changes to be almost entirely capacitance changes.) These were first seen in quick swept wavelength experiments on the chromium doped sample studied in Chapter Four. When similar experiments were performed on the vanadium doped sample E11-V-1 a similar, but not identical, set of high photon energy "thresholds" was found.

First the similarities between the two sets of thresholds, shown in their original form as wavelengths in table 5.3, will be examined and possibilities advanced to explain the common "thresholds". Then the differences will be looked at and comments made for the two different impurity systems.

In the table very close matching of wavelengths in the two materials has been noted by use of the same line of the table for the two entries. *Close* is taken to mean within 2 or 3 nm of each other at maximum. All the "thresholds" are reproducible to within 1nm (0.005eV at 500nm). The common energies are 1.834eV (676nm), 2.230eV (556nm – multiple line structure), 2.357eV (526nm), 2.403eV (516nm), 2.431eV (510nm), 2.446eV (507nm), 2.546eV (486nm), 2.594eV (478nm), 2.707eV (458nm – approximately bandgap energy), 3.116eV (398nm) and 3.280eV (378nm). The results are quoted here because of the data reproducibility. The

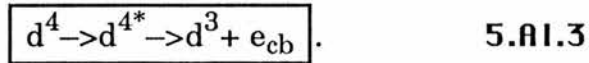
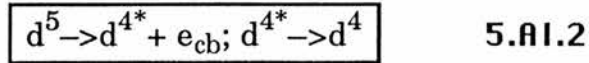
bandwidth of the excitation source was, however, typically 20nm except for the results in column three of table 5.3 which were performed using a slit width corresponding to 10nm, and a much slower wavelength scanning rate than was usual, over a limited range of photon energies.

The capacitance always increased at a "threshold" when light of below bandgap energy was used and always decreased with above bandgap energy light. Capacitance increases indicate electrons entering the conduction band leaving more charge in the depletion region.

The "thresholds" above the bandgap energy are common to both systems except for the chromium "threshold" at 434nm (discounting the weak feature at 454nm). We suggest that these transitions are due to one or more of the following possibilities. 1- copper complexes in the lower half of the bandgap. 2- Transitions from intrinsic defects producing levels in the lower bandgap. Aluminium, the donor impurity, complexing to form deep levels. The transition at around the bandgap energy might be due to excitonic effects, although it must be noted that 150K is a high temperature to observe excitonic related phenomena.

In the case of chromium there are several transitions not matched by those in the vanadium doped samples. From the references already studied in Chapter Four it was noticed that there a correlation existed between the photocapacitance "thresholds" observed here and the excitation peaks of the chromium d^4 (${}^5E \rightarrow {}^5T_2$) luminescence seen by Grebe *et al.*^[60] The correspondences were reasonable but not excellent (not expected with a different technique and the large bandwidths used here). The "thresholds" closest to the PLE peaks are all unique to the chromium sample except for the lowest energy transition at 1.834eV (676nm). We suggest these transitions are most probably photothermal excitations.

There were four possibilities that came to mind. The first three, all possible photothermal processes, are summarised in the equations below,



The last possibility considered was that the transitions were due to direct photoionisation of a set of impurity defects including chromium complexes.

In vanadium there are similar ideas to those summarised in eqns. 5.A1.1–3. As well as the problem of identification, the reason why we do not see any evidence of the complementary transitions to the valence band ($d^2 \rightarrow d^3 + h_{vb}$ for example), through decreases in capacitance is still unclear.

Table 5.3 High Photon Energy Photocapacitance Features

<u>ZnSe:Cr</u>	<u>ZnSe:V</u>	<u>ZnSe:V</u> (limited range - high sensitivity)
	697	
	679	
676*	676	
	660	
	638	
632		
	619.5	
614*		
606		
594		
575		
555	559.5	
552	557.5	
	555.5	
	541	
	540	
534		
532*		
526		525.2
		524.8
		523.8
		522.9
	520	520
	519.5	519.7
516		516.1
510		509.9
507		508
		505.9
		503.7
		501.6
		499
486	487	487.2
		484.2
		483.1
		481.2
477	478.5	
475*		
461		
458	458	
454*		
434*		
415	418	
399	398	
378	377	

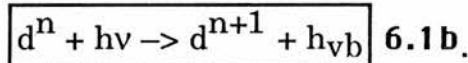
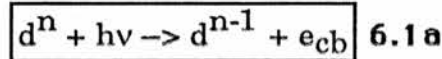
Raw data – all figures are in units of wavelength (nanometres). All results were taken at a temperature 150K. Repeatability $\pm 2\text{nm}$. * indicates nearest transition in the table to PLE peaks seen by Grebe *et al* [60].

Chapter Six:

Absolute Photoionisation Cross Sections: A Review

6.1 Introduction

Photoionisation is the removal of a particle from a bound state to a continuum. The energy to do this is supplied by a quantum of light. In this work the term photoionisation refers to either of the processes:



The term photoneutralisation is used by some authors^[82] to refer to transitions which result in configurations which are neutral with respect to the lattice. They reserve the term photoionisation for transitions from initially lattice neutral configurations.

The photoionisation cross section is a measure of the probability that a photon will cause a transition from a d^n configuration to a $d^{n\pm 1}$ configuration, with a carrier generated in the appropriate band. It is measured in terms of a theoretical equivalent diameter for unit photon flux. It can be calculated in principle by applying the Fermi golden rule to obtain an expression:

$$\boxed{\sigma(h\nu) = \frac{A}{h\nu} |\langle \phi_i | \hat{H} | \phi_f \rangle|^2 \rho(E)} \quad \mathbf{6.2}$$

where: A is a constant independent of the photon energy; $h\nu$ is the photon energy; ϕ_i is the initial state of the impurity and the operator

\hat{H} corresponds to $e\underline{r}$, which is proportional to the perturbation Hamiltonian for an electric dipole transition. The final state wavefunction, Φ_f , must include the new configuration wavefunction of the impurity ion and the wavefunction of a free carrier in the appropriate band. $\rho(E)$ is the density of states in the appropriate carrier band. The photoionisation cross section shows how the impurity interacts with the host material through the initial configurational wavefunction and the combined final state wavefunction. In particular the modifications of the configurational wavefunction due to the host must be included. There have been a number of papers published showing how the impurity wavefunction can be approximated in order to calculate the shape of a cross section^[62,83,84]. In Section two of this chapter we shall be examining the extent to which impurity orbitals can mix with neighbouring atom/ion orbitals.

The wavefunction for 3d impurities in semiconductors is believed to consist of two parts. There is a d-like core part close to the nucleus which is very similar to the atomic 3d wavefunctions. At larger distances the wavefunction must hybridise with the host wavefunctions and thus be more like the host wavefunctions. A crude picture with a sharp spatial change-over between core and tail parts of the wavefunction is shown in figure 6.1. Other workers have proposed three regions with a core, a Coulomb region and a screened region.

If measured accurately, the photoionisation cross section provides a stiff test for both the semi-empirical models used by many experimenters and state-of-the-art calculations from first principles. The most rigorous test is if the models are required to reproduce both the shape and the absolute values of the cross section spectrum over a wide range of photon energies. In this chapter we will not examine details of the different

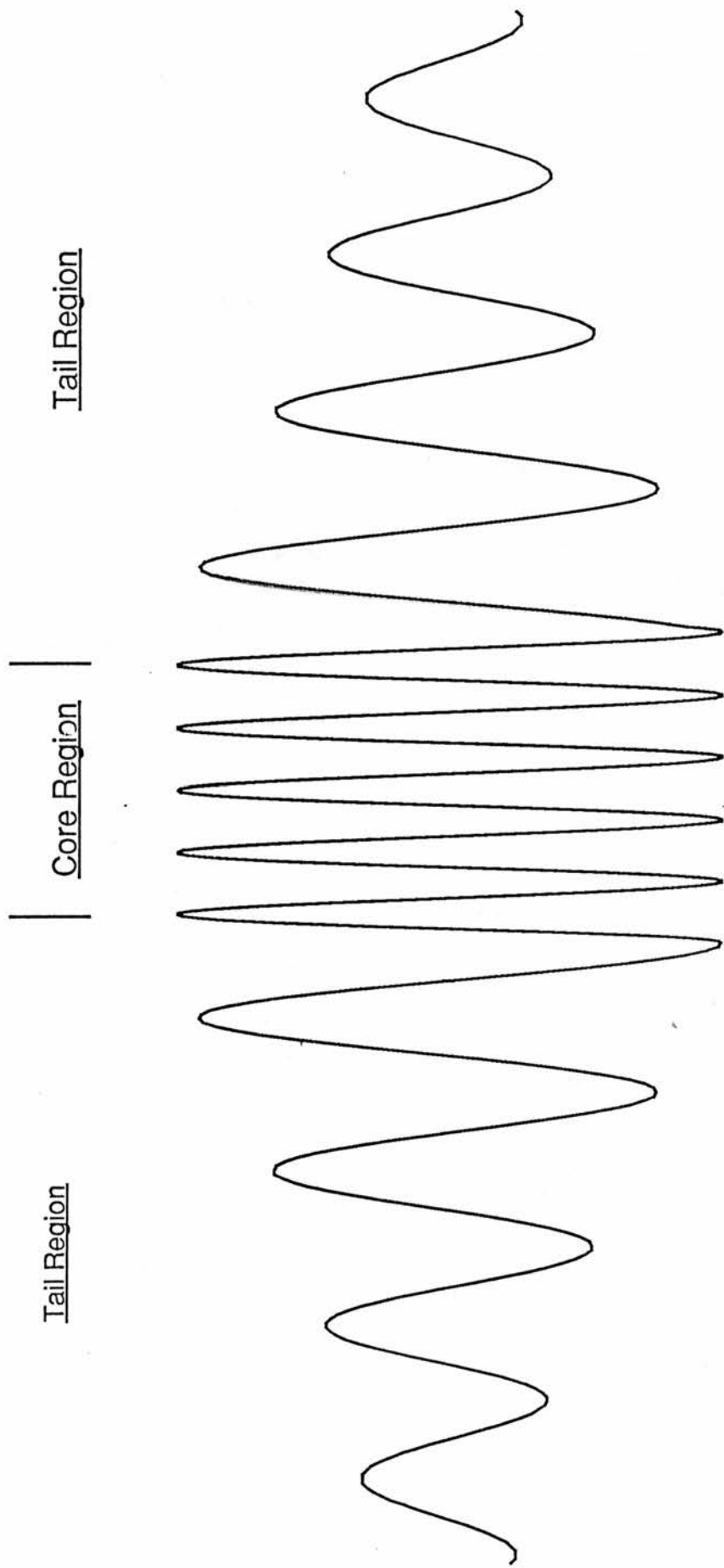


Figure 6.1 The 3d impurity wavefunction is commonly divided into an atomic-like core region and an evanescent tail region.

shapes of photoionisation cross section spectra which have been found experimentally, nor will we discuss in detail any of the models proposed to account for differences in the spectral shape. It is noted, however, that some of the proposed models require a large number of parameters^[85] and that the experimental data is not usually of sufficient accuracy for more than one, or at most two, parameters to be used as fitting factors.

To my knowledge, no systematic studies of the magnitudes of comparative absolute magnitudes of the maximum photoionisation cross section values have been published, except that of Martinez^[86]. Martinez only looked at chromium transitions for which data was available. The data consisted of the $d^4 \rightarrow d^5$ transitions in ZnS, ZnSe, ZnTe, and CdTe. For the III-V compounds he looked at the $d^3 \rightarrow d^4$ transitions in InP and GaAs and the $d^2 \rightarrow d^3$ transition in GaAs. In total Martinez examined six cross section values^[57,85,88-90]. The tables of the present study might be the most comprehensive set of absolute optical photoionisation cross sections of 3d series impurities in binary semiconductors yet compiled. There are 30 values for III-V materials and 18 values for II-VI materials listed in the Tables.

Parameters which can be deduced (in theory) from cross section spectra include the following. E_{opt} , the optical depth of an impurity from the band to which the transition takes place. Γ , the thermal broadening parameter can be obtained from fitting a thermally broadened cross section model to experimental data. Γ depends not only on temperature but on phonon mode energies and the relaxation energy for the transition (Franck-Condon energy), E_{rel} . Thus we can work out the value of the relaxation energy for the transition in practice if the effect of all the phonons present is replaced by an effective average phonon energy. If the

relaxation energy and the optical depth are both known the thermal depth of the impurity can be calculated as

$$\boxed{E_t = E_{\text{opt}} - E_{\text{rel}}} \quad \mathbf{6.3.}$$

An analysis of a thermally broadened photoionisation transition was given in Chapter Four ($d^4 \rightarrow d^5$ of chromium in ZnSe:Cr, model due to Piekara *et al.*^[63]).

This section is completed by a quick look at the contents of the rest of Chapter Six. In Section 6.2 some of the basic ideas necessary for the later discussion of photoionisation data is given. In Section 6.3 we review the methods which have been used to determine photoionisation cross sections: not examining them in experimental detail but from the point of view of their relative merit as tools for accurate determination of the data. Section 6.4 gives an insight into possible selection rules for photoionisation transition, with more consideration given to the most promising candidate. Some of the trends to be expected in the cross section data are outlined. In Section 6.5 the compiled photoionisation data are formally introduced to the reader before looking at the data in the light of the information in Section 6.4. Section 6.6 is a brief summary of the main conclusions.

6.2 Basic Theory: Symmetries, Crystal Fields and e & t₂ orbitals.

In this section the basic background theory of 3d electronic levels in semiconductors is given. Tetrahedral symmetry is assumed to be appropriate. This assumption is not a trivial statement. Within it is subsumed that both Jahn–Teller distortions^[91] and spin–orbit interactions^[92] are either not present or are small enough to ignore for our purposes. The information contained in this section is given as general background and as an introduction to some of the arguments to be used later in the discussion of the compiled results and tables.

The d electrons of the impurity in a crystal are subject to interactions with: (1) the screened nucleus (Coulomb) (2) each other (exchange and Coulomb) (3) an average potential from all the other electrons/ions in the crystal (crystal field). This potential is sometimes approximated by the potential due to neighbouring ligands. The terms labeled (1) and (2) occur for free atoms or ions, but (3) does not. The extra term, as we shall see, can greatly change the properties of the system from those of the atomic limit.

Firstly, some comments about crystal symmetries are in order. The appropriate point-group symmetry for substitutional sites in cubic binary crystals (a tetrahedrally coordinated environment) is the T_d point group^[92]. This group has a five–dimensional irreducible representation with a basis set given in terms of the {1, 1, 2, 3, 3}–fold degenerate basis representations usually denoted by the set $\{A_1, A_2, E, T_1, T_2\}$. For one–electron states the lower case letters are used $\{a_1, a_2, e, t_1, t_2\}$. The only representations to contain d-like components are the e and t₂ representations. We can describe d electrons in T_d symmetry in terms of these two representations. It is noted that the distribution of the n 3d

electrons between the e and t_2 one-electron levels is referred to as the single-electron configuration or the one-electron configuration.

If we approach the problem from looking at a five-fold degenerate atomic d state then the crystal field, due to all the other point charges in the crystal, lifts the degeneracy of the e and t_2 levels. The t_2 levels are raised in energy and the e levels lowered with respect to their zero crystal field energies. The manner in which this happens is illustrated in figure 6.2a. The difference between the e and t_2 one-electron orbitals is the crystal field energy Δ , sometimes denoted by $10Dq$.

Now we consider the spin dependent exchange terms. Electrons can have either spin up or spin down. The exchange interaction between electrons of different spin orientation splits both the e and t_2 levels into e_+ , e_- , t_{2+} and t_{2-} single-electron levels. This splitting is illustrated in figure 6.2b. The magnitudes of the crystal field and the two single-electron exchange splittings determine the energetic ordering of the spin-split single-electron levels and hence give the ground state configurations of the substitutional impurities in the strong field limit. In traditional crystal field theory^[92] fitting, and is indeed the case in almost all well understood systems, the ground state is found to be that corresponding to the maximum possible spin. This can be referred to as a 'Hund rule' system in the same way as Hund's rules are used to find the ground state configuration (determining L , S and J) of partially filled atomic d and f shells^[92]. The spin-split one-electron levels in this case are in the increasing energetic order: e_+ , t_{2+} , e_- , t_{2-} . The ground state configurations, in terms of e and t_2 orbital occupation, are given in Table 6.1 together with excited state single-electron configurations. If, however, the crystal field splitting is large compared to the exchange splitting, then both the e_+ and e_- levels will lie lower than either of the t_2 levels and the ground states will

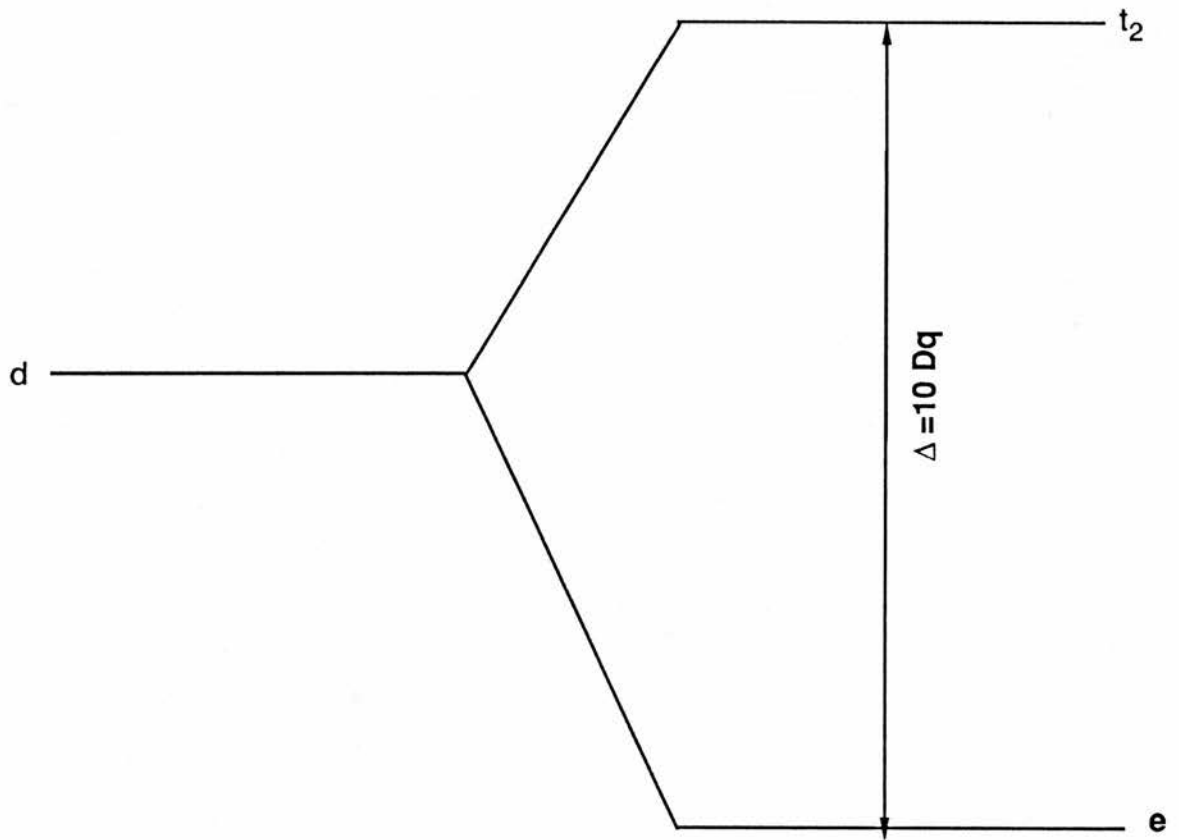


Figure 6.2a The d electron shell Crystal Field Splitting under T_d symmetry.

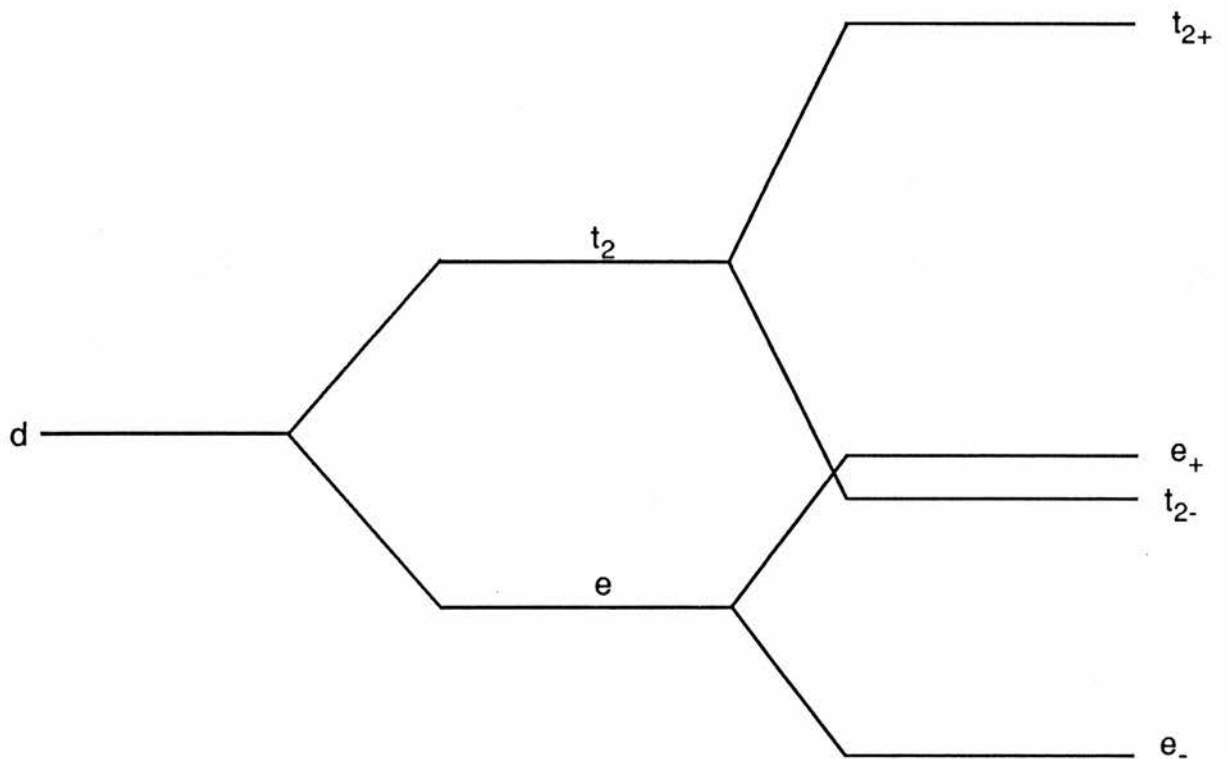


Figure 6.2b d shell crystal field splitting and one-electron exchange splitting.

have the minimum possible number of unpaired spins^[93]. This situation can be referred to as the low-spin regime.

When we look at many-electron levels rather than single-electron levels we find that the mutual interactions between the electrons cause a lifting of many of the degeneracies of the multiplets which make up each one-electron level. For example, in a d^2 system the e^2 orbitals are comprised of the representations A_1 , A_2 and E ; the t_2^2 level is comprised of the A_1 , E , T_1 and T_2 representations and the et_2 combination is comprised of the T_1 and T_2 representations. A systematic treatment including spin in a double-group treatment shows a total of 11 multiplets. A similar breakdown for other d^n systems is given in several of the references.^[92,94,95] The full multiplet spectrum depends, in the Tanabe-Sugano model, on the crystal field Δ and on two adjustable parameters B and C which derive from the free ion Racah parameters B_0 and C_0 .

It is found that in this point group symmetry, unlike the continuous group for 3d rotations, states of certain orbital angular momentum (l) are allowed to mix with some other orbital angular momentum states. The t_2 levels are allowed to mix with p ($l=1$) as well as d ($l=2$) states. In contrast the e levels are not allowed to mix with s , p or even f states. The neighbouring ligands are p -like because the valence electrons of all group VA and VIA elements are $l=1$ states. From the point of view of the impurity ion, the four nearest-neighbour ligands symmetry description contains an element of T_2 character. This fact allows hybridisation of the impurity t_2 orbitals with the outer p -shells of the nearest-neighbour ions. The t_2 orbitals can not then be said to be essentially d -like. The parity selection rule (Laporte rule), that electric dipole transitions (electric dipole operator, $e\mathbf{z}$, has a t_2 representation) are allowed to states with an opposite parity $\{(-1)^l\}$ and forbidden to states of the same parity, becomes invalid.

An alternative view-point (chemical) is that the t_2 orbitals can form σ orbitals with the nearest neighbours.

If there were no mixing of d and p states then the impurity wavefunction would be highly localised, as in the case of a free atom or ion. Hybridisation of the orbitals leads to a 'spreading' of the impurity wavefunction in real space. (In momentum space there are still too many lattice wavefunctions required to adequately represent the impurity wavefunction by a tractable number of Bloch states in a linear combination.) The e wavefunctions are expected to delocalise to a much smaller extent compared to the wavefunctions of the t_2 orbitals because of the symmetry bar on e states mixing with states of p-like origin. When the e orbitals do begin to delocalise they do so by symmetric radial expansion. This delocalisation is in a sense equivalent to covalency and should therefore correlate with other measures of covalency.

Table 6.1 High-Spin Strong Crystal Field Single-electron Configurations

<u>Number of d electrons</u>	<u>High-spin Configurations</u>	<u>Next Highest Spin Configurations (Excited States)</u>		
1	e^1	t_2^1		
2	e^2	$e^1 t_2^1$	t_2^2	
3	$e^2 t_2^1$	$e^1 t_2^2$	t_2^3	e^3
4	$e^2 t_2^2$	$e^1 t_2^3$	$e^3 t_2^1$	t_2^4
5	$e^2 t_2^3$	$e^3 t_2^2$	$e^1 t_2^4$	
6	$e^3 t_2^3$	$e^2 t_2^4$	$e^4 t_2^2$	$e^1 t_2^5$
7	$e^4 t_2^3$	$e^3 t_2^4$	$e^2 t_2^5$	$e^1 t_2^6$
8	$e^4 t_2^4$	$e^3 t_2^5$	$e^2 t_2^6$	
9	$e^4 t_2^5$	$e^3 t_2^6$		
10	$e^4 t_2^6$			

The ordering of excited states given here is first by decreasing spin (highest spin first), then with the minimum t_2 orbitals occupied.

List of transitions between ground states involving a change in the occupancy of the e orbitals.

$$d^0 \rightarrow d^1 \text{ and } d^1 \rightarrow d^0,$$

$$d^1 \rightarrow d^2 \text{ and } d^2 \rightarrow d^1,$$

$$d^5 \rightarrow d^6 \text{ and } d^6 \rightarrow d^5,$$

$$d^6 \rightarrow d^7 \text{ and } d^7 \rightarrow d^6.$$

6.3 Methods used to Measure the Cross Section

Three categories of experimental technique have been used to measure the optical photoionisation cross sections tabulated at the end of Section 6.5. They are optical absorption, junction capacitance based measurements and the photo-dependent electron paramagnetic resonance (photo-EPR) technique, in order of the frequency with which impurity-host systems have been investigated. In this section we shall have a short look at each technique. We will indicate how the cross section is calculated, as well as trying to elucidate the advantages of each technique for transition identification and cross section determination. We will also look at the separability of the photoionisation transition under study from possible effects that might obscure the measurement. A more systematic treatment of these obscuring effects is left until Section 6.4.

6.3.1 Optical Absorption

The optical absorption of pure semiconductors is usually very low (a few cm^{-1} at most) in the energy range corresponding to energies above those of free carrier absorptions (when present) up to photon energies corresponding to the energy gap. In this region the absorption due to impurity centres, present sometimes only in ppm concentrations, can be measured. Absolute absorption measurements have been performed since the 1960's.

The absorption cross section is equal to the absolute absorption coefficient, $\alpha(h\nu)$, divided by the active population of the impurity centre, N , usually the number of ions in a particular charge state.

$$\boxed{\sigma_{n \text{ or } p}^{\circ}(h\nu) = \frac{\alpha(h\nu)}{N}} \quad 6.4$$

This concentration is not necessarily equal to the concentration of impurity atoms, N , determined from charge state insensitive techniques (including mass spectroscopy, SIMS, and radioactive isotope doping). If the internal transitions of the initial charge state are well established, such that the oscillator strength has been determined, (and the lines are strong enough) then the concentration of a particular charge state can be determined in this spectroscopic manner.

There are several possible reasons why there can be a difference between the concentrations N and N , some of which will now be mentioned.

(1) Impurities can form different centres in the same host by being incorporated on different lattice sites (although there is little evidence of other than cationic substitution for Ti through Ni in III-V and II-VI semiconductors, Mn in silicon is known to occupy both substitutional and interstitial sites).

(2) Even if all impurities are incorporated on the cationic substitutional site, the local environment can be different in a number of ways. The impurity could be close enough to a like impurity so as to form a pair (most likely in high concentrations- solubility involved [96]); it could be close to an introduced donor or acceptor to form a complex [97]; complexes could also be formed with near lying native defects (vacancies most likely, also interstitials and antisites).

(3) Different charge states can be present at some temperatures for very long periods depending on the exact position of the Fermi level. An example is found in Chapter Two where it was seen from the literature that the same sample (GaP:Ni) could show the ${}^5T_2 \rightarrow {}^5E$ internal

absorption of the d^9 configuration as well as some d^8 transitions.

Internal transitions can obscure the absorption edges characteristic of photoionisation processes^[98,99]. This obscuring is in addition to that observed using methods which involve the detection of charge transferred to a band (e.g. DLOS – see Section 6.3.2) or which offer the possibility of direct observation of relative level concentration (e.g. photo-EPR – see Section 6.3.3).

6.3.2 Optical Capacitance based techniques

The techniques included in this category are photocapacitance and DLOS (Deep Level Optical Spectroscopy)^[20]. Both methods rely on the transfer of charge to the conduction or valence band from the depletion region of a junction (usually a metal Schottky contact), thus altering the capacitance of the depletion region. Photocapacitance has been used routinely for cross section measurement since the early-1970's and DLOS since the early 1980's.

Photocapacitance usually measures either the initial rate of change of the capacitance upon illumination (if the transient is exponential) or the calculated time constant of the change some time after the start of the illumination. From either of these measurements the cross section can be obtained:

$$\sigma_{n;p}^q(h\nu) = \frac{1}{\phi\Delta C} \left. \frac{dC}{dt} \right|_{t=0}, \quad 6.5a$$

$$\sigma_{n;p}^q(h\nu) = \frac{1}{(\phi\tau)}. \quad 6.5b$$

C , is the capacitance of the depletion layer, ΔC is the change in capacitance upon illumination, Φ is the photon flux incident on the depletion region and τ is the time constant for the exponential part of the capacitance transient.

The sign of the capacitance change indicates the band to which the transition is taking place: an increase in capacitance is a transition to the conduction band and a decrease is one to the valence band. Relative cross sections can be obtained, in special cases, by the DLSS method of photocapacitance (see Chapter Two).

6.3.3 Photo-EPR

The photoenhancement or photoquenching of an electron spin resonance signal would seem to be a technique likely to give clear information as to which impurity charge state is responsible for a particular transition. The photostimulation of EPR signals has been studied since the 1960's, but not applied to cross section determination until the late 1970's.

EPR signals are characterised by g values and fine structure lines which can, in many cases, be calculated well from theory and used to identify the impurity, its charge state and the symmetry to which it is subject. The EPR signal growth and quenching under monochromatic illumination should establish the position of the level in the gap and the kinetics of the changes give the cross section. A cross section should be calculable thus: the intensity of the EPR signal for a particular level is monitored with time as the sample is illuminated with monochromatic light. The spectral dependence of the time constant of the EPR signal rise

or fall gives a measure of relative cross section^[100], in the same way as simple photocapacitance. Again the absolute value of the cross section can be calculated if the photon flux is known in absolute terms (eqn. 6.5b).

This is an idealised picture and naturally we can not in practice do so well. The possibility of recombination exists in samples suitable for EPR (not carrier depleted) and what is measured is in fact a sum of photoionisation terms convoluted with functions due to recombination phenomena^[101]. Recombination can be reduced by performing experiments at liquid helium temperatures but often can not be sufficiently reduced for a good cross section measurement to be made.

There are other reasons why this technique does not account for more of the cross section data. The accuracy of the determination of cross sections from photo-EPR is almost always inferior to the accuracy of junction capacitance methods. The d^6 and d^8 states are invisible to EPR and so can only be inferred from the changes in d^5 , d^7 or d^9 (whichever is appropriate) signal intensities in EPR studies.

Photoconductivity is a good tool for obtaining a qualitative picture of a photoionisation cross section but is limited by recombination effects in a similar manner to photo-EPR. This technique can be used either in bulk samples, or in carrier depleted regions where its interpretation is more straightforward because of a reduction in recombination due to the lack of carriers.

6.4 Possible Selection Rules and Consequent Expected Trends in Cross Section values

We would like to see if there are any selection rules operating for photoionisation cross sections. The first suggestion for such a rule was the Laporte rule forbidding transitions to the conduction band but allowing those to the valence band. This simple rule has already been dismissed as an exact rule in the discussion of the non-orthogonality of orbital wavefunctions under T_d symmetry, given in Section 6.2. It can not be used as an empirical rule either because it does not work. For example the chromium $d^5 \rightarrow d^4$ transition in ZnSe studied in Chapter Four has almost equal values for the cross sections to the conduction and to the valence bands.

Symmetry group arguments are here used to find a selection rule for the strength of the absolute photoionisation cross section of substitutional 3d impurities in binary semiconductors. The general validity of the rule will then be established by comparing expectations with available data.

For a transition to be allowed the direct product of the symmetry representations of the initial state, the electric dipole operator and the final state must contain the A_1 representation. The operator for electric dipole transitions has been stated already to have a T_2 representation. The final state symmetry is the direct product of the final d^n electronic symmetry and the appropriate carrier band symmetry. The conduction band minimum has been taken to be s-like (A_1 representation) and the valence band maximum to be p-like (T_2 representation) (again spin-orbit splitting is ignored)^[102]. The multiplication table for the T_d group has been used to find the allowed and forbidden transitions. Table 6.2 shows the results when all the ground states were assumed to be high-spin

states. The table shows that the only forbidden transitions are those which involve a change of e level occupancy and result in an electron in the conduction band. These comprise the $d^1 \rightarrow d^0$, $d^2 \rightarrow d^1$, $d^6 \rightarrow d^5$ and $d^7 \rightarrow d^6$ transitions.

This result was then found to be more general. All transitions involving a change in e orbital occupancy of one (and no t_2 orbital occupancy change) were found to be allowed when resulting in a hole in the valence band and forbidden when producing an electron in the conduction band. A logical exposition of the symmetry arguments is given as Appendix 6.1. Because the arguments used in Appendix 6.1 do not involve the assumption of any particular ordering of the spin-split one-electron levels, we can therefore apply the selection rule to a regime in which all ground states have low-spin or to a mixed high-spin low-spin regime, as well as to the high-spin regime already detailed in Table 6.2. In the case of transition between low-spin systems this rule has been applied. The only ground states whose symmetries differ in the low-spin regime from those of the high-spin regime are the d^3 , d^4 , d^5 and d^6 cases. The selection rule leads to different levels (e or t_2) being involved in the photoionisation transition only in the cases of the d^2/d^3 , d^3/d^4 , d^5/d^6 and d^6/d^7 pairs of transitions. The differences between the low-spin and high-spin regimes are summarised in Table 6.3.

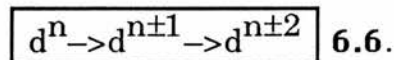
Increased hybridisation of the levels should lead to higher cross sections because the two types of level become such that their symmetries are not completely described solely by e and t_2 representations. More covalent systems should show increased hybridisation. III-V materials are more covalent than II-VI materials. Therefore it is expected that cross sections will be in general larger in III-V materials than in II-VI materials. A similar trend is predicted for particular impurities in a

series of semiconductors, for example $\sigma_{\text{ZnS:Cr}} \sim \sigma_{\text{ZnSe:Cr}} < \sigma_{\text{ZnTe:Cr}}$.

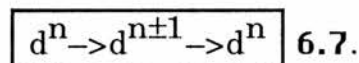
At higher photon energies we expect to see transitions to higher bands taking place. We must however be careful in interpreting real or apparent charge transfer bands in spectra. Such 'bands' can be due to many possible effects. Some of these possibilities, which can be seen both in bulk samples and in carrier depleted regions, are listed below.

1- Transitions might take place to higher extrema of the conduction^[103] or valence bands^[85]. These extrema are the Γ , X and L minima (with the Γ band lowest in direct gap materials) in the case of the conduction band and to the split-off valence band. The separation between light and heavy hole bands is usually very small at $\underline{k}=\underline{0}$.

2- There could be a second level in the gap for the same impurity and thus three stable charge states. Thus a second ionisation might be possible:

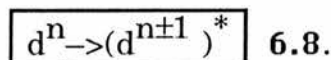


3- In some cases, when the Fermi level is suitably placed, the complementary transition might be possible:



4- A second centre of similar concentration or cross section times concentration product might be present^[32].

5- A transition to an excited state of the final configuration is a possibility^[104]:



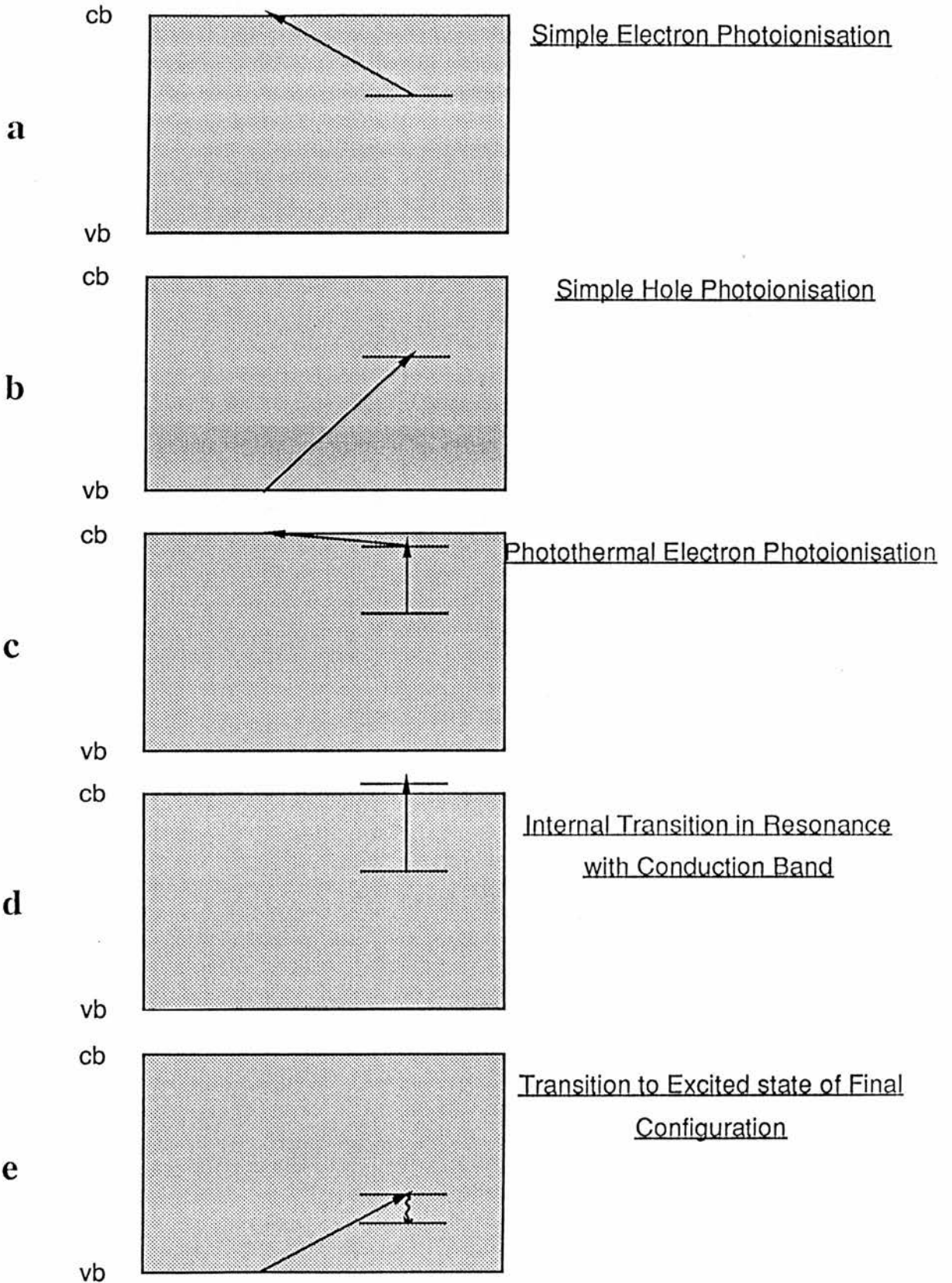
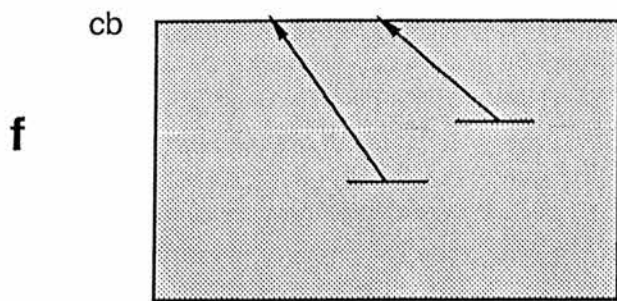
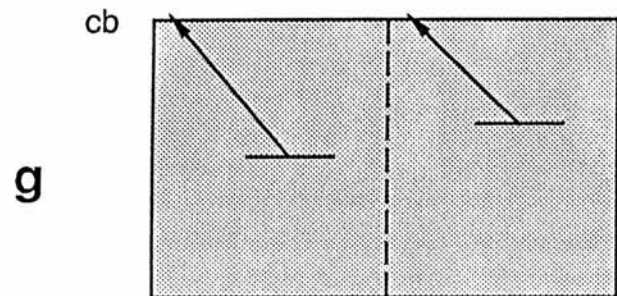
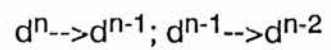


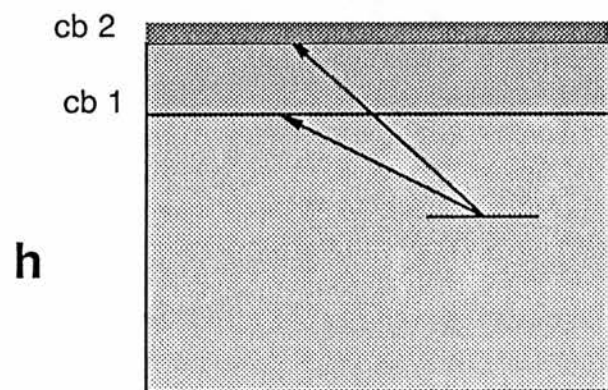
Figure 6.3a-e Types of transition possible with one Level and excited States.



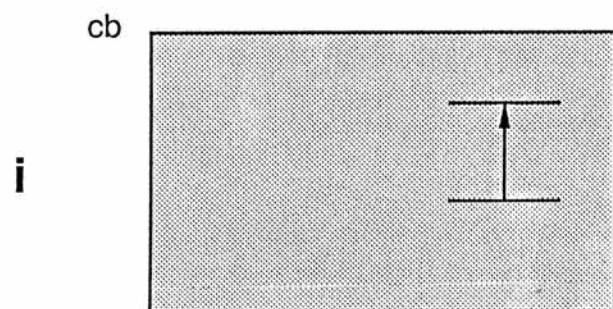
Two Stage Photoionisation



Photoionisation of Two Different Centres



Transitions involving higher Extrema

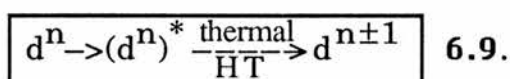


Internal Absorption

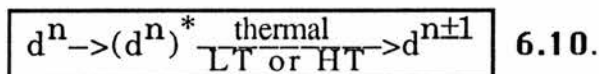
No charge transfer

Figure 6.3f-i: Other processes possible with more than one charge state; more than one centre or more than one band involved. Internal absorptions in mid-gap are only observed in optical absorption experiments.

6— A photoionisation transition could take place through an intermediate state. If there was an excited state very close to the band edge, thermal processes could then ionise the centre. A peak in the spectrum should appear at energies just below the photoionisation edge at high temperatures and disappear at low temperatures. This is a photothermal peak as was found in n-type GaP doped with nickel (Chapter Three)^[30,32]. This can be expressed as:



7— If there is an excited state at an energy corresponding to it lying just within a carrier band, i.e. in resonance with the band, this could produce a peak which obscured the threshold of the ground state photoionisation behaviour.



Resonances can, in some circumstances, produce not increases in absorption coefficient, but small dips.

These various processes are illustrated in figure 6.3c-i in the form of excitation-ionisation level diagrams. These must be recognised as being handy, simple representations of complex processes. Care must be taken that one does not rely too much on one particular modelling aid. For example, at least a one-dimensional configuration coordinate diagram is needed to account for the difference between thermal and optical depths of levels.

Table 6.2 Symmetry Based Photoionisation Selection Rules under T_d Symmetry

	Transition	$\Gamma_i \otimes \Gamma_{h\nu}$	$\Gamma_f \otimes \Gamma_{band}$
to cb	$d^1 \rightarrow d^0$	$E \otimes T_2 = T_1 + T_2$	$A_1 \otimes A_1 = E$
	$d^2 \rightarrow d^1$	$A_2 \otimes T_2 = T_1$	$E \otimes A_1 = E$
	$d^3 \rightarrow d^2$	$T_1 \otimes T_2 = A_2 + E + T_1 + T_2$	$A_2 \otimes A_1 = A_2$
	$d^4 \rightarrow d^3$	$T_2 \otimes T_2 = A_1 + E + T_1 + T_2$	$T_1 \otimes A_1 = T_1$
	$d^5 \rightarrow d^4$	$A_1 \otimes T_2 = T_2$	$T_2 \otimes A_1 = T_2$
	$d^6 \rightarrow d^5$	$E \otimes T_2 = T_1 + T_2$	$A_1 \otimes A_1 = A_1$
	$d^7 \rightarrow d^6$	$A_2 \otimes T_2 = T_1$	$E \otimes A_1 = E$
	$d^8 \rightarrow d^7$	$T_1 \otimes T_2 = A_2 + E + T_1 + T_2$	$A_2 \otimes A_1 = A_2$
	$d^9 \rightarrow d^8$	$T_2 \otimes T_2 = A_1 + E + T_1 + T_2$	$T_1 \otimes A_1 = T_1$
to vb	$d^0 \rightarrow d^1$	$A_1 \otimes T_2 = T_2$	$E \otimes T_2 = T_1 + T_2$
	$d^1 \rightarrow d^2$	$E \otimes T_2 = T_1 + T_2$	$A_2 \otimes T_2 = T_1$
	$d^2 \rightarrow d^3$	$A_2 \otimes T_2 = T_1$	$T_1 \otimes T_2 = A_2 + E + T_1 + T_2$
	$d^3 \rightarrow d^4$	$T_1 \otimes T_2 = A_2 + E + T_1 + T_2$	$T_2 \otimes T_2 = A_1 + E + T_1 + T_2$
	$d^4 \rightarrow d^5$	$T_2 \otimes T_2 = A_1 + E + T_1 + T_2$	$A_1 \otimes T_2 = T_2$
	$d^5 \rightarrow d^6$	$A_1 \otimes T_2 = T_2$	$E \otimes T_2 = T_1 + T_2$
	<i>>> $d^5 \rightarrow d^6$</i>	$A_1 \otimes T_2 = T_2$	$T_2 \otimes T_2 = A_1 + E + T_1 + T_2$ <<
	$d^6 \rightarrow d^7$	$E \otimes T_2 = T_1 + T_2$	$A_2 \otimes T_2 = T_1$
	$d^7 \rightarrow d^8$	$A_2 \otimes T_2 = T_1$	$T_1 \otimes T_2 = A_2 + E + T_1 + T_2$
	$d^8 \rightarrow d^9$	$T_1 \otimes T_2 = A_2 + E + T_1 + T_2$	$T_2 \otimes T_2 = A_1 + E + T_1 + T_2$

(>> Transition to first excited state of d^6 <<)

Orbital symmetry forbidden transitions $\{(\Gamma_i \otimes \Gamma_{h\nu}) \otimes (\Gamma_f \otimes \Gamma_{band})$ which do not contain the identity element $A_1\}$ are shown in *Italics*.

Table 6.3 Low and High-spin Configurations Compared and Differences Noted.

<u>d electrons</u>	<u>low-spin</u>	<u>(common)</u>	<u>high-spin</u>
<u>Symmetry</u>			<u>Symmetry</u>
1		e^1	
		e	
2		e^2	
		e	t_2
3	2E	e^3	$e^2t_2^1$ 4T_1
		e	t_2
4	1A_1	e^4	$e^2t_2^2$ 5T_2
		t_2	t_2
5	2T_2	$e^4t_2^1$	$e^2t_2^3$ 6A_1
		t_2	e
6	3T_1	$e^4t_2^2$	$e^3t_2^3$ 5E
		t_2	e
7		$e^4t_2^3$	
		t_2	
8		$e^4t_2^4$	
		t_2	
9		$e^4t_2^5$	

The letters e , t_2 , e , t_2 refer to the type of orbital which is involved in a photoionisation transitions involving the two configurations listed above and below. The outlined letters show that there is a different type of orbital involved in transitions between high-spin systems and those between low-spin systems. The symmetries given for the configurations are different in the two cases.

6.5 Discussion

A comparison is made in this section between the expectations outlined in the preceding section and the experimental results available. There will be comments on the tables in general and about particular experimental results. The differences between the observed and expected trends will be given. Finally some observations are made which could account for the observed discrepancies and preserve the present theory to await the test of future experimental results.

The cross sections found in the literature for 3d impurities in the three most common wide bandgap III-V materials (InP, GaAs and GaP) are given in table 6.4a. In table 6.4b the cross sections found in three II-VI materials are given (ZnS, ZnSe and CdSe). For other II-VI materials ZnTe and CdTe the few entries (two each) are listed beneath the body of the table. Values taken by optical absorption have in some cases been calculated by the authors and others I have had to calculate using eqn. 6.4. The data so calculated has been vetted carefully^[105]. Annotations to the table entries give the experimental method used and the reference(s) from which the data were taken. The many blank positions in the table should be noted. There are several reasons for this incompleteness. The first is that no suitable experimental results have been made, as in the case of ZnS:Ti. Secondly, in some cases the data is not in a suitable form from which to calculate the absolute cross section; some papers do not contain impurity concentration data; others measure only a relative absorption coefficient.

There are several ways in which a complex set of data such as has been compiled for the 3d ion photoionisation cross sections can be analysed. Firstly, we will look at the type of orbital (e or t_2) involved in the transition, working from the supposition that the ground states of

impurities are given by considering the Hund rule single-electron configurations. Next we shall attempt to look at trends across the 3d series and then to examine the case of single impurities in different host crystals. Geometric means are used to compare different subsets of the cross section data numerically. The geometric mean is a better "averaging" procedure than an arithmetic mean when one wishes to give equal weightings to data which differ by an order of magnitude.

All the data show that for transitions involving a change of t_2 orbital occupancy, under the Hund rule scheme, the cross sections for complementary transitions are of the same order of magnitude. There are eight such examples in the tables: three in II-VI materials and five in III-V hosts. When one looks at the availability of measured complementary transition data for supposed e orbital occupancy changes, there is a relative scarcity compared to the t_2 data. There are, neglecting iron in the III-V materials, only three such transitions in III-V materials and only the ZnS:Fe data in II-VI materials. All of these transition pairs, except in InP:Co, show transitions to the conduction band about an order of magnitude smaller than the transitions resulting in holes in the valence band. Iron in III-V compounds has the curious property that there is a weak $d^5 \rightarrow d^6$ transition, of the same order of magnitude in GaAs and GaP as the $d^6 \rightarrow d^5$ transition, and at 0.3–0.4eV higher energies there is a much stronger transition, of the same order of magnitude as those transitions of undoubted t_2 orbital occupancy change^[103,106–109]. This strong transition can produce luminescence corresponding to the internal d^6 transition 5E to 5T_2 ^[110]. Spectra similar in form to the iron doped binaries are also seen in the ternary alloys GaAsP^[111] and AlGaAs^[112] over all studied compositions.

It is clear that the Hund rule t_2 transitions to the valence band in II-

VI materials are much weaker than in III-V materials. The geometric mean of eleven results in III-V hosts is $5 \times 10^{-17} \text{ cm}^2$, whereas that of six results in II-VI hosts is $1 \times 10^{-17} \text{ cm}^2$, a difference of a factor of five. Likewise for t_2 transitions to the conduction band we find: in III-V materials the geometric mean is $5 \times 10^{-17} \text{ cm}^2$ (five results); and in II-VI materials it is $8 \times 10^{-18} \text{ cm}^2$ (six results). In this case the factor is about six greater for the III-V materials. A similarly sized ratio of approximately six is found for the e transitions to the valence band in III-V semiconductors compared to II-VI materials, using the III-V data which do not include the anomalous iron results. The uncertainty in the geometric means for the e transitions to the conduction band is very large. The geometric mean data has been summarised in Table 6.5.

From the two preceding paragraphs we can conclude in addition to the question of a selection rule forbidding e transitions to the conduction band: 1– In general photoionisation cross sections are significantly smaller in II-VI semiconducting materials than in III-Vs. This fact is consistent with the increased delocalisation in III-V materials which comes from their greater covalency. 2– The transitions to the valence band are of approximately the same magnitude as those to the conduction band when there is a change of t_2 orbital occupation.

Since achieving the categorisation of the the data by semiconductor type, e or t_2 orbital involvement and band involved we are now in a position to note that the Gnatenko *et al.*^[113] value for the transition interpreted by the authors as the cobalt $d^7 \rightarrow d^6$ transition in zinc telluride is anomalous. This is expected to be an e orbital transition to the conduction band on the high-spin ground state model. Its magnitude ($1.5 \times 10^{-17} \text{ cm}^2$) is large compared to the typical (geometric mean) value for II-VI t_2 transitions ($0.8 \times 10^{-17} \text{ cm}^2$) to the conduction band. The only other value for ZnTe

transitions is $2.0 \times 10^{-17} \text{ cm}^2$ for the chromium $d^4 \rightarrow d^5$ transition (which is a high-spin t_2 orbital transition). It now appears that there are two transitions which do not fit the theory constructed, both apparently involving the $d^7 \rightarrow d^6 + e_{cb}$ transition of cobalt. Indium phosphide and zinc telluride are the only two materials for which (as far as we are aware) photoionisation cross section data exists for this transition. We will examine in Section 6.5.1 the possible reasons why this material should not fit a theory which otherwise works well.

The next approach taken to analysing the data is to look for trends in the cross sections within a single host material across the 3d transition series. The material with the most complete set of photoionisation cross section data is indium phosphide. Of the possible 10 pairs of different $d^n \rightarrow d^{n+1}$ configurations only three pairs of transitions are not available. All these transitions have been measured by one basic technique, DLOS, and with this fact the data are more easily compared to one another. The cross sections for indium phosphide are plotted with a logarithmic ordinate for the cross section value in figure 6.4. We note that according to our previous analysis of Section 6.4, we should look at transitions presumed to be t_2 transitions separately from those taken to involve e orbital electrons. The following points are noted.

- 1) Except for cobalt, the remarks made for the geometric means in III-V materials hold specifically in InP.

- 2) The cobalt transitions have large cross sections even for t_2 orbital transitions.

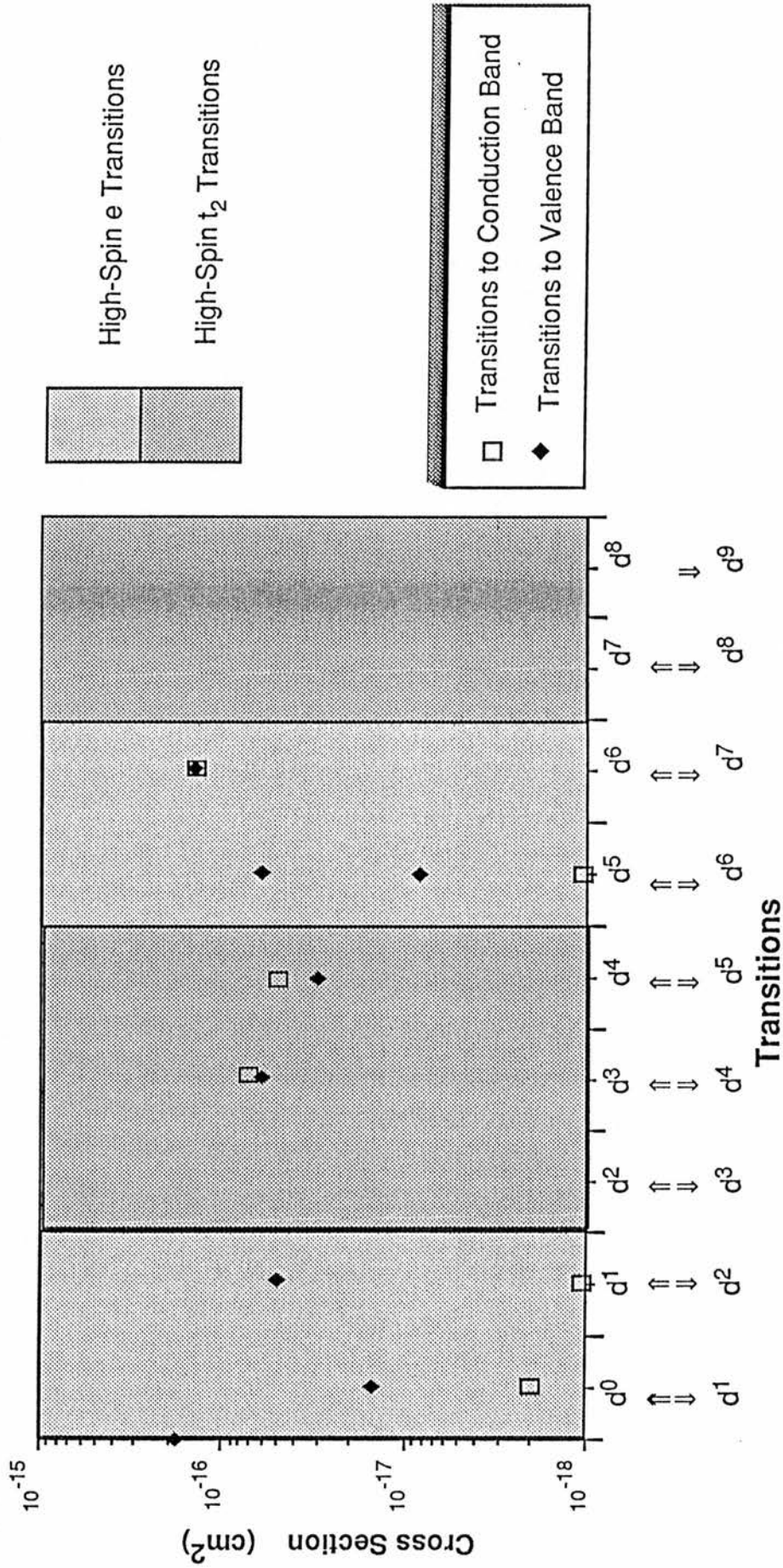


Figure 6.4 A logarithmic plot of the known maximum photoionisation cross sections for 3d transition metal impurities in indium phosphide. Both the transitions to the conduction band and the valence band are given.

3) Unfortunately the second group of unequivocal t_2 transitions, d^7/d^8 and d^8/d^9 , is not represented in the data making trend analysis of t_2 orbital cross sections impossible.

Comparison of the cross sections in InP, GaAs and GaP, in all cases where data is available for the same transitions in all three materials, reveals the decreasing order GaAs, InP, GaP. The most marked decreases occur between indium phosphide and gallium phosphide. The energy gap is much larger in GaP than in either InP or GaAs.

The data for alloy cross sections is interesting to see the variation of cross section with host material. The cross sections are available only for two materials, $\text{GaAs}_{1-y}\text{P}_y:\text{Fe}$ ($0.0 \leq y \leq 0.76$)^[111] and $\text{Al}_x\text{Ga}_{1-x}\text{As}:\text{Fe}$ ($0.0 \leq x \leq 0.77$)^[112]. In each of these alloys the cross sections to both the ^5E and the $^5\text{T}_2$ levels decreases by more than one order of magnitude as x or y increases. As far as it is possible to tell, since the transition to the $^5\text{T}_2$ level obscures the maximum of the ^5E transition, the ratio of the two maximum cross sections is independent of composition. The maximum cross section to the $^5\text{T}_2$ level in both the alloys is shown in figure 6.5. What causes this vast change? There are a number of possibly relevant factors which change with composition and which might be responsible for the variation with host material. Firstly, due to alloy mixing the local symmetry of the iron ions changes. There are three possible symmetries (T_d , C_{3v} or C_{2v})^[111] if one assigns a point-group symmetry based solely on the four nearest-neighbours and forgets longer range effects. There is no obvious reason why the reduction of symmetry should lead to a decrease of cross section, indeed one expects the reverse when considering symmetry alone. Secondly, the bandgap of the materials is increasing as the composition deviates from GaAs. In addition to this there is a change from the direct

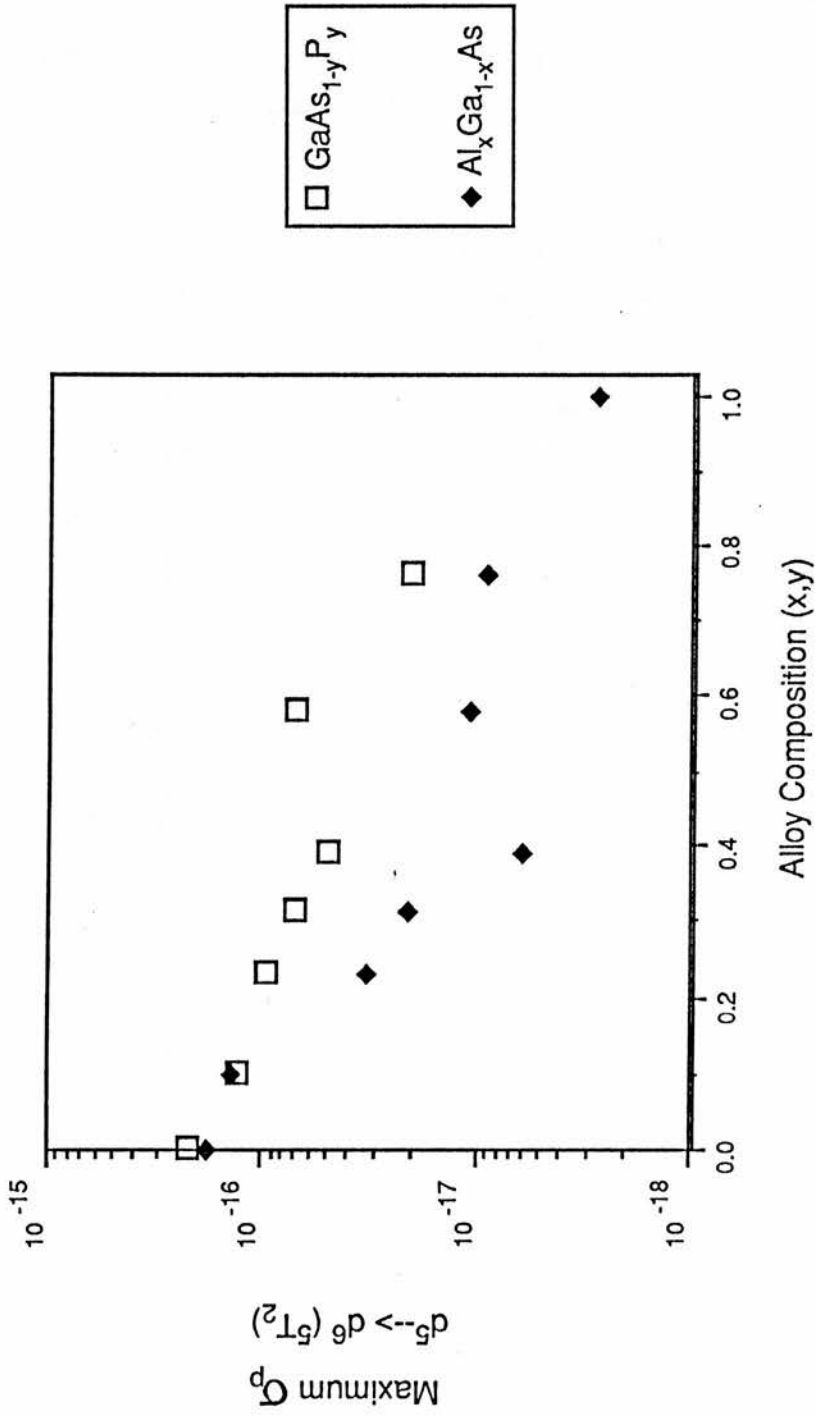


Figure 6.5 A plot of the maximum photoionisation cross section against composition for the $d^5 \rightarrow d^6 ({}^5T_2)$ transition of iron in the ternary alloys AlGaAs and GaAsP.

gap GaAs to an indirect gap in both the $\text{GaAs}_{1-y}\text{P}_y$ ($y > 0.47$) and $\text{Al}_x\text{Ga}_{1-x}\text{As}$ ($x > 0.45$) alloys but here we are concerned with transitions to the valence band, not to the conduction band.

In summary it would appear, looking at the alloy data in isolation, that the energy gap increase is most likely to be responsible for the large change in cross section, but that symmetry reduction through alloy disorder causes a small enhancement of the cross section in the region of maximum disorder (x, y at $\sim 50\%$). This is not in full agreement with the fact that the energy gap ordering (InP, GaAs, GaP) does not exactly match the overall transition magnitude ordering (GaAs, InP, GaP) in III-Vs.

There are models which predict that the cross section to the valence band depends on the carrier mass in the band^[85]. This is found to be stronger than a linear dependence. It is also suggested that only heavy-hole masses, m_{hh} , need to be included to obtain the approximate magnitude of the cross section. In the III-V materials this can not be a major factor influencing the geometric mean cross section because the heavy-hole masses in GaP and InP are very similar and in GaAs m_{hh} is smaller – exactly the opposite trend to the one that we were seeking.

A similar analysis could be performed for other host material parameters (e.g. permittivity or ionicity). Even if correlations can be found with "average" cross sections the information is of limited use until it is incorporated within a wider theoretical framework. One practical application of this study is it provides an estimate of the maximal cross section in a particular material to within an order of magnitude. Thus if one were to calculate from experiment a cross section in GaP of, say $2.5 \times 10^{-16} \text{ cm}^2$, then it should be re-examined more carefully.

6.5.1 Are low-spin states possible? The cases of InP:Co and ZnTe:Co.

In this section we examine the evidence for the existence of low-spin ground states. First the theoretical possibilities will be discussed then the specific case of the d^6 configuration will be examined in more detail. Finally we compare the experimental evidence and suggest possible further investigations.

The low-spin regime is favoured for the case of crystal fields which are strong compared to the one-electron exchange splitting energy.

The d^6 system ground state is found to change as a function of Δ in standard crystal field theory^[92] (B, C, Δ theory). BC Δ theory shows that the cross over to a low-spin ground state occurs at a Δ/B value of 3.0, a lower value than for any other d^n electron configuration except for d^4 .

O'Neill^[94] has developed a semi-empirical crystal field theory ($\mathcal{E}\tau\Delta_p$ theory) which takes into account differential delocalisation of the e and t_2 orbitals. The delocalisation is explicitly accounted for in two parameters \mathcal{E} and τ which are unity for a completely localised (atomic) system and decrease with increasing delocalisation. The reduction of τ is a measure of hybridisation with nearest-neighbour electrons and the reduction of \mathcal{E} measures the radial expansion of the e orbitals. In the limit ($\mathcal{E}, \tau = 1$) the theory reduces to BC Δ crystal field theory. O'Neill predicts that the d^6 , d^4 and d^7 configurations are capable of showing low-spin ground states if certain conditions on the crystal field parameter and the e and t_2 localisation parameters are satisfied. The d^6 configuration meets these conditions for a larger (and more physically reasonable) range of values of Δ , \mathcal{E} and τ than do the d^4 and d^7 configurations. We have given a phase

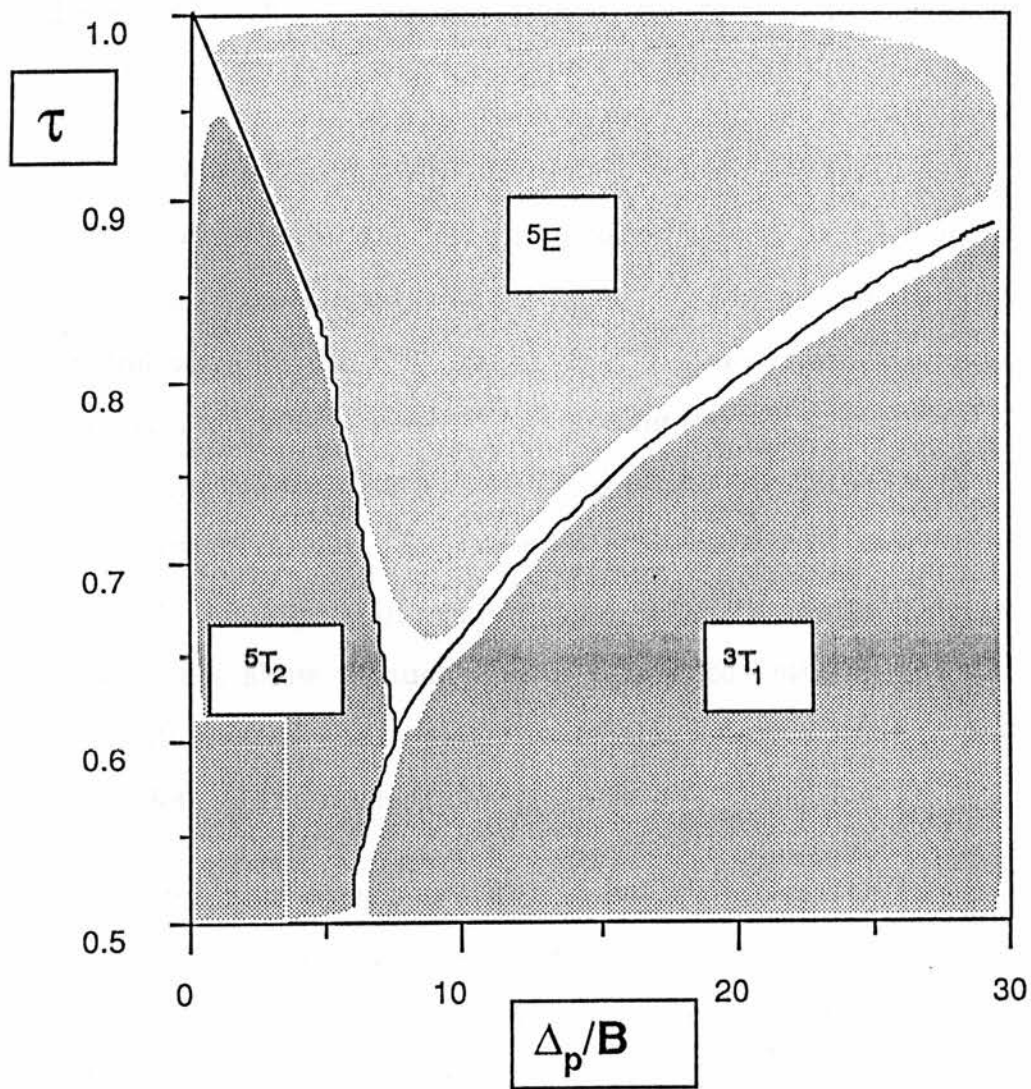


Figure 6.6 The d^6 configuration ground state symmetry phase diagram in the O'Neill model (T_d symmetry) with $C_0/B_0=4.81$ (free ion value) and covalency parameter ϵ fixed at 1.00.

diagram for the d^6 configuration in figure 6.6. Such diagrams are two-dimensional projections of a surface in four-dimensions (energy, Δ , \mathcal{E} , \mathcal{T}).

Other workers have predicted unseen low-spin ground states, or systems close to having low-spin ground states, in the more covalent III-V materials. Fazzio, Caldas and Zunger^[72] (FCZ) predict a possible low-spin ground state for the V d^3 ion in GaP. Watanabe and Kamimura^[73], in 59 atom cluster calculations^[114] and using the effective crystal field theory of FCZ, have constructed a diagram showing the GaAs:Co d^6 (Co^{3+}) excited state structure. The 3T_1 low-spin state is shown as lying only $\sim 0.05\text{eV}$ above the 5E high-spin ground state, whereas similar calculations for the Fe d^6 state show a much larger difference between the two multiplets. This illustrates the sensitivity of the relative energy position of the multiplets to the nuclear charge.

The same arguments apply, *but with less confidence*, to ZnTe:Co. Zinc telluride is the most covalent member of the zinc cationic II-VI semiconductor series and shows greater delocalisation of orbitals than ZnS or ZnSe do. If we continue this very simple argument then we have to predict a low-spin ground state in CdTe which is more covalent than ZnTe.

In summary, d^6 having a low-spin ground state is a possibility which has a number pieces of circumstantial evidence supporting it. A high-spin d^7 to a low-spin d^6 transition would involve a t_2 orbital electron — a T_d symmetry allowed photoionisation transition to the conduction band. This explanation brings the cobalt data in InP and ZnTe into line with vast majority of analysed data. The range of values needed for orbital delocalisations and the crystal field in the O'Neill covalent crystal field theory to produce a low-spin d^6 state are not physically unreasonable in

InP. The consequence of this is we expect Co d^6 to be a low-spin or almost a low-spin system in GaAs, GaP and CdTe.

Table 6.4a Maximum Absolute Photoionisation Cross Sections for InP, GaAs, and GaP ($\times 10^{-16} \text{ cm}^2$)

	d^n/d^{n+1}	InP		GaAs	GaP
Ti	0/1	0.02 ^{a1,*}	0.15 ^{a2,*}	α	α
V	1/2	<0.01 ^{a3,†}	0.5 ^{a4,†}		0.5 ^{b0}
Cr	2/3			1.0 ^b	2.1 ^b
Cr	3/4	0.7 ^{a4}	0.6 ^a		0.9 ^c 0.08 ^f 0.1 ^f
Mn	4/5	0.5 ^a	0.30 ^{a,‡}		0.8 ^{f2,\$} 0.6 ^f
Fe	5/6	0.005 ^{a5}	0.6 ^{a#}	<0.001 ^d	2.0 ^{e,e0} ⁵ T ₂ <0.08 ^f 0.2 ^{f1} ⁵ T ₂
		⁵ T ₂ [↑]	0.08 ^{5E}		0.2 ^{d,e} ⁵ E 0.02 ^{e1} ⁵ E
Co	6/7	1.4 ^a	1.4 ^a		0.5 ^{f2}
Co	7/8				>0.6 ^{f3}
Ni	7/8			>0.5 ^g	0.3 ^h
Ni	8/9				0.2 ⁱ 0.2 ⁱ

Outlined results are those transitions which result in holes in the valence band, plain text - electrons in the conduction band.

OA is used to denote Optical Absorption data.

a [103] DLOS Ti,V,Cr data published in references contained therein. 1 Excited state just above threshold energy and second onset at 1.25eV. 2 Maximum photon energy 1.2eV. 3 No transition found. 4 Spectrum contains an excited state and a second onset. 5 Spectrum contains a second onset. * [89] DLOS. † [115] DLOS. ‡ [116] OA. They obtained $5 \times 10^{-17} \text{ cm}^2$. # [117] Photocapacitance. Several levels in gap.

b0 [4] OA.

b [90] Photocapacitance.

c Ref. [85]. OA.

d [104]. Photocapacitance..

e [111]. Photocapacitance.

e0 [118] $> 9 \times 10^{-16} \text{ cm}^2$ OA. with [108] OA.

e1 [30] Photocapacitance, combined

f [107]. Photocapacitance.

f1 [108]. OA.

f2 [119] OA.

f3 [120] OA..

g [121] also [122] OA.

h [47] OA.

i [30]. Photocapacitance.

α OA results of [98] suggest that the transition to the valance band is stronger than that to the conduction band in GaAs:Ti.

£ [123] OA.

\$ [124] have $2.5 \times 10^{-16} \text{ cm}^2$. OA.

Table 6.4b Maximum Absolute Photoionisation Cross Sections for ZnS, ZnSe and CdSe ($\times 10^{-18} \text{ cm}^2$)

	<u>ZnS</u>		<u>ZnSe</u>		<u>CdSe</u>	
	n	p	n	p	n	p
	0/1					
Ti	1/2					8^a
V	2/3		9^b	$>12^c$	9^a	
Cr	3/4				$10^{d,j}$	
Cr	4/5	5^e	5^f	10^g	8^f	
Fe	5/6	$0.8^{h,i}$	8^h	7^j	0.7^k	
	6/7					
Ni	7/8				$>5^l$	
Ni	8/9		14^m			

a [125] Optical Absorption.

b Result from Chapter Five of the present work. Photocapacitance.

c [79] Optical Absorption.

d [126] Optical Absorption. This is the most recent reference found.

e [127] Optical Absorption.

f [57] Optical absorption.

g See Chapter Four of the present work. Photocapacitance.

h [82] Photo-EPR.

i. [128] Optical absorption.

j [129] Photo-EPR.

k [130] Optical Absorption. Less certainty in measurement than in [55].

l [99] Optical Absorption. Another onset occurs at 1.7eV.

m [131] Optical Absorption.

Other known absolute photoionisation cross sections in II-VI materials include the following (all from optical absorption): ZnTe:Cr $d^4 \rightarrow d^5$ ($2.0 \times 10^{-17} \text{ cm}^2$) [87], ZnTe:Co $d^7 \rightarrow d^6$ ($1.5 \times 10^{-17} \text{ cm}^2$) [113] and CdTe:Cr $d^4 \rightarrow d^5$ ($1.5 \times 10^{-17} \text{ cm}^2$) [88].

Table 6.5 Comparing e and t_2 (High-spin Assignments)
Transitions to the Conduction and Valence Bands

Geometric Means of Available Data.

III-V	<u>e to cb</u> $<1.5 \times 10^{-18} \text{ cm}^2$ a $1.0 \times 10^{-18} \text{ cm}^2$ b $7 \times 10^{-18} \text{ cm}^2$ c	<u>e to vb</u> $5 \times 10^{-17} \text{ cm}^2$ a $2.0 \times 10^{-17} \text{ cm}^2$ b $7 \times 10^{-18} \text{ cm}^2$ c
II-VI	<u>e to cb</u> $7 \times 10^{-19} \text{ cm}^2$	<u>e to vb</u> $8 \times 10^{-18} \text{ cm}^2$
III-V	<u>t_2 to cb</u> $5 \times 10^{-17} \text{ cm}^2$	<u>t_2 to vb</u> $5 \times 10^{-17} \text{ cm}^2$
II-VI	<u>t_2 to cb</u> $8 \times 10^{-18} \text{ cm}^2$	<u>t_2 to vb</u> $1.0 \times 10^{-17} \text{ cm}^2$

a not including iron data.

b including iron data.

c iron data only.

6.6 Conclusions

In this chapter some theoretical properties of incomplete 3d shell electronic systems, in binary semiconductors, under T_d symmetry, have been examined. The consequences for the magnitudes of the photoionisation cross sections have been explored. An extensive literature review has resulted in the compilation of tables of known photoionisation cross sections in both III-V and II-VI materials. The absolute magnitudes of the cross sections, but not the spectral shapes, were compared to one another. A good correlation of the cross section magnitudes was found to the predictions of a symmetry–argument–based selection rule. The two exceptions to this selection rule, when high-spin ground states are assumed, can be accommodated within the same framework if the cobalt d^6 ion has a low-spin ground state in the more covalent materials.

Other trends in the cross section data have been noted. Comparisons between III-V and II-VI semiconductors have been made showing III-V cross sections to be typically the order of five times larger than II-VI materials. A tentative proposition is put forward that cross sections will in general be larger in hosts of smaller bandgap.

Appendix 6.1Deriving the Photoionisation Selection Rule

In this appendix the selection rule forbidding e transitions to the conduction band and allowing other types of transition under T_d symmetry is determined explicitly and systematically but not in a rigorous mathematical manner.

The identity element must be contained within the direct product $(\Gamma_i \otimes \Gamma_\gamma) \otimes (\Gamma_f \otimes \Gamma_{\text{band}})$ which can be rearranged, because of the group commutivity and associativity, to $(\Gamma_i \otimes \Gamma_f) \otimes (\Gamma_\gamma \otimes \Gamma_{\text{band}})$. For the transitions to the valence band $(\Gamma_\gamma \otimes \Gamma_{\text{band}})$ contains the representations A_1 , E, T_1 and T_2 . Therefore the transition will be forbidden only if $(\Gamma_i \otimes \Gamma_f)$ contains A_2 only. Thus $A_2 \leftrightarrow A_1$ transitions are not allowed. In changing the number of d electrons by one this is not possible. Therefore all transitions between high-spin ground states are allowed which result in a hole in the valence band.

In the case of transitions to the conduction band $(\Gamma_\gamma \otimes \Gamma_{\text{band}})$ contains only T_2 . Therefore $(\Gamma_i \otimes \Gamma_f)$ must contain a T_2 representation to be allowed. We now consider changing the e orbital occupation and changing the t_2 orbital occupation separately. For e transitions we must have empty, half-full or full t_2 levels with representations A_1 , A_2 and A_1 respectively. The e orbital symmetry must change from an A state (0, 2 or 4 electrons) to an e state (1 or 3 electrons), or vice-versa. Therefore $(\Gamma_i \otimes \Gamma_f)$ must contain only the representation E. Therefore all e orbital changes to the conduction band are forbidden.

When the t_2 orbital occupation changes, the e level symmetry must contain either A_1 or A_2 . The t_2 orbital symmetry can change from $A_1 \leftarrow$

$T_2 \leftrightarrow T_1 \leftrightarrow A_2$ as one adds an extra t_2 electron (\rightarrow) or takes it away (\leftarrow). The resultant possible sets of representations contained within $(\Gamma_i \otimes \Gamma_f)$ are $\{T_2\}$ and $\{A_2, E, T_1, T_2\}$, both of which include T_2 . Therefore, since $(\Gamma_\gamma \otimes \Gamma_{\text{band}})$ contains only T_2 , t_2 transitions to the conduction band are allowed.

The same procedure could be used to derive symmetry selection rules for photoionisation transitions under different point group symmetries. The most relevant symmetry groups would be C_{2v} and C_{3v} .

Appendix 6.2Further Comments on low-spin systems

A d^4 phase diagram showing ground state against λ_e^4 and λ_t^4 for several values of Δ_{eff} was given in full by Fazzio *et al.* [72]. In the present work the equivalent O'Neill–Allen^[94,132] theory phase diagram has been calculated using the same Racah C/B ratio (that appropriate to the free ion $\text{Cr}^{2+} - d^4$)^[95] for comparison. A close correspondence between the ground state predictions in the two formulations of crystal field theory which include delocalisation effects was observed.

We will now comment on the positions of the cobalt d^6/d^7 level with respect to vacuum energies in II-VI materials. Deep levels for a particular transition metal impurity are often found to be approximately the same depth below the vacuum level for a group of similar semiconductors^[133] (III-V vacuum related energies are different from II-VI materials). For the case of ZnSe and ZnTe doped with cobalt, the level is believed to lie 1.4–1.5eV above the valence band maximum in ZnS^[134], 0.3eV above the maximum in ZnSe^[93] and is 0.86eV above it in ZnTe^[113]. These values translate into vacuum related values of -6.05eV, -6.10eV and -4.90eV (photoemission has been used to establish the position of the band gap relative to the vacuum level^[135,93]).

The discrepancy between the anticipated approximately equal values^[133] could be due to one of two reasons, the formation of a low-spin ground state for the d^6 configuration, or the experimental level seen is not the cobalt d^6-d^7 level. Comparison with the position of the d^8-d^7 level is needed. In the III-V materials we find valence band related energies of 0.41eV, 0.16eV and 0.25eV respectively in GaP^[136], GaAs^[137] and InP^[103]. These values are -5.54eV (in GaP), -5.37eV (GaAs) and -5.52eV

(InP) with respect to the vacuum level. These values are in reasonable agreement with each other. There are several alternative reasons why these values are all similar: 1- all have low-spin d^6 ground state. 2- Low-spin ionisation values agree with high-spin values. 3- The data or its assignment to the $d^7 \rightarrow d^6$ transition is wrong. 4- There is another as yet unexplained reason to break the apparent selection rule ($e \rightarrow cb$ is weak).

Chapter Seven : Conclusions

In this the final chapter the most important results presented in this thesis are re-stated, along with possible lines of future research following on from this work. A more detailed summary of the results and conclusions for particular impurity systems can be found at the end of each relevant chapter.

Chapter One contained a very brief introduction to deep levels in semiconductors, their pictorial representations and some of the experimental methods used to characterise and then identify the centres responsible for deep levels. Also, it was felt that the introduction was the appropriate place for a short discussion of deep level kinetics which would be pertinent to the discussions in subsequent chapters. Chapter Two discussed the experimental apparatus, experimental procedures adopted and the problems encountered in taking the phot capacitance results in Chapters Three, Four and Five.

Gallium phosphide doped with nickel was the subject of the study in Chapter Three. It was shown, by repeating an earlier manually operated experiment, that the automation of the phot capacitance experiment (control and data acquisition) had been successful. The automation project had been started by Mudhar^[31] but was completed by the author. Double light source steady-state experiments with different pump light energies showed that the ground state could be influenced substantially by the pump light. When a 2.00eV photon energy pump light source was used the d^9 state was populated. This was deduced from the photothermal peak in the DLSS spectrum which corresponded to a transition to the conduction band via the 2E crystal-field split excited state of the $^2T_2 d^9$ ground state. If

a 1.00eV photon energy pump light beam was used the most likely interpretation of the DLSS spectrum was that transitions were being observed from the d^8 state to the conduction band, both directly and via excited states.

In Chapter Four the $d^5 \rightarrow d^4 + e_{cb}$ transition of chromium in zinc selenide was studied. It was shown that a previously recorded level, of relatively low concentration, with an onset in the 0.6–0.7eV range, had been mistakenly attributed to the Cr $d^5 \rightarrow d^4$ transition. The optical transition energy found for the $d^5 \rightarrow d^4$ transition was about 1.1eV, in keeping with several published studies on the complementary ($d^4 \rightarrow d^5$) transition. Computer fitting of the photoionisation model thought appropriate to this centre gave a thermal broadening factor inconsistent with the literature values. In general, though, a configuration coordinate diagram was found to provide a good description of the level properties. A measurement of the absolute value of the $d^5 \rightarrow d^4 + e_{cb}$ photoionisation cross section was obtained. The value was of the same order of magnitude as that for the $d^4 \rightarrow d^5 + h_{vb}$ transition.

Chapter Five contains what is probably, at the present, a unique phot capacitance study of vanadium in zinc selenide. A level was discovered to be present at very high concentrations 1.0–1.1eV below the conduction band minimum. This level is believed to be the vanadium d^2-d^3 level. The energy depth is consistent with recent theoretical predictions. The photoionisation cross section spectrum for the presumed $d^3 \rightarrow d^2$ transition is given in absolute units, having been calibrated relative to two absolute measurements. The cross section value was consistent with other transition metal systems in II-VI materials and with the model explored in Chapter Six. One obvious further investigation is to observe the

properties of the complementary $d^2 \rightarrow d^3$ transition, both the energy depth (optical and thermal) from which the relaxation energy can be estimated and cross section absolute magnitude. It might be possible to do this on an n -type sample using a low temperature photocapacitance experiment if one first empties the level with an intense light source of suitable photon energy.

In Chapter Six, tables were compiled of all the absolute photoionisation cross sections of levels arising from transition-metal impurities in III-V and II-VI semiconductors, found after an extensive literature search. These tables include the two results from Chapters Four and Five. Some simple models to obtain selection rules for the transitions were examined and tested against the experimental data. The most likely candidate model was based on differing T_d symmetry selection rules for the cases of changes in e or t_2 orbital occupation upon photoionisation (in shorthand e transitions or t_2 transitions). It was found that e transitions to the conduction band were symmetry forbidden whereas all t_2 transitions or e transitions to the valence band were allowed. Assigning the conventional high-spin ground states to the d^n configurations showed two anomalies: cobalt $d^7 \rightarrow d^6$ cross sections in indium phosphide and in zinc telluride were unexpectedly large. This could be accounted for by invoking a low-spin d^6 ground state in these semiconductors. A physically reasonable argument was found to explain this by taking account of the differential delocalisation of the e and t_2 orbitals due to covalency effects.

There is obviously scope for the completion, as far as levels lie within the bandgap, of the photoionisation cross section tables in Chapter Six. In particular the systematic use of junction capacitance techniques is strongly encouraged.

References

- [1] Lax M *J. Chem. Phys.* 20, 1752 (1952)
- [2] Clerjaud B, Naud C, Deveaud B, Lambert B, Plot B, Brémond G,
Benjeddou C, Guillot G and Nouailhat A
J. Appl. Phys. 58, 4207 (1985)
- [3] Gladkov P S, Monova E N and Ozanyan K B
Phys. Stat. Sol. (a) 104, K121 (1987)
- [4] Hennel A M, Brandt C D, Ko K Y, Lagowski J and Gatos H C
J. Appl. Phys. 62, 103 (1987)
- [5] Ulrici W, Eaves L, Friedland K, Halliday D P and Kreißl J
Mat. Sci. Forum 10-12, 637 (1986)
- [6] Ulrici W, Kreißl J, Vasson A, Vasson A M and En-Naqadi M
Phys. Stat. Sol. (b) 143, 195 (1987)
- [7] Hennel A M, Brandt C D, Ko K Y and Pawlowicz L M
Mat. Sci. Forum 10-12, 645 (1986)
- [8] Brémond G, Guillot G, Nouailhat A, Lambert B, Toudic Y, Gauneau M
and Deveaud B
Mat. Sci. Forum 10-12, 657 (1986)
- [9] Lambert B, Toudic Y, Coquille R, Grandpierre G and Gauneau M
Mat. Sci. Forum 10-12, 651 (1986)
- [10] Klein P B, Furneaux J E and Henry R L
Appl. Phys. Lett. 42, 638 (1983)
- [11] Dean P J *Prog. Cryst. Growth & Charact.* 5, 89 (1982)
- [12] Ayling S G and Allen J W *J. Phys. C* 20, 4251 (1987)
- [13] Zakrzewski A and Godlewski M *Phys. Rev. B* 34, 8993 (1986)
- [14] Dreyhsig J
M.Sc. Thesis, St Andrews Univ., Scotland (1987) [Unpublished]

- [15] Lang D V *J. Appl. Phys.* 45, 3023 (1974)
- [16] Morimoto J, Fudamoto M, Tahira K, Kida T, Kato S and Miyakawa T
Japan. J. Appl. Phys. 26, 1634 (1987)
- [17] Hurtes C, Boulou M, Mitonneau A and Bois D
Appl. Phys. Lett. 32, 821 (1978)
- [18] Sze S M *Physics of Semiconductor Devices*,
John Wiley & Sons, New York, USA (1981)
- [19] Grimmeiss H G and Ovrén C *J. Phys. E* 14, 1032 (1981)
- [20] Chantre A, Vincent G and Bois D *Phys. Rev. B* 23, 5335 (1981)
- [21] Godlewski M *Phys. Stat. Sol. (a)* 90, 11 (1985)
- [22] Brozel J and Bitter F *Phys. Rev.* 86, 308 (1952)
- [23] Cavenett B C *Adv. Phys.* 30, 475 (1981)
- [24] Davies J J *J. Cryst. Growth* 86, 599 (1988)
- [25] Feher G *Phys. Rev.* 103, 834 (1956)
- [26] van Engel P and Sie S G *Sol. State Comm.* 30, 515 (1979)
- [27] Ueda Y, Niklas J R, Spaeth J M, Kaufmann U and Schneider J
Sol. State Comm. 46, 127 (1983)
- [28] Hage J, Niklas J R and Spaeth J-M
Mat. Sci. Forum 10-12, 259 (1986)
- [29] Rees G J, Grimmeiss H G, Janzén E and Skarstam B
J. Phys. C 13, 6157 (1980)
- [30] Yang X-G, Samuelson L and Grimmeiss H G
J. Phys. C 17, 6521 (1984)

- [31] Mudhar P S
Ph.D. Thesis, St Andrews Univ., Scotland (1985) [Unpublished]
- [32] Szawelska H R, Mudhar P S and Allen J W
J. Phys. C 17, 6521 (1984)
- [33] Mead C A
Sol. State Electron. 9, 1023 (1966)
- [34] McCaldin J O, McGill T C and Mead C A
J. Vac. Sci. Technol. 13, 802 (1976)
- [35] Szawelska H R
Ph.D. Thesis, St. Andrews Univ., Scotland (1980) [Unpublished]
- [36] Mangelsdorf P
J. Appl. Phys. 30, 442 (1959)
- [37] Noras J M and Szawelska H R
J. Phys. C 15, 2001 (1982)
- [38] Yang X-Z and Allen J W
[Private Communication]
- [39] Yang X-Z and Allen J W
J.Lum. 40/41, 373 (1988)
- [40] Brunwin R F, Hamilton B, Hodgkinson J, Peaker A R and Dean P J
Sol. State Elect. 24, 249 (1981)
- [41] Szawelska H R, Noras J M and Allen J W
J. Phys. C 14, 4141 (1984)
- [42] Bishop S G, Dean P J, Porteous P and Robbins D J
J. Phys. C 13, 1331 (1980)
- [43] Kaufmann U and Schneider J
Sol. State Comm. 25, 1113 (1979)
- [44] Kaufmann U, Kochel W H and Schneider J
Phys. Rev. B 19, 3343 (1979)
- [45] Baranowski J M, Allen J W and Pearson G L
Phys. Rev. 167, 758 (1967)

- [46] Jeźnewski M, Liro Z and Godlewski M J. Phys. C 20, 311 (1987)
- [47] Abagyan S A, Ivanov G A and Koroleva G A
Sov. Phys. Semicond. 10, 1056 (1976)
- [48] Peaker A R, Kaufmann U, Wang Z-G, Wörmer R, Hamilton B
and Grimmeiss H G J. Phys. C 17, 6161 (1984)
- [49] Saidov M S, Abdrinov K, Saidov A S and Makarenko V G
Sov. Phys. Semicond. 17, 332 (1983)
- [50] Ennen H and Kaufmann U J. Appl. Phys. 51, 1615 (1980)
- [51] Clerjaud B J. Phys. C 18, 3615 (1985)
- [52] Hamilton B and Peaker A R
2nd. Lund Conference on Deep Levels in Semiconductors,
St. Maxime, France (1979) [Unpublished]
- [53] Fung S and Nicholas R J J. Phys. C 15, 7355 (1982)
- [54] Baranowski J M
Deep Levels in Semiconductors (Ed. Pantelides S T), Academic Press,
New York, USA (1986)
{The d^3-d^4 level is expected to lie close to the valence band. Although
Baranowski is probably correct in his claim that the d^3 state can be
observed in ZnSe the evidence he quotes is not well founded
(EPR data of
Rai R, Savard J Y and Tousigant B Phys. Lett. 25A, 443 (1967)).}
- [55] Title R S Phys. Rev. 133, A1613 (1964)
- [56] Röppischer H, Elssner W and Bottner H [In German]
Phys. Stat. Sol. (a) 27, 375 (1975)
- [57] Kamińska M, Baranowski J and Godlewski M
Inst. Phys. Conf. Series 43, 303 (1979)

References

U

- [58] Vallin J T, Slack G A, Roberts S and Hughes A E
Sol. State Comm. 7, 1211 (1969)
- [59] Grebe G, Roussos G and Schultz H-J
J. Lum. 12/13, 701 (1976)
- [60] Grebe G, Roussos G and Schultz H-J
J. Phys. C 9, 4511 (1976)
- [61] Mead C A
Phys. Letts. 18, 218 (1965)
- [62] Lucovsky G
Sol. State Comm. 3, 299 (1965)
- [63] Piekara U, Langer J M and Krukowska-Fulde B
Sol. State Comm. 23, 583 (1977)
- [64] Suto K, Aoki M, Nakada M and Ibuki S
J. Phys. Soc. Japan 22, 1121 (1967)
- [65] Fujiwara Y, Nishino T and Hamakawa H
Japan. J. Appl. Phys. 21, L727 (1982)
- [66] Skolnick M, Brozel M and Tuck B
Sol. State Comm. 43, 379 (1982)
- [67] Baranowski J M , Jeżewski M and Liro Z
Proc. 16th. Int. Conf. on the Phys. of Semicond., North-Holland (1982)
- [68] Vallin J T and Watkins G D
Phys. Rev. B 9, 2051 (1974)
- [69] More discussion on this subject can be found in Chapter Six and papers referred to therein..
- [70] Hite G E, Marple D T F, Aven M and Segall B
Phys. Rev. 156, 850 (1967)
- [71] Vasil'ev A V, Ippolitowa G K, Omel'yanovskii É M and Ryskin A M
Sov. Phys. Semicond. 10, 341 (1976)
- [72] Fazzio A, Caldas M and Zunger A
Phys. Rev. B 30, 3430 (1984)
- [73] Watanabe S and Kamimura H
J. Phys. Soc. Japan 56, 1078 (1987)

- [74] Meijer G and Avinor M Philips Res. Rep. 15, 225 (1960)
- [75] Avinor M and Meijer G J. Phys. Chem. Solids 12, 211 (1960)
- [76] Allen J W Physica 29, 764 (1963)
- [77] Holton W C, Schneider J and Estle T L Phys. Rev. 133 A1 638 (1964)
- [78] Allen J W and Wray E M J. Phys. C 4, 512 (1971)
- [79] Hoang Le Man and Baranowski J M Phys. Stat. Sol. (b) 84, 361 (1977)
- [80] Szawelska H R [Private Communication]
- [81] Depletion formula $\Delta n = \frac{k(C+\Delta C)^2}{V} - N$. Also refer to Chapter Six.
- [82] Godlewski M and Zakrzewski A
ZnS:Fe J. Phys. C 18, 6615 (1985)
- [83] Allen J W J. Phys. C 2, 1077 (1969)
- [84] Inkson J C J. Phys. C 14, 1093 (1981)
- [85] Martinez G, Hennel AM, Szuszkiewicz W, Balkanski M and Clerjaud B
GaAs:Cr Phys. Rev. B 23, 3920 (1981)
- [86] Martinez M Proc. ICDS-14, Mat. Sci. Forum 10-12, 603 (1986)
- [87] Komura H and Sekinobu M
ZnTe:Cr J. Phys. Soc. Japan 29, 1100 (1970)
- [88] Cieplak M Z, Godlewski M and Baranowski J M
CdTe:Cr Phys. Stat. Sol. (b) 70, 323 (1975)
- [89] Brémond G, Guillot G, Nouailhat A and Picoli G
InP:Cr J. Appl. Phys. 59, 2038 (1986)
- [90] Ulrici W and Kleinert P
GaAs:Cr Phys. Stat. Sol. (b) 129, 339 (1985)

- [91] Jahn H A and Teller E Proc. Roy. Soc. A 161, 220 (1937)
- [92] Sugano S, Tanabe Y and Kamimura H
Multiplets of Transition Metal Ions in Crystals,
Academic Press, New York (1970)
- [93] Zunger A Sol. State Phys. 39, 275 (1986)
- [94] O'Neill A G
Ph.D. Thesis, University of St Andrews, Scotland (1984) [Unpublished]
- [95] Griffith J S The Theory of Transition Metal Ions,
Cambridge University Press, London, England (1964)
- [96] McClure D S J. Chem. Phys. 30, 2850 (1963)
- [97] Ennen H, Kaufmann U and Schneider J
GaP:Ni Appl. Phys. Lett. 38, 355 (1981)
- [98] Hennel AM, Brandt C D, Wu Y-T, Bryskiewicz T, Ko K Y, Lagowski J
and Gatos H C GaAs:Ti Phys. Rev. B 33, 7353 (1986)
- [99] Baranowski JM and Phuong An
CdSe:Ni Phys. Stat. Sol. (b) 122, 331 (1984)
- [100] Godlewski M and Kamińska M
J. Phys. C 13, 6537 (1980)
- [101] Brunthaler G and Jantsch W Acta Phys. Polon. A71,
355 (1987)
- [102] The assumption of the conduction band being completely s-like and
the valence band being p-like will not stand up to close scrutiny.
Wentzcovitch *et al.*^[138] have performed calculations for ZnSe and
CdTe which suggest about 90% p, 10% d character at Γ_{15}^v , 100% s
character at Γ_1^c but only 26% s character at X_c^1 .
- [103] Brémond G, Guillot G and Nouailhat A [In French]
InP:Ti,V,Cr,Mn,Fe,Co,Cu Revue de Phys. Appl. 22, 873 (1987)

- [104] Kleverman M, Omling P, Ledebø L-Å and Grimmeiss H G
GaAs:Fe J. Appl. Phys. 54, 815 (1983)
- [105] The absorption data was checked as follows. The concentrations were checked to see how they had been calculated and if the magnitude was reasonable. If more than one sample, with a different concentration, was used the agreement of values between the two were checked. The absorption spectrum was examined for obscuring effects (such as given in figure 6.3).
- [106] Yang X-Z, Grimmeiss H G and Samuelson L
GaP:Fe Sol. State Comm. 48, 427 (1983)
- [107] Glorizova RI and Kolesnik L I
GaP:Cr, GaAs:Cr Sov. Phys. Semicond. 12, 66 (1978)
- [108] Abagyan S A, Ivanov G A and Kuznetsov Yu N
Sov. Phys. Semicond. 8, 1096 (1975)
- [109] Brehme S GaP:Fe J. Phys. C 18, L319 (1985)
- [110] Clark M G and Dean P J Inst. Phys. Conf. Series 43, 291 (1978)
- [111] Qisheng Huang, Grimmeiss H G and Samuelson L
GaAs/P:Fe J. Phys. C 18, 5443 (1985)
- [112] Wang Z-G, Ledebø L-Å and Grimmeiss H G
Ga/AlAs:Fe J. Appl. Phys. 56, 2762 (1984)
- [113] Gnatenko Yu P, Zhmurko A I, Potykevich I V and Farina I A
ZnTe:Co Sov. Phys. Semicond. 18, 689 (1984)
- [114] Fifty-nine atoms is a large cluster computationally, but corrections must be applied to obtain results for a physically reasonable crystal size. There are also problems with the bonds at the cluster edge.
- [115] Deveaud B, Plot B, Lambert B, Brémont G, Guillot G, Nouailhat A, Clerjaud B and Naud C InP:V J. Appl. Phys. 59, 3126 (1986)

- [116] Kurbatov VA, Omel'yanovskii ÉM, Polyakov AYa, Raïkhshteïn V I,
Karataev V V, Nashel'skii A Ya and Yakobson S V
InP:Mn Sov. Phys. Semicond. 19, 1084 (1985)
- [117] Grushko N S and Gutkin A A
InP:Fe Sov. Phys. Semicond. 8, 1179 (1975)
- [118] Andrianov D G, Omel'yanovskii É M, Rashevskaya E P
and Suchkova N I GaAs:Fe Sov. Phys. Semicond. 10, 637 (1976)
- [119] Brown W J and Blakemore J S
GaAs:Co,GaAs:Mn J. Appl. Phys. 43, 2242 (1972)
- [120] Jeżewski M, Baranowski J M and Radliński A
GaP:Co Proc. XI Conf. Phys Semicond. Compounds,
Warsaw , p. 255 (1983)
- [121] Suchkova N I, Andrianov D G, Omel'yanovskii É M,
Rashevskaya E P and Solov'ev N N
GaAs:Ni Sov. Phys. Semicond. 9, 469 (1975)
- [122] Bazhenov V K, Rasevskaya E P, Solov'ev N N and Foigel' M G
GaAs:Ni Sov. Phys. Semicond. 7, 1067 (1974)
- [123] Abagyan S A, Ivanov G A, Koroleva G A, Kuznetsov Yu N
and Okunov Yu A GaP:Mn Sov. Phys. Semicond. 9, 243 (1975)
- [124] Chapman R A and Hutchinson W G
GaAs:Mn Phys. Rev. Lett. 18, 443 (1967)
- [125] Langer J M and Baranowski J M
CdSe:V Phys. Stat. sol. (b) 44, 155 (1971)
- [126] Jastrebski L and Baranowski J M
CdSe:Cr Phys. Stat. Sol. (b) 58, 401 (1973)
- [127] Godlewski M ZnS:Cr J. Appl. Phys. 56, 2901 (1984)
- [128] Skowroński M and Godlewski M
ZnS:Fe J. Phys. C 17, 2901 (1984)

References

H

- [129] Martynov V N and Gorn I A
ZnSe:Fe Sov. Phys. Semicond. 20, 843 (1986)
- [130] Baranowski J M and Langer J M
CdSe:Cr,Fe Phys. Stat. Sol. (b) 48, 863 (1971)
- [131] Clerjaud B, Gélinau A, Gendron F, Porte C, Baranowski J M
and Liro Z ZnS:Ni J. Phys. C 17, 3837 (1984)
- [132] O'Neill A G and Allen J W
ZnSe:Co Sol. State Comm. 46, 833 (1983)
- [133] Ledebø L-Å and Ridley B K
J. Phys. C 15, L961 (1982)
- [134] Noras J M, Szawelska H R and Allen J W
ZnSe:Co,ZnS:Co J. Phys. C 14, 3255 (1981)
- [135] Swank R K
Phys. Rev. 153, 844 (1967)
- [136] Loescher D M, Allen J W and Pearson G L
GaP:Co J. Phys. Soc. Japan 21 (Suppl.), 239 (1966)
- [137] Baranowski J M, Grynberg M and Magerranov E M
GaAs:Co Phys. Stat. Sol. (b) 50, 433 (1972)
- [138] Wentzcovitch R M, Richardson S L and Cohen M L
Phys. Lett. 114A, 203 (1986)